MAX-PLANCK-INSTITUT FÜR PLASMAPHYSIK
Garching bei München

STELLARATOR EXPERIMENTS AT IPP GARCHING

1965 - 1990

compiled by Horst Wobig and Fritz Rau

IPP 2 / 311 February 1991

This collection of publications on stellarator experiments in Garching is dedicated to
Dr. Günter Grieger
on the occasion of his 60th birthday.

Die nachstehende Arbeit wurde im Rahmen des Vertrages zwischen dem Max-Planck-Institut für Plasmaphysik und der Europäischen Atomgemeinschaft über die Zusammenarbeit auf dem Gebiet der Plasmaphysik durchgeführt.

Contents

IAEA Brussels, 1980	Neutral Injection in the Wendelstein VII-A Stellarator with Reduced Ohmic Current W VII-A Team, NI Team
IAEA Baltimore 1982	Neutral-Injection Heating in the Wendelstein VII-A Stellarator W VII- A Team, NI Group
IAEA Baltimore 1982	Concept of an Advanced Stellarator U. Brossmann et al.
IAEA London, 1984	Plasma Confinement and the Effect of Rotational Transform in the Wendelstein VII-A Stellarator W VII-A Team, NI-Group, Pellet Injection Group
IAEA London, 1984	Some Aspects of Modular Stellarator Reactors E. Harmeyer, J. Kißlinger, F. Rau, H. Wobig
EPS Budapest 1985	Confinement of Stellarator Plasmas with Neutral Beam and RF Heating in W VII-A G. Grieger et al.
Nucl. Fus., 25, 1231, 1985	Wendelstein Stellarators G. Grieger, H. Renner, H. Wobig
Nucl. Fus., 25, 1593, 1985	Impurity Transport in the Wendelstein VII-A Stellarator W VII-A Team, NI Group
Fus. Techn., 7, 275, 1985	Electron Cyclotron Resonance Heating Experiments in the Wendelstein VII-A Stellarator V. Erckmann et al., W VII-A Team
EPS Schliersee 1986	Electron Cyclotron Resonance Heating in the Wendelstein VII-A Stellarator V. Erckmann et al.
IAEA TC Yalta, 1986	Advanced Stellarator Reactor and Burner Studies G. Grieger, E. Harmeyer, J. Kißlinger, F. Rau, H. Wobig
IAEA TC Yalta, 1986	Engineering Consideration of Modular Coils for ASRA6C, an Advanced Stellarator Reactor E. Harmeyer, J. Kißlinger, F. Rau, H. Wobig
IAEA TC Yalta, 1986	Magnetic Field Studies for Advanced Stellarator Reactors E. Harmeyer, F. Herrnegger, J. Kißlinger, F. Rau, H. Wobig
IAEA TCYalta, 1986	Heating and Burn Scenarios for ASR and ASB E. Harmeyer, J. Kißlinger, F. Rau, H. Wobig
Nucl. Fus., 26, 678, 1986	Evaluation of the Local Heat Conductivity Coefficient by Power-Modulated Electron Cyclotron Heating in the Wendelstein VII-A Stellarator H.J. Hartfuss et al., W VII-A Team
IAEA Kyoto, 1986	Plasma Confinement in the Wendelstein VII-A Stellarator H. Wobig et al., W VII-A Team, ECRH Group, NI Group

IAEA Kyoto, 1986	Impurity Behaviour in the Wendelstein VII-A Stellarator H. Ringler et al., W VII-A Team, ECRH Group, NI Group
EPS Madrid 1987	Stellarator Research-Status and Trends H. Wobig
IAEA Nice 1988	Physics Studies for Helical-Axis Advanced Stellarators G. Grieger et al.
Pl. Phys. and Contr. Fus., 30, 283, 1988	Studies on Electron Cyclotron Heating at the Wendelstein VII-A/AS Stellarators U. Gasparino et al., W VII-A Team, ECRH Group
Nucl. Fus., 28, 1737, 1988	Effect of Tearing Modes on Temperature and Density Profiles and on the Perpendicular Transport in the W VII-A Stellarator R. Jaenicke, W VII-A Team
EPS Venezia 1989	Initial Operation of the Wendelstein 7 AS Advanced Stellarator H. Renner, W 7-AS Team, NBI Group, ICF Group, ECRH Group
Fus. Techn., 17, 61, 1990	Stellarator Wendelstein VII-AS: Physics and Engineering Design J. Sapper, H. Renner
Fus. Techn., 17, 76, 1990	Electron Cyclotron Resonance Heating Transmission Line and Launching System for the Wendelstein VII-AS Stellarator V. Erckmann et al. W VII-AS Team
Fus. Techn., 17, 148, 1990	Physics and Engineering Design for Wendelstein VII-X C. Beidler et al.
Fus. Eng. and Des., 11, 399, 1990	Design and Engineering Aspects of the Main Components for the Wendelstein VII-AS Stellarator Experiment R. Mathis, J. Sapper
EPS Amsterdam, 1990	Confinement Studies on the Wendelstein VII-AS Stellarator H. Ringler et al., W VII-AS Team, NBI Team, ECRH Group
IAEA Washington, 1990	Confinement Properties of the "Advanced Stellarator" Wendelstein 7-AS H. Renner et al., W 7-AS Team, NBI Group, Pellet Injection Group, ECRH Team
IAEA Washington, 1990	Electron Cyclotron Current Drive and Wave Absorption Experiments in the W 7-AS Stellarator V. Erckmann et al., W 7-AS Team
IAEA Washington, 1990	Physics and Engineering Studies for Wendelstein 7-X G. Grieger et al.

COMPARISON OF ALKALI PLASMA LOSS RATES IN A STELLARATOR AND IN A TOROIDAL DEVICE WITH MINIMUM MEAN-B PROPERTIES

D. ECKHARTT, G. VON GIERKE AND G. GRIEGER
MAX-PLANCK-INSTITUT FÜR PHYSIK UND ASTROPHYSIK,
MUNICH, FEDERAL REPUBLIC OF GERMANY

Abstract — Résumé — Аннотация — Resumen

COMPARISON OF ALKALI PLASMA LOSS RATES IN A STELLARATOR AND IN A TOROIDAL DEVICE WITH MINIMUM MEAN-B PROPERTIES. The confinement of toroidal low-β plasmas in the absence of ohmic heating currents has been studied by using a thermal Cs plasma in a stellarator with $\ell = 3$ helical windings. These experiments gave evidence that the surfaces of constant pressure roughly coincided with the surfaces of constant magnitude of B, rather than being identical with the magnetic surfaces as would normally be expected for a stellarator in magnetohydrodynamic equilibrium. We have extended these experiments to the stellarator with $\ell = 2$ windings which provide a constant rotational transform to all lines of force of the magnetic confining field.

Secondary currents as well as macroscopic mass motions along the lines of force are required for equilibrium in a stellarator in which the confining field is mainly azimuthal in direction. In a toroidal device of azimuthal symmetry with a purely meridional magnetic field, however, equilibrium can be achieved without any currents of macroscopic motions along B. In addition, stability against flutes can be provided for low-β plasmas if $\nabla \oint d\ell/B$ is directed parallel to ∇p. We have constructed a machine with the above-mentioned properties. It consists essentially of four current-carrying ring conductors immersed in the plasma (similar to the arrangement of Okhawa et at.) The conductors are fed by direct currents in order to avoid azimuthally directed electric fields within the plasma. Plasma confinement in this device is studied by using thermal alkali plasmas which are produced by contact ionization. The operating conditions can be chosen so that plasma losses due to "classical" mechanisms (collisonal diffusion to the walls and to the ring conductors, particle losses to the supports, volume recombination, etc.) become small compared to the high loss rates ascribed to "pump-out".

Preliminary experimental results with the Wendelstein stellarator and with the octopole device indicate that in both arrangements the observed particle loss rates agree quite well with theoretical calculations in which resistive diffusion and surface recombination on supports has been assumed. "Pump out" losses would yield particle loss rates one to two orders of magnitude larger than observed.

COMPARAISON DES TAUX DE PERTE D'UN PLASMA ALCALIN DANS UN STELLARATOR ET DANS UN APPAREIL TOROIDAL AYANT DES PROPRIETES DE B MOYEN MINIMUM. Le confinement de plasmas toroïdaux à β faible, en l'absence de courants de chauffage ohmique, a déjà fait l'objet de recherches au cours desquelles on a utilisé un plasma thermique de césium dans un stellarator à enroulements hélicoïdaux du type $\ell = 3$. Ces expériences ont montré que les surfaces de pression constante coïncident approximativement avec les surfaces de B constant et ne sont pas identiques aux surfaces magnétiques, comme on pourrait s'y attendre pour un stellarator en état d'équilibre magnétohydrodynamique. Les auteurs ont étendu ces expériences au stellarator à enroulements du type $\ell = 2$ qui fournit une transformation rotationnelle constante pour toutes les lignes de force du champ magnétique de confinement.

Des courants secondaires ainsi que des mouvements macroscopiques de matière le long des lignes de force sont nécessaires pour assurer l'équilibre dans un stellarator dans lequel le champ de confinement a une direction essentiellement azimutale. Toutefois, dans un appareil toroïdal à symétrie azimutale et à champ magnétique purement méridien, l'équilibre peut être établi sans courant ou mouvement macroscopique le long de B. De plus, l'instabilité en cannelures peut être évitée dans des plasmas à β faible si la direction de $\nabla \oint d\ell/B$ est parallèle à ∇p. Les auteurs ont construit un appareil ayant les propriétés mentionnées ci-dessus. Il consiste principalement en quatre conducteurs annulaires dans lesquels circule le courant et qui sont plongés dans le plasma (dispositif semblable à celui de Okhawa et coll.). Les conducteurs sont alimentés

en courants continus de manière à ne pas créer de champs électriques à direction azimutale à l'intérieur du plasma. Les auteurs étudient le confinement du plasma dans cet appareil en employant des plasmas alcalins thermiques produits par ionisation de contact. Les conditions de fonctionnement peuvent être choisies de telle manière que les pertes de plasma dues aux mécanismes classiques (diffusion collisionnelle vers les parois et vers le conducteurs annulaires, perte de particules vers les supports, recombinaison volumique, etc.) soient petites par rapport aux taux de perte élevés attribués au «pompage».

Les résultats expérimentaux préliminaires obtenus au moyen du stellarator Wendelstein et du dispositif octopolaire montrent que, dans les deux cas, les vitesses élevées de perte de particules sont en assez bon accord avec les résultats des calculs dans lesquels on suppose une diffusion résistive et une recombinaison superficielle sur les supports. Des pertes par pompage donneraient des vitesses de perte de particules plus grandes (de un à deux ordres de grandeur) que les vitesses observées.

СРАВНЕНИЕ СКОРОСТЕЙ ПОТЕРЬ ЩЕЛОЧНОЙ ПЛАЗМЫ В СТЕЛЛАРАТОРЕ И В ТОРОИДАЛЬНОЙ УСТАНОВКЕ С МИНИМУМОМ СРЕДНЕГО В. С помощью термической цезиевой плазмы в стелларатore с трехзаходными винтовыми обмотками исследовалось удержание плазмы с низким значением β при отсутствии омических токов. В результате этих экспериментов получены доказательства того, что поверхности постоянного давления скорее совпадают с поверхностями постоянного В, чем с магнитными поверхностями, что обычно ожидалось бы для стелларатора в магнитогидродинамическом равновесии. Мы поставили также эксперименты на стелларатore с двухзаходными обмотками, которые обеспечивают постоянное вращательное преобразование всех силовых линий удерживающего магнитного поля. Для обеспечения равновесия в стелларатore, в котором удерживающее поле имеет главным образом азимутальное направление, необходимы вторичные токи, а также макроскопические движения массы вдоль силовых линий. Однако в тороидальной установке с азимутальной симметрией с чисто меридиональным магнитным полем равновесия можно достигнуть без каких-либо токов или макроскопических движений вдоль В. Кроме того, устойчивость относительно желобковых возмущений на поверхности плазмы можно обеспечить для плазмы с низким значением β, если $\vec{\nabla}\phi\partial\ell/B$ направлено параллельно $\vec{\nabla}_p$. Мы построили установку с вышеуказанными свойствами. Она состоит главным образом из четырех токонесущих кольцевых проводников, погруженных в плазму (аналогично системе Окава и др.). Проводники питаются постоянными токами с тем, чтобы избежать образования азимутально направленных электрических полей в плазме. Изучается удержание плазмы в этой установке с помощью термической плазмы щелочных металлов, которая получается в результате контактной ионизации. Можно выбрать такие рабочие условия, при которых потери в плазме в результате "классических" механизмов (столкновительная диффузия на стенки и кольцевые проводники, потери частиц на держателях, объемная рекомбинация и т.д.) становятся незначительными по сравнению с большими скоростями потерь, приписываемыми "откачке".

Предварительные результаты экспериментов на стелларатore Вендельштейн и на октупольной установке показывают, что в обоих случаях наблюдаемые скорости потери частицы хорошо согласуются с теоретическими расчетами, в которых учтена резистивная диффузия и поверхностная рекомбинация на опорах. Потери "выкачки" привели бы к увеличению скорости потери частиц на один-два порядка по сравнению с наблюдаемой.

COMPARACION DE LAS VELOCIDADES DE PERDIDA DE PLASMAS ALCALINOS EN UN STELLARATOR Y EN UN APARATO TOROIDAL CON PROPIEDADES DE B MEDIO MINIMO. Se ha estudiado el confinamiento de plasmas toroidales de β pequeño, en ausencia de corrientes de calentamiento óhmico, utilizando un plasma térmico de cesio en un Stellerator con arrollamientos helicoidales del tipo $\ell = 3$. Estos experimentos han demostrado que las superficies de presión constante coincidían aproximadamente con las superficies en las que la magnitud de B permanece constante, en vez de ser idénticas a las superficies magnéticas, como sería de esperar en un Stellarator que se encuentra en equilibrio magnetohidrodinámico. Los autores han ampliado dichos experimentos al Stellarator con arrollamientos del tipo $\ell = 2$ que proporcionan una transformación rotacional const. te a todas las líneas de fuerza del campo magnético de confinamiento.

Las corrientes secundarias y los movimientos macroscópicos de masas a lo largo de las líneas de fuerza son necesarios para asegurar el equilibrio en un Stellarator en el cual el campo de confinamiento está dirigido principalmente en dirección azimutal. Sin embargo, en un aparato toroidal de simetría azimutal, con un campo magnético puramente meridiano, se puede conseguir el equilibrio sin corrientes ni movimientos macroscópicos a lo largo de B. Además, las inestabilidades estriadas pueden evitarse en los plasmas de β pequeño si $\nabla\phi\, d\ell/B$ es paralelo a ∇p. Los autores han construido un aparato que reúne las propiedades antes mencionadas. En esencia, consta de cuatro conductores anulares, por los que circula la corriente y que están sumergidos en el plasma (la disposición es similar a la de Okhawa y colaboradores). La corriente que circula por dichos conductores es continua, para evitar, dentro del plasma, los campos eléctricos azimutales. Se estudia el

confinamiento del plasma en este aparato utilizando plasmas alcalinos térmicos que se producen por ionización de contacto. Se pueden elegir las condiciones de funcionamiento de modo que las pérdidas de plasma debidas a mecanismos «clásicos»(difusión por colisión hacia las paredes y los conductores anulares, pérdidas de partículas en los soportes, recombinación en volumen, etc.) sean pequeñas en comparación con las elevadas velocidades de pérdidas atribuidas al «bombeo».

Los resultados iniciales de carácter experimental obtenidos con el stellarator de Wendelstein y con el aparato octopolar indican que en ambos dispositivos las velocidades observadas de pérdida de partículas concuerdan satisfactoriamente con los cálculos teóricos que se basan en la difusión resistiva y en la recombinación de las superficies en los soportes. Las pérdidas por «bombeo»parecen indicar velocidades de pérdida de partículas superiores en uno o dos órdenes de magnitud a las observadas.

Introduction

The intention of the experiments described in this paper was to investigate in toroidal devices the confinement of low-ß plasmas which should be quiescent and as close as possible to thermal equilibrium. Therefore, a thermal cesium plasma has been produced by contact ionization, thus limiting the plasma temperature to a narrow range around 2300 ^{o}K. But by proper choice of particle density and magnetic field strength many properties of a high temperature plasma can be simulated.
From earlier experiments of this type in stellarators it was not clear to us to which extent the "pump out" effect usually observed in these devices might be related to secondary currents required for equilibrium. Therefore, we thought it would be worthwhile to compare the experimental results obtained in stellarators with those from a toroidal octopol device where the divergence of the diamagnetic currents vanishes locally and thus no secondary currents exist. In addition, stability should be provided according to the $\nabla p \cdot \nabla \oint \frac{dl}{B} > 0$ - principle.

Stellarator

In previous experiments [1] we investigated the confinement of cesium plasmas in the stellarator WENDELSTEIN WIa which was equipped with $\ell = 3$ helical windings in order to provide equilibrium and stability as well. The measured surfaces of constant particle density (under the experimental conditions being identical with the surfaces of constant pressure) did not coincide with the magnetic surfaces. The deviations were larger than expected for a stellarator in magnetohydrodynamic equilibrium. In contrary, the surfaces of constant pressure coincided roughly with the surfaces of constant magnetic field with the consequence that secondary currents are required only near the walls [3]. The measured mean particle life time was shorter than computed under the assumption that resistive diffusion is the predominant loss process.
A possible reason for the results obtained - at least with higher densities - is the rather small rotational transform in the neighbourhood of the magnetic axis. In order to check this hypothesis further experiments have been performed with a stellarator equipped with $\ell = 2$ helical windings (WIb) thus providing a constant rotational transform, ι , over the plasma cross-section. Now, ι , can be made large near the magnetic axis.
A schematic drawing of the WENDELSTEIN stellarator is shown in fig. 1. Cesium plasma is produced by contact ionization on a piece of tantalum metal (4 mm dia) located on the axis of the vacuum tube and heated to a temperature of about 2300 ^{o}K.
The input flux of ions, ϕ_o , is measured by the ion saturation current upon applying a suitable voltage between the tantalum

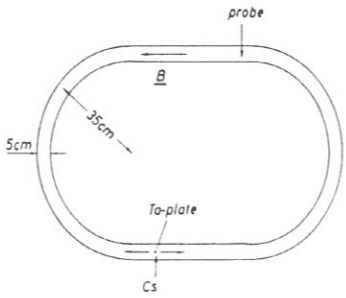

FIG. 1. Schematic drawing of the stellarator WENDELSTEIN WI

piece and the metal vacuum tube. The local particle density, n , is determined from the ion flux to a shielded double-double probe (for more details v. ref. [1]). The magnetic fields are switched on for about half a second which is long enough to have stationary state conditions. During this time interval the tantalum piece is allowed to assume its floating potential.
The mean particle life time, τ , is then obtained from the relation

$$\phi_o \cdot \tau = \int n \, dV = N \qquad (1)$$

The integral $\int n dV = N$ is evaluated by integrating the measured distribution of particle density over the cross-section of the vacuum tube and multiplying by L , the length of the machine.

Most experiments were performed with a main magnetic field B_o = 10 kGauss and an angle of rotational transform $\iota = 70^o$. Four current loops allowed to apply a small magnetic correction field directed perpendicular to the magnetic axis.
These correction fields have been adjusted for optimum plasma conditions, i.e. maximum plasma density and minimum density fluctuations. It turned out, thereby, that the plasma conditions could be further improved if the same angle of rotational transform was produced by energizing the helical winding only on one U-bend instead of feeding a correspondingly lower current through the windings on both U-bends. (See fig. 2). Therefore, all further experiments have been done this way.
In fig. 3 an example of contours of equal particle density is shown. In contrast to our earlier measurements with a rotational transform of type $\ell = 3$ [1], these contours are rather close to rotational symmetry.
In fig. 4 the relation between the total input flux of ions, ϕ_o , and the mean particle density, N/V , is plotted where V is the plasma volume defined by the radius of aperture which in turn is determined by the applied helical fields. The results of our measurements are represented by crosses and circles. The solid curves in this figure are the results of calculations assuming different particle loss mechanisms (for B = 10 kGauss). In these calculations the plasma source is thought to be uniformly spread out along the axis of the machine. As for curve ϕ_p , it is assumed that the particles diffuse across the magnetic field at a rate given by the diffusion coefficient found by STODIEK et al. describing the "pump out" effect in the B-3 stellarator [4]. (The B-3 stellarator has about the same dimensions as our machine WIb). Recombination can be neglected in this case. Curve ϕ_{re} represents the particle loss rates due to resistive diffusion. It should be borne in mind that equilibrium in stellarators requires

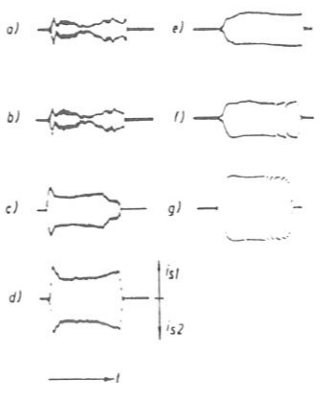

FIG. 2. Optimizing procedure in the stellarator WIb.
a) Oscillogramms of ion saturation current, i_s, to a double-double probe before adjusting the correction fields. The two traces represent the ion flux to either side of the probe. $\iota = 70°$, B = 10 kG, $\phi_0 = 6.9 \times 10^{14}$ sec^{-1}, gain: 0.5 V/cm, time base: 0.1 sec/div. b) Same conditions as a) showing the reproducibility. c) B = 10 kG, $\phi_0 = 5.6 \times 10^{14}$ sec^{-1}, gain: 0.5 V/div, time base, 0.1 sec/div, $\iota = 70°$ produced by both sets of helical windings, correction fields near optimum. d) Same conditions as before except for generating the same rotational transform by only one set of helical windings. e) Correction fields optimized, B = 10 kG, $\phi_0 = 5.0 \times 10^{14}$ sec^{-1}, $\iota = 70°$ (one set of helical windings), gain: 1 V/div, time base: 0.1 sec/div. f) Same conditions as e) but the input flux increased to 5.3×10^{14} sec^{-1}. g) Input flux increased to 9×10^{14} sec^{-1}.

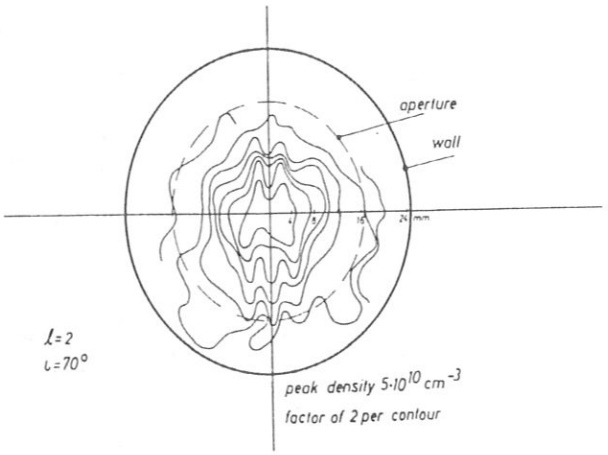

FIG. 3. Distribution of particle density over the tube cross-section for $\ell = 2$ and $\iota = 70°$ in the stellarator WIb (logarithmic scale). Wall radius and radius of aperture are shown.

secondary currents flowing parallel to B which, on account of the finite resistivity of the plasma, cause additional dissipative effects. This leads to an enlargement of the usual coefficient for resistive diffusion, $\frac{\eta_\perp \cdot n \cdot k T}{B^2}$, by a factor $\left(1 + \frac{4\pi^2}{\iota^2}\right)$, [5], [3]

$$D_{re} = \frac{\eta_\perp \cdot n \cdot k \cdot T}{B^2}\left(1 + \frac{4\pi^2}{\iota^2}\right) \qquad (2)$$

This diffusion coefficient has been used in calculating curve ϕ_{re}

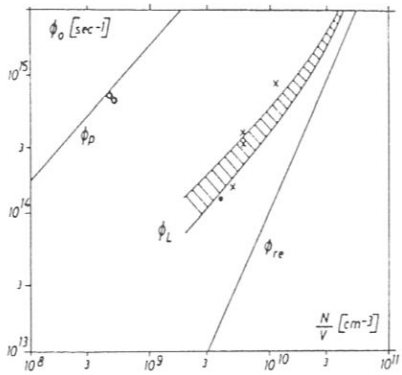

FIG. 4. Total ion input flux, ϕ_o, vs mean particle density, N/V in the stellarator WIb.
x: 10 kG, $\iota = 70°$. O: 10 kG, $\iota = 0°$. ●: 5 kG, $\iota = 150°$.
ϕ_p: Calculated loss flux due to "pump out" vs mean particle density for a field strength of 10 kG. ϕ_L: Calculated loss flux due to resistive diffusion plus recombination on the ceramic support of the tantalum piece for a field strength of 10 kG (lower curve). The upper curve includes recombination on the hot tantalum piece.
ϕ_{re}: Calculated loss flux due to resistive diffusion.

Before comparing our experimental results with the calculations it has to be considered that the ceramic tube supporting the tantalum piece (plasma source) provides a particle sink by recombination of the thermal ion flux on its surface.
Smearing out this recombination effect over the individual magnetic surfaces a volume recombination coefficient, α, can be defined by the relation

$$\alpha \cdot n^2 \cdot L \cdot 2\pi r dr = \frac{1}{4} n \cdot v_{ith} \cdot 2b \cdot dr \qquad (3)$$

where b is the effective width of the ceramic support. The radial dependence of particle density, n, and particle flux, ϕ, is then obtained by integrating the following system of differential equations

$$\frac{d\phi}{dr} = -L \cdot 2\pi r \cdot \alpha \cdot n^2$$
$$\frac{d(n^2)}{dr} = -\frac{\phi \cdot n}{L \cdot \pi \cdot r \cdot D_{re}} \qquad (4)$$

starting from the edge of the plasma (n = 0 at the aperture) up to r = 2 mm (radius of the plasma source), thus yielding the particle flux, ϕ_o, leaving the source region. The lower curve limiting the shadowed region, ϕ_L, represents the relation between ϕ_o and N/V computed in this way. The upper limit of the shadowed region is given by adding recombination losses on the hot tantalum piece assuming a recombination probability of 0,5. It is seen that it is enough to assume resistive diffusion across the magnetic lines of force and recombination on the support of the plasma source to explain the experimental results. "Pump out" losses - if they would occur in this experiment - should yield a mean particle density more than one order of magnitude less than the observed one.
The full circle stands for an experiment where B was reduced by a factor of two and ι was increased by about the same factor. This leaves the diffusion coefficient D_{re}, eq. (2), nearly un-

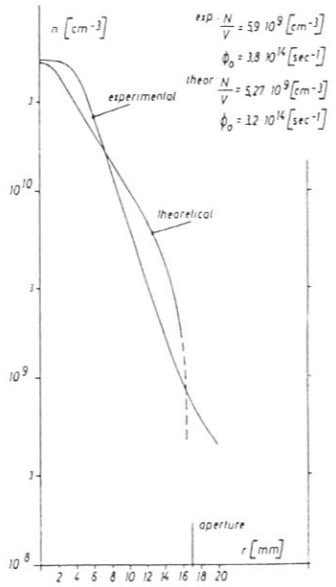

FIG. 5. Comparison of experimental and theoretical density profiles in the stellarator Wlb

changed. Also this experimental result agrees quite well with the theoretical predictions.
The mean particle life-times computed according to eq. (1) vary from 30 to 90 ms thus being still short enough to have stationary state conditions during the time the magnetic field was switched on.
Fig. 5 shows a comparison between the theoretical density profile calculated for classical diffusion and surface recombination and - for about the same absolute value of the input ion flux - of the observed radial dependence of the particle density. In calculating this theoretical density profile under the above assumptions it has been neglected that near the center the resulting density gradients would lead to balancing mass flows the velocity of which exceeds the thermal velocity of the ions [3]. Therefore, the actual density gradients should be slightly less steep in this region.
If the particle density is enlarged by increasing the total input ion flux, the central region where the velocity of the balancing mass flow would be required to exceed the thermal ion velocity, grows radially outwards and, finally, equilibrium will be lost. Comparing figs. 2e to 2g, where the input flux is increased step by step with all other conditions kept constant, the appearance of the sudden reductionsin particle density might be interpreted as an indication that this effect occurs.
The open circles in fig. 4 show the results of our measurements without rotational transform, i.e., in a purely toroidal magnetic field. The measured contours of equal density, fig. 6, indicate that in a rough approximation the pressure is constant on surfaces B = const (similar to our results for $\ell = 3$, [1]). These results could be understood as an effect of the presence of the conducting walls [3].

Octopole Device

A schematic drawing of the octopole device is shown in fig. 7, the diameter of the vacuum vessel is 127 cm. Four ring-

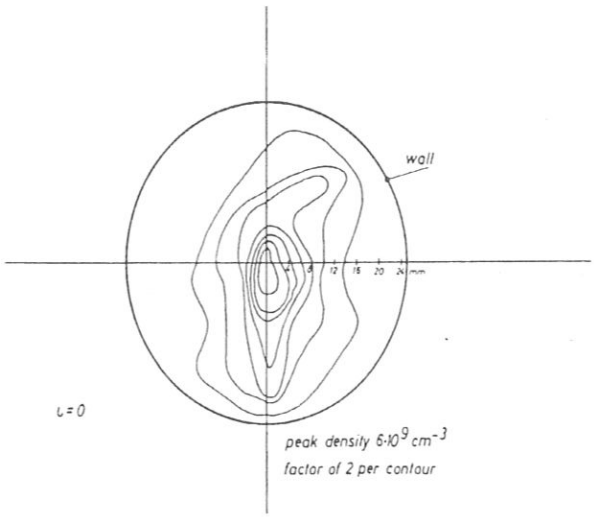

FIG. 6. Distribution of particle density over the tube cross-section for a purely toroidal field ($\iota = 0$), (logarithmic scale)

shaped conductors carry currents in equal directions and, for suitably chosen relative magnitudes of the currents through the outer and inner rings, the field line pattern of fig. 8 is generated, if, in addition, a reversed magnetic field by currents through the outer windings is superimposed [6]. In the plane of symmetry, z = 0 , $\nabla\oint \frac{dl}{B}$ points towards the region of vanishing B_M between r = 28,4 cm and r = 57,3 cm. Therefore, the field line which intersects the midplane at the above points encloses a volume where flute-stable confinement of plasma should be possible [6]. As the magnetic field lines lie in meridian planes the diamagnetic currents flow in azimuthal direction and, for azimuthal symmetry of the arrangement, no secondary currents are necessary for equilibrium.

The machine has been built for steady operation in order to prevent electric fields inside the plasma which arise with inductivily driven currents through ring conductors of finite conductivity. Current and cooling water are fed to each ring conductor through one support; two more supporting rods keep the ring in its position. These supports cross the plasma and intercept the original pathes of the diamagnetic currents, j . Thus, they represent a particle sink where the losses are given by the thermal ion flux onto their surfaces.

In order to satisfy the condition div j = 0 also in the neighbourhood of the supports, a small azimuthal magnetic field, B_ι , has been superimposed which provides a small translational transform to the meridian field, B_M . (This translational transform allows the diamagnetic currents to pass by the supports, so to speak).

We were aware of the fact that the losses to the supports exceed the losses due to resistive diffusion across the magnetic field to the walls. But it was our intention to perform a relatively simple experiment where it was possible to decide the question whether in such a device "pump out" loss rates would appear although no secondary currents were needed for equilibrium. This decision is possible even in the presence of the supports as may be seen from fig. 9.

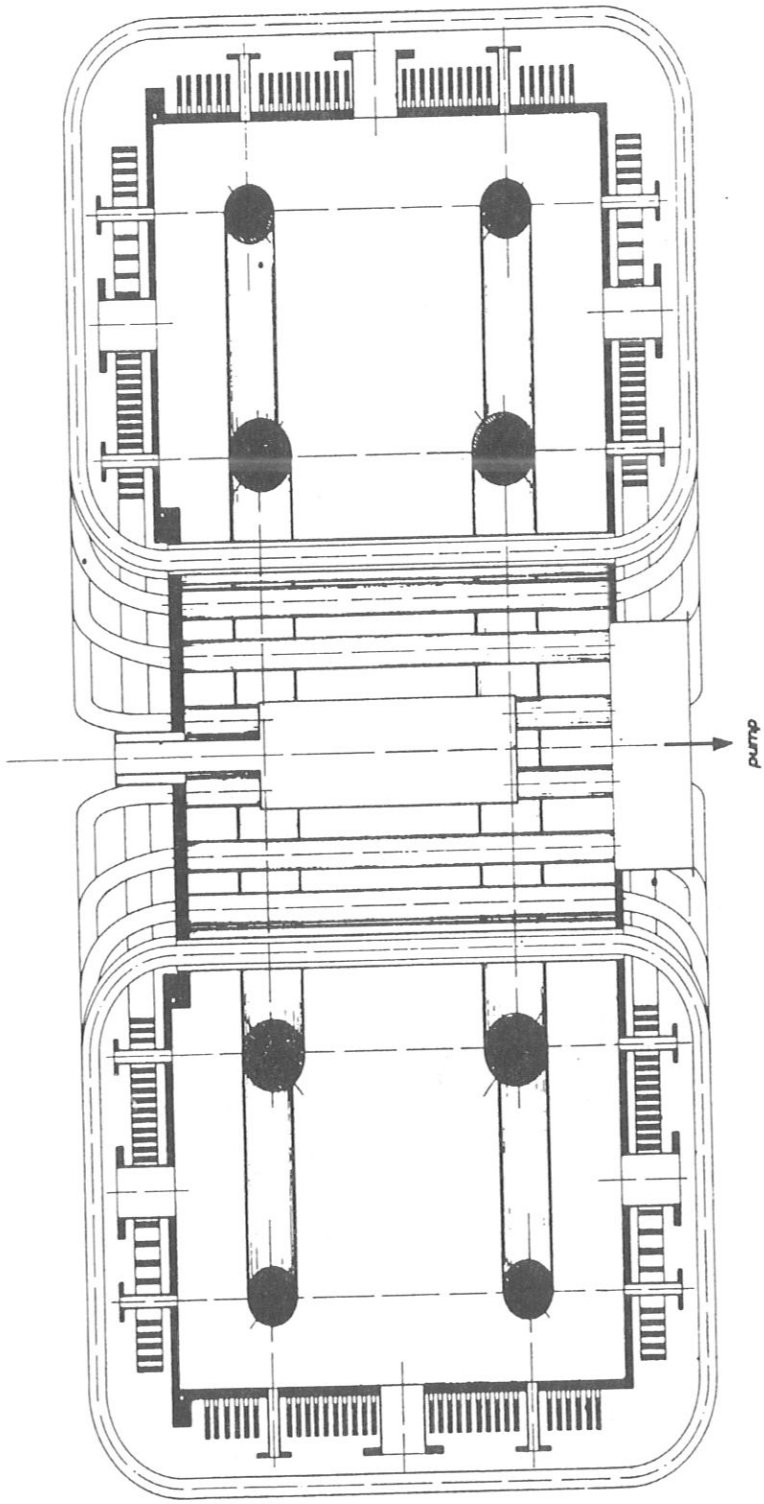

FIG. 7. Schematic drawing of the octopole device

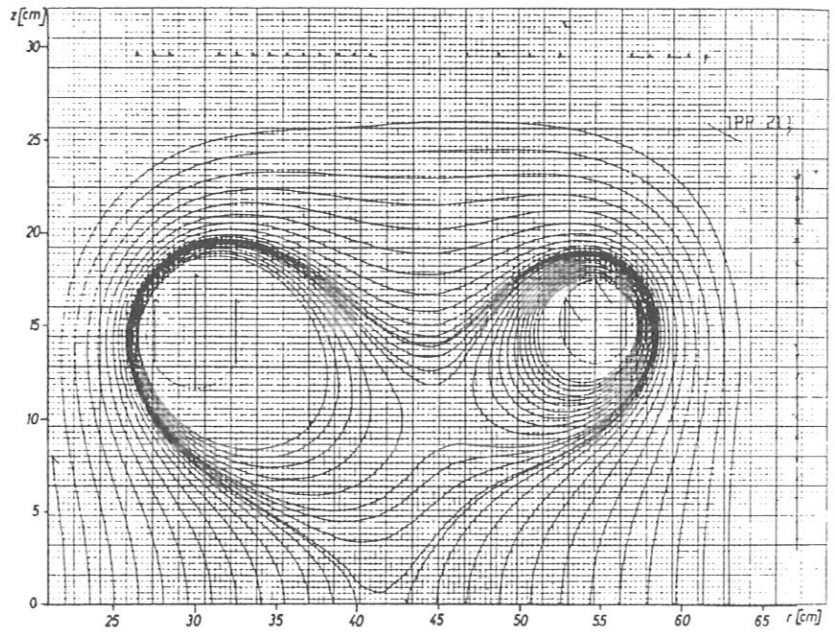

FIG. 8. Field line pattern in a meridian plane of the octopole device

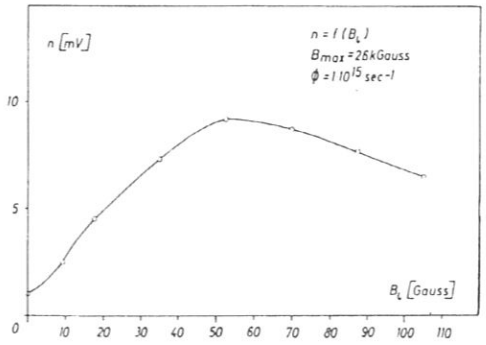

FIG. 9. Particle density vs azimuthal magnetic field, B_t, for fixed input flux in the octopole device

The plasma has been generated in the same way as in the stellarator experiment except for the diameter of the tantalum piece which has been increased to about 15 mm. The tantalum piece was located in the region where B_M vanishes. Two double-double probes, identical to those used in the stellarator experiment, were arranged diametrically opposite to the plasma source to measure the particle density. One of them could be moved perpendicular to the plane of symmetry, the other one could be moved radially in this plane.

We want to report the following preliminary results obtained with magnetic fields near the inner ring conductor varying from 1,3 to 3,9 kGauss.

One of the first experiments was to study the influence of the magnitude of the translational transform on the mean particle life time. This has been done by keeping the input flux of ions con-

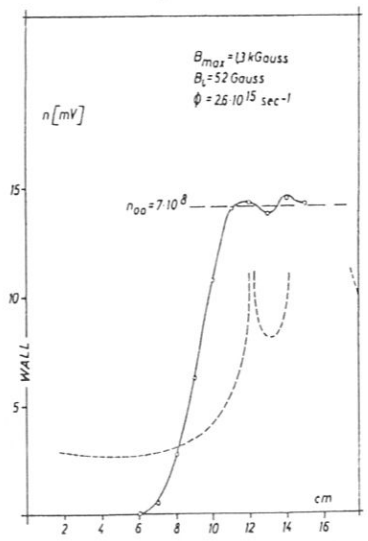

FIG. 10. Density profile in the octopol device perpendicular to the plane of symmetry in the middle between two ring conductors (solid curve); ϕ dl/B in arbitrary units vs distance from the wall (dotted curve)

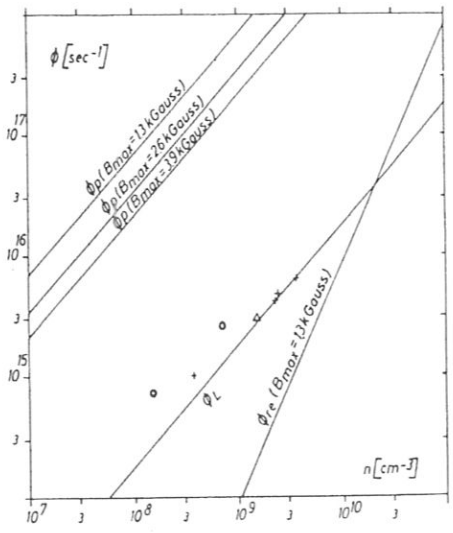

FIG. 11. Total ion input flux, ϕ_0, vs plateau density, n, in the octopole device.
O: B_{max} = 1.3 kG; + : B_{max} = 2.6 kG; Δ: B_{max} = 3.9 kG.
ϕ_p: Calculated losses due to "pump out". ϕ_{re} : Calculated losses due to resistive diffusion. ϕ_L : Calculated losses due to recombination on the supports.

stant and measuring the resultant particle density at a fixed probe position. From the results shown in fig. 9 it can be seen that for zero transform the resultant particle density is comparatively small. With increasing B_L the particle density goes up and very soon reaches a maximum for our experimental conditions. The further experiments, therefore, have been done with $B_L \approx 50$ Gauss.

Fig. 10 shows a plot of the particle density versus probe position measured from the inner wall of the vacuum vessel. The density

goes down to zero far away from the wall, in the region where the magnitude of $\oint \frac{dl}{B}$ has its minimum. The point where the density reaches zero appears to be independent of the field strength within the range investigated.
From these density profiles, and assuming the density to be constant along a line of force, the particle loss fluxes to the supports have been calculated. This was done by multiplying the thermal ion flux density with the surface of the supports as the ion radii of gyration are of about the same order of magnitude as the linear dimensions of the supports. This relation between the peak density and the loss fluxes to the supports is drawn as a straight line in fig. 11 (curve ϕ_L). It may be seen that for the range of densities investigated these losses exceed the losses due to resistive diffusion to the outer walls and the surfaces of the ring conductors, represented by the curve ϕ_{re} as mentioned above. The experimental points, namely the connection between the ion input flux and the resultant plateau density for the different magnetic field values investigated are denoted by circles, crosses and triangles, respectively. If the "pump out" effect would occur in this device, the relation between input flux and peak particle density would be represented by the straight lines, ϕ_p . In these calculations the particle density is set equal to zero at the same field line as observed experimentally.
The experimental results indicate that the particle losses in this device are due to recombination on the supports of the ring conductors. If "pump out" losses would dominate the resultant particle density should be less by about two orders of magnitude than it is observed experimentally.

Conclusions

The confinement of a low-ß cesium plasma has been investigated in a stellarator with $\ell = 2$ windings and in a toroidal device with Minimum Mean-B properties. If we compare the two experiments we have to conclude that in both cases the measured particle loss rates seem to agree with the assumption of resistive diffusion across the confining fields and surface recombination. "Pump out" effects would lead to loss rates one to two orders of magnitude higher than observed. Further measurements with refined methods are necessary to support these preliminary results.

Acknowledgements

The authors wish to thank Dr. K.U.v.Hagenow and Mr. K. Katterbach for performing the calculations. They have greatly benefited from discussions with Prof. A.Schlüter and Dr. D.Pfirsch. They gratefully acknowledge the help of the engineers Messrs. C.Freudenberger, J.Kolos, and M.Zippe for their designing and supervising work during the construction of the octopole device. Finally they wish to thank their technicians and the workshop of the Max-Planck-Institut für Physik und Astrophysik who made it possible to build and put into operation this device within less than half a year.

REFERENCES

[1] D'ANGELO, N. DIMOCK, D. FUJITA, J. GRIEGER, G. HASHMI, M. STODIEK, W., VI. International Conference on Ionization Phenomena in Gases, Paris (1963), paper III,c,9.

[2] OKHAWA, T. YOSHIKAWA, M. SCHUPP, A. VOORHIES, H.G., Sixth Annual Meeting of the Plasma Physics Division of the APS, New York (1964).

[3] ECKHARTT, D. GRIEGER, G., Max-Planck-Institut Rep. MPI-PA-29/64.

[4] STODIEK, W. ELLIS, R. GORMAN, J., Nuclear Fusion Suppl. Part I (1962) 193.

[5] PFIRSCH, D. SCHLÜTER, A., Max-Planck-Institut Rep. MPI-PA-7/62.

[6] ECKHARTT, D. VON GIERKE, G. GRIEGER, G., Max-Planck-Institut Rep. MPI-PAE/Pl. 6/65.

DISCUSSION

A.A. WARE: Were your plasmas in the l = 2 and octopole experiments free of instabilities? Did you look for fluctuations?

D. ECKHARTT: In the stellarator we found sudden interruptions in particle density if the input flux surpassed a certain value. This may be seen in Fig.2. We have not yet looked into the details of this phenomenon.

S.J. BUCHSBAUM: Was there any shear in your machine?

D. ECKHARTT: In the l = 2 stellarator, there was shear only to the amount that higher harmonics of the helical fields might be present with our windings. The octopole device has shear, as mentioned.

V.S. MUKHOVATOV: Is the difference in results obtained by you in the l = 3 and l = 2 devices caused by the different stability conditions or by the different degree of plasma stability?

D. ECKHARTT: We have reason to believe that in our l = 3 system, equilibrium is not achieved near the axis, where the rotational transform is small. This should be the case at least for higher densities. In the l = 2 system we apparently have equilibrium. This could explain the difference between our results for the two systems.

M.B. GOTTLIEB: It has not been established that the loss discussed in the papers on the Tokamak-3 device*, the stellarator at Princeton** and the stellarator at Munich is in fact diffusion; it could be another type of loss. The difference between the reported results may be due to a different ion mass.

---

* These proceedings (CN-21/147, CN-21/245 and 246).

** These proceedings (CN-21/119 and CN-21/120).

RESISTIVE DIFFUSION OF CESIUM PLASMA IN A STELLARATOR*

E. Berkl, D. Eckhartt, G. v. Gierke, and G. Grieger
Institut für Plasmaphysik, Garching bei München, Germany
(Received 29 August 1966)

We have continued our investigations on particle losses from cesium plasmas in the Wendelstein stellarator. At the Culham Conference we reported on measurements[1] obtained in a stellarator magnetic field with helical windings of type $l=2$.[2] We found particle-loss rates to be much less than the anomalously high "pump-out" losses usually encountered in stellarators.[3] Moreover, the relationship observed between ion input flux and the resultant particle density distribution was in agreement with calculations which assumed resistive diffusion across the magnetic confining field and recombination on the insulating surfaces of the supports of the plasma source, the latter constituting the predominant loss process.[4]

In recent experiments, which will be described in this Letter, surface recombination losses within the plasma volume were made negligibly small by minimizing the surfaces of the supports of the plasma source. In this way we have been able to show the radial transport of the plasma to be governed by resistive diffusion.

Our machine has a race-track shape with an axial length of 319 cm and a tube diameter of 5 cm. The main magnetic field can be pulsed up to 15 kG for about one second; the $l=2$ helical windings yield a maximum angle of rotational transform of 0.4π at a main field strength of 11 kG. A small correction field transverse to the magnetic axis can be applied from two pairs of auxiliary windings which encircle the machine. The plasma is produced by contact ionization on a hot tantalum sphere, 5 mm in diameter, which is hung from a thin (25 μm in diameter) tungsten wire. The emitting sphere is heated by bombardment with a beam of energetic electrons from a gun outside the plasma volume. This electron beam is switched off during the time of the experiment and the emitting sphere is allowed to assume its floating potential. The total ion input flux is determined from the ion saturation current drawn when a voltage is applied between the emitting sphere and the vacuum vessel with no magnetic field present. Two small cylindrical electrostatic probes (50 μm diam, 5 mm length) —one located close to the emitting sphere ("near probe"), the other one half-way around the machine ("distant probe")—are situated at the axis of the plasma volume. They are biased negatively with respect to the emitting sphere, and the plasma density is determined from the measured probe current. An annular particle detector which defines the cross section of the plasma volume by its open area is situated near the position of the distant probe. Particles which have left the so-defined plasma volume can be detected by this detector if they move along the magnetic field lines toward its surface. With these measuring devices we obtained the following results:

(1) With fixed magnetic field and for a typical ion input flux of 10^{12} sec^{-1} we found the resultant plasma density to be nearly independent of the temperature of the emitting sphere between 1800 and 2200°K. Beyond these limits the density dropped sharply. This behavior could be explained in terms of plasma production and interaction with the surface of the emitting sphere.

(2) Since the particle density determined by the probes depends strongly on the correction fields, we adjusted them for maximum probe signal. This adjustment was made keeping all other parameters constant. Reversal of all magnetic fields left the plasma properties unchanged. If the emitting sphere was displaced, the correction fields had to be readjusted. This resulted in a displacement of the magnetic axis which was apparently the same as that of the sphere. The temperature of the emitting sphere and the correction fields are adjusted in the following as described above.

(3) The measured output signal of the annular detector represents about 25% of the ion input flux to the machine. If we estimate that about the same fraction of the input flux is lost on the insensitive area of the annular detector, we can account for the rest of the input flux as being lost on the probes and their shafts as well as by recombination on the source. This means that approximately all particles which have left the plasma volume hit the annular detector. This excludes the existence of a large radial plasma transport velocity.

(4) Moving the probes to their maximum sig-

nal positions and correcting for the difference in sensitive areas, we found that the signal of the distant probe was only slightly smaller than that of the probe near the emitting sphere. If the losses had been due to pump-out, the associated high radial plasma flux would have caused a rapid decay of the particle density in the axial direction away from the source (see Fig. 1).

(5) Simultaneous observation of the central particle density, n_0, and of the flux to the annular detector, Φ_R, yielded a relation that allowed a quantitative check on the diffusion mechanism governing the radial plasma transport. For resistive diffusion one would expect

$$\Phi_{re} = C_1 \frac{n_0^2}{B^2}\left(1+\frac{4\pi^2}{\iota^2}\right);$$

if pump-out losses were dominant, the result would be

$$\Phi_B = C_2 \frac{n_0}{B},$$

where C_1 and C_2 are coefficients which include plasma temperature and geometrical dimensions, and which take into consideration that only a fraction of the radial plasma flux will be measured by the annular particle detector.

The quantities n_0 and Φ_R have been measured in three different types of experiments: (a) B and ι were varied to the limits of our power supply; (b) ι was changed keeping all other parameters constant (Fig. 2); (c) the ion input flux was varied leaving the magnetic fields unchanged (Fig. 3).

In Figs. 2 and 3 two curves are drawn to represent the connection between n_0 and Φ_R as calculated from the two loss processes mentioned above. For both cases axial uniformity of the radial particle density distribution was assumed, although in case of pump-out losses a large axial gradient of particle density would be expected. Furthermore, it is taken into account that the annular particle detector —due to its particular geometry— measures only about one-half of the flux arriving on its surface. The experimental results show agreement with the curves for resistive diffusion and disagree with those for pump-out losses in the range of experimental parameters investigated, except for the deviations from the theoretical curve in Fig. 2. These deviations could be interpreted as an indication of incomplete plasma thermal equilibrium when the radial

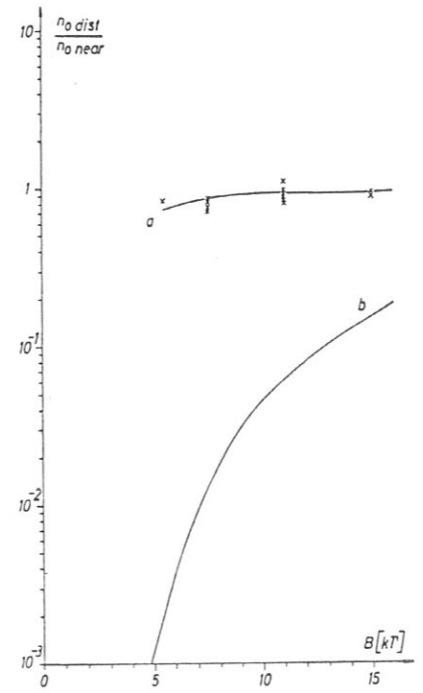

FIG. 1. Ratio of probe signals—distant probe to near probe—versus main magnetic field. Crosses indicate experimental values. Solid curves represent calculated ratios of densities at the two probe positions: curve (a), assuming resistive diffusion; curve (b), pump-our losses.

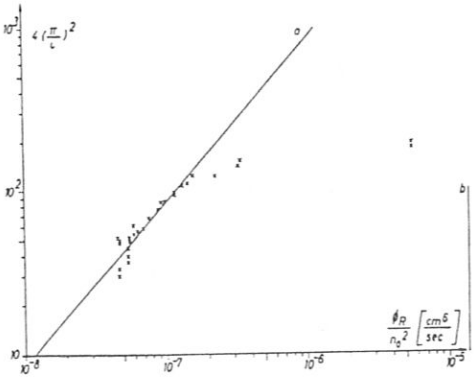

FIG. 2. Total signal of the particle detector related to the central particle density versus $4(\pi/\iota)^2$ for $B = 11$ kG. ι is the angle of rotational transform, n_0 was determined from the probe current. Experimental values are indicated by crosses. Curve (a) represents the calculated relationship assuming resistive diffusion. Curve (b) shows the calculated ratio of Φ_R and n_0^2 if pump-out losses were operative, n_0 having the average value found in this particular experiment.

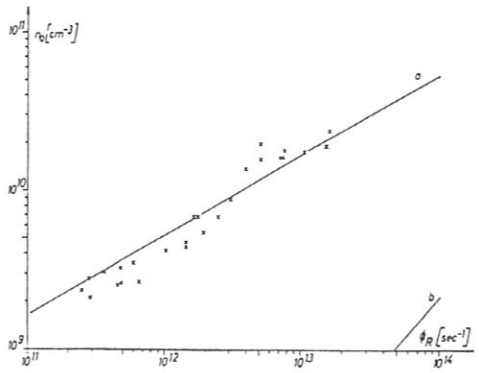

FIG. 3. Relationship between central particle density and flux of diffusing particles for $B = 11$ kG and $\iota = 0.3\pi$. Crosses indicate measured values determined from probe current and particle detector, respectively. Curve (a) is calculated assuming resistive diffusion, curve (b), from pump-out losses.

losses become excessively large for too small values of ι.

We wish to thank Professor A. Schlüter for his continuous interest and for many helpful discussions. The assistance of Dr. W. Ohlendorf and Mr. A. Roland is gratefully acknowledged.

---

*This work was performed under the terms of the agreement on association between the Institut für Plasmaphysik and EURATOM.

[1]D. Eckhartt, G. v. Gierke, and G. Grieger, in Proceedings of a Conference on Plasma Physics and Controlled Nuclear Fusion Research, Culham, England, 1965 (International Atomic Energy Agency, Vienna, 1966), Vol. II, p. 719.

[2]L. Spitzer, Jr., Phys. Fluids 1, 253 (1958).

[3]W. Stodiek, R. A. Ellis, Jr., and J. G. Gorman, Nucl. Fusion, Suppl., Pt. I, 193 (1963).

[4]It should be kept in mind that the coefficient of resistive diffusion has to be multiplied by $(1+4\pi^2/\iota^2)$, where ι is the angle of rotational transform,[2] so as to allow for the power required to drive the secondary currents in a plasma of finite conductivity [D. Pfirsch and A. Schlüter, Max-Planck-Institut für Physik und Astrophysik Report No. MPI-PA 7/62, 1962 (unpublished); D. Eckhartt and G. Grieger, Max-Planck-Institut für Physik und Astrophysik Report No. MPI-PA 29/64, 1964 (unpublished)].

CONFINEMENT OF CONTACT-IONIZED BARIUM PLASMA IN THE WENDELSTEIN STELLARATOR W II *

E. BERKL, D. ECKHARTT, G. v. GIERKE, G. GRIEGER, E. HINNOV**,
K.U. v. HAGENOW AND W. OHLENDORF
INSTITUT FÜR PLASMAPHYSIK, GARCHING, MUNICH,
FEDERAL REPUBLIC OF GERMANY

Abstract

CONFINEMENT OF CONTACT-IONIZED BARIUM PLASMA IN THE WENDELSTEIN STELLARATOR W II. The confinement of low-β plasmas in a stellarator magnetic field has been studied experimentally as a continuation of our previous work. A new stellarator, W II, allows d.c. operation. It has circular shape, avoids interruptions of the helical windings generating an $\ell = 2$ helical field, and possesses five-fold rotational symmetry. It has practically no shear but a small average magnetic well, 3% in depth. Barium plasma was produced by contact ionization on a radiation-heated tantalum sphere located on or near the magnetic axis. Measurements of the density distribution were performed for various values of the magnetic field, the angle of rotational transform and the magnitude of the input ion flux. The ion density was determined by two independent methods, namely (i) by Langmuir probes and (ii) by resonance fluorescence. The measured relation between input ion flux and peak ion density is in agreement with numerical calculations of this dependence assuming resistive diffusion across a stellarator magnetic field and recombination on the surfaces of the emitter and its supporting wire as well as on the surfaces of any probe introduced into the plasma. This confirms earlier measurements done in the apparatus W Ib. For the higher emitter temperature assumed in the calculations the flux lost on the emitter is negligibly small compared to the flux radially outwards. It has also been found that for input ion flux and main magnetic field kept constant the peak ion density decreases markedly whenever $\iota/2\pi$ is a rational fraction.

Introduction

Previous experiments on the confinement of a Cs plasma in the Wendelstein stellarator W Ib [1, 2, 3] gave evidence that - in comparison to "pump-out" - the plasma loss rate only slightly exceeds that expected for resistive diffusion (including the factor $(1 + \iota^{-2})$ for stellarator confinement [4]) and recombination on the emitter and the probes. This statement holds after a critical revision of the previous results based on current knowledge [5, 6] ($\iota/2\pi$ is here denoted by ι).
However, the uncertainty introduced by the use of probes for density measurement, the relatively short duration of 0.8 sec of the magnetic field pulse, the time dependence of the emitter temperature, the complicated magnetic field structure of the W Ib stellarator and the restriction on plasma radius required a new experiment in order to put the results on a safer ground.

---

* This work was performed under the terms of the agreement between the Institut für Plasmaphysik GmbH, Garching near Munich, and Euratom to conduct joint research in the field of plasma physics.

** On leave from Princeton University, USA.

Therefore, a new stellarator, W II, has been built. This is a circular torus with a comparatively large aspect ratio of 0.1 and the highest degree of symmetry achievable for a $\ell = 2$ stellarator. It has practically no shear, but does possess a small average magnetic well about 3 % in depth. Steady-state operation can be achieved for 20 sec or more. Observation ports as large as consistent with these requirements have been provided to allow spectroscopic investigations in addition to the diagnostic techniques previously used.

Experimental Arrangement

The stellarator W II (fig. 1) is a circular torus with radius of curvature R = 50 cm and an effective tube diameter 2r = 12 cm. The main field is produced by 44 coils, equally spaced and connected in series. The maximum field strength is 9 kG d.c. or about 15 kG pulsed. The helical windings are of the type $\ell = 2$, and are wrapped uniformly around and directly upon the vacuum tube with a field period of five. The only deviation from five-fold rotational symmetry is caused by the current leads. The requirements of symmetry unfortunately limit the location and size of the observation ports.

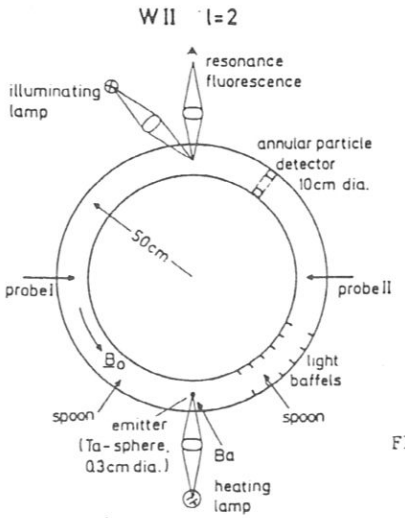

FIG. 1. Schematic drawing of the stellarator W II.

The rotational transform, the existence and the shape of the magnetic surfaces have been measured by means of a pulsed electron beam [7]. The magnitude of the rotational transform agrees closely with calculations [8], as shown in fig. 2. The magnetic surfaces are nearly elliptical in cross-section. In the range of $\iota = \frac{t}{2\pi}$ investigated the ratio of the two axes of the ellipses can be approximated by the formula

$$\frac{a}{b} = 1.14 + 1.46\ \iota$$

So far only magnetic fields of 5 and 7.5 kG have been used. The maximum rotational transform for these cases are $\iota = 0.5$ and $\iota = 0.22$ respectively. The plasma diameter is limited by the magnetic surface tangent to an annular particle detector with an inner radius

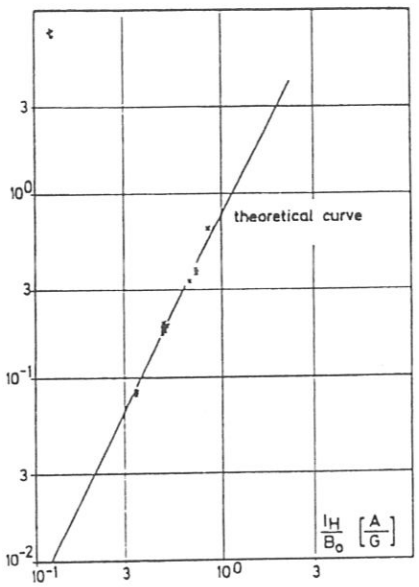

FIG.2. Rotational transform, ι, vs the ratio between the current in the helical windings and the strength of the main magnetic field, measured by means of a pulsed electron beam. The calculated curve is shown for comparison.

27.5.68 20006

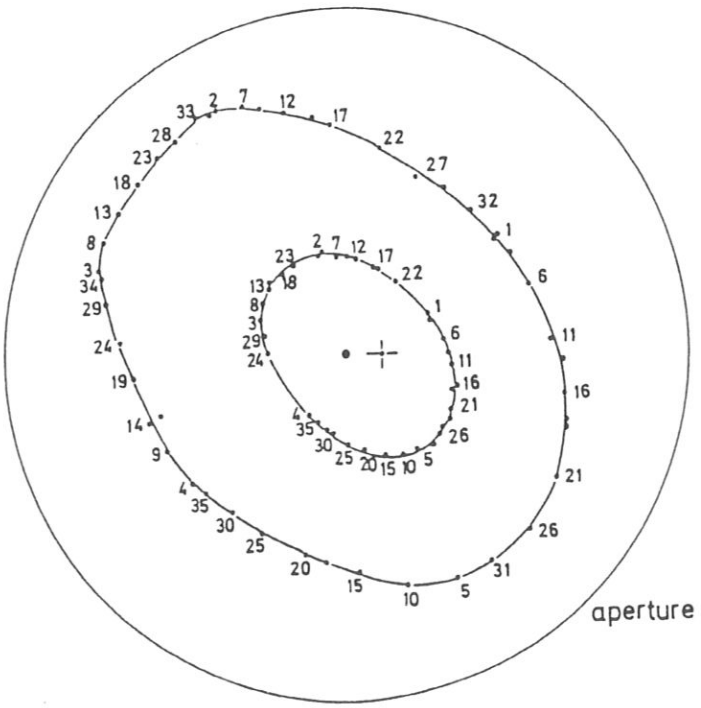

FIG.2a. An example of the drift surfaces in the stellarator W II found by the use of a pulsed electron beam.

of r_p = 5 cm. This yields an effective aperture with the radius $r_{eff} = 5.0 - 1.65\,\epsilon$ cm.

Ba plasma is produced by contact ionization on a Tantalum sphere of 3 mm diameter. The sphere was suspended by a Tungsten wire of 50 µm diameter on or near the magnetic axis. It was heated to a temperature of about 2150 °K by focussing a 6.5 kW high pressure Xe arc upon its surface. The measured current of thermally emitted electrons allowed the formation of an electron sheath up to densities of about $3 \cdot 10^9$ cm^{-3}. Higher temperatures could not be achieved by this means because of the limited solid angle available.

Two removable spoon probes are arranged on either side of the emitter. With the help of these probes the total input flux of ions, Φ_B, could be determined from the ion saturation current also in the presence of the magnetic field. The ion density was measured in two different ways. (i) Probes could be introduced 90° azimuthally displaced from the plasma source. The probe tips were 30 µm in diameter and 3 - 5 mm in length. The probe shafts had a diameter of 0.1 mm. The probes were biased with respect to the emitter. The ion density has been evaluated in the usual way from the probe signal except that an "increased sensitivity factor" of 2.5 was taken into account [9, 10]. (ii) At 180° around the machine the density was measured by the method of resonance fluorescence [11]. A capillary high pressure Xe lamp was used to excite the Ba^+ resonance lines. The spatial resolution used was about 2.5 x 2.5 x 12 mm^3 with the long dimension orientated parallel to the main magnetic field. Horizontal scans could be made by shifting the illuminating lamp and vertical scans by deflecting the image of the stellarator by means of a variprism [12]. The particle detector (fig. 10) was intended to measure the flux leaving the confinement region. It was of the double-double probe type described previously [13]. The sensitive parts of the particle detector were divided into four segments, each consisting of three azimuthal strips of 2 mm radial extension.

Experimental Results and Discussion

Two main relationships were subject to experimental investigation: (i) the peak particle density as function of the input ion flux, Φ_B, for fixed magnetic fields; and (ii) the dependence of the peak ion density on ϵ with input flux and main magnetic field kept constant. For some of the parameters particle density profiles were determined and the influence of the presence of a probe within the plasma on the ion density studied.

The experimental results are compared with a theoretical model which considers resistive diffusion across the stellarator magnetic field in the approximation of small t and recombination on the emitter and its supporting wire as the dominant loss processes. If probes are introduced into the plasma the losses on their surfaces are also taken into account. This model has been found to describe successfully the experimental results obtained with the W Ib stellarator [6] and has been modified only for the different parameters present in this experiment. The curves shown for comparison with the experimental results are calculated for emitter temperatures of 2320 ^{o}K, i.e. U_{th} = 0.2 V, and 2100 ^{o}K, i.e. U_{th} = 0.18 V. In the former case the flux lost by recombination on the emitter is small compared to the flux lost by diffusion and therefore has only a minor influence on the peak particle density, except for the highest values of t and n.

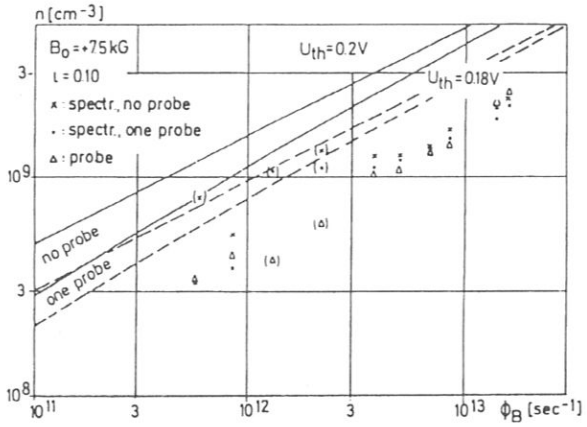

FIG. 3. Peak ion density vs input ion flux measured by resonance fluorescence and by probe for B_0 = 5 kG and t = 0.10. Calculated curves for U_{th} = 0.2 V and 0.18 V respectively are shown for comparison.

Figs 3 - 5 give the dependence of the measured density on the input flux for different parameters. There are three different measurements of the density: a) by resonance fluorescence with no probe introduced into the plasma; b) by resonance fluorescence with one probe in the plasma; and c) by the probe itself. The measured points follow a $n \sim \sqrt{\Phi_B}$ dependence as expected for the model discussed above, except for a few points shown in brackets. With the latter points there exists some uncertainty with respect to the experimental parameters present during the measurement. The absolute density is smaller by a factor of 2 or 3 than the one calculated for U_{th} = 0.2 V but exceeds the Bohm value by two orders of magnitude for $\Phi_B = 10^{12}$ sec^{-1}. If the loss rates are that small, the introduction of an obstacle into the plasma should reduce the density considerably. This effect is realized by introducing a probe into the plasma,

i.e. a glass-covered wire of 0.01 cm outer diameter. In this case the density as measured by resonance fluorescence is reduced by 20 - 30 %, in agreement with the calculations. The residual disagreement between the density measured and calculated might find its explanation in the fact that the temperature of the emitter was only 2150 ^{o}K i.e. $U_{th} \approx 0.18$ V yielding a much larger recombination coefficient. On the other hand, the appropriate value of the work function of Ta for these operating conditions is not known to us and seems to be in disagreement with the usual assumptions. This involves some uncertainties in the flux lost by surface recombination and will be subject to further investigations. It was in fact a surprising result that Ta could be used so effectively to produce a Ba plasma.

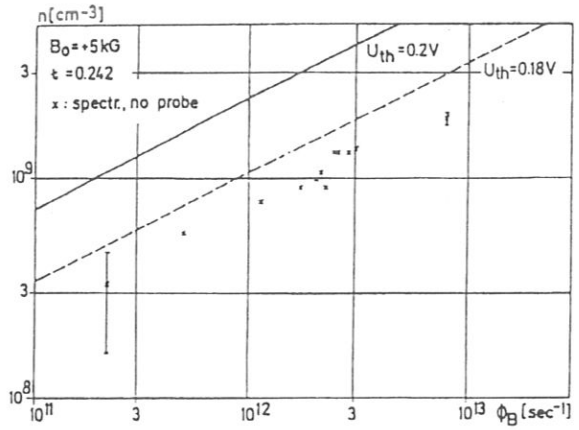

FIG. 4. Peak ion density vs input ion flux measured by resonance fluorescence for B_0 = 5 kG and t = 0.242. Calculated curves for U_{th} = 0.2 V and 0.18 V respectively are shown for comparison.

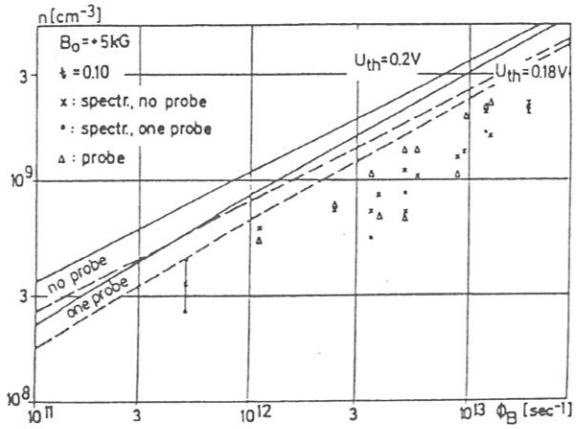

FIG. 5. Peak ion density vs. input ion flux measured by resonance fluorescence and by probe for B_0 = 7.5 kG and t = 0.10. Calculated curves for U_{th} = 0.2 V and 0.18 V respectively are shown for comparison.

The increase in density when increasing the magnetic field strength from 5 to 7.5 kG is calculated to be 40 %. An increase of roughly this magnitude was observed by resonance fluorescence

measurements at higher fluxes. At lower input fluxes the experimental error is of the same order as the effect expected.

In figs 6-8 the dependence of the peak ion density on t is shown. It can be seen that above a certain t the density rises steeply. This critical value of t decreases with increasing Φ_B and increasing B which might be explained in terms of thermalization of the plasma and supports earlier explanations [2]. It should also be emphasized that for small values of t it is not permitted to neglect the ion inertia terms as has been done in the calculations.

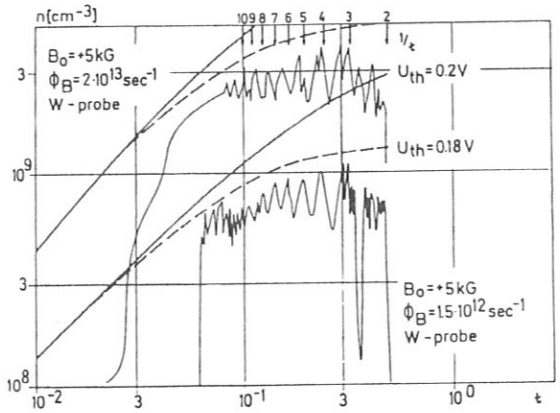

FIG.6. Peak ion density vs t measured by probe for B_0 = 5 kG and $\Phi_B = 1.5 \cdot 10^{12}\,s^{-1}$ and $\Phi_B = 2 \times 10^{13}\,s^{-1}$ respectively. For comparison calculated curves are shown for U_{th} = 0.2 V and 0.18 V respectively.

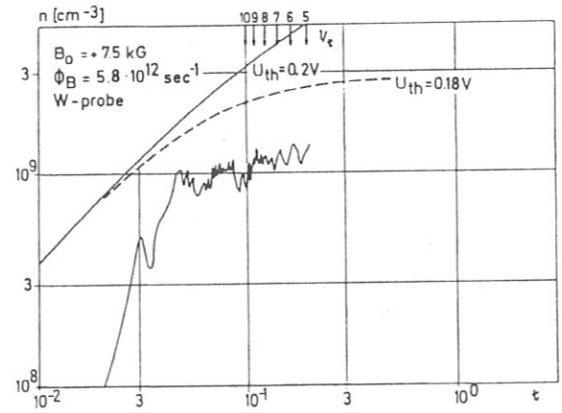

FIG.7. Peak ion density vs. t measured by resonance fluorescence for B_0 = 5 kG and $\Phi_B = 9.5 \times 10^{12}\,s^{-1}$. For comparison calculated curves are shown for U_{th} = 0.2 V and 0.18 V respectively.

For larger t the density shows discrete maxima and minima. Within the experimental error the minima occur if $1/t$ is a rational number[+], some of them being indicated on the top of the figures.

+) The term "rational number" in this connection should be understood as $1/t = \frac{m}{n}$ with m, n being not too large integers.

Unfortunately, no precise statement can be made about this fact, since the currents of the generators showed some fluctuations with time and could not be measured with sufficient precision to reduce the error in ι below 3-4 %. That the fine structure of the confinement properties could be observed so clearly is ascribed to the fact that the W II device has practically no shear. In this case ι becomes rational for a large part of the plasma cross-section simultaneously. When ι

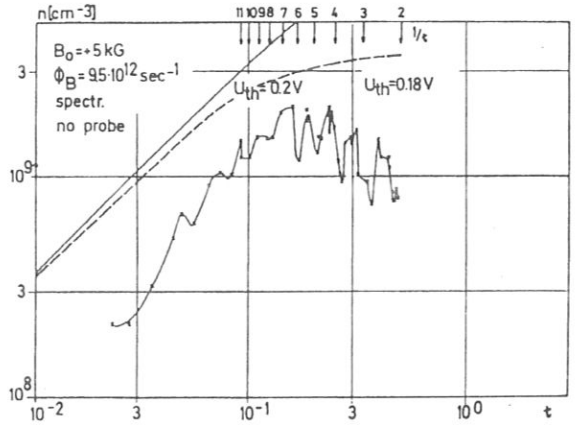

FIG.8. Peak ion density vs. ι measured by probe for B_0 = 7.5 kG and $\Phi_B = 5.8 \times 10^{12}\ s^{-1}$. Calculated curves for U_{th} = 0.2 V and 0.18 V, respectively, are shown for comparison.

is a rational fraction magnetic surfaces are no longer defined since the magnetic lines close upon themselves after a certain number of revolutions around the machine. In this case the condition $\nabla_{\parallel} p = 0$ no longer requires that the pressure is constant on the magnetic surfaces but only along the individual closed lines. Equilibrium between plasma pressure and magnetic field forces in such degenerate cases requires $p = f(q)$ where $q = \oint \frac{dl}{B}$. In general surfaces of constant q will differ from the magnetic surfaces (as defined by a slight change of ι) but it has been found by numerical calculations that closed q-surfaces in fact exist in W II in the immediate neighbourhood of the magnetic surfaces, at least for $\iota = 0.5$. Therefore, the appearance of such drastic changes of the confinement properties are not to be expected simply on the basis of the absence of well-defined magnetic surfaces. It is not clear, on the other hand, how the stability is affected if ι becomes a rational fraction particularly as the device has negative V''- properties. One possible explanation for the observation might be found in the development of convective cells if ι is rational since the supporting wire of the emitter - even though it was very thin - might influence the potential on those magnetic lines which pass through or near it. In contrast, if magnetic surfaces exist, i.e. if ι is an irrational fraction, these surfaces must closely agree with the surfaces of constant potential,

prohibiting the generation of convective cells oriented perpendicular to the magnetic surfaces. All these possibilities are being investigated both theoretically and experimentally.

As far as the maxima of n are concerned, they follow closely the calculated curve if one uses the actual temperature of the emitter (0.18 V) except for the highest values of t where the deviation seems to become larger.

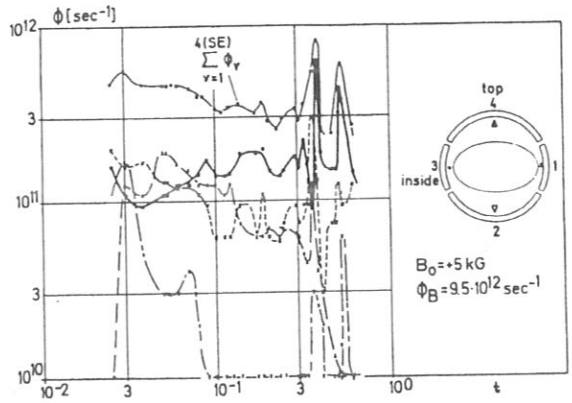

FIG.9. Fluxes to the individual segments of the particle detector and the sum of these fluxes vs t for B_0 = 5 kG and $\Phi_B = 9.5 \times 10^{12}\ s^{-1}$. No probe was present within the plasma. These data were taken simultaneously with the ones shown in Fig.7. For the meaning of the symbols see insert.

In fig. 9 the ion flux collected by the particle detector vs. t is plotted. These data were taken simultaneously with the ones shown in fig. 7. No probe was present within the plasma in this case. It can be observed that for increasing t the plasma is lost preferentially in the plane of the torus towards the segments 1 and 3, which is in agreement with the orientation of the elliptical cross section of the magnetic surfaces as shown in the insert of fig. 9. Upon reversing the direction of the helical currents the orientation of the ellipse is rotated by 90° and the plasma is found to be lost towards the segments 2 and 4. Furthermore, by comparison with fig. 7 it can be seen that the flux found at the particle detector increases if the centre density decreases. It has not yet been investigated, however, why the direction of the increased loss flux is not always the same but depends very sensitively on the magnitude of t . The answer might, perhaps, be found in a change of the orientation of convective cells possibly generated by the presence of the wire suspending the emitter. The total flux found on both sides of the detector is only about 10 % of the input ion flux. The flux reaching the wall of the vacuum chamber should be negligibly small as the flux decreases sharply in the radial direction (see fig. 11). There use has been made of the radial splitting of the sensitive segments of the particle detector. These results probably find their explanation in a larger recombination on the emitter and,

preferentially, on the suspending wire than assumed. This is supported by the observation that there is only a small change of the signal detected by the particle detector if a probe is introduced into the plasma. Further experimental investigations of this effect are planned. If only the main magnetic field is switched on ($\iota = 0$) the plasma is lost preferentially in the outward direction (Fig.12). In that case no signal is found on the inner segments of the detector.

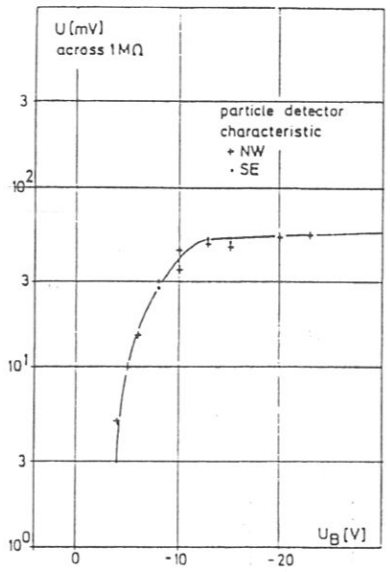

FIG.10. Characteristic of the particle detector. The electron-collecting grids were always electrically connected with the wall of the vacuum chamber.

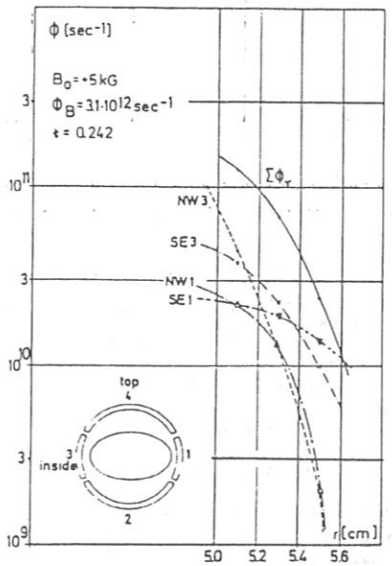

FIG.11. Radial dependence of the flux collected by the particle detector. Use has been made in this case of the radial splitting of the individual segments.

In fig. 13 a profile of particle density is shown for a case with the emitter positioned 7 mm off the magnetic axis. The profile was measured by probe and by resonance fluorescence without

the probe. One observes fair agreement between both curves. The dip in the centre is produced by the probe acting as a particle sink and could be observed by resonance fluorescence+) as well.

The measured amplitude of the fluctuations is less than 1 % of the total density if ϵ is carefully adjusted for optimum conditions. This holds for regions around the plasma centre and for a cut-off frequency of the probe circuit of 500 kHz (see fig. 14). No

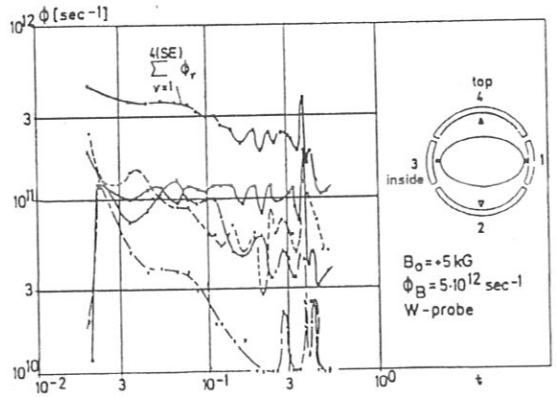

FIG. 12. Fluxes to the individual segments of the particle detector and the sum of these fluxes vs. ϵ for B_0 = 5 kG and $\Phi_B = 5 \times 10^{12}\ s^{-1}$. In this case a probe was introduced into the plasma.

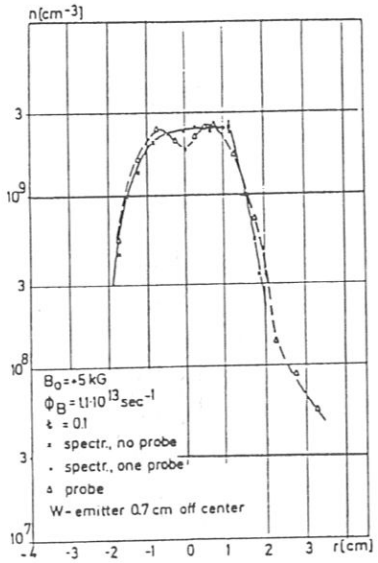

FIG. 13. Profile of particle density measured by resonance fluorescence without any probe being present within the plasma except for one point showing the reduction in central density when introducing the probe and by probe. The position of the emitter was 7 mm off axis, B_0 = 5 kG, $\Phi_B = 1.1 \times 10^{13}\ s^{-1}$.

+) An additional result of this investigation is that this type of probes, if evaluated as described above, shows close agreement with the density measured by resonance fluorescence not only in Q-machines but also in closed configurations outside the emitter region.

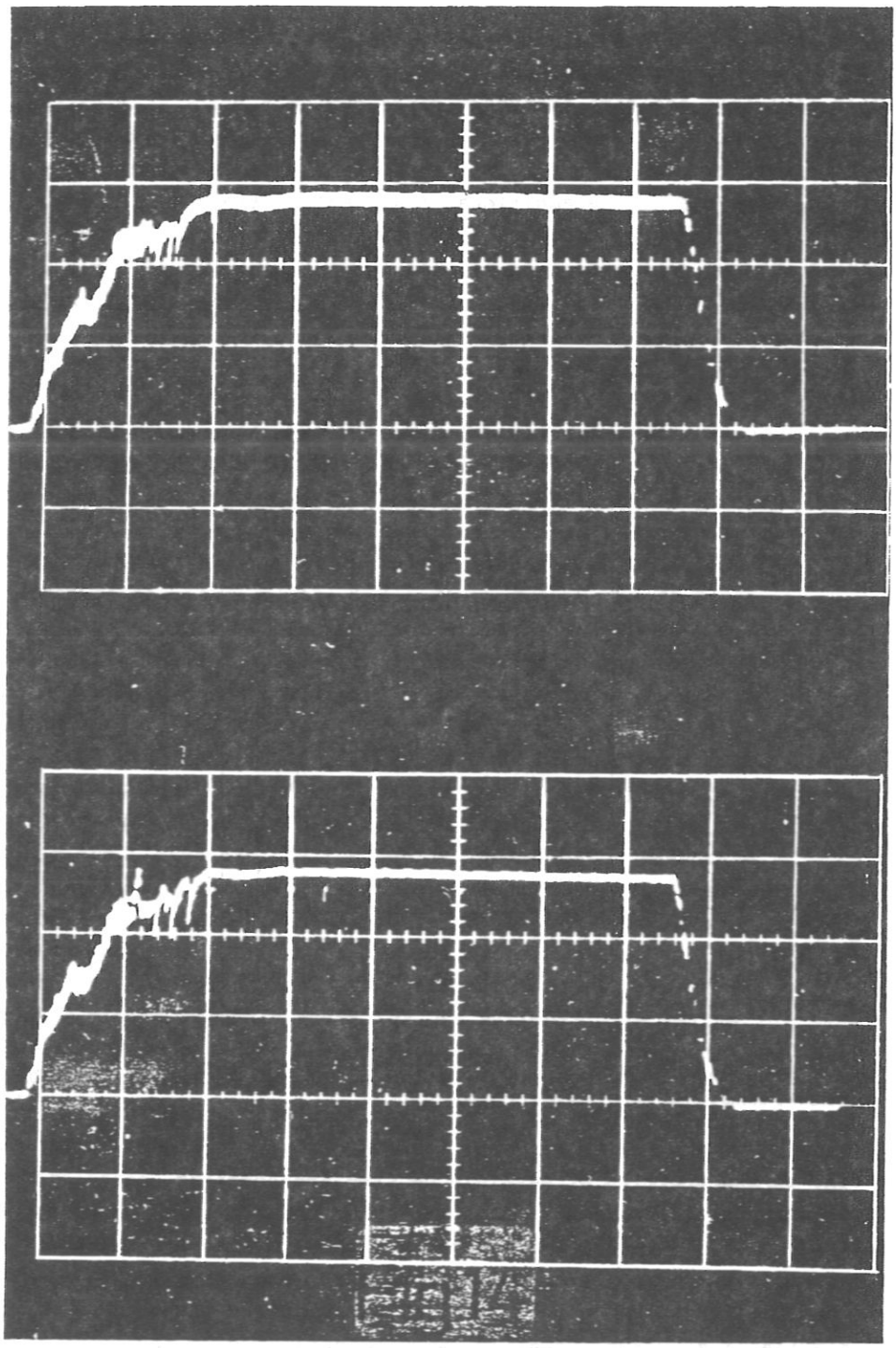

FIG. 14. Example of the probe signal for a case with carefully adjusted τ. The sweep is 5 s per division. On the lower picture a low pass filter with a cut-off frequency of 30 kHz has been used. The upper picture is taken without such a filter, the cut-off frequency of the probe circuit being 500 kHz. Small residual oscillations observed in this case are identified as pick up from a radio station located nearby and operating at ν = 800 kHz.

particular investigations were performed on fluctuations in the region of steep density gradients. For values of ι other than optimum, low-frequency fluctuations of 0.1 - 500 Hz were observed which fall into the same frequency range as the current fluctuations of the generators. Therefore, these fluctuations are believed to be fluctuations of the confinement properties with fluctuating ι . This is supported by the additional observations that: a) quiescent plasma conditions could also be found for n being a minimum as function of ι , and b) rapid changes of the orientation of the loss fluxes as indicated by the signals of the particle detector were observed.

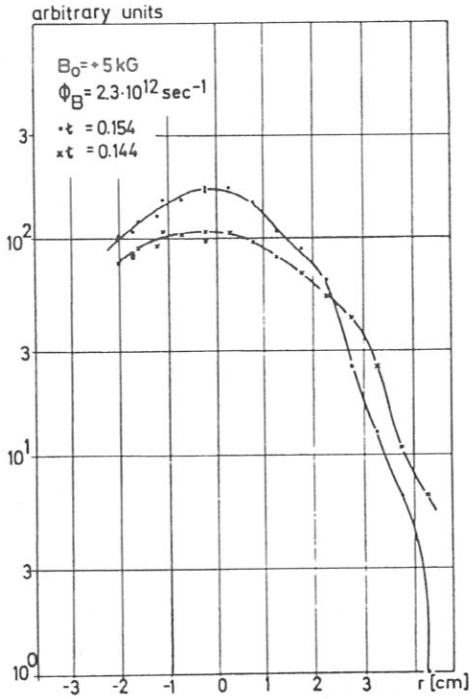

FIG. 15. Comparison of two profiles of particle density for identical B_0 = 5 kG and Φ_B = 2.3 × 10^{12} s^{-1} but for different ι being 0.154 and 0.144 (~ 1/7) respectively.

In fig. 15 two profiles of particle density are compared, one taken for n being a maximum (ι = 0.154) and one for the adjoining minimum (ι = 0.144 ~ 1/7). One sees that the profiles are quite different in shape, so that fluctuations in ι should yield considerable fluctuations in n. Some of the profiles taken preferentially at higher densities were integrated over the plasma volume and this number divided by the input flux. The confinement time obtained this way is of the order of 1 sec which is about a factor of 2 shorter than that calculated. Again this might be caused by a recombining flux larger than assumed in the calculations.

For the low temperature of the emitter and the parameters present in this experiment no strong dependence of the peak ion density on the correction fields is expected according to our earlier explanations [2]. This is in agreement with observations carried out at B = 5 kG and $\Phi_B > 1.9 \cdot 10^{12}$ sec^{-1}. The highest density investigated is just below the limit where, even for larger values of ι, the ion inertia, which has been neglected in the calculations, should strongly influence the confinement properties and therefore the peak density [6].

Summary

A circular stellarator with $\ell = 2$ helical windings yielding practically no shear but a mean magnetic well of 3 % depth has been built. It has been shown that a quiescent Ba plasma can be established by contact ionization on an electron-emitting Ta sphere covering only 0.1 % of the plasma cross section. Over 2 orders of magnitude of the input flux of ions one finds an $n \sim \sqrt{\Phi_B}$ dependence which coincides within a factor of 2 with curves calculated on the basis of classical assumptions only. The residual discrepancy might be caused by the underestimation of the flux recombining on the surface of the emitter. For $\Phi_B = 10^{12}$ sec^{-1} the density found is two orders of magnitude higher than would be the case if the particle losses were governed by "pump-out". These results are obtained with no probe present within the plasma and the ion density measured by resonance fluorescence, they hold if the plasma temperature is assumed to be equal to the emitter temperature which fact remains still to be measured. The confinement properties have been found to be strongly dependent on the value of the rotational transform, showing minima probably where $1/\iota$ is rational. The maxima in between follow closely the theoretical curve if one uses $U_{th} = 0.18$ V which is close to the actual temperature of the emitter. Confinement times of the order of 1 sec are observed. Finally, it should be mentioned once more that the ionizing properties of Tantalum surfaces require detailed investigation as considerable deviations from the "equilibrium model" seem to be indicated.

Acknowledgement

We wish to thank Prof. A. Schlüter for many helpful discussions. For technical help, for scientific discussions, numerical calculations, evaluations and drawings we are indebted to so many people that it is impossible to enumerate all of them individually.

Without their enthusiastic help it would have been impossible to perform this work in such a short time. Special thanks are due to the house Osram, and the DVL Institut für Raumsimulation, which provided us with high-pressure Xenon lamps in a very critical phase of the experiment.

REFERENCES

[1] ECKHARTT, D., v. GIERKE, G., GRIEGER, G., in Plasma Physics and Controlled Nuclear Fusion Research (Proc. Conf. Culham, 1965) 2, IAEA, Vienna (1966) 719.
[2] ECKHARTT, D., v. GIERKE, G., GRIEGER, G., Institut für Plasmaphysik Report IPP 2/52 (1966).
[3] BERKL, E., ECKHARTT, D., v. GIERKE, G., GRIEGER, G., Phys. Rev. Letters 17 (1966) 906.
[4] PFIRSCH, D., SCHLÜTER, A., Max-Planck-Institut Report MPI-PA-7/62.
[5] BERKL, E., v. GIERKE, G., GRIEGER, G., Institut für Plasmaphysik Report IPP 2/69 (1968).
[6] v. GIERKE, G., GRIEGER, G., v. HAGENOW, K.U., Institut für Plasmaphysik Report IPP 2/70 (1968).
[7] to be published.
[8] to be published.
[9] HASHMI, M., van der HOUVEN van OORDT, A.J., WEGROWE, J.-G., 2nd European Conf. on Controll. Fusion and Plasma Physics, Stockholm (1967). (To be published in Plasma Physics).
[10] La FRAMBOISE, J.G., Institute for Aerospace Studies, University of Toronto, UTIAS Rep. No.100.
[11] RYNN, N., HINNOV, E., JOHNSON, L.C., Rev. scient. Instrum. 38 10 (1967) 1378.
[12] HIRSCHBERG, J.H., Journal Appl. Opt. 4, No.6 (1965) 759.
[13] D'ANGELO, N., DIMOCK, D., FUJITA, J., GRIEGER, G., HASHMI, M., STODIEK, W., in Ionization Phenomena in Gases, (Proc. 6th Int. Conf., Paris, 1963) 1 (1964) 399.

DISCUSSION

R.M. SINCLAIR: Is the dependence on rotational transform that you observe consistent with your earlier results (obtained two years ago) concerning the dependence of confinement on transverse field?

G. GRIEGER: The results are consistent with our earlier ones. Owing to the relatively low temperature of the emitter (2150°K), there should be only a weak dependence of the confinement on transverse fields, as long as the displacement of the magnetic axis does not become large compared with the diameter of the emitter.

S. YOSHIKAWA: Existing experimental data do not show L^2 dependence above $L/2\pi = 0.1$. Although recombination may explain this behaviour, we cannot at present rule out the additional loss. Do you agree?

G. GRIEGER: Yes, I agree. However, I would like to point out that, under the conditions of the experiment, the factor by which the cross-field losses might exceed resistive diffusion cannot be a very large one (as indicated in the figures).

S. YOSHIKAWA: What is the agreement or the difference between calculated and experimental density profiles?

G. GRIEGER: The density profile is determined by recombination on the support of the emitter and diffusion across the field. However, the recombination is difficult to take into account accurately. Estimates show rough agreement with the observed density profile.

A. GIBSON: What limit can you place on the amplitude of the fluctuations observed?

G. GRIEGER: If ι is properly adjusted to optimum conditions, $\Delta n/n$ should not exceed about 1%.

Testplasma im Wendelstein-Stellarator W IIa

G. GRIEGER

Institut für Plasmaphysik, Garching bei München

Vor etwa zwei Dezennien wurde zunächst in den USA, der UdSSR und Großbritannien mit Arbeiten zur gesteuerten Kernfusion begonnen, und vor etwas mehr als zehn Jahren sind auch in der Bundesrepublik Deutschland nach schon früher begonnenen theoretischen Untersuchungen Experimente zu diesem Thema aufgenommen worden. Das große Interesse an diesen Forschungen gründet sich auf die Möglichkeit, nach diesem Prinzip sehr große, relativ ungefährliche und hinsichtlich der Abfallprodukte auch sehr saubere Energiequellen zu erschließen. Ein Plasma aus einem Deuterium-Tritium-Gemisch kann große Mengen Fusionsenergie abgeben, wenn es gelingt, es bei einer Temperatur von über 100 Millionen °K so lange zusammenzuhalten, bis genügend viele Fusionsprozesse zwischen den Atomkernen stattgefunden haben. So war auch in den ersten Jahren der im Meerwasser vorhandene fast unvorstellbar große „Brennstoffvorrat" an schwerem Wasser das Hauptargument für die Aufnahme dieser Arbeiten. In der Zwischenzeit haben jedoch angesichts der zunehmenden Siedlungsdichte und der wachsenden Besorgnis über die Änderung der Umweltsbedingungen, wie z.B. die Luftverschmutzung, die *Sauberkeit* und die *Sicherheit* dieser Energiequellen eine mindestens gleichrangige Bedeutung erlangt.

Der Stellarator im Vergleich zu anderen Fusionsexperimenten

Die beiden für eine rationelle Gewinnung von Fusionsenergie zu lösenden Aufgaben, nämlich ein Plasma auf so hohe Temperaturen zu heizen, daß überhaupt Fusionsprozesse stattfinden können und es dann so lange zusammenzuhalten, daß auch hinreichend viele solcher Prozesse stattfinden können, sind im Prinzip voneinander unabhängig. So konnten z.B. im Institut für Plasmaphysik in einer linearen Theta-Pinch-Apparatur die erforderlichen Temperaturen von 100 Millionen °K nahezu erreicht werden, doch war diese Apparatur ungeeignet zur Erzielung langer Einschlußzeiten. Das einzige bekannte praktikable Mittel, die Expansion eines heißen Plasmas drastisch zu reduzieren, sein Einschluß in ein Magnetfeld, kann seine Expansion nur senkrecht zur Feldrichtung stark herabsetzen. Bewegungen parallel zum Magnetfeld werden dagegen nur dann reduziert, wenn sie in Richtung steigender Stärke des Feldes erfolgen. Dieser Effekt ist jedoch bei Berücksichtigung der technischen Realisierungsmöglichkeiten solcher Feldanordnungen vergleichsweise klein und erfaßt auch nicht alle im Plasma vorhandenen Teilchen gleich. Da aus diesen Gründen bei linearen Anordnungen die Verluste durch aus beiden Enden herausfließende Teilchen vermutlich intolerabel groß sind, hat sich das allgemeine Interesse jetzt fast ausschließlich auf ringförmig geschlossene Apparaturen konzentriert, die Endverluste völlig ausschließen und die Einschließungseigenschaften des Magnetdeldes nur senkrecht zu seiner Richtung ausnutzen.

Die Stärke dieses Magnetfeldes relativ zum Druck des einzuschließenden Plasmas unterscheidet die beiden Hauptarbeitsrichtungen in der Plasmaphysik.

Ist die Energiedichte des einschließenden Magnetfeldes vergleichbar mit dem Druck des einzuschließenden Plasmas, so hat man die elegante und im Hinblick auf zukünftige Fusionsreaktoren zweifelsohne sehr attraktive Möglichkeit, mit ein und demselben Magnetfeld während seiner ansteigenden Phase das Plasma zu erzeugen und zu heizen und es dann, nach Erreichen des Spitzenwertes, weiter einzuschließen. Allerdings sind unter diesen Bedingungen alle Parameter des Plasmas auf das Engste miteinander verknüpft, so daß die Änderung eines Parameters die gleichzeitige Änderung vieler anderer nach sich zieht. Ein nach diesem Prinzip gebauter Fusionsreaktor kann nur intermittierend arbeiten. Im anderen Grenzfall, und zu diesem gehört der Stellarator, bleibt der Plasmadruck stets klein gegen die Energiedichte des Magnetfeldes, das dann nur die Aufgabe des Einschließens des Plasmas übernimmt und in seiner Stärke und Geometrie weitgehend unbeeinflußt von dessen Eigenschaften bleibt. Erzeugung und Heizung des Plasmas werden unabhängig davon vorgenommen. Die so mögliche Trennung der Parameter ist im Stadium der Forschung natürlich besonders verlockend. Darüber hinaus bietet ein nach dem Stellaratorprinzip gebauter Fusionsreaktor grundsätzlich die Möglichkeit des stationären Betriebes. Die dafür notwendigen recht starken und ausgedehnten Magnet-

felder können mit zwar teuren supraleitenden Spulen, aber ohne großen Leistungsaufwand stationär aufrecht erhalten werden. Bringt man Plasma in ein Magnetfeld, so wird senkrecht zu dessen Richtung dem Plasmadruck dadurch nahezu das Gleichgewicht gehalten, daß ein als Folge einer langsamen Expansion des Plasmas in diesem induzierter Strom gerade die erforderliche, dem Produkt aus Strom- und Magnetfeldstärke proportionale, rücktreibende Kraft auf das Plasma ausübt. Dieses Gleichgewicht kann sich jedoch nur in solchen toroidalen Magnetfeldern einstellen, in denen die erforderlichen Ströme sich im Plasma selbst schließen können.

Nach diesen Gesichtspunkten sind die sog. Multipolanordnungen die einfachsten unter den toroidal geschlossenen. Sie entstehen durch Ströme — in Fig. 1 sind es zwei —, die in konzentrisch angeordneten Ringleitern gleichsinnig fließen. Das so erzeugte Magnetfeld hat keine Komponente in azimutaler Richtung, d. h. in Richtung der Ströme. Damit sind aber auch die zur Erzielung des Druckgleichgewichtes notwendigen Plasmaströme azimutal gerichtet und können sich wegen der Rotationssymmetrie der Anordnung kreisförmig schließen. Bei allen bisher existierenden stationär betreibbaren Apparaturen dieser Art jedoch ist die dafür notwendige Rotationssymmetrie gestört, da an mehreren Stellen Stromzuführungen und Stutzen durch das Plasma zu den Ringleitern geführt werden müssen. Es gilt heute als sicher, daß die dadurch verursachten Störungen ganz wesentlich das Verhalten des Plasmas bestimmen und zu einer Erhöhung der Plasmaverluste führen. Um diesen Nachteil zu beheben, werden in den USA, in Großbritannien und auch in unserer Gruppe Apparaturen entwickelt, bei denen die ringförmigen Stromleiter ohne jede materielle Verbindung nach außen in einem überlagerten, ebenfalls rotationssymmetrischen Stützmagnetfeld schweben sollen. Da jedoch in den Ringen zur Erzeugung des das Plasma einschließenden Magnetfeldes Ströme von bis zu 400000 A über lange Zeiten ohne Änderung fließen sollen, sind die Wicklungen der Ringe aus supraleitendem Material hergestellt und die Ringe selbst auf etwa 5—7 °K abgekühlt. Die Notwendigkeit solcher Maßnahmen zeigt aber zugleich, daß derartige Anordnungen für Fusionsreaktoren kaum zu verwenden sind, da die Ringleiter durch das heiße sie umgebende Plasma in kürzester Zeit auf unzulässig hohe Temperaturen aufgeheizt würden. Im jetzigen Forschungsstadium jedoch verdienen diese Apparaturen ein außerordentliches Interesse, da sie wegen der im Vergleich zum Stellarator einfachen Geometrie des Magnetfeldes eine Vereinfachung der zugehörigen Theorie erlauben. Auf diese Weise wird eine detailliertere Prüfung der theoretischen Vorstellungen möglich, deren Ergebnis in vielen Fällen auch für andere, kompliziertere Apparaturen relevant sein kann.

Schließt man also für künftige Fusionsreaktoren alle Anordnungen mit materiellen Körpern innerhalb des Plasmas aus, so muß man das einschließende Magnetfeld mit Spulen erzeugen, die ganz außerhalb des Plasmas verlaufen, und darf es zusätzlich nur durch die Felder solcher Ströme modifizieren, die zwar von außen induziert, doch vom Plasma selbst getragen werden. Schematisch erhält man das Grundmagnetfeld dieser Klasse von Apparaturen durch Vertauschen der Feldlinien und der felderzeugenden Ströme der Fig. 1 und gelangt so zu einer Reihe von kreisförmigen auf einem Kreis angeordneten Spulen (Fig. 2). Innerhalb des für die Einschließung von Plasmen vorgesehenen Volumens sind dann alle Feldlinien kreisförmig in sich geschlossen. In einer solchen Anordnung müssen auch die dem Plasmadruck das Gleichgewicht haltenden Ströme im Plasma nicht mehr in azimutaler Richtung, sondern entlang des kurzen Weges um das Plasma herum fließen. Da die Stärke des toroidalen Magnetfeldes mit steigendem Radius R proportional $1/R$ abnimmt und sich die Plasmaströme auf ihrem Weg im Plasma schließen müssen, ist wegen des dort größeren Magnetfeldes die auf der Innenseite des Plasmaschlauches auf das Plasma ausgeübte Kraft größer als die auf die Außenseite wirkende. Als Folge der daraus resultierenden Nettokraft wird der ganze Plasmaschlauch an die äußere Wand des Vakuumgefäßes getrieben und geht dort verloren.

Um diesem Effekt zu begegnen, werden beim Stellarator [1] durch außen angebrachte Zusatzwicklungen (Fig. 3) die Feldlinien um eine mittlere — die magnetische — Achse schwach verdrillt. Jetzt können sich die senkrecht zum Magnetfeld gerichteten Komponenten der Plasmaströme so einstellen, daß sie in dem lokalen Magnetfeld dem Plasmadruck das Gleichgewicht halten, und „Ausgleichsströme", die „kraft-

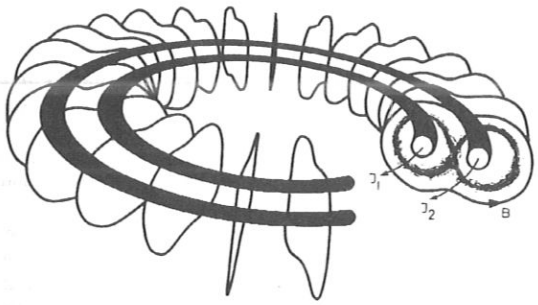

Fig. 1. Schematische Darstellung einer Quadrupolanordnung. Die in den Ringleitern fließenden Ströme I_1 und I_2 erzeugen das Magnetfeld B. Etwa der schraffierte Bereich wird vom Plasma eingenommen

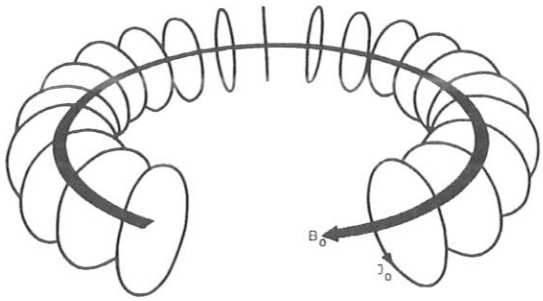

Fig. 2. Schematische Darstellung des Grundmagnetfeldes des Stellarators und des Tokomaks. Die in den kreisförmigen Spulen fließenden Ströme I_0 erzeugen das toroidale Magnetfeld B_0

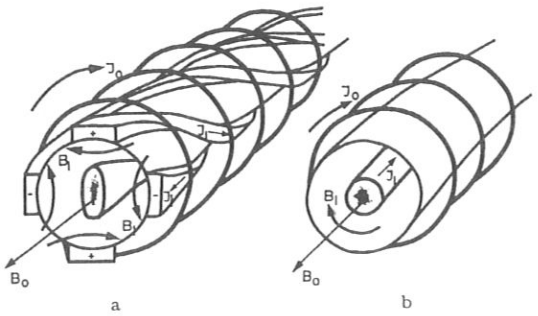

Fig. 3a u. b. Schematische Darstellung a des Stellarator- und b des Tokomakprinzips. Beim Stellarator wird die Verdrillung der Feldlinien des Grundmagnetfeles durch die in den verschraubten Zusatzwindungen fließenden Ströme I_1 über deren Magnetfeld B_1 erzeugt, während beim Tokomak das erforderliche Magnetfeld B_1 durch einen im Plasma induzierten Strom I_1 hervorgerufen wird. Der Plasmabereich ist wieder durch Schraffur angedeutet

frei" parallel zum Magnetfeld abfließen können, sorgen für das Schließen der Stromlinien innerhalb des Plasmas.

Leider verhindert jedoch der endliche Widerstand des Plasmas das ungehinderte Fließen dieser Ausgleichsströme, so daß die auf das Plasma wirkende Nettokraft zwar erheblich vermindert, nicht aber völlig zum Verschwinden gebracht wird. An dieser Stelle greift die Verdrillung der Feldlinien ein zweites Mal ein. Das wird am deutlichsten, wenn man von der Vorstellung ausgeht, der Plasmaschlauch habe sich bereits ein kleines Stück nach außen verlagert.

Sind dann die Feldlinien um die Seele S (Fig. 4a) verdrillt und greift man eine Feldlinie etwa am Punkt A heraus und folgt ihr auf ihrem Weg um die Apparatur, so gelangt man schließlich wegen der Verdrillung des Feldes auf die Innenseite des Plasmaschlauches, z.B. nach A'. Dort ist aber wegen der Verlagerung des Plasmaschlauches nach außen der Plasmadruck kleiner als in A. Durch die hohe Beweglichkeit des Plasmas parallel zu den Feldlinien setzt nun eine Strömung in diese Richtung ein (Fig. 4b), die das Plasma auf dem Weg um die Apparatur herum der Innenseite des Plasmaschlauches wieder an einem anderen Azimut zuführt. Die Folge ist ein raumfestes Strömungsprofil, wie es in Fig. 4c in der Projektion auf eine Querschnittsebene angedeutet ist. Die so aufgefangene radiale Expansion des Plasmas muß jedoch mit einer Erhöhung der Plasmaverluste gegenüber einer geraden Anordnung bezahlt werden.

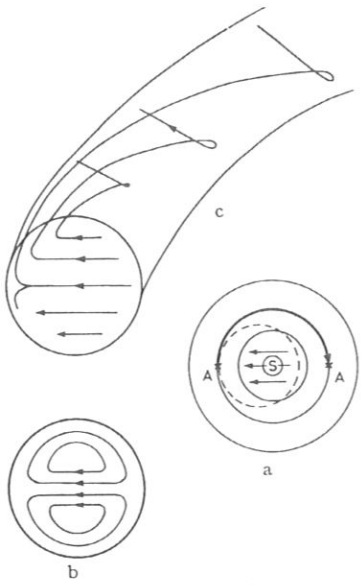

Fig. 4. a Die konzentrischen Kreise werden jeweils von einer der um die magnetische Achse verdrillten Feldlinien gebildet. Die Plasmasäule sei dagegen etwas nach links versetzt. Weiter siehe Text. — b Die radial nach außen gerichtete Strömung fließt vor Erreichen der Rohrwand parallel zum Magnetfeld ab und wird so der Innenseite an einem anderen Azimut wieder zugeführt. — c Projektion dieses Strömungsbildes auf eine Querschnittsebene

Voraussetzung für das Ablaufen der eben beschriebenen Prozesse ist eine weitgehend raumfeste Struktur des Magnetfeldes, die durch das Plasma selbst nicht wesentlich beeinflußt wird. Da beim Stellarator das gesamte einschließende Magnetfeld durch außerhalb des Plasmas angebrachte Spulen erzeugt wird, ist dieser Bedingung Rechnung getragen. Erzeugt man dagegen die Verdrillung der Feldlinien durch einen von außen induzierten starken azimutalen Strom im Plasma selbst, wie das bei den russischen Tokomak-Apparaturen (Fig. 3b) der Fall ist, so verliert man zunächst den Vorteil, solche Apparaturen stationär betreiben zu können. Darüber hinaus kann sich die Magnetfeldstruktur mit einem sich bewegenden Plasma, d. h. mit einem sich bewegenden Stromkanal, mitbewegen, und es müssen zusätzliche Maßnahmen ergriffen werden, um in der Apparatur eine raumfeste Lage für das Plasma zu schaffen. Das geschieht beim Tokomak dadurch, daß man entweder Wirbelstromeffekte in einer gut leitenden, das Plasma umgebenden Wand heranzieht oder durch Überlagerung zusätzlicher, auf der Torusebene senkrecht stehender Magnetfelder die erforderlichen Kräfte auf den Plasmastrom ausübt. Vorteilhaft ist dagegen, daß das Magnetfeld des Tokomak einfacher und von höherer Symmetrie ist als das des Stellarators und daß der induzierte starke azimutale Strom zugleich eine Heizquelle für das Plasma darstellt. Leider reicht diese nicht aus, um das Plasma auf Fusionstemperatur zu heizen, da der Widerstand des Plasmas und damit auch die Leistung der Quelle mit steigender Temperatur stark abnimmt. Trotzdem konnten mit diesen Apparaturen in der UdSSR in letzter Zeit große Erfolge erzielt werden. Plasmen mit einer Temperatur von einigen Millionen °K konnten erzeugt und relativ lange eingeschlossen werden. Wegen der starken Verwandtschaft zwischen Tokomak und Stellarator wird es lohnend sein, die weitere Entwicklung dieser Apparatur aufmerksam zu verfolgen.

Experimente im Stellarator mit durch Kontakt-Ionisierung erzeugten Plasmen

Vor einigen Jahren schien es das Ergebnis aller Experimente zu sein, daß das Plasma aus dem für seinen Einschluß vorgesehenen Volumen viel schneller als theoretisch verständlich verloren ging. Die Verlustgeschwindigkeit war so hoch, daß man dem Effekt den treffenden Namen „pump out" gegeben hatte. Es war auch gelungen, eine einfache empirische For-

mel aufzustellen, die die Abhängigkeit der experimentell gefundenen Einschlußzeit von der Temperatur des Plasmas, der Stärke des Magnetfeldes usw. richtig wiedergab. Der Grund jedoch für das Auftreten der hohen Plasmaverluste war unklar. Insbesondere blieb offen, ob das Auftreten von Instabilitäten, mangelndes Gleichgewicht aufgrund unzulänglicher Einschließungseigenschaften der Apparaturen, die Plasmaeigenschaften selbst oder andere Gründe dafür verantwortlich waren. Deshalb schien es uns seinerzeit erforderlich, eine Serie von Experimenten so auszulegen, daß man bevorzugt nur eine der Gruppen von möglichen Ursachen für die kurzen Einschließungszeiten testet. Hier war natürlich die vordringlichste Frage, ob die benutzten Apparaturen überhaupt geeignet sind, Plasma effektiv einzuschließen. Diese Frage war in der Tat erlaubt, da den detaillierten Parametern der Apparaturen angepaßte Theorien so schwierig sind, daß über Jahre hinaus keine zuverlässige Aussage zu erwarten war. Andererseits mußten die existierenden Theorien unter so vielen vereinfachenden Annahmen hergeleitet werden, daß die Gültigkeit ihrer Aussagen für die reale Apparatur keineswegs sicher war.

Durch Kontakt-Ionisierung gewonnene Metalldampfplasmen boten sich dafür an, bevorzugt die Einschließungseigenschaften des Stellarators zu untersuchen. Wegen der speziellen Art der Erzeugung sind diese Plasmen sehr nahe dem thermischen Gleichgewicht, und ihre Eigenschaften sind sehr genau bekannt. Leider ist ihre Temperatur auf einen engen Bereich um 2300 °K begrenzt, doch waren in vielen Apparaturen mit Wasserstoffplasmen auch in diesem Temperaturbereich erheblich höhere Teilchenverluste gefunden worden als sie die Theorie des Plasmaeinschlusses voraussagt. Wegen der hohen Masse der Metall-Ionen werden sogar einige Eigenschaften von Wasserstoffplasmen höherer Temperatur durch sie imitiert. Ferner hatte man mit kontaktionisierten Plasmen in einem homogenen Magnetfeld senkrecht zu diesem bereits Verlustraten beobachtet, die erheblich kleiner waren als die pump-out-Verluste [2].

Nach einigen sehr positiv verlaufenden Versuchen in kleineren Apparaturen [3] führten diese Experimente zum Bau des Stellarators *Wendelstein W IIa*, und allein die mit dieser Apparatur gewonnenen Ergebnisse sollen hier besprochen werden [4]. Dieser Stellarator war unter Beibehaltung der höchstmöglichen Symmetrie gebaut worden, um einerseits die zugehörige Theorie nicht mit unnötigen Schwierigkeiten zu belasten und andererseits durch Abweichungen von der Symmetrie eventuell auftretende Effekte von vornherein auszuschließen. Außerdem wurde er für stationären Betrieb ausgelegt, um unabhängig von dem viel schwerer interpretierbaren Aufbau des Plasmas dessen stationären Zustand studieren zu können.

Nach Fertigstellung der Apparatur wurde zunächst der Verlauf der magnetischen Feldlinien mittels eines eingeschossenen Elektronenstrahles gemessen und mit dem berechneten verglichen. In Fig. 5 sind die Durchstoßpunkte des Elektronenstrahles durch eine auf der magnetischen Achse senkrecht stehende Querschnittsebene aufgetragen, und man erkennt die Verdrillung der Feldlinien deutlich daran, daß der Durchstoßpunkt mit jedem Umlauf um einen bestimmten

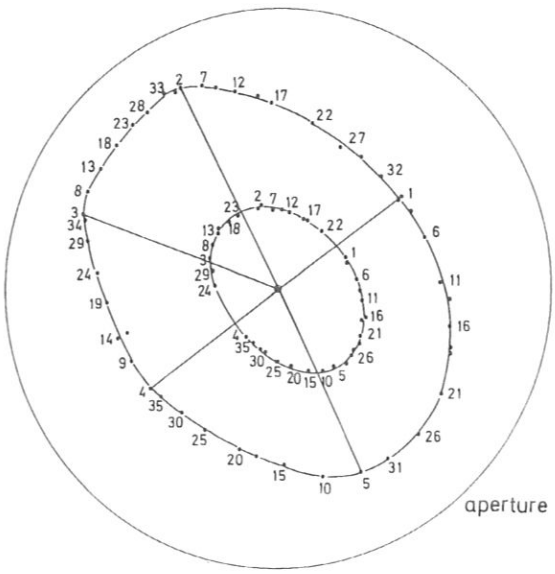

Fig. 5. Durchstoßpunkte eines Elektronenstrahles durch eine auf der magnetischen Achse senkrecht stehende Querschnittsebene für zwei verschiedene mittlere Radien. Die Zahl der Umläufe um die Apparatur ist neben jedem Durchstoßpunkt angegeben. Durch Vergleich der aufeinander folgenden Durchstoßpunkte erkennt man die Verdrillung der Feldlinien um die magnetische Achse

Winkel versetzt ist. Der Mittelwert dieser Versetzungswinkel ist der Winkel der Rotationstransformation, iota.

Die Plasmaquelle hatte nach einigen Zwischenstufen folgende Gestalt: Möglichst genau auf der magnetischen Achse ist eine Wolframkugel von 3 mm Durchmesser an zwei Wolframfäden von je 10 µm Dicke aufgehängt. Diese Kugel wird durch einen CO_2-Laser auf etwa 2300 °K stationär aufgeheizt und von einem Ofen her mit einem kollimierten Strahl von Barium-Atomen beschossen. Diese Atome werden auf der Oberfläche der Kugel mit einer berechenbaren Wahrscheinlichkeit ionisiert und stellen zusammen mit den durch Glühemission erzeugten Elektronen eine lokale und in ihrer Stärke und räumlichen Ausdehnung genau bekannte Plasmaquelle dar. Da das Plasma auf der Oberfläche eines materiellen Körpers erzeugt wird, befindet es sich auch mit diesem recht genau in thermischem Gleichgewicht. Im Stellarator entspricht diese Quelle dann wegen der hohen Beweglichkeit des Plasmas parallel zum Magnetfeld einem entlang der magnetischen Achse verlaufenden ringförmigen Quellschlauch vom Querschnitt der Kugel. Er erfüllt damit nur $1\,‰$ des dem Plasma zur Verfügung stehenden Querschnitts und erlaubt damit die Untersuchung der Diffusion des Plasmas durch das einschließende Magnetfeld in einem quellenfreien Gebiet. Information über die Einschließungseigenschaften des Stellarators erhält man aus der mittleren Lebensdauer eines Ions in der Apparatur. Diese gewinnt man durch Division der stationär in der Apparatur vorhandenen Ionen durch die Zahl der pro Sekunde verlorenen. Unter stationären Bedingungen ist die Verlustrate der Ionen gleich ihrer Erzeugungsrate, und diese Größe läßt sich leicht und genau dadurch messen,

daß man alle auf der Oberfläche der Wolframkugel erzeugten Ionen mit zwei großen Löffelsonden absaugt.

Etwas problematischer ist die Bestimmung der Gesamtzahl der stationär in der Apparatur vorhandenen Ionen, d. h. des Volumenintegrals über die Ionendichte. Diese Größe bestimmt man zwar am einfachsten mit Sonden, doch bei den in dieser Apparatur gefundenen langen Einschließungszeiten führt die Anwesenheit der Sonden im Plasma zu nicht mehr vernachlässigbaren Störungen. Selbst wenn der Durchmesser der Sonden nur 50—100 μm beträgt, geht noch bis zur Hälfte des Plasmas auf ihrer Oberfläche verloren, statt nach der Diffusion durch das Magnetfeld auf der Wand des Vakuumrohres. Noch dünnere Sonden sind technisch kaum noch herstellbar und ihre Signale vor allem nicht mehr zuverlässig interpretierbar.

Hier zeigten sich die Vorzüge von Barium als Ausgangsmaterial für das verwendete Plasma. Das Barium-Ion verfügt über so günstig im sichtbaren Bereich liegende Resonanzspektrallinien, daß die Bestimmung der Ionendichte über die Resonanzfluoreszenz möglich ist [5]. Dazu wird das Plasma über die Abbildung einer intensiven Lichtquelle optisch angeregt und die remittierte Strahlung senkrecht dazu gemessen. Das empfangene Signal ist dann proportional der Ionendichte an dem Ort, an dem sich Beleuchtungs- und Beobachtungsstrahlengang kreuzen. Dieses Verfahren erlaubt also eine Messung der lokalen Ionendichte ohne das Plasma zu stören.

Zunächst am interessantesten ist die Abhängigkeit der Einschlußzeit von der Stärke der Plasmaquelle, da sie ein Maß für das allgemeine Einschließungsvermögen der Apparatur ist. In Fig. 6 ist als Beispiel einer solchen Messung die erreichte Ionendichte auf der magnetischen Achse als Funktion der Quellstärke für einen festen Winkel der Rotationstransformation aufgetragen. Dabei ist die Ermittlung der für eine bestimmte Quellstärke erreichbaren Ionendichte gleichwertig mit der Bestimmung der Einschlußzeit; steigt

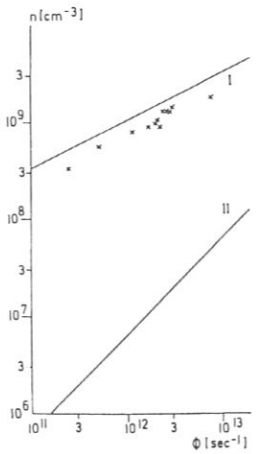

Fig. 6. Teilchendichte auf der Seele der Plasmasäule in Abhängigkeit von der Stärke der Plasmaquelle, d. h. von der Zahl der pro Sekunde erzeugten Ionen, für $B_0 = 5{,}0$ kGauss und $\iota/2\pi = 0{,}242$. Vergleichsgerade *I* gibt den aufgrund der klassischen Theorie erwarteten Verlauf wieder, während ein Verlauf nach Kurve II bei „pump-out"-Verlusten erwartet würde

für eine festgehaltene Quellstärke die Ionendichte, so steigt gleichermaßen die Einschlußzeit. Man sieht, daß die experimentell gefundenen Werte der Ionendichte mit den von der Theorie geforderten innerhalb eines Faktors 2 übereinstimmen und insbesondere auch dieselbe Abhängigkeit von der Quellstärke zeigen. Schon aus diesen Messungen läßt sich schließen, daß ein Stellarator grundsätzlich ein Plasma so lange einschließen kann wie es die klassische Diffusionstheorie zuläßt. Würden „pump-out"-Verluste in der Apparatur vorherrschen, so wären die erreichbaren Ionendichten um 2—3 Größenordnungen kleiner als die tatsächlich erreichten (Fig. 6). Angesichts dieses großen Abstandes zwischen den beiden Vergleichsgeraden ist auch die Abweichung von den theoretischen Werten ohne Belang, zumal sicher auch die theoretischen Vorhersagen wegen der verwendeten Näherungen Unsicherheiten um einen Faktor 2 zulassen.

Eine bereits etwas detailliertere Fragestellung ist die nach der Abhängigkeit der Einschlußzeit vom Winkel der Rotationstransformation, iota. Diese Abhängigkeit gibt Aufschluß darüber, ob alle im vorigen Kapitel beschriebenen Ausgleichvorgänge auch wie erwartet ablaufen. Ein Beispiel einer solchen Messung ist in Fig. 7 für festgehaltenes Hauptmagnetfeld und festgehaltene Quellstärke wiedergegeben. Zunächst würde man erwarten, daß die Teilchendichte und damit auch die Einschlußzeit mit zunehmendem Winkel iota ansteigt, wie es durch die zum Vergleich eingetragene, monoton ansteigende Kurve angedeutet ist. Die experimentellen Werte zeigen dagegen charakteristische Maxima und Minima, wobei die Maxima durchaus in die Nähe der theoretischen Kurven reichen. Eine genauere Analyse zeigt, daß Minima in der Dichte offenbar immer dann auftreten, wenn der Winkel iota gerade so groß ist, daß eine Feldlinie schon nach einigen Umläufen um die Apparatur wieder in sich zurückläuft, statt eine ganze Fläche auszufüllen. In Fig. 5 würde das bedeuten, daß nach jeweils n Umläufen (wobei n eben eine nicht zu große ganze Zahl ist) der $(n+1)$. Durchstoßpunkt wieder auf den ersten fällt, der $(n+2)$. auf den zweiten usw. Für davon abweichende Winkel iota füllen dagegen die Durchstoßpunkte eine geschlossene Kurve ganz aus. Es ist nun ein experimentelles Ergebnis, daß gutes Einschließungsvermögen der Apparatur nur

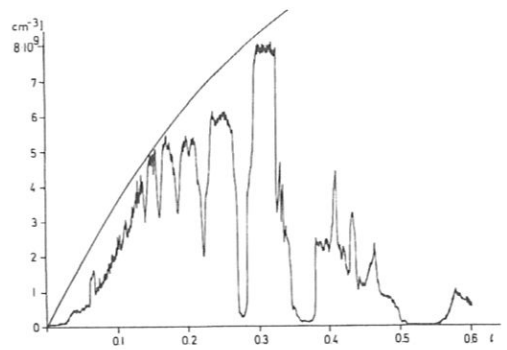

Fig. 7. Teilchendichte auf der Seele der Plasmasäule in Abhängigkeit vom Winkel der Rotationstransformation, iota, für $B_0 = 4{,}5$ kGauss und Quellstärke $\Phi_0 = 1{,}2 \cdot 10^{13}$ Teilchen/sec. Die Vergleichskurve gibt den nach der einfachen klassischen Theorie erwarteten Verlauf an

dann möglich ist, wenn die Feldlinien nicht nach wenigen Umläufen in sich zurücklaufen. Der theoretische Grund für dieses Verhalten ist noch nicht genau bekannt, doch gibt es mehrere Ansätze zur Erklärung dieses Effektes.

An sich wäre auch das Auftreten dieser Minima nicht beunruhigend, da es für einen Fusionsreaktor nur wichtig ist, daß es wenigstens einen Wert von iota gibt, für den langer Plasmaeinschluß erreicht wird. Man will jedoch andererseits eine ganze Reihe von möglichen Instabilitäten dadurch ausschließen oder zumindest in ihrem Einfluß reduzieren, daß man eine Verscherung des Magnetfeldes einführt. Dazu wählt man den Winkel iota nicht über den ganzen Plasmaquerschnitt weitgehend konstant wie bei unserer Apparatur, sondern läßt ihn von der magnetischen Achse aus nach außen gehend ansteigen. Dabei werden jedoch Bereiche durchlaufen, in denen die Feldlinien sich schließen oder in denen sie eine ganze Fläche ausfüllen. Es wird dann wichtig, welcher der beiden Effekte überwiegt, schlechter Einschluß für geschlossene Feldlinien oder guter in den Bereichen dazwischen.

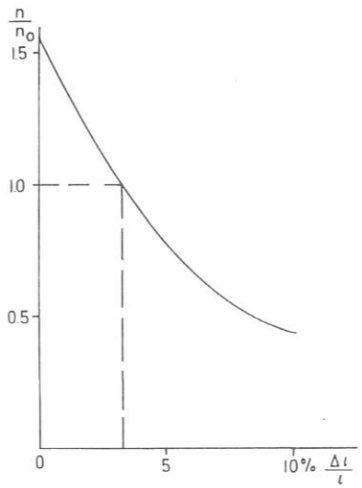

Fig. 8. Auf den normalen Betriebszustand normierte Teilchendichte auf der Seele der Plasmasäule in Abhängigkeit von der relativen Änderung der Rotationstransformation über dem Plasmaquerschnitt

Aus diesem Grunde haben wir einige Experimente durchgeführt und dabei durch ein zusätzliches, überlagertes Magnetfeld eine kleine Verscherung der Feldlinien eingeführt. In dem in Fig. 8 aufgeführten Beispiel dieser Meßreihe beobachtet man, daß mit steigender Verscherung das Einschlußvermögen der Apparatur abnimmt. Es ist also fraglich, ob man eine Verscherung des Magnetfeldes zur Stabilisierung des Plasmas wird einführen dürfen. Es muß jedoch betont werden, daß bisher noch nicht auszuschließen ist, daß diese Ergebnisse auch auf sekundäre, behebbare Ursachen zurückgehen können. Untersuchungen dazu sind im Gange.

Die in unserer Apparatur gefundenen langen und mit den theoretischen Erwartungen übereinstimmenden Einschlußzeiten des Plasmas eröffnen auch die Möglichkeit, die Einschlußzeit des Plasmas durch gezielte störende Einflüsse wesentlich herabzusetzen. Aus den Ergebnissen solcher Versuche können dann Toleranzen für die Größen der einzelnen Störeffekte hergeleitet werden. Die wichtigste Frage in diesem Zusammenhang ist die tolerable Größe von Störmagnetfeldern. Solche Felder sind stets am Ort der Apparatur vorhanden. Einerseits können die Wicklungen zur Erzeugung der Nutzmagnetfelder nur mit endlicher Genauigkeit hergestellt werden, andererseits können stromführende Leitungen und größere Eisenmassen in der Nähe der Apparatur die Felder modifizieren. So benutzt man typischerweise große Eisentransformatoren, um das längs des Hauptmagnetfeldes gerichtete elektrische Feld zur Heizung des Plasmas mittels eines starken elektrischen Stromes zu induzieren.

Für einen quantitativen Versuch haben wir dem Stellarator sowohl weitgehend homogene als auch mehr lokale Störmagnetfelder überlagert. Dabei ergab sich zunächst wie erwartet ein starker Einfluß auf das Einschließungsvermögen der Apparatur, doch wurden für einige Werte des Winkels der Rotationstransformation sogar Verbesserungen der Einschlußzeit gefunden. In allen diesen Fällen hatten sich in der Einschlußzeit zuvor noch Abweichungen von der theoretischen Kurve ergeben, obwohl die Feldlinien sich nicht schon nach wenigen Umläufen um die Apparatur schlossen. Dieses Ergebnis kann nur so verstanden werden, daß auch unser Stellarator mit kleinen Fehlern hergestellt und Störfeldern ausgesetzt ist, die durch ein bestimmtes überlagertes Feld kompensiert werden können. In Fig. 9 ist für festes iota

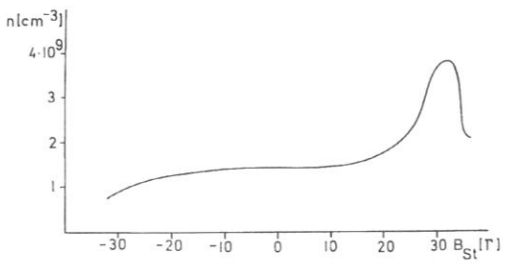

Fig. 9. Teilchendichte auf der Seele der Plasmasäule in Abhängigkeit von der Stärke eines nahezu homogenen, in der Torusebene verlaufenden Störfeldes für $B_0 = 4{,}5$ kGauss und $\iota/2\pi = 0{,}450$. Quellstärke $\Phi_0 = 7 \cdot 10^{12}$ Teilchen/sec

und feste Quellstärke die Stärke des überlagerten Störmagnetfeldes variiert und die erreichte Ionendichte aufgetragen. Das Hauptfeld beträgt 5 kGauss. Man sieht, daß die Verbesserung der Einschlußzeit nur für einen engen Bereich mit einer Halbwertsbreite von etwa 5 Gauss, also $1^0/_{00}$ des Hauptfeldes, auftritt. Eine solche Genauigkeit des Feldverlaufes ist insbesondere bei Verwendung großer Eisentransformatoren nur schwer einzuhalten, doch zeigen die Experimente erfreulicherweise auch, daß eine Summe mehrerer kleiner Feldfehler durch ein einziges überlagertes Feld geeigneter Größe und Richtung kompensiert werden kann, ohne daß man die Fehler im einzelnen kompensieren muß.

So positiv alle diese Ergebnisse auch sind, so muß man sich doch stets vor Augen halten, daß sie für ein Plasma mit recht niedriger Temperatur gewonnen

sind. In einem solchen Plasma legen die Teilchen zwischen zwei Zusammenstößen mit anderen Teilchen im Mittel nur Wege zurück, die den Umfang der Apparatur nicht wesentlich überschreiten. Mit steigender Temperatur jedoch nimmt diese freie Weglänge stark zu und es gibt sowohl theoretische Argumente als auch experimentelle Hinweise dafür, daß dann Teilchen, die verglichen mit ihrer Senkrechtgeschwindigkeit nur eine kleine Geschwindigkeitskomponente parallel zum Magnetfeld haben, schneller aus der Apparatur verloren gehen. Da nun durch Stöße der Teilchen untereinander immer wieder solche mit den genannten Vorzugsgeschwindigkeiten erzeugt werden, bedeutet dieser Effekt eine Erhöhung der Verlustrate und damit eine Reduzierung der erreichbaren Einschlußzeit. In dem von uns untersuchten Parameterbereich sollte dieser Effekt nicht auftreten.

Es ist daher jetzt die Aufgabe, ausgehend von unseren Resultaten das Plasma zu heizen und damit schrittweise die freie Weglänge für Stöße der Teilchen untereinander zu erhöhen. Unsere bisherige Plasmaquelle läßt jedoch ein solches Verfahren nicht zu, da die thermische Kopplung zwischen Plasma und der das Plasma erzeugenden Wolframkugel zu intensiv ist. Wir haben deshalb diese Plasmaquelle inzwischen durch eine andere ersetzt und beleuchten nun den aus dem Ofen kommenden kollimierten Strahl von Barium-Atomen in der Umgebung der magnetischen Achse mit einer äußerst intensiven Lichtquelle. Auf diese Weise gelingt es, im Kreuzungsbereich des Atomstrahles und des Lichtbündels durch Photo-Ionisierung eine der früher verwendeten sehr ähnliche Plasmaquelle zu schaffen, die jedoch keinen materiellen Körper im Plasma mehr erfordert. Erste Experimente mit dieser Plasmaquelle haben zu Ergebnissen geführt, die mit den bisherigen in Einklang sind. Damit ist eine wichtige Frage bereits positiv beantwortet, daß nämlich im Gegensatz zu einigen auf theoretischen Argumenten beruhende Vermutungen die Anwesenheit der Kugel im Plasma nicht erforderlich ist, um die gefundene lange Einschlußzeit zu ermöglichen.

Diese neue Plasmaquelle schließt nun die bisherige Serie von Versuchen ab und leitet über zu einem neuen Abschnitt unserer Experimente, dem Einschließen heißer Plasmen in die auf ihre Einschließungseigenschaften getesteten Stellaratoren. Der damit gleichzeitig verbundene Übergang zu größeren freien Weglängen wird Aufschluß darüber geben, ob und in welchem Umfange neue Verlustmechanismen in Erscheinung treten. Gleichzeitig haben wir mit dem Bau eines größeren Stellarators begonnen, der vor allem die Erzeugung erheblich stärkerer Magnetfelder zuläßt als bisher. Da solche Magnetfelder sich mit konventionellen Spulen nicht mehr mit vertretbaren Kosten aufrecht erhalten lassen, wird das Hauptmagnetfeld dieser Apparatur mittels supraleitender Spulen erzeugt. Damit wird es gleichzeitig auch möglich, Erfahrungen zu sammeln für den Aufbau und den Betrieb großvolumiger toroidaler Magnetfeldanlagen, wie sie für spätere Fusionsreaktoren Voraussetzung sind.

Diese Arbeit wurde im Rahmen des Vertrages zwischen dem Institut für Plasmaphysik GmbH, München-Garching, und Euratom über die Zusammenarbeit auf dem Gebiete der Plasmaphysik durchgeführt.

[1] Spitzer jr., L.: Phys. Fluids **1**, 253 (1958). — [2] D'Angelo, N., Rynn, N.: ibid. **4**, 1303 (1961). — [3] Eckhartt, D., Gierke, G. v., Grieger, G.: Plasma Physics and Controlled Nucl. Fusion Res. Vol. II, 719 (1966). — [4] Berkl, E., et al.: Plasma Physics and Controlled Nucl. Fusion Res. Vol. I, 513 (1969). — [5] Rynn, N., Hinnov, E., Johnson, L. C.: Rev. Sci. Instr. **38**, 1378 (1967).

Eingegangen am 25. Februar 1970

Universitätsdruckerei H. Stürtz AG Würzburg

Printed in Germany

PAPER CN-28/H-3

FOURTH CONFERENCE ON PLASMA PHYSICS AND CONTROLLED NUCLEAR FUSION RESEARCH

Madison, Wisconsin, U.S.A.

17 - 23 June 1971

INVESTIGATION OF THE MINIMA IN THE PARTICLE CONFINEMENT TIME IN THE WENDELSTEIN II a-STELLARATOR

G. Grieger, W. Ohlendorf, H.D. Pacher, H. Wobig, G.H. Wolf
Max-Planck-Institut für Plasmaphysik, 8046 Garching
Fed. Rep. of Germany

ABSTRACT

For not too large values of iota, previous experiments in contact ionized barium plasmas have demonstrated confinement in accordance with classical theory, except in the neighbourhood of the low order rational values of iota. The minima in confinement there observed may be understood as the result of stationary or nonstationary convection. The present experiments are concerned with the investigation of these minima. In particular, measurements of the dependencies of the peak density on the input flux, magnetic field strength, and neutral pressure have been carried out at various iota to test theoretically predicted relations. Low frequency oscillation have been observed and the influence of shear on the position of the minima has been investigated. The conclusion is drawn that the most probable explanation for the observed minima is an unstable transition between the classical diffusion and a stationary or nonstationary convection.

This work was performed as part of the agreement between the Max-Planck-Institut für Plasmaphysik, Munich-Garching, and Euratom.

I. INTRODUCTION

As reported earlier (Ref. 1) the confinement in the $\ell = 2$ Wendelstein II a stellarator under certain conditions showed a behaviour predictable from classical theory. The dependence of the maximum ion density on various parameters, such as shear, disturbing magnetic fields etc., has been investigated. In the neighbourhood of certain values of iota ($\iota = 1/2$, $1/3$, $1/4$ ...[+]), minima in the traces of ion density versus iota were observed, for which until now no explanation could be found. It is the purpose of this work to obtain more information on these minima and to discuss various effects which might be responsible for their occurrence.

Theoretically, higher losses at rational values of iota can be the result of stationary or nonstationary convective motion. This motion could be initiated by one of the following effects.

+) It should be noted that the iota scale, which one deduces from the assumption that the minima occur at rational values of iota, disagrees by 10 % from the numerically calculated one. This discrepancy is thought to be due to errors in the mechanical positioning of the helical field windings and is presently being investigated by electron beam measurements.

1) Destruction of magnetic surfaces
2) Noncoincidence of the rational magnetic surfaces and $\oint \frac{il}{B}$ surfaces
3) Inappropriate boundary conditions
4) Spatially localized plasma source
5) Instability

In order to study the behaviour of the minima and their dependence on various parameters barium plasma was used as in the earlier measurements. This plasma was produced by contact ionization on a tungsten ball of 3 mm diameter which was heated by laser irradiation to a temperature of about 2500 ^{o}K and suspended on 3 tungsten wires of 10 µm diameter each. The base pressure was 10^{-6} Torr. In some cases argon was added in order to increase the neutral background.

The ion density was measured spectroscopically using resonance fluorescence (Ref. 2). The ball potential was monitored with a high impedance voltmeter and recorded. In addition the flux to the particle detector was measured.

II. EXPERIMENTAL RESULTS

In order to study the properties of the minima the following parameters were varied:

a) the toroidal magnetic field B between 3 kG and 6 kG
b) the ion input flux ϕ between 5×10^{12} and 2×10^{13} sec^{-1}
c) the neutral pressure between 1×10^{-6} Torr and 6×10^{-5} Torr by the addition of argon

The main object of this experiment was the plasma behaviour in the minima. The experimental conditions were not optimized specifically to achieve a close approach of the maximum density towards the classical value; at low neutral pressure agreement within a factor of 3 was typical.

1. Conditions for the Existence of the Minima

Most observations were made at minima No. 5 ($\iota \approx 1/5$) and No. 6 ($\iota \approx 1/6$); minima No. 4 ($\iota \approx 1/4$) and No. 7 ($\iota \approx 1/7$) have also been investigated.

In general, minima No. 5 and 6 behave in the following manner:

a) There exists a critical magnetic field above which the minimum occurs (see for example Fig. 1). Fig. 1 shows that minimum No. 5 occurs above a value of the magnetic field lying between 4 and 5 kG, whereas for minimum No. 6 this critical field lies between 5 and 6 kG. This critical magnetic field decreases with increasing neutral pressure, as shown in Fig. 2.

b) The width of the minima does not depend on neutral pressure but increases slightly with increasing magnetic field (see Fig. 1).

c) At low values of argon pressure, peaks in the middle of the minima were observed under some conditions. These peaks vanish at higher magnetic field and at higher neutral pressures.

d) As iota is changed the transition between maxima and minima extends over a very small range of ι ($\delta\iota \approx 0.005$).
Simultaneously oscillations of the floating potential of the ball and of the flux to the particle detector were observed, with frequencies between 1 and 25 Hz.

2. Dependence on Magnetic Field

From the variation of the n vs iota curve with magnetic field the following results were obtained:

a) At low pressure ($p_{Ar} < 5 \times 10^{-6}$ Torr) the density in the maxima appears to scale as $B^{3/2}$ (Fig. 3), while at higher neutral pressure (p_{Ar} up to 10^{-5} Torr) it scales as B. The $B^{3/2}$ scaling at low neutral pressure is probably a mixture of the classical B scaling and an anomalous effect which scales as B^2.

b) The density in the minima stays constant or decreases with increasing magnetic field (Fig. 4). The decrease was found at higher neutral pressure (10^{-5} Torr), where the minima No. 5 and 6 were more pronounced than at low pressure.

3. Dependence on Ion Input Flux

For various magnetic fields, $n, \frac{n}{\sqrt{\phi}}, \frac{n}{\phi}$ have been plotted versus ϕ (Fig. 5). It was found that at low pressure the density scales as ϕ, but at higher neutral pressure a proportionality to $\phi^{1/2}$ resulted. With respect to the dependence on ion input flux there was no significant difference between minima and maxima.

4. Influence of Argon Pressure

The effect of friction between plasma and neutral particles was studied by adding argon at pressures up to 5×10^{-5} Torr. With an increase of the pressure up to 10^{-5} Torr the plasma density in the maxima increased by approximately 100 %, while between 1×10^{-5} and 2×10^{-5} Torr the density decreased below its value at low pressure (Fig. 6).

In the high pressure regime the ion-neutral collisions begin to dominate over the electron-ion collision.

As for the minima, a distinction must be drawn between Nos. 5 and 6 and No. 4. In the minima No. 5 and 6 the density was independent of neutral pressure in most cases. At high ion input flux (2×10^{13} sec^{-1}) and at high magnetic field an increase of the neutral pressure resulted in a decrease of the density (Fig. 7).

In the minimum No. 4 the density first increased with increasing neutral pressure (up to 8×10^{-6} Torr) but decreased for even higher pressure. Simultaneously the minimum becomes wider. This broadening of the minimum occurs as a discontinous process. As the neutral pressure increases, more and more minima appear in the neighbourhood of the original minimum, and at even higher neutral pressure these maxima between the minima vanish.

At high neutral pressure (2.1×10^{-5} Torr) minimum No. 4 shows the same unexpected scaling with B as the minima Nos. 5 and 6, i.e. a decrease of the density with increasing magnetic field.

5. Oscillations

In the present experiment, high level, low frequency oscillations are observed under some conditions. As iota is changed slowly, the onset of oscillations is followed by a transition of the density from the adjacent maximum to the density of the minimum. The oscillations show an increase in frequency (from 5-10 Hz to 11-20 Hz) and a decrease in amplitude as the center of the minimum is approached.

The main diagnostic used to investigate these oscillations in a preliminary manner has been the floating potential of the hot sphere. A typical example of the oscillations is shown in figure 8 in which a frequency spectrum from 1-20 Hz is also demonstrated.

The oscillations in this example appear to be a single mode, but measurements at other values of iota show a more broader spectrum. The oscillations of the flux to the particle detector and of the floating potential and density signal of a probe are also observed.

Unfortunately, lack of detailed experiments does not permit conclusions about the amplitude of the density fluctuations and their phase relation to the potential fluctuations.

A discontinuous transition between a higher density and a lower density state as iota is varied can be subject to a hysteresis effect, that is, the transition occurs at a lower value of ι when ι is decreasing than when ι is increasing (see Fig. 9). The upward as well as the downward transitions are preceded by a hard onset of oscillations.

Little can be said at this point about the type of oscillations observed. However, the available body of data indicates that the amplitude of the oscillations increases with magnetic field. In the minima the oscillations show a decrease of frequency with increasing magnetic field, although this trend is not very definite. For all magnetic fields, an increase in frequency of oscillations at the edges of the minima with increasing argon pressure is observed.

In summary, the low frequency oscillations that are observed are strongly correlated with the transition between the maxima and the minima in density. The presence of oscillations of comparable amplitude in adjacent maxima and minima makes it possible that the oscillations are not directly responsible for the observed particle loss but rather accompany the transition from one state to another.

6. Influence of Shear on the Position of the Minima

To decide whether the occurrence of the minima results from the coincidence of a particular value of iota with a certain plasma radius, the magnetic shear was changed by superimposing a quadrupole magnetic field. For several plasma radii the variation of the relative change of the local iota with the shear producing currents was calculated numerically (Fig. 10), and was markedly different on the axis ($r = o$) and in the outer plasma region. In the latter, the sign of the shift of iota is independent of the direction of the "shear current", while on and near the axis a reversal of the "shear current" changes the sign of the shift of iota. Therefore, if the minima can only occur, when a particular value of iota lies on some radius in the inner region, the experimentally observed shift of a minimum should change sign on reversal of the shear current, while for the outer region the sign should remain constant. The experimental data are shown in figure 10 by the dotted line. They clearly indicate that one may exclude the region with $r < 3$ cm as a possible origin of the observed minima. However, from this result one cannot decide which effect near the plasma boundary, determined by the limiter, is responsible for the poor confinement in the minima.

An additional experimental result was that the width of the minima did not vary with the shear.

III. DISCUSSION

The possible causes for the occurrence of the minima, as stated in the introduction, will now be discussed on the basis of the experimental results.

1. Destruction of Magnetic Surfaces

Numerical calculations, starting from an ideal current distribution, showed the existence of magnetic surfaces, but also islands of relatively small radial extent were found at rational values of iota ($\iota = 1/2, 1/3, \ldots$). Besides, it could not yet be ruled out that the magnetic surfaces in the device are destroyed by unknown magnetic field perturbations. If, however, the plasma were to stream freely along the field lines to the boundary, an addition

of neutral gas would inhibit the flow and therefore increase the plasma density. On the contrary, a decrease of plasma density with neutral pressure was observed in some cases (see section II.4). By the same reason enhanced radial transport by parallel flow along the islands is also considered to be unlikely.

2. $\oint \frac{dl}{B} \neq$ const. on Rational Surfaces

A theoretical model (Ref. 3) which was developed for this case predicts a stationary convection at rational values of iota. But the asymmetries in the magnetic field needed to explain the experimental results are much larger than those possibly present in the machine. Furthermore, again, the theory predicts increasing density with increasing neutral pressure. In some cases, this dependence is apparently not observed (see II.4).

3. Boundary conditions

If the outer boundary does not coincide with a magnetic surface, a static equilibrium with n = const. on this surface is no longer possible. The more closely the iota on this surface approaches a rational value of low order, the larger is the stationary convection which might occur. This convection, again, should be inhibited by increasing the neutral pressure. Although some of the experiments show a decrease of the density with increasing neutral pressure, the boundary conditions cannot be excluded as a possible cause for the minima. However, a description by continuous variation of a unique equilibrium state seems to be implausible.

4. Spatially Localized Plasma Source

This cause can be ruled out by the result of the shear experiment (II.6), since there the region near the axis was excluded.

5. Non-stationary Processes

The experimental results clearly indicate that the transition between a maximum and a minimum is correlated with an instability (II.5). This conclusion is supported by the existence of a critical magnetic field and a critical neutral pressure (II.1). The results reported above show a great similarity to the nonstationary convection of a fluid heated from below (Ref. 4). Here also saw-tooth-like oscillations and hysteresis effects are predicted. As far as the critical and anomalous scaling with B is concerned, an analogous situation exists in the case of the instability of a positive column (Ref. 5,6).

IV. CONCLUSIONS

From these results it can be concluded that the most probable explanation for the minima in particle confinement time is an unstable transition between the classical equilibrium and a stationary or nonstationary convection. Although the experimental observations give no clear indications, the shear experiment gives some hint that the convective state might be determined by the conditions at the plasma boundary.

ACKNOWLEDGEMENTS

The authors would like to thank Dr. J. Hugill for his significant contributions in conducting the experiments as well as to the discussions. The help of J. Eisert in the computer evaluation of the experiments has been invaluable. The voluminous calculations of S. Rehker, as well as the calculations of B.Streibl, on the magnetic field structure have been necessary for the interpretation. Furthermore, the capable and untiring help of D. Köhler and the technical staff and of Miss H. Rupprecht is greatly appreciated.

REFERENCES

1) E.g. E. Berkl et al. in "Plasma Physics and Controlled Nuclear Fusion Research" , IAEA, Vienna, 1969, p. 513

2) F.W. Hofmann, Phys. of Fluids, Vol. 7, No. 4, April 1964, p. 532 ff

3) H. Wobig, to be published

4) F.H. Busse, J. Fluid Mech. (1967) Vol. 28, pt. 2, p 223 ff

5) Golant et al., Zhur. Tekh. Fiz. 33 (1963), 1043

6) Kadomtsev, Plasma Turbulence, Academic Press, London (1965)

FIGURE CAPTIONS

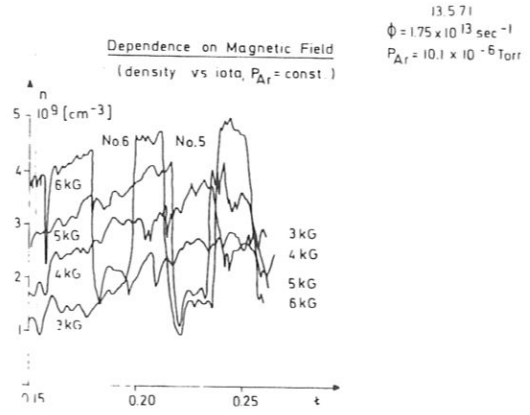

Fig. 1: Density versus iota at different magnetic fields

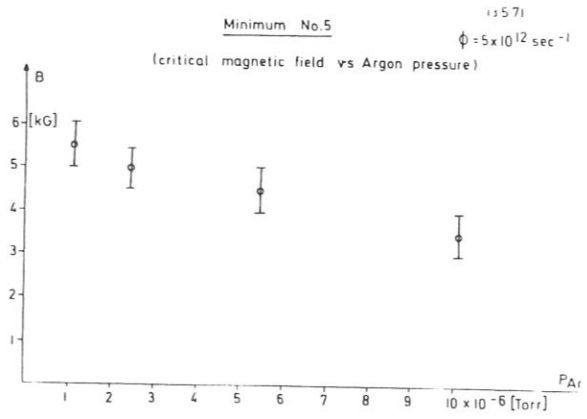

Fig. 2: Critical magnetic field for minimum No. 5 versus argon pressure

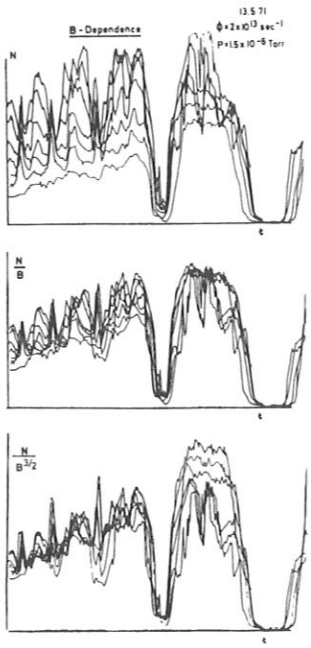

Fig. 3: N, $\frac{N}{B}$, $\frac{N}{B^{3/2}}$ as a function of iota for various magnetic fields

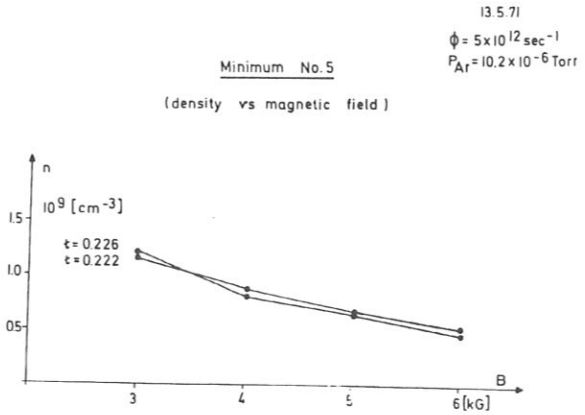

Fig. 4: Density versus magnetic field in the minimum No. 5

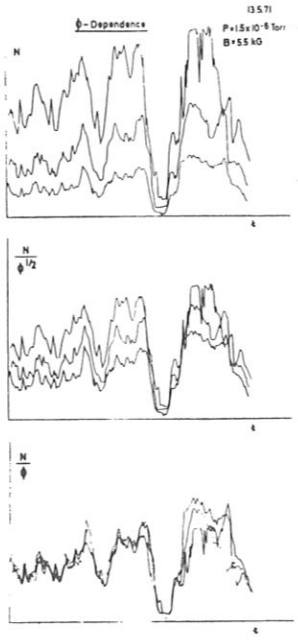

Fig. 5: N, $\frac{N}{\sqrt{\phi}}$, $\frac{N}{\phi}$ as a function of iota for different fluxes

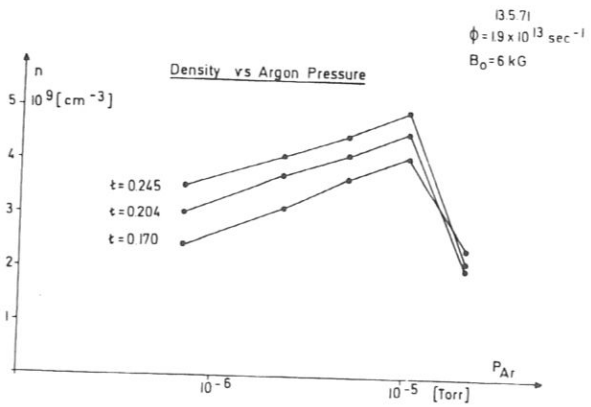

Fig. 6: Density versus argon pressure at various maxima

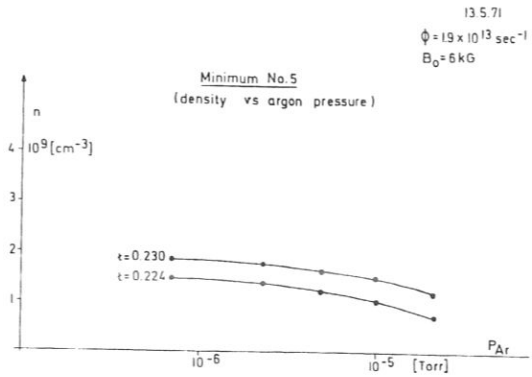

Fig. 7: Density versus argon pressure in minimum No. 5

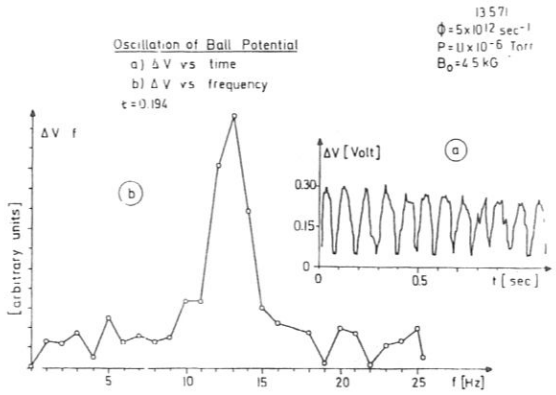

Fig. 8: Oscillation of ball potential versus time, and frequency spectrum

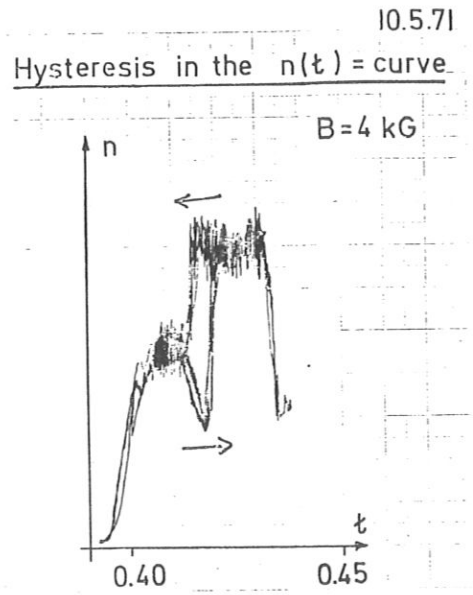

Fig.9: Example for a hysteresis effect

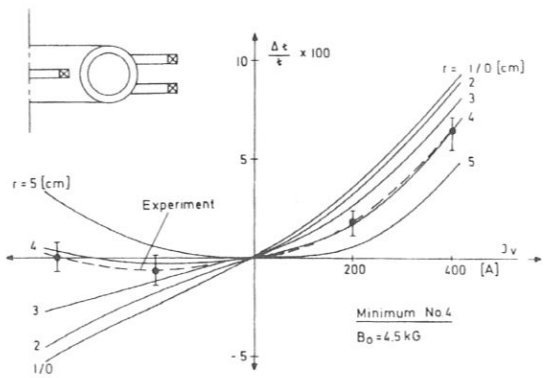

Fig. 10: Experimental and theoretical results for the relative shift in iota for minimum No. 5

APPENDIX TO PAPER CN-28/H-3 OF THE IV. CONF. PLASMA PHYS. CONTR. FUSION - MADISON 1971

OHMIC HEATING IN THE WENDELSTEIN STELLARATOR W II b

G. Grieger, J. Hugill[+)], R. Jaenicke, C.O.L. Juulman, I. Katsumata, W. Ohlendorf, H.D. Pacher, H. Renner, J.-G. Wegrowe, H. Wobig, G.H. Wolf
Max-Planck-Institut für Plasmaphysik, EURATOM-Assocation, 8046 Garching
Fed. Rep. of Germany

W II b

In order to expand the barium plasma experiments on the W II a stellarator to hydrogen plasmas of higher temperatures and densities, another apparatus with similar constructional features was built: $\ell = 2$ stellarator with major radius R = 50 cm, minor radius r = 9 cm. The internal limiter restricts the plasma radius to 6.5 cm. The toroidal magnetic field can achieve 7.5 kG in a stationary state, 15 kG pulsed.

The preionized plasma is subject to ohmic heating applied in two steps. For the preheating stage the energy of a capacitor bank of 30 kJ is discharged into an air core transformer. The loop voltage induced in the torus reaches 40 V over 0,3 msec. The subsequent heating pulse applied by a second air core transformer should allow for quasistationary operation with a loop voltage of up to 3 V over 50 msec. Estimates yield expected temperatures of $T_i \simeq T_e \sim 40$ eV and densities of $n \sim 10^{13}$. Preionization is accomplished with an RF discharge or ECRH, supplemented by an electron emitting filament.

The first test runs are used to obtain some information on the build-up and properties of the preheated plasma. Initial parameters are: filling pressure of H_2 of 10^{-4} Torr, toroidal magnetic field 7.3 kG and $\iota_0 \simeq 0.1$. The plasma current thus achieved was about 1.5 kA. An estimate based on classical resistivity gives for the electron temperature $T_e \lesssim 20$ eV. A five-beam microwave interferometer operating at 70 GHz shows peak plasma densities of 5×10^{12} cm^{-3}, assuming a plasma radius of 5 cm and a decay time of typically 1.5 msec. The density reaches its maximum in 0.3 msec, in correlation with the time dependence of the plasma current, the latter decaying during 0.5 msec.

An X-ray energy analyzer pointed at the limiter shows a bremsstrahlung spectrum with energies up to about 40 keV, the maximum of its intensity occurring at the characteristic iron line. The emission of the bremsstrahlung is restricted to the build-up phase of the plasma density. Additional diagnostics as laser scattering, particle energy analyzers, spectroscopic and photographic methods, magnetic probes etc. are installed and will be put into operation in the near future.

ACKNOWLEDGEMENTS

The authors gratefully acknowledge scientific discussions with their colleagues, in particular with Dr. G. v. Gierke. They are further indebted to the technical staff and its unflagging support. The leading contributions were made by: J.Kolos, K. Freudenberger, H. Goss and H. Ihmann, design; M. Zippe and H. Holitzner, electronics; U. Weber and E. Würsching, microwave techniques; W. Spensberger, J. Bömerl, A. Gronmayer and G. Preißer, construction.

Cs-PLASMA IN THE GARCHING OCTOPOLE W V

C. W. ERICKSON, G. v. GIERKE, G. GRIEGER, F. RAU AND H. WOBIG
INSTITUT FÜR PLASMAPHYSIK, GARCHING, MUNICH,
FEDERAL REPUBLIC OF GERMANY

Abstract

Cs-PLASMA IN THE GARCHING OCTOPOLE W V. In the Octopole a Cs plasma in the density range of typically some 10^8 cm^{-3} is produced by contact ionization with an ion input flux of the order of $\Phi = 10^{15}$ s^{-1}. The influence of an applied azimuthal magnetic field is studied. In accordance with a previous experiment an improvement in density by a factor of 10 is found, when superimposing $B_\varphi = 65$ G. Axial density profiles show a maximum near the lower small separatrix. No appreciable azimuthal density gradient is found, however a large density gradient parallel to the magnetic field towards the rings is to be concluded. n proportional to Φ is found. The experimental confinement time is $\tau_\varphi \approx 20$ ms for $B_\varphi = 65$ G and $\tau_0 = 2$ ms for $B_\varphi = 0$. The confinement is discussed in terms of a collisionless model where non-conservation of magnetic moment and large Larmor radii lead to recombination of particles at the rings.

Introduction

Preliminary results on the Octopole were reported [1] in 1965, at the Culham Conference. After several technical improvements regarding the current-carrying rings the investigation of the confinement of a Cs plasma in the Octopole has been resumed. For the sake of continuity as well as to check the possible influence of the above-mentioned changes on the physics in this machine the experimental conditions are chosen in the same range of operation as in 1965. In this paper, however, we concentrate on experiments where the main magnetic field as well as the temperature of the plasma source, is kept constant.

Apparatus

A description of the apparatus is already given in ref. [1]. Here we only list the main features and give details of certain changes made in the meantime.

When energizing appropriately a system of two pairs of inner rings along with outer reverse windings a meridional field as shown in fig. 1 is produced. The maximum magnetic field at the big separatrix, $B_0 = 2.3$ kG, is near the inner ring at $z \approx 15$ cm, near the outer ring there is B = 0.84 kG. Vertically between the crossing

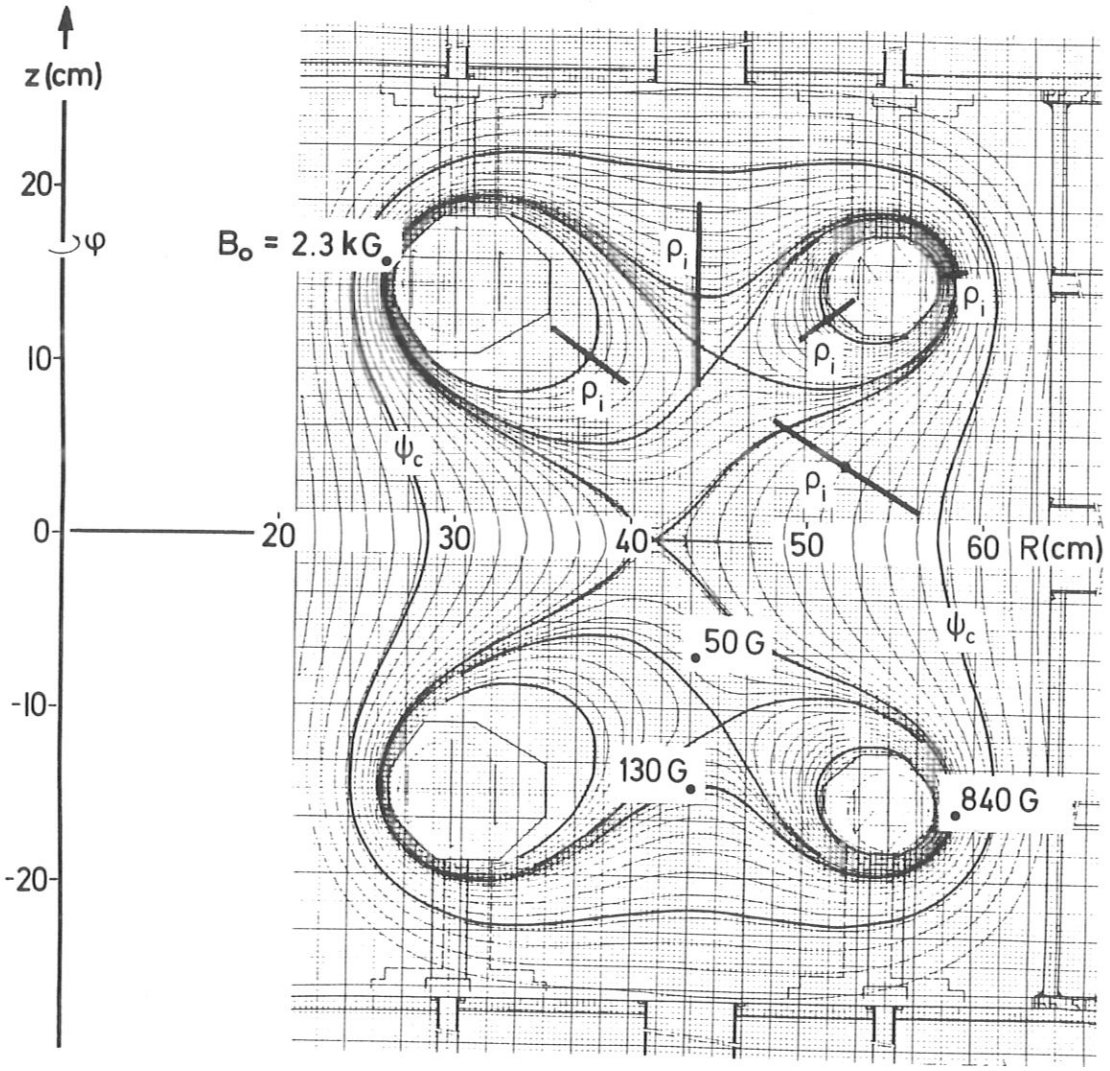

FIG. 1. Magnetic field plot of octopole W V.

points of the separatrices there is B ≈ 50 G. The theoretical limit of a flute-stable confinement, ψ_c, is inside the vacuum tank. Considering Cs ions with energy of 0.2 eV there are about 3.3 Larmor radii ρ_i between ψ_c and the big separatrix in the plane z = 0. Near the outer ring, however, there is only one Larmor radius between the shell of the ring and the small separatrix. Generally, ρ_i is of the order of a scale length in the magnetic field.

These statements also were valid for the experiment described in ref. [1]. In the meantime more rigid structures of the shells around the coils with also three supports for each ring were constructed. Care was taken to keep the new shells inside the same magnetic flux lines as were those described in ref. [1]. The dimensions of the

supports have been increased slightly, the long sides still being parallel to the field lines of the meridional field. The surfaces of the supports are insulated by silicon paint, the shells of the coils are connected electrically with the vacuum tank.
The magnetic field is switched on for two seconds, this time being long compared to the experimental confinement time as well as to the rise time of current in the inner rings. An azimuthal magnetic field B_φ up to several hundred gauss can be superimposed upon the meridional field.
We use contact ionization of Cs-vapour which is directed vertically from the bottom of the machine towards a hot conical spiral of about 2 cm diameter and 1.6 cm height, made of 2 mm dia tantalum wire. The tip of the cone is pointing downward. The spiral is heated by d.c. up to 2500 ^{o}K. The heating is switched off during the pulse time of the magnetic field. As the spiral is well insulated it can assume its floating potential. The plasma source is placed at the same azimuth as the big supports of the rings in order to have a maximum of azimuthal symmetry in the machine. We use single Langmuir probes and special double-double probes as described in ref. [2] as diagnostic tools. The single probes are of 0.5 mm diameter and 2 mm length biased with respect to the spiral. Ion density is calculated the usual way. An empirical correction factor of 2.5, see e.g. ref. [3, 4], is applied.
The probe signals are evaluated at t = 1 s. At this time the spiral is cooled down from 2500 ^{o}K to about 2300 ^{o}K. No corrections regarding recombination at the probe itself and at the shaft are made.

Experiments

We first investigate the influence of an applied azimuthal magnetic field B_φ on the density of the Cs plasma in this machine. In the previous experiment, ref. [1], an increase of nearly one order of magnitude in peak density was reported when superimposing a weak magnetic field $B_\varphi \approx 50$ G on the main meridional field. In fig. 2 we give the results of our investigation. Using an ion input flux $\Phi = 10^{15}$ s^{-1} the density n vs azimuthal field $\pm B_\varphi$ is measured at azimuthal position $\varphi = 180^{o}$ with respect to the plasma source, at several points of the big separatrix, as indicated in the insert. There is a close agreement with the 1965 results when normalizing the 1965 data at the maximum of the curve. With increa-

sing B_φ the density rises monotonically up to a factor of 10 as compared to the density at $B_\varphi = 0$. The maximum of the curve is reached near $B_\varphi = 65$ G; beyond this maximum there is a slow decrease. The same behaviour is found when measuring axially at R = 30 cm above the inner ring.

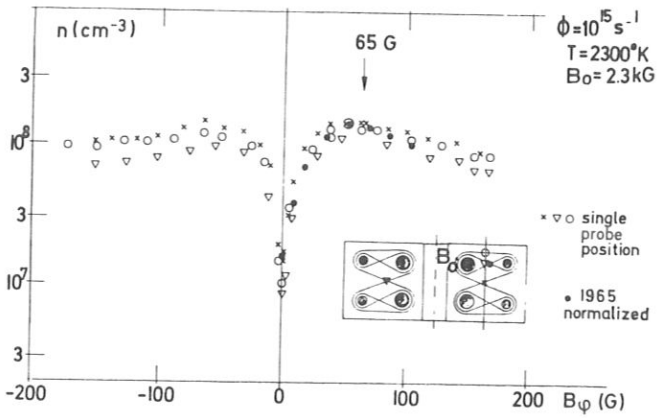

FIG.2. Density versus azimuthal magnetic field B_φ. Probe position indicated in insert.

In fig. 3 we give axial and radial profiles of Cs ion density n in the Octopole. The data of these curves is gained during several days of experiments where the ion input flux Φ was varying from $9 \cdot 10^{14}$ to $3.4 \cdot 10^{15}$ s^{-1}. Corresponding to the result of the following fig. 4 (n proportional to Φ) we normalized the profiles to $\Phi = 1 \cdot 10^{15}$. The vertical profiles at azimuthal angles $\varphi = 60^\circ$ and 180° are taken with the identical probes, the vertical profile at $\varphi = 180^\circ$ is measured with double-double and with single probe, resp. The radial profiles are obtained with two different single probes. All these profiles are taken with an azimuthal field $B_\varphi = 65$ G; with $B_\varphi = 0$ we only show a vertical profile at $\varphi = 180^\circ$. The relative agreement of the 4 different probes used is within a factor of 2.

We note the following details of the profiles:

i) with $B_\varphi = 65$ G and $B_\varphi = 0$ we find in the axial profiles a maximum of density in the lower half of the machine, peaked around the lower small separatrix.

This asymmetry is not changed when using the reverse polarity of the currents which produce the meridional field.

ii) the radial profiles are rather flat-topped and centered around the big separatrix.

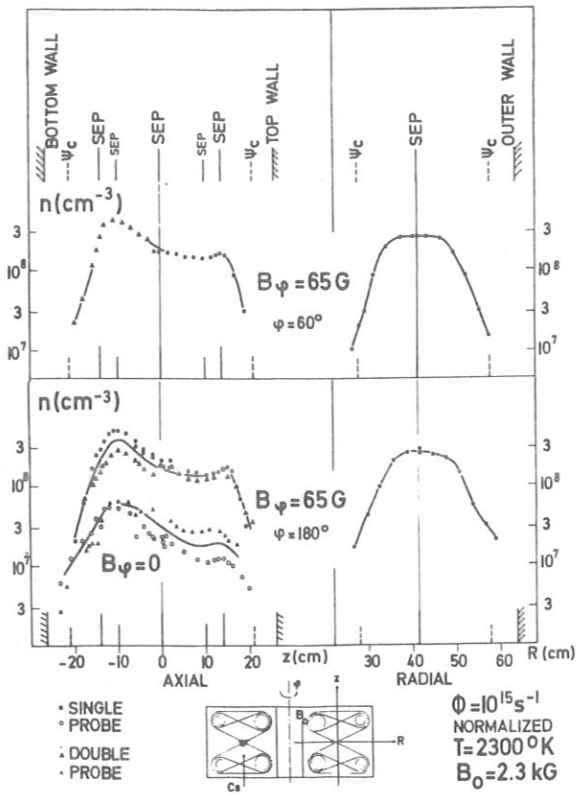

FIG.3. Axial and radial density profiles.

iii) the density at the big separatrix is approximately constant at the different points in the profiles shown. However, when measuring axial profiles above the rings at an azimuth of 180° we find peak densities of about one order of magnitude lower than those as given in fig. 3. This information is obtained with another double-double probe of the same construction and dimensions as were used in the profiles shown. Assuming the same sensitivity this means that a remarkable density gradient parallel to the magnetic lines is to be concluded.

iv) apparently there is no appreciable azimuthal density gradient to be observed.

A comparison of confinement mechanisms as predicted by theoretical considerations with the experimental data can be undertaken by a study of a n vs Φ plot, e.g. as shown in fig. 11 of ref. [1].

In fig. 4 we present our data obtained by single and double-double probes at several points of the big separatrix. The bulk of the experimental points follows the relation n proportional to Φ. Vertically above the upper rings, however, but still near the separatrix we find the density to be an order of magnitude lower. The density above the inner ring (x) appears to be higher by about a factor of 2 as compared to the density above the outer ring (+).

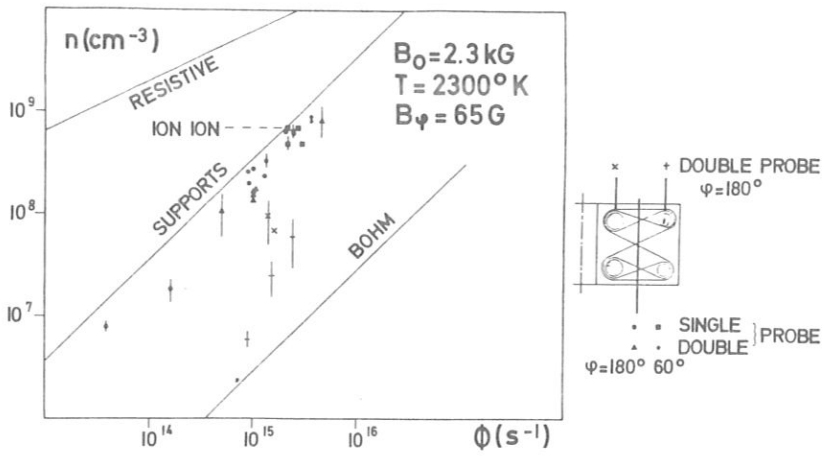

FIG. 4. Density at large separatrix-versus-ion input flux and theoretical particle losses.

Discussion

In fig. 4 three theoretical curves (straight lines) are reproduced from fig. 11 of ref. [1], corresponding to resistive and Bohm-type diffusion and to recombination at the supports, resp., as predominant loss processes. In order to take into account our changes in the size of the supports we shifted the line "SUPPORTS" by a factor of 1.5 towards lower densities. The curve "RESISTIVE" also is adjusted to a magnetic field higher by a factor of 2 as compared to the corresponding line in fig. 11 of ref. [1].
The dashed line marked ION-ION is taken from a report of GRAWE [5].

i) Resistive diffusion

Resistive diffusion as the predominant loss process in the Octopole W V is not to be expected.

ii) Bohm diffusion

This type of loss mechanism yields n proportional to Φ. However, the bulk of the experimental points is found to be about a factor of 60 higher in density than predicted by this model. Furthermore, the experimental radial profile is not as broad as the Bohm profile (ref.[6]).

iii) Support losses

Recombination of the ions at the supports of the Octopole was concluded to be the predominant loss process in the 1965 experiment [1]. Similar statements were made e.g. by OHKAWA et.al. [7] and KERST et.al. [8]. Our experimental data obtained axially above the rings at the same radii where the supports are situated, however, do not yield constant density along the big separatrix, but typically show one order of magnitude less density than in the region of low magnetic field. Consequently this would shift the curve SUPPORTS of fig. 4 higher by the same amount beyond the experimental error of the measured $n(\Phi)$ curve. Therefore it is to be concluded that - assuming unchanged probe sensitivity as mentioned above - in the Octopole with magnetic fields as used in this experiment the confinement of a Cs plasma of 0.2 eV mean thermal energy is not governed by recombination at the supports.

iv) Like particle diffusion

This was considered by GRAWE [5] using the experimental data of the 1965 experiment [1]. Numerically he solved a transport equation and succeeded in a nearly perfect fit of the vertical density profile given in ref.[1], fig. 10. The result of his calculation, however, was very insensitive with respect to a variation of the ion input flux Φ; as shown in fig. 4 of this paper, dashed curve, marked "ION ION" . Since in 1965 n proportional to Φ was found, GRAWE concluded that like particle diffusion is not likely to be predominant.

In our present investigation the meridional field was higher by a factor of 2 as compared to the conditions of fig. 10 in ref. [1]. As the probability of like particle

diffusion is proportional to ρ_i^4 [9] (ρ_i..ion Larmor radius), we are of opinion that like particle diffusion is to be excluded as the main loss process.

Collisionless model with large Larmor radii

Following the procedure as described in ref. [8] to evaluate the absolute confinement zones we calculate a vertical density profile by integration over the distribution function of the Cs ions. This was taken to be Maxwellian with a mean thermal energy of 0.2 eV at the source. The losses due to recombination at the supports are taken into account. Electric fields which should be present in the machine are neglected. According to the energy dependence of the confinement zones the confinement of particles with energy higher than 0.2 eV should be poor. This profile is shown in the middle part of fig. 5, (bold curve), adjusted at the mid plane to fit the experimental curve taken with B_φ= 65 G at $\varphi = 180^\circ$ (light curve).

Due to the magnetic flux between the big and the small separatrix the calculated profile shows a marked dip at the small separatrix. Experimentally, this dip is not observed. However, at the lower small separatrix there is a maximum of density, the origin of which has to be studied in the future.

In the case of a toroidal multipole with a collisionless plasma the energy H and the momentum p_φ are conserved, see e.g.ref. [8]. Whenever a charged particle penetrates the zone of low magnetic field the magnetic moment μ may change. This may be regarded as an elastic collision where the momentum vector is rotated about some angle in velocity space.

In the case of a superimposed perpendicular field this statement also holds true, as can be seen in the upper part of fig. 5. There, for a linear quadrupole we calculate numerically the path of a charged particle with given Larmor radius and starting direction. One percent of the maximum magnetic field at the separatrix is superimposed.

In this connection we now discuss a loss mechanism which might be applicable to this experiment. This model yields a

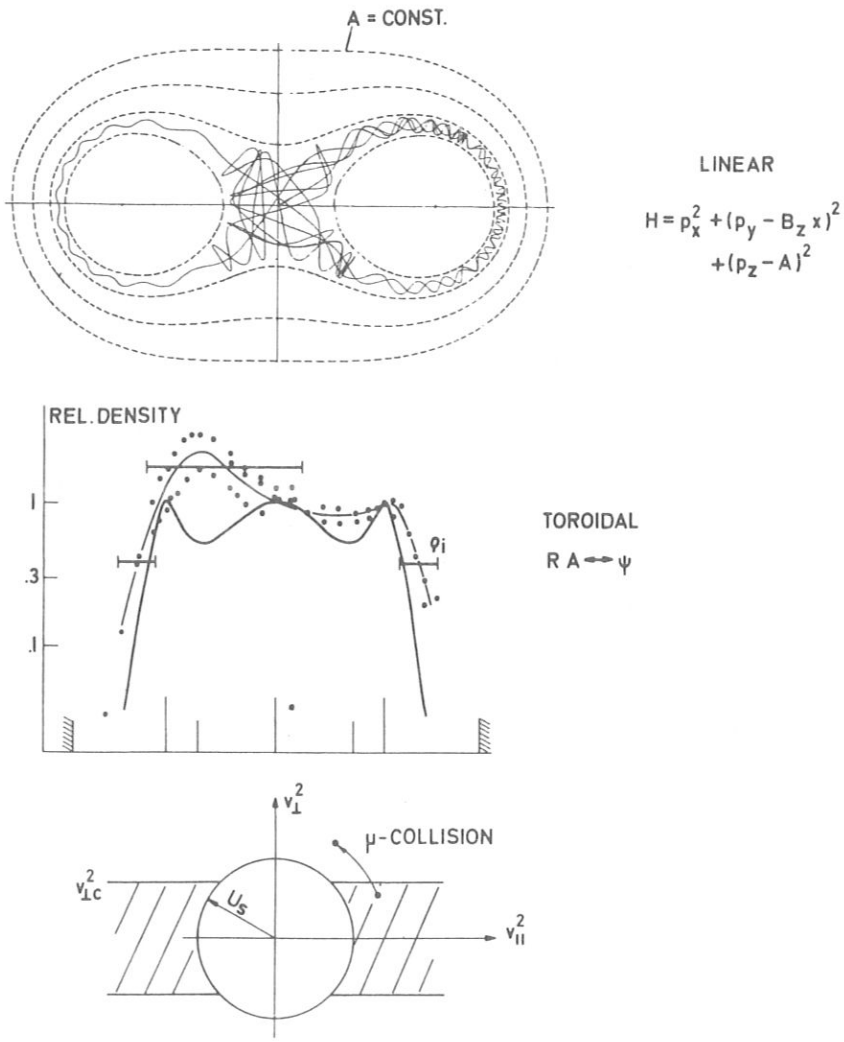

FIG. 5. Collisionless model with non-conservation of magnetic moment and large Larmor radii.

relation of n proportional to Φ. Qualitatively the improvement of the confinement by applying the azimuthal field B_φ can be shown, however no prediction can be made with respect to the reduction of particle density beyond the optimum value of $B_\varphi \approx 65$ G.

Since in the Octopole between the outer ring and the small separatrix the distance is only one Larmor radius ρ_i of a 0.2 eV Cs ion those particles having by chance a larger radius of gyration than this distance are lost by recombination at the shell. This effect depletes the velocity distribution beyond a critical perpendicular velocity $v_{\perp c}$. Whenever

a Cs ion is passing near the zone of lower field at a rate $\nu \approx 4 \frac{v_{ith}}{L} \approx 2 \cdot 10^3 \ s^{-1}$ (L ≈ 1 m being the length of the big separatrix), μ might change. There is a probability $c < 1$ that this change transfers part of the parallel velocity to perpendicular velocity beyond the critical value.

In order to calculate the losses in stationary state we have to balance the input flux Φ and the losses $\Phi = c \nu n V$; n being an average density in the confinement volume $V \approx 10^5 \ cm^3$.

Inserting the experimental values of the measurement without azimuthal field (see fig. 3) we find $c_o = 0.2$ corresponding to a confinement time $\tau_o \approx 2$ ms. This time is short as compared to ion-electron or ion-ion collision times, respectively. This value reduces to $c_{\varphi} \approx 0.02$ when considering the results of the measurement with optimal B_{φ}. Since in the case with azimuthal field (non-zero-min-B-device) μ is a better adiabatic constant, the confinement should be improved.
Particles with energy $E < \frac{m}{2} v_{\perp c}^2$ cannot leave the plasma in the model discussed above. Those low velocities, presumably do not exist in the Octopole at the conditions of this experiment. With a Ta-spiral at about T = 2300 °K and at densities of typically $10^8 \ cm^{-3}$ there exists an electron sheath with sheath voltage U_s large as compared to 0.2 V. In the collisionless regime the distribution function (assumed to be at the source half-Maxwellian with temperature T) is accelerated in the sheath[+].
Thus the distribution of velocities in this experiment might well be as asymmetric as shown in the lower part of fig. 5, with only the shaded area of the velocity space being populated.

In the loss model discussed here characteristic distances in the machine are compared with local Larmor radii of a 0.2 eV Cs ion. Considering the influence of the sheath acceleration one might argue that larger Larmor radii have to be taken into account.
Up to now we have totally neglected effects of electrical fields which at least are caused by the large factor between

+) In accordance with ref. [3] this introduces no marked error in our evaluation of probe signals.

ion and electron Larmor radii. Taking into account the gradient of the measured floating potential, however, leads to the conclusion that the Larmor radius of an Cs ion can be reduced up to a factor of 2. This counteracting effect might balance part of the increase of Larmor radii caused by energy gain in the sheath in front of the emitter.

Conclusion

From the experimental data and the results of a simple collisionless model of particle losses taking non-conservation of magnetic moment as well as effects of Larmor radii into account we believe that confinement of Cs ions in this experiment on the Octopole is governed mostly by recombination at the surfaces of the rings.

To test this model more experiments are to be made, especially those using smaller Larmor radii and an emitter with less sheath voltage. The decrease of density beyond the optimum value of $B_\varphi \approx 65$ G is to be investigated further. Up to now no explanation of this feature is given.

This work was performed under the terms of the agreement between the Institut für Plasmaphysik GmbH, Munich-Garching, and Euratom to conduct joint research in the field of plasma physics.

References

[1] Eckhartt, D. et.al. Proceedings of the Culham Conf. 1965, Vol.II,718,paper CN 21/50.

[2] D'Angelo, N. et.al. VI ICPIG Paris, 1963, paper III c, 9.

[3] Hashmi, M. et.al. Proc. of Conf. on Phys. of Quiescent Plasmas, Frascati 1967, paper I, 1.

[4] Hashmi, M. et.al. 2nd Eur.Conf.on Controlled Fusion and Plasma Phys., Stockholm 1967, paper Wa BI.

[5] Grawe, H. Report IPP 6/61, 1967.

[6] Eckhartt, D. et.al. Report MIP/PAE/PL 6/65.

[7] Ohkawa, T. et.al. Proc.of the Culham Conf. 1965, Vol. II, 531, paper CN 21/115.

[8] Kerst, D.W. et.al. Phys.Fl. 9, 997 (1966).

[9] Simon, A. Ph.Rev.100, 1557 (1955).

DISCUSSION

J. L. TUCK: In Fig. 3, the two peaks are of unequal height. Is there any asymmetry in the geometry of the apparatus to which this inequality can be related?

F. RAU: As I mentioned in my oral presentation, the device has two independent quadrupoles, and asymmetries in plasma production can lead to preferred filling of one of the two quadrupoles even when the conical spiral is located near the mid-plane of the device.

J. L. TUCK: When you say "recombination of particles at the rings" are you implying something different from "loss to the rings"? Once an ion has reached the rings, it is a loss as regards confinement, whether it chooses to recombine or not.

F. RAU: Of course, there is a sheath near the surface of the rings. By "surface recombination" we simply mean that particles are lost at the surface of solid materials.

S. J. BUCHSBAUM: At the temperatures obtained in your experiment, how did the thickness of the sheath compare with the Larmor radius?

F. RAU: The sheath thickness, which is governed by the Debye length, was about 0.3 mm. This is small compared with the Larmor radius, especially when one bears in mind that the magnetic field is high at the surface of the ring.

F. F. CHEN: Does the toroidal field needed for a tenfold increase in density correspond to that which gives a sufficient pitch of the lines of force for the injected ions to miss the filament on the first turn?

F. RAU: It gives a much larger pitch.

Plasma Physics, Vol. 15, pp. 151 to 155. Pergamon Press 1973. Printed in Northern Ireland

RESEARCH NOTE

Effect of rational transform on the ohmically heated plasma in the WIIb stellarator

(*Received* 18 *May* 1972)

THE WIIb stellarator is similar in size and construction to the WIIa stellarator used to study the confinement of barium plasma (GRIEGER *et al.* 1971; GRIEGER *et al.* 1971). The major radius is 0·50 m, the vessel internal radius 90 mm, the main magnetic field up to 15 kG pulsed, and the left-handed $l = 2$ helical winding has five field periods, giving a rotational transform, $t_0 \leqslant 0{\cdot}6$ on the axis with very little shear. The vacuum vessel has an insulating gap to allow for ohmic heating. An adjustable limiter consisting of two semicircular tantalum annuli, electrically insulated from the vacuum vessel, is positioned near the gap.

Figure 1 shows the disposition of the air-cored transformers for ohmic heating. These are of toroidal shape to minimise stray flux. The coupling to the plasma circuit is very weak so that the primary is effectively decoupled from the plasma, and we apply a given voltage to the plasma in contrast to the usual arrangement. The two smaller transformers are intended for preheating, and the larger transformer for quasistationary operation.

In the present experiments only the preheating transformers are used. They are energised from a 30 kJ capacitor bank via ignitrons to give a quarter cosinusoidal loop voltage with a peak value of 30 V and a duration of 360 μs. At this time the bank is crowbarred and the residual loop voltage is initially -5 V, slowly decaying. The main magnetic field is adjusted to 4·2 kG and the limiter diameter to 130 mm.

Various methods of preionisation were tried, including r.f. applied to ring-shaped electrodes within the vacuum vessel, a hot filament biased to -200 V and a plasma gun of the type used on the Proto-Cleo experiment (ADLAM *et al.*, 1969), fired both into a vacuum ($p = 10^{-6}$ torr) and into hydrogen gas ($p = 5 \times 10^{-5}$ torr). The highest plasma current and plasma temperature are obtained using the plasma gun fired into a vacuum. The ohmic heating pulse is applied 50 μs after the gun injection process, which lasts for 100 μs. This timing is found to give maximum induced current. The densities reached are higher than would be expected from the gun alone according to previous experience. It is thought that during the pulse gas is evolved from the walls of the vacuum vessel, which are not yet clean, and ionised within the plasma column.

Diagnostics presently employed are: gap voltage measurement, plasma current measurement by a Rogowski coil inside the vacuum vessel, optical spectroscopy, ruby laser light scattered at 90° for density and temperature, multichannel μ-wave interferometry for density vs time, and detection of X-rays from part of the limiter.

Figure 2 shows the gap voltage, the plasma current I, the X-ray intensity and the integrated electron density along two beams of the 4 mm μ-wave interferometer for $t_0 = 0{\cdot}27$. The electron density at the centre of the discharge, n, increases to a maximum of 10^{13} cm^{-3} between 80 μs and 300 μs after current maximum. The electron temperature T_e, measured by the laser diagnostic at current maximum is approximately 10–20 eV and the density agrees with $\int n \, \mathrm{d}l$ from the μ-wave interferometer assuming a plasma profile rather flatter than parabolic. Bursts of X-rays are generated at the limiter during current decay, accompanied by small steps in current of 100 A. This suggests that a substantial fraction of the plasma current is carried by runaways. The rather low initial value of $\mathrm{d}I/\mathrm{d}t$ also suggests that the inertial effect of a small number of high energy current carriers is present. If $\mathrm{d}L/\mathrm{d}t = 0$ at current maximum we can use the gap voltage to calculate the plasma resistance and hence a conductivity temperature. Figure 3 shows the temperature thus calculated, assuming the ions are singly ionised, for both flat and parabolic current distributions (extreme points on lines) against T_e measured by the scattering of laser light. In general T_e (conductivity) $>$ T_e (laser) which again suggests the presence of a substantial runaway current, especially when T_e is low. In general the reproducibility of the voltage and current is within 5 per cent while that of the laser-measured n and T_e is poor, 50 per cent from shot to shot. This result probably reflects the variable amount of energy absorbed by the plasma and the runaway electrons respectively, depending on both the initial conditions and the amount of gas evolved from the vacuum wall during the discharge.

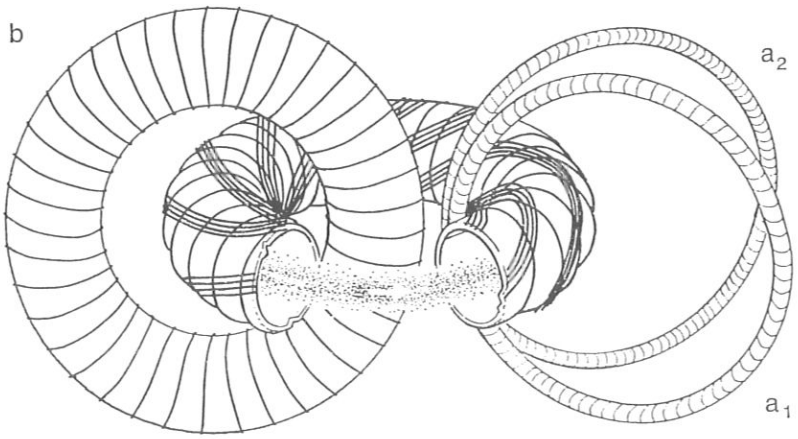

FIG. 1.—The disposition of the ohmic heating transformers in WIIb.

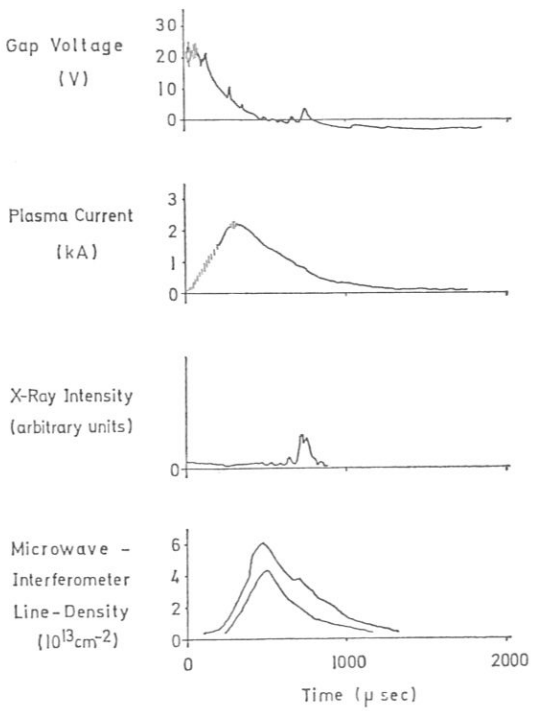

FIG. 2.—Typical oscillograms of measured parameters during a preheating pulse.

The variation in the peak current, I_{max}, with the initial value of the rotational transform on the magnetic axis t_0, is shown in Fig. 4. Three regions can be distinguished. At $t_0 = 0{\cdot}0$, I_{max} is nearly zero, i.e. we do not obtain a tokamak-type discharge. This may be related to inaccuracies in the main field or to the poor confinement of the gun-injected plasma. The 2 cm thickness of the stainless-steel vacuum vessel should be adequate to allow tokamak equilibrium on our time scale. However an initial $t_0 = 0{\cdot}02$ is already sufficient to provide nearly maximum peak current, where the rotational transform produced by the current is 0·2 at the plasma boundary. For $0{\cdot}05 < t_0 < 0{\cdot}25$, I_{max} is nearly constant, and appears to be limited principally by the plasma inductance and the available flux, 0·007 Vs, from the preheat transformer. However, as t_0 is increased from 0·25 to 0·5, I_{max} decreases linearly towards zero. If we interpret this result as an effect of rational total transform, $t_0 + t_j = 0{\cdot}5$, where t_j is the transform due to the plasma current (in the same direction as that of the helical windings in our experiment), then the current produces a transform of $0{\cdot}1\,I$, where I is in kA. This corresponds with the transform produced at a radius of 5 cm, that is near

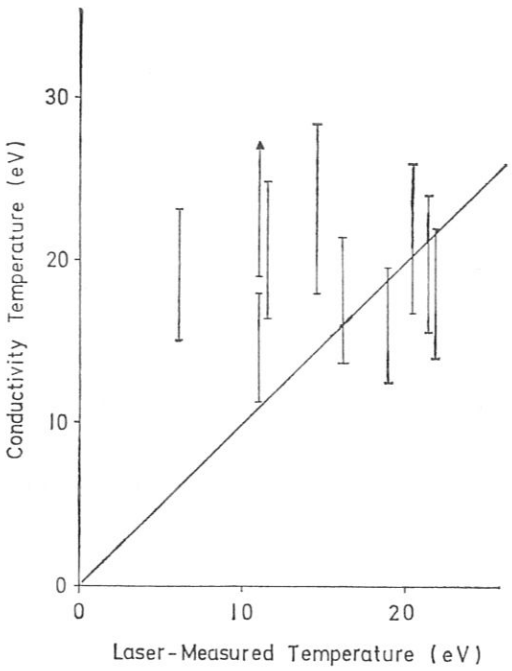

FIG. 3.—Comparison of conductivity temperature with that measured by the laser diagnostic.

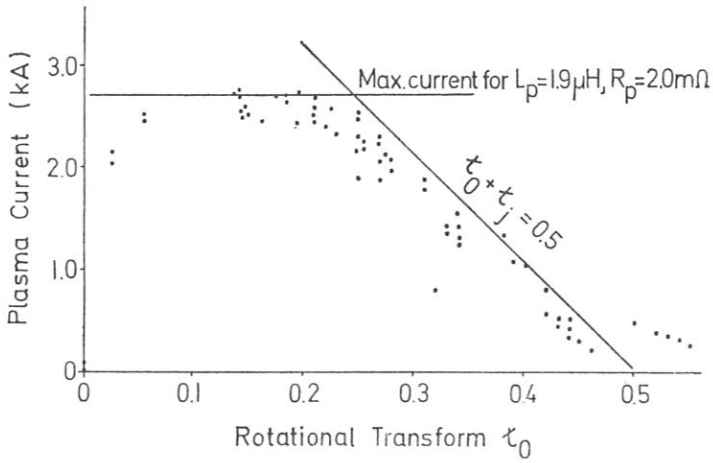

FIG. 4.—Variation of maximum plasma current with the rotational transform of the vacuum field.

the outer boundary of the plasma column, or at any radius within a uniform current distribution with a mean radius of 5 cm.

The cause of the limitation of the plasma current can be seen by looking at the dI/dt signal from the Rogowski coil. At $t_0 = 0{\cdot}5$, dI/dt has a low mean value accompanied by violent oscillations. Typically these disappear as the driving voltage falls, and the dI/dt trace becomes clean: then I rises slightly to its maximum value. The mean value of dI/dt increases as t_0 is reduced allowing I to rise to the values given in Fig. 4. As t_0 is further reduced several regions of instability in the dI/dt signal can be seen separated by more or less stable regions. An example is shown in Fig. 5 for $t_0 = 0{\cdot}21$. The regions of instability are quite well defined and are marked by arrows in the figure. Oscillation frequencies in the unstable regions are typically 200 kHz, about 5–10 × the electron diamagnetic drift frequency. Notice that the dI/dt trace becomes much cleaner after current maximum ($dI/dt = 0$). Minima in dI/dt are also observed after this time. These are not associated with rapid oscillations of the dI/dt signal but with X-rays from the limiter, which are not observed during periods of instability.

In Fig. 6 the values of the current at which well-defined instabilities occur like those shown in Fig. 5, are plotted as a function of t_0. The straight lines drawn in Fig. 6 correspond to values of $t_h + t_j = 1/2, 1/3, 1/4$, where t_h is the transform of the helical field at the limiter ($t_h = 1{\cdot}12 \times t_0$) and t_j is the transform produced by the plasma current at a mean radius of 5.0 cm. There are no fitted parameters. The observed instabilities seem to be convincingly related to these lines. They could only be consistent with rational transform at other radii if the current distribution were nearly

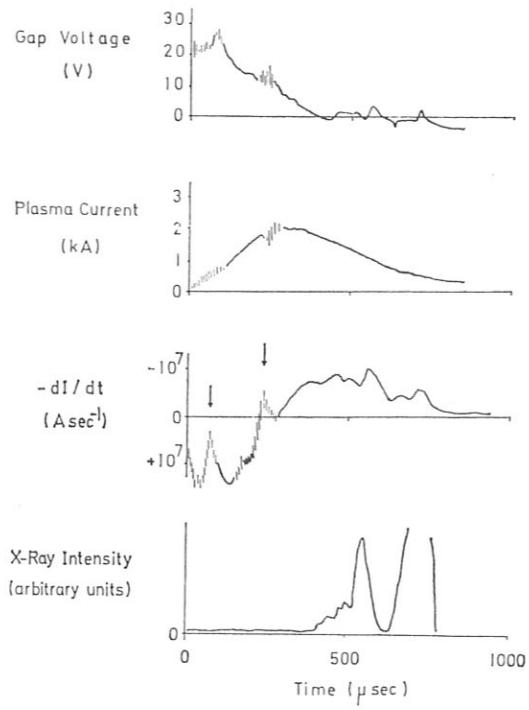

FIG. 5.—Oscillograms showing instabilities in the plasma current, marked by arrows.

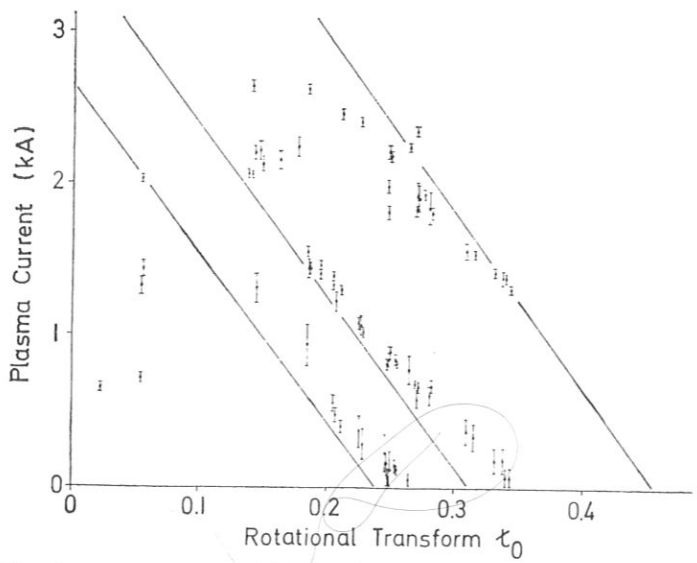

FIG. 6.—The plasma currents at which instabilities occur as a function of the rotational transform of the vacuum field. The straight lines are calculated as described in the text. For t_0 from 0·35 to 0·5 the instability is strongest and occurs from zero to nearly maximum current. There is always some noise on the current trace at low current (see Fig. 5), partly caused by interference from the plasma gun and the ignitron switch of the preheat transformer. At $t_0 \leqslant 0{\cdot}14$ we still see regions of instability but these are very weak and difficult to analyse in detail. They have not all been included in the figure.

uniform; but bell-shaped current distributions should give lines with a different slope when the rational surfaces occur appreciably inside the plasma boundary.

We conclude that instabilities of the plasma current have been observed when the transform near the plasma boundary is rational, whose strength decreases with increasing mode number. The $t = 1/2$ instability is sufficiently strong to limit the current attainable. The instabilities do not seem to depend strongly on other plasma parameters such as n and T_e which can vary 50 per cent from shot to shot. Similar phenomena observed in the early B and C stellarator work (SINCLAIR *et al.*, 1965) and in present tokamaks (HOSEA *et al.*, 1971) are usually attributed to MHD instabilities; the variation of instability strength with t in WIIb is also reminiscent of these experiments. However the minima in confinement time observed in the similarly constructed WIIa stellarator in experiments with Ba plasma may equally provide an explanation for our results. These are also found to be associated with rational transform at the plasma boundary, and their strength decreases with decreasing t.

Acknowledgement—The authors would like to acknowledge the technical support of the WIIb engineering group. E. WUERSCHING was responsible for the operation of the μ-wave interferometer.

Max Plank Institut für Plasmaphysik
Garching
Germany

G. GRIEGER
R. JAENICKE
C. O. L. JUULMAN
C. MAHN
H. RENNER
H. RINGLER
G. SCHILLING
G. H. WOLF

Culham Laboratory
Abingdon, Berks.
England

J. HUGILL

REFERENCES

ADLAM J. H., ASHBY D. E. T. F., BICKERTON R. J., BURCHAM J. N., FRIEDMAN M., HAMBURGER S. M., HOTSON E. S., LEES D. J., MALEIN A., REYNOLDS P., SHATFORD P. A. and WHITE B. M. (1969) *Plasma Phys. and Contr. Nuc. Fus. Res.* I p. 573, I.A.E.A., Vienna.

GRIEGER G., HUGILL J., JAENICKE R., JUULMAN C., RENNER H., RINGLER H., SCHILLING G., WEGROWE J.-G. and WOLF G. H. *Bull. Am. Phys. Soc.* (1971) **11**, 16 1280.

GRIEGER G., OHLENDORF W., PACHER H. D., WOBIG H. and WOLF G. H. (1971) *Plasma Phys. and Contr. Nuc. Fus. Res. Paper* CN-28/H-3, I.A.E.A. Vienna.

HOSEA J. C., BOBELDIJK C. and GROVE D. J. (1971) *Plasma Phys. and Contr. Nuc. Fus. Res. Paper* CN-28/F-7, I.A.E.A., Vienna.

SINCLAIR R. M., YOSHIKAWA S., HARRIES W. L., YOUNG K. M., WEIMER K. E. and JOHNSON J. L. (1965). *Phys. Fluids* **8**, 118.

PARTICLE AND ENERGY CONTAINMENT IN THE WII-b STELLARATOR

H. HACKER, G. PACHER, H. RENNER, S. REHKER,
H. RINGLER, E. WÜRSCHING
Max-Planck-Institut für Plasmaphysik,
EURATOM-Association,
Garching,
Federal Republic of Germany

Abstract

PARTICLE AND ENERGY CONTAINMENT IN THE WII-b STELLARATOR.

The WII-b machine is an Ohmically heated stellarator (with $\ell = 2$, $m = 5$ helical windings) with a major radius $R = 0.5$ m and a plasma radius $a = 0.05$ m. The experiments reported here have been performed in hydrogen and helium gas. The energy confinement times are shown to be consistent with a heat loss process dominated by pseudoclassical heat conduction. The particle containment time is in the neighbourhood of neoclassical values.

INTRODUCTION

The major characteristics of the WII-b stellarator have been described in detail elsewhere [3] and are summarized here in Table I and Fig.1.

In hydrogen, the starting plasma is produced by a Bostick gun, followed by the OH1 transformer system for pre-heating. In helium, it is possible to pre-ionize with HF [1], producing a density in the neighbourhood of 10^{12} cm^{-3}, which is sufficient to immediately initiate the quasi-stationary phase by using the OH2 transformer. Relatively high starting density seems to be imperative in stellarator operation since the good containment properties, even in the starting phase, favour the production of runaway electron currents [2]. Measures to limit this current, all of which have been used, include voltage reversal in the starting phase, temporally increasing helical rotational transform, and, in particular, destruction of the magnetic surfaces for several milliseconds by perturbing magnetic fields.

PARAMETER RANGE

The low voltages and poor coupling of the air core transformers severely limit the accessible parameter range. The regions for H_2 and He discharges are indicated in Fig.2. For lower densities, large runaway currents result, whereas at too high densities the voltage is too small to provide sufficient energy input at the corresponding low temperature.

The range of ι available is also limited by the small heating voltage because the increased losses at rational values of total rotational transform (i.e. integer values of q) cannot be compensated by increasing the energy input [3]. Only if the plasma current contribution to ι provides sufficient shear and thus limits these losses, is it possible to pass through such rational values in the time development of the discharge.

TABLE I. CHARACTERISTICS OF WII-b STELLARATOR

major radius: 0.5 m
vessel minor radius: 0.09 m
limiter radius: 0.055 m, Tungsten
plasma minor radius: 0.04 - 0.05 m
main field: 0.5 - 1.2 T
helical winding: $l=2$ $m=5$, shear free
$\varepsilon_{helix} < 0.3$ ($B_0 = 1.2$ T)

transformer OH_1: $3 \cdot 10^{-3}$ Vs, 20 V peak
transformer OH_2: 0.05 Vs, 5 V peak

pre-ionization: H_2 Bostick gun
He 300W, HF generator, 98 MHz

cleaning: 50 Hz discharge in Ne:He, followed by pulse cleaning

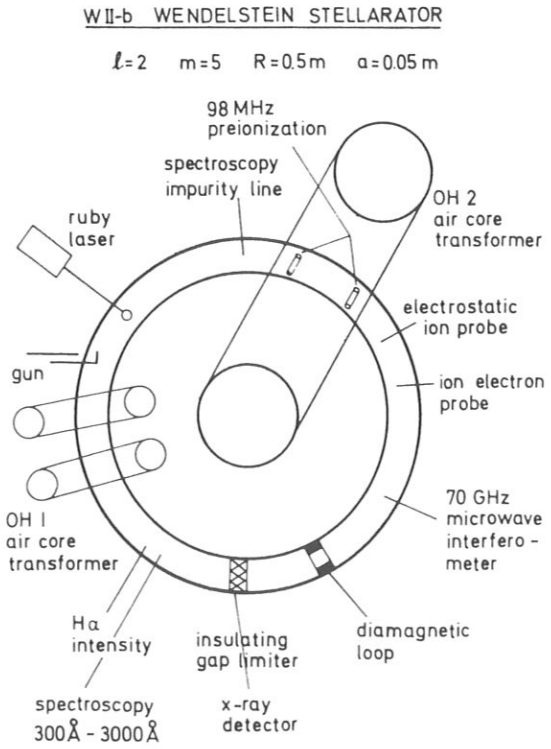

FIG.1. Schematic of the device.

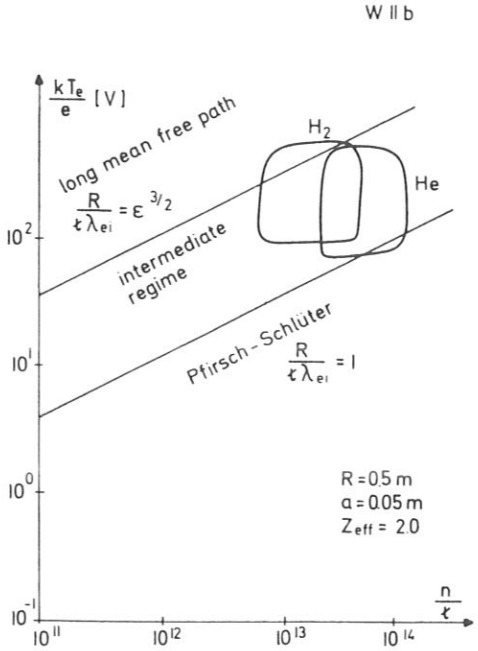

FIG.2. Parameter ranges.

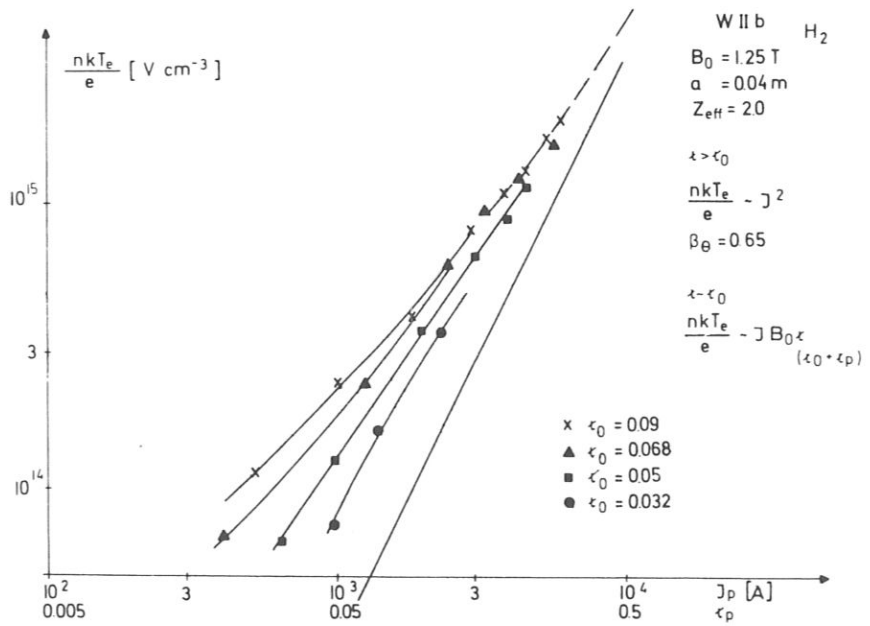

FIG.3. Energy density nkT_e for different values of the helical rotational transform ϵ_0 versus plasma current J_p.

ENERGY CONTAINMENT

In describing the energy containment of the WII-b stellarator analogous to tokamak descriptions, it should be remembered that the poloidal field consists of a contribution from the helical windings in addition to that from the plasma current. The assumption that the dominant energy loss is determined by a pseudoclassical heat conductivity with $\chi_e = C^2 \rho_{e\theta}^2 \nu_{ei}$ [4] leads to the expression $\tau_E' \sim 1/\chi_e$. For energy balance, this must be equal to the containment time derived from energy input,

$$\tau_E' = \frac{\int nkT_e \, dV}{J_p U}$$

in a quasi-stationary model. We then arrive at the expression for energy density

$$nkT_e = \frac{1}{\alpha Rc} \, \iota \, J_p B_0 \sim J_p^2 + \gamma \, \iota_0 J_p B_0 \qquad (1)$$

where R is the major radius, J_p the plasma current, ι the rotational transform, equal to $\iota_0 \pm \iota_p$, B_0 the main field, and α a proportionality constant which depends on physical and profile factors.
It follows then that the energy content nkT_e varies as $J_p B_0$ for $\iota_0 > \iota_p$ [5] and approaches a variation with J_p^2, independent of B_0, for $\iota_p > \iota_0$. Figure 3 illustrates this relationship with experimental values at $B_0 = 1.25$ T for different values of ι_0. In Fig.4, these points are replotted against ιJ_p and are seen to fall on a straight line as is expected from Eq.(1). Recently, it has been observed that the equation is also obeyed for the discharges obtained in helium which have a completely different time development. Figure 5 shows the typical time development of density and electron temperature for different discharges, one in hydrogen, the other one in helium. Figure 6 shows that both discharges behave according to Eq.(1) over the duration of the discharge, in spite of changing parameters. The constant c^2 in the diffusion constant may then be obtained from the experimental value of the proportionality constant $1/\alpha Rc$ so that comparison with other experiments is possible. In tokamaks, c^2 normally assumes values between 4-6, while for Uragan [5] and WII-b, the result is given in Table II. Remarkable quantitative agreement is found, despite the different conductivity mechanisms in the two machines [5]. For both hydrogen and helium discharges in WII-b, the plasma resistance is compatible with Spitzer resistivity with a $Z_{eff} = 2$ for the electron temperatures as measured by Thomson scattering. The ratio of electron drift to thermal velocity is $\lesssim 0.1$

It is possible to relate energy containment to conductivity σ by using relation (1):

$$\tau_E' \sim \frac{\iota}{\iota_p} \sigma \sim \left(1 + \frac{\iota_0}{\iota_p}\right) \sigma \qquad (2)$$

In the Moscow Conference, this relationship was illustrated by a plot of τ_E' against kT_e [6], where ι/ι_0 was used as a parameter and the appropriate discharge conditions were selected. In Fig.7, the energy containment time

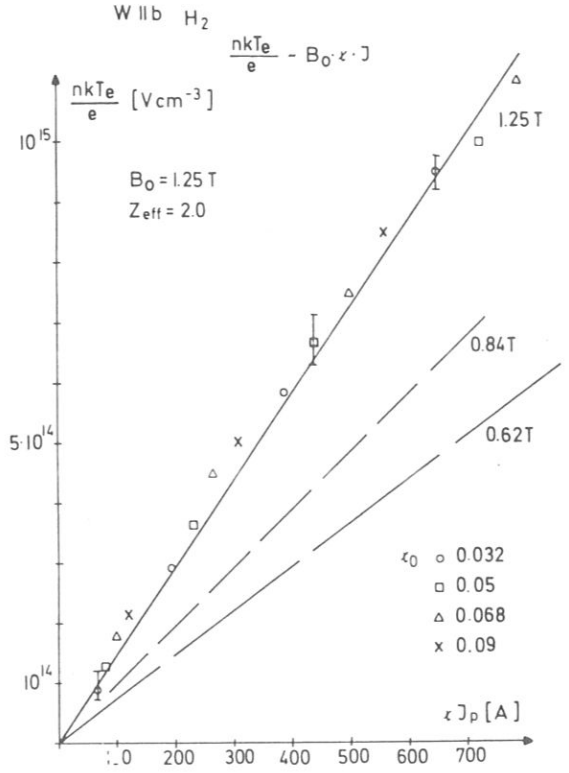

FIG.4. Energy density depending on εJ_p for varying main field B_0.

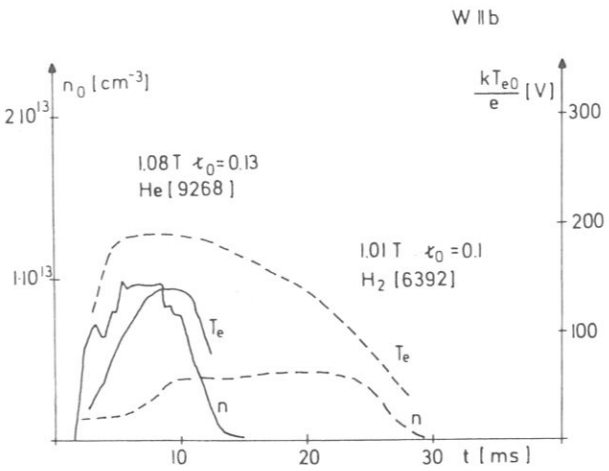

FIG.5. H_2 and He discharges: density and temperature.

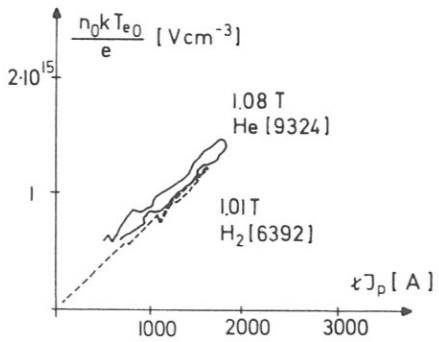

FIG.6. Electron energy density for H_2 and He discharges.

TABLE II. PSEUDOCLASSICAL HEAT CONDUCTIVITY. COMPARISON WII-b - URAGAN–TOKAMAK

$\chi_e = C^2 \varrho_{e\theta}^2 \upsilon_{ei}$	$nkT_e = \frac{1}{\alpha RC} \tau \cdot J_p \cdot B_0$	
W II b He H_2	URAGAN He	'TOKAMAK'
$\frac{1}{\alpha RC} = (1.1 \pm 0.2)\ 10^8$	$\frac{1}{\alpha RC} \tau = 2 \cdot 10^7 \left[\frac{eV}{cm^{-3} A \cdot G}\right]$	
$R = 0.5$ m	$R = 1.9$ m	$\beta_\theta = 0.5$
	$\tau = 0.8$	
$C^2 = 7$	$C^2 = 7.8$	$C^2 = 4 - 6$

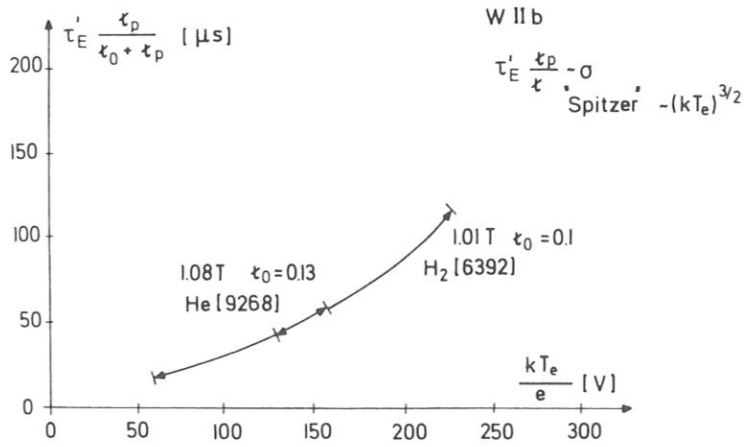

FIG.7. Energy containment time $\tau'_E = \frac{\int nkT_e \, dV}{J_p U}$ normalized to $\tau'_E \sim \frac{\tau_0 + \tau_p}{\tau_p} \sigma$.

is multiplied by t_p/t to normalize the experimental values throughout the time development of the two discharges mentioned above. The ratio t_p/t here varies between 0.3 and 0.7. We observe a $T_e^{3/2}$ dependence.

The energy containment of electrons is thus consistent with a loss process determined by pseudoclassical heat conductivity for both the hydrogen and helium discharges in WII-b. The energy loss to the ions and the radiative losses seem to be negligible in the energy balance. For example, in a typical discharge with energy input of 25-30 kW, the estimated radiated power is less than 3 kW, the power to the ions less than 1 kW.

PARTICLE CONTAINMENT

At the Garching Conference 1973 [7] we have reported two estimates of particle confinement time, one based on the time dependence of the ion temperature, and the other on the neutral gas balance. Both methods indicated a particle confinement time which was by a factor of 10 larger than the energy confinement time τ_E'.

We have now measured the particle confinement time by determining the ionization rate in H_2 discharges.

Using the equation of balance between particle loss rate and the ionization of neutrals in the plasma column we obtain

$$\frac{d\bar{n}_e}{dt} = -\frac{\bar{n}_e}{\tau_p} + \sum \text{ionization rates}$$

We assume that the dominant ionization rate is that of hydrogen. We can obtain the ionization rates by using the relative rate coefficients for excitation and ionization which have been calculated by Hinnov et al. [8]. The ratio of these rate coefficients gives the number of ionization events per H_α-photon. By measuring the total flux of photons for the H_α-line and knowing $\bar{n}_e$ from microwave interferometry and Thomson scattering, we can obtain the particle confinement time τ_p.

Since the ionization rates depend on radial and axial position, the H_α-radiation had to be recorded as a function of radius and along the axis of the machine. The distribution of light intensity around the machine was observed to peak at the fast gas inlet with a maximum ten times as large as at the opposite port. The full width at half maximum of this distribution was approximately equal to twice the minor diameter of the vacuum tube. The radial distribution turned out to be constant across the plasma column. Taking these axial and radial dependences into account we have calculated τ_p for our experiment.

The results confirm the first estimates. In the region investigated, with $t = 0.05\text{-}0.4$, $kT_e = 80\text{-}250$ eV, $n_e = 3 \times 10^{12}\text{-}1.5 \times 10^{13}$, and $B_0 = 0.5\text{-}1.2$ T (i.e. intermediate regime), particle containment times between 1 and 3 ms were obtained. For comparison with other stellarator experiments, the measured particle containment times, normalized to τ_{PS} for a toroidal plasma, are plotted in Fig.8. They lie a factor of 2-3 below the values for the intermediate regime of neoclassical theory. A description of the temperature dependence according to $\tau_p \sim t B_0^2/(kT_e)^{3/2}$ is not in contradiction to the experimental values, either.

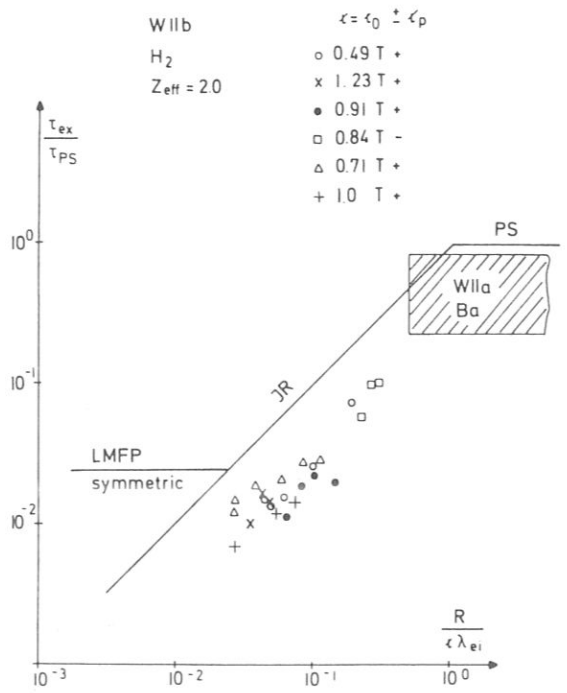

FIG.8. Particle containment time τ_p normalized to the toroidal confinement time τ_{ps}.

First results of the investigation of the helium discharges seem to indicate a similar behaviour of τ_p. In helium, also the particle containment times determined from He I and He II intensities lie around one millisecond. The reduction of the containment time by taking into account the absolute intensities of the spectral lines of hydrogen and oxygen remains below 30%. The effect of impurities, both by changing the particle balance and by radiation, thus seems to be insufficient to account for the discrepancy between particle and energy containment times.

CONCLUSION

We could show that a description of the energy containment of the WII-b stellarator with Ohmic heating is possible in terms of pseudoclassical heat conductivity. However, particle containment times are nearly an order of magnitude larger and exhibit different temperature dependence. Further careful investigations, especially of the impurity content and the runaway electron behaviour, will be necessary to obtain detailed information on the transport processes determining the discharge.

ACKNOWLEDGEMENTS

We wish to thank our colleagues Drs V. Suprunenko and O. Pavlichenko for many helpful discussions during their visit at Garching, October 1973.

We are grateful to Dr. E. Hinnov for his present participation in the experiment. Our thanks are also extended to our technical staff J. Bömerl, P. Iraschko, P. Voigt and Mrs H. Pacher.

REFERENCES

[1] HOOKE, B., Bull. Am. Soc. 4F10 (1973) 1314.
[2] ROME, J.D., ORNL-TM-3880 (1972).
[3] GRIEGER, G., et al., in Contr. Fusion and Plasma Physics (Proc. 6th Europ. Conf., Moscow, 1973) 101.
[4] ARTSIMOVICH, L.A., Nucl. Fusion 12 (1972) 215.
[5] DIKY, A.G., et al., Nucl. Fus. Suppl. (1972) 295.
[6] GRIEGER, G., et al., in Contr. Fusion and Plasma Physics (Proc. 6th Europ. Conf., Moscow, 1973) Suppl. paper 2 (1973) 334.
[7] GRIEGER, G., Third Int. Symp. on Toroidal Plasma Confinement (1973) D3,1.
[8] JOHNSON, L.C., HINNOV, E., J. Quant. Spectrosc. Radiat. Transfer 13 (1973) 333.

OHMIC HEATING IN THE W VII A-STELLARATOR

W VII A TEAM

M. BLAUMOSER, G. CATTANEI, A. CAVALLO, D. DORST,
A. ELSNER, G. GRIEGER, H. HACKER, H. JÄCKEL,
R. JAENICKE, J. JUNKER, R.-C. KUNZE, F. LEUTERER,
E. v. MARK, S. MARLIER, G. MÜLLER, A. v. OORDT,
F. RAU, S. REHKER, H. RENNER, H. RINGLER,
J. SAFFERT, J. SAPPER, P. SMEULDERS, M. TUTTER,
A. WELLER, E. WÜRSCHING, H. WOBIG, M. ZIPPE
Max-Planck-Institut für Plasmaphysik,
Euratom-Association,
Federal Republic of Germany

Abstract

OHMIC HEATING IN THE W VII A-STELLARATOR

First results of experiments with Ohmic heating in the W VII A-stellarator are reported. At $B_0 = 2.5$ T, a comparison of discharges with large ($\iota_0 = 0.23$) and small ($\iota_0 = 0.055$) rotational transform of the external helical field is made. In the parameter regime, $\bar{n}_e = 5 \times 10^{18} - 6 \times 10^{19}$ m^{-3}, $T_e = 200 - 900$ eV, $T_i = 100 - 220$ eV, energy confinement and MHD-instabilities are investigated. The energy density nT follows the scaling $nT \sim \iota J_p B_0$ (J_p = plasma current, B_0 = toroidal field, ι = rotational transform), the energy confinement time increases with n_e and T_e. Disruptive instabilities do not occur in discharges with large helical fields ($\iota_0 = 0.23$). Gas puffing during the discharge leads to higher densities ($n_{e0} \approx 8 \times 10^{19}$ m^{-3}), low Z_{eff} and heating of the ions. Internal relaxations are not only observed on X-ray signals but also on various other diagnostic signals outside the plasma.

INTRODUCTION

The W VII stellarator was built in order to heat and to confine a plasma, the parameters of which are comparable with those in a standard-size tokamak. In its first experimental phase with the small vacuum tube (W VII A) ohmic heating is the only heating mechanism, consequently all those effects as disruptions, kink instabilities and other current driven effects are expected. During the first three months of operation the aim of the experimental activities was to study the effect of the external helical field on confinement and stability of the plasma. By reducing the external helical field, a stepwise transition to tokamak operation was possible.

In this paper attention is given to the comparison of "tokamak" operation with "stellarator" operation, the discussion of other effects not concerning this question will be reduced to a minimum.

MACHINE PARAMETERS AND MAGNETIC SURFACES

W VII A is a circular $\ell = 2$ stellarator with 40 main field coils and an air core transformer for ohmic heating. The basic machine parameters are listed in Table I. Technical details of the apparatus are described elsewhere [1].

Tolerances of the mechanical setup have been chosen as small as possible in order to avoid deviations from axisymmetry. The only major deviation is the ripple of the helical field ($\delta_h \leqslant 5\%$). Magnetic surfaces measured by means of an electron beam agree well with the theoretical ones (Fig.1), magnetic islands with $\Delta > 3$ cm could not be detected [2]. The effective plasma radius as

TABLE I. BASIC MACHINE PARAMETERS

Major radius	$R_0 = 2$ m	Rotational transform	$0 \leqslant \iota_0 \leqslant 0.23$
Vacuum tube	$r_i = 0.17$ m	Shear	$\Delta\iota_0/\iota_0 = 10^{-2}$
Limiter radius	$r_L = 0.135$ m	Toroidal field	2.5 T (4 T in Jan. 77)
Helical windings	$\ell = 2$, m = 5	Air core transformer	$\phi = 1.2$ Vs (2.2 Vs in Jan.77)

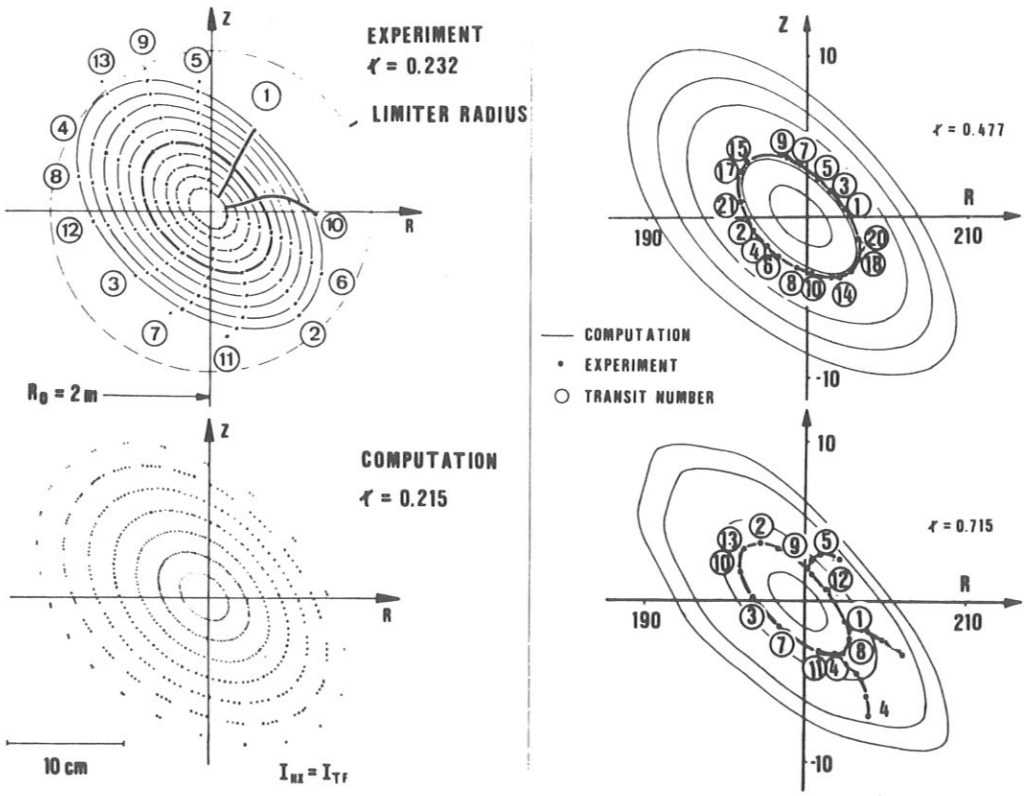

FIG.1. Calculated and measured magnetic surfaces for various values of the rotational transform.

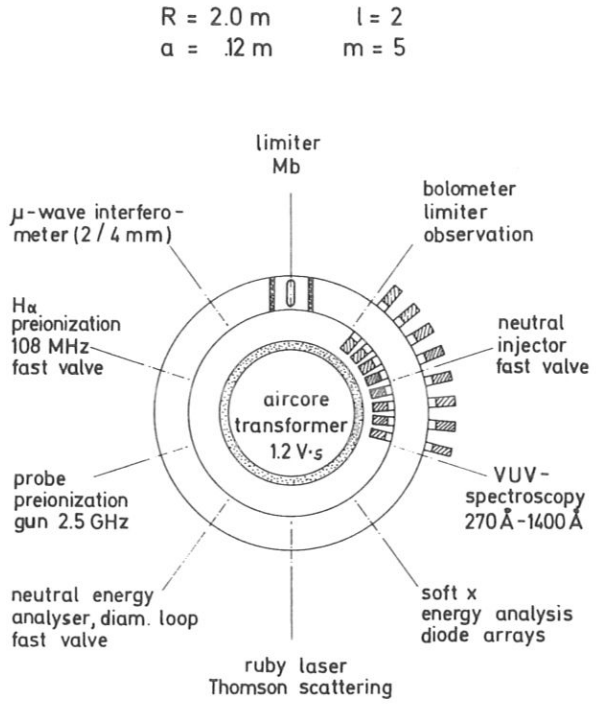

FIG.2. Position of the instrumentation for diagnostics.

defined by the magnetic surface contacting the molybdenum limiter is a = 10 cm (a = geometric mean of the axis of the ellipse.) The plasma current does not modify this result appreciably [3]. This result is also confirmed by the measured temperature and density profiles.

MODE OF OPERATION

During the first period of operation cleaning discharges at 50 Hz, $B_0 = 0.4$ T, $\iota_0 = 0.23$ and the study of effective preionization methods were carried out. The base pressure in the vacuum chamber which is not bakeable could be reduced below 10^{-7} torr with H_2O being the dominant impurity.

Two hours of cleaning discharges in Ne (50 Hz at 5 kW) precede the normal pulsed operations with ohmic heating. The time sequence of a pulse consists of a 10 ms rf pulse (108 MHz, 3 kW) started by a Ti/H_2 gun which produces a plasma with $n_e \leqslant 10^{18}$ m^{-3}. The length of the following OH-discharge normally is 100–200 ms. Preionization with 2.4 GHz and (or) with a neutral injector (30 kW) will be available in the future.

Since for technical reasons the coupling between air core transformer and plasma current is weak and control of the loop voltage is not yet available, the voltage always decays as programmed by the passive circuitry. Shaping of the plasma current is only possible by additional neutral gas

pulses during the discharge. Additional gas feeding is necessary since recycling from the wall is not sufficient to maintain the plasma density. With an elaborate system of fast acting valves around the machine (response time < 1 ms) the neutral particle flux of $\Gamma = 10^{19} - 10^{21}$ part./s is controlable. Although the external helical field defines the equilibrium of the plasma, a programmed vertical field is used for corrections of the plasma position.

In addition to the basic magnetic and electrical parameters, results from all diagnostic methods distributed around the machine (see Fig.2) are available. For further improvements methods to measure profiles of ion temperature, VUV radiation, plasma current and the spectrum of synchrotron radiation are in preparation.

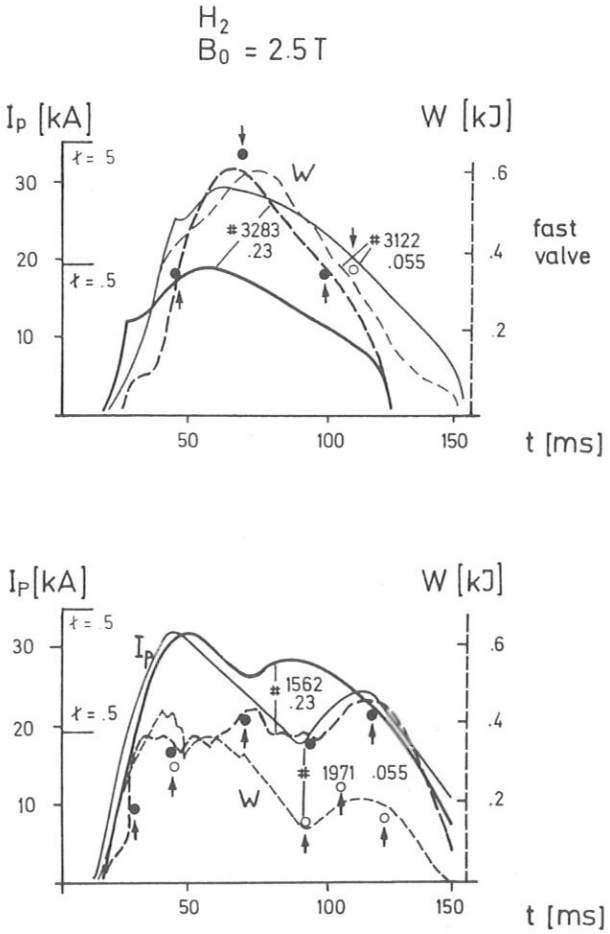

FIG.3. Typical discharges (upper part with gas pulsing) for different external rotational transforms $\iota_0 = 0.055$, $\iota_0 = 0.23$ at $B_0 = 2.5$ T. W(J), the total energy, is measured by diamagnetic loops; marked dots give plasma energy as calculated from profiles of kT_e, n and kT_i.

PARAMETER RANGE

The experiments were performed at 2.5 T toroidal field and mainly at two values of the external helical field: $\iota_0 = 0.23, \iota_0 \gtrsim \iota_p$ ("stellarator" operation) and $\iota_0 = 0.055, \iota_0 \ll \iota_p$ ("tokamak" operation). ι_p is the rotational transform of the plasma current at the edge of the plasma. In all discharges described hereafter the total rotational transform is $\iota = \iota_0 + \iota_p; \iota = 1/q$.

With discharges in hydrogen (filling pressure $5 \cdot 10^{-5}$ torr $- 3 \cdot 10^{-4}$ torr) the following parameter range could be investigated: $\bar{n}_e = 5 \times 10^{18} - 6 \times 10^{19}$ m^{-3}; $kT_{e0} = 200 - 900$ eV; $kT_{i0} = 100 - 220$ eV, plasma current $I_p \leq 37$ kA, loop voltage $3 - 8$ V; energy density $\langle nT \rangle \leq 10^{22}$ eV/m^3.

The Kruskal limit under tokamak conditions ($a \approx 0.1$ m) is 70 kA.

EXPERIMENTAL RESULTS

a) Energy confinement

In order to demonstrate the effect of the helical windings some typical discharges (see Fig.3) with equal current and without additional gas pulse (lower picture) or equal energy density (upper picture) are compared. Without gas pulse the plasma density cannot be increased above 1.5×10^{19} m^{-3}.

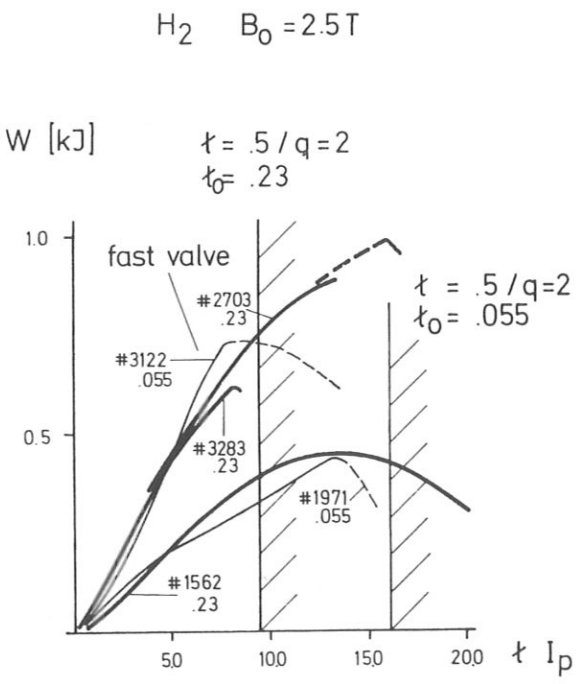

FIG.4. Description of plasma energy versus ιI_p for the discharges given in Fig.3. $\iota = 0.5$ marked for $\iota_0 = 0.055$ and $\iota_0 = 0.23$.

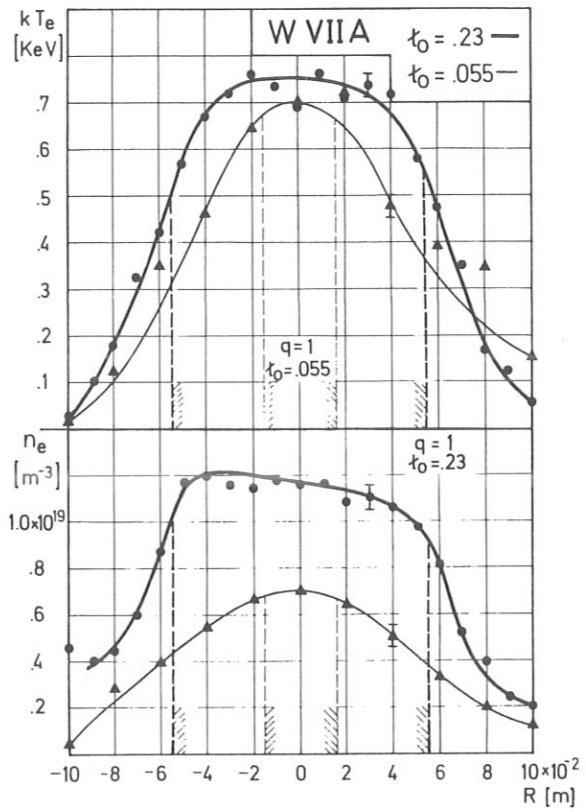

FIG.5. Electron temperature and density profiles:
ι_0 = 0.055, J_p = 23 kA, discharge numbers 2004 – 2014
ι_0 = 0.23, J_p = 22 kA, discharge numbers 1610 – 1641 } *B_0 = 2.5 T*
Radius of q = 1 indicated (calculated from kT_e for Z_{eff} = const.)

During the current rise anomalous loss of density accompanied by onset of MHD-oscillations and bursts of rf oscillations ($\omega = \omega_{ci} \rightarrow \omega_{pi}$) occurs whenever the value of ι at the plasma edge is near a rational number. In discharges with higher density these rf oscillations show pronounced maxima around harmonics of the ion cyclotron frequency.

In the second phase of the discharge the energy density is higher in the "stellarator" case than in the equivalent "tokamak" case. As shown in Fig.3 the difference is roughly a factor 2 at a current of 25 kA. This effect can be explained by the flattened n_e, T_e-profiles of the "stellarator" case (Fig.5) and by the additional confining effect of the helical field. In order to obtain the same plasma energy content in stellarator operation a lower current is needed (Fig.3, upper picture, 18 kA for $\iota_0 = 0.23$ and 28 kA for $\iota_0 = 0.055$). The plasma energy derived from the diamagnetic loop and from the profile measurements agree very well.

The energy density follows the scaling already found in W II B [4] and Uragan [5] : $\langle nT \rangle = A\,\iota\, I_p B_0$, if the current is below a critical value (see Fig.4). The factor A depends on the density regime. The improvement of energy confinement with increasing density can clearly be seen.

The temperature and density profiles measured by Thomson scattering (Fig.5) show the flattening effect of the stellarator field. This effect may be due to m = 1 MHD-modes and internal disruptions within the $\iota \geqslant 1$-surface.

TABLE II. PARAMETERS DERIVED FROM PROFILE MEASUREMENTS OF TWO GROUPS OF DISCHARGES WITH EQUAL CURRENTS.
($k\overline{T} = \int nkT\, r\, dr / \int n\, r\, dr$; $\bar{n} = 2\int n\, r\, dr/d^2$; β_θ includes the field of the plasma current only, τ_E' = electron plasma energy/Ohmic power, τ_E = total plasma energy/Ohmic power).

	Without gas pulse		With gas pulse	
	$\iota_0 = 0.23$	$\iota_0 = 0.055$	$\iota_0 = 0.23$	$\iota_0 = 0.055$
Discharge numbers	1610 – 1641	2004 – 2014	3248 – 3263	3110 – 3129
ι_p/ι_0	1.61	6.6	1.1	4.9
ι	0.6	0.42	0.53	0.32
I [kA]	22.0	23.0	18.2	17.5
U [V]	5.7	3.8	4.6	3.8
t [ms]	120	160	70	110
n_{e0} [10^{19} m^{-3}]	1.1	0.7	5.9	2.92
$\bar{n}_e$ [10^{19} m^{-3}]	0.68	0.33	3.4	1.6
kT_{e0} [eV]	760	674	251	526
$\overline{kT_e}$ [eV]	432	390	178	269
kT_{i0} [eV]	220	95	185	180
W [J]	390	142	566	358
β_θ	0.78	0.28	1.8	1.3
Z_{eff}	8.7	3.7	1.2	2.3
$j(0)$ [$A \cdot m^{-2}$]	199×10^4	212×10^4	106×10^4	234×10^4
τ_E' [ms]	2.7	1.6	6.8	5.5
τ_E [ms]	2.0	1.4	4.4	4

A slight asymmetry found in some density profiles cannot yet be explained.

The energy confinement time τ_E' derived from the profiles varies between 1 ms and 7 ms. The difference to the Bohm time is a factor of 10–20. The confinement time increases with electron temperature and density, the measurements are not yet detailed enough in order to show a scaling with the helical field.

A comparison of the two types of discharges and the quantitites derived from the profiles are given in Table II. The energy confinement time τ_E including the ion energy is 2–8 ms. Without gas pulse Z_{eff} which is calculated from the temperature profiles is between 2.5 and 8.7, in the discharge with gas pulse these numbers are reduced to 1.2–2.5. In the latter case these results are confirmed by X-ray measurements. The two groups of discharges described above represent the state of art.

b) MHD-oscillations and disruptive instability

A remarkable difference between the two types of discharges is the behaviour of the disruptive instability. It is not possible to cross the $\iota = 0.5$ limit in "tokamak" operation since the discharge is terminated at $I_p = 32$–35 kA by a disruption. Also incorrect positioning of the plasma

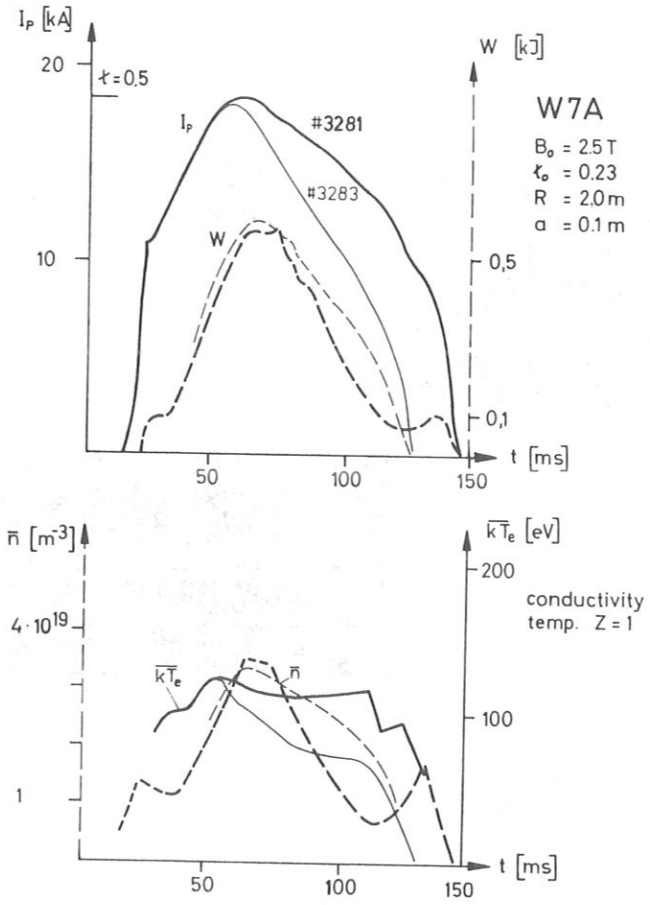

FIG. 6. Loss of plasma energy near $\iota = 0.5$. W plasma energy, $\bar{n}$ plasma density and $k\overline{T_e}$ (calculated for $Z_{eff} = 1$) are given for discharges with slightly changed $I_{p,max}$.

column and a strong gas pulse lead to a disruption, sometimes at $\iota = 0.33$ (q (a) = 3). Already below these critical values the energy confinement decreases due to the onset of strong MHD-oscillations (see Fig.4) as seen by pick-up coils.

In "stellarator" operation the current can be raised to a value of 37 kA ($\iota \approx 0.8$) without a disruption. Also here the energy content is reduced at high currents, the optimum current being between 20 and 25 kA. $\iota = 0.5$ is passed at 16–18 kA. This drop in energy density seems to be correlated with the enhanced MHD-activities at rational values of ι, ($\iota = \frac{1}{3}, \frac{1}{2}, \frac{2}{3}$). At these numbers of ι during current buildup also large voltage spikes (up to 200 V) are observed at the limiter, which consists of four insulated segments. The four signals obtained are different and depend on the orientation of the magnetic surfaces and the plasma position. The investigation of a discharge close to $\iota = 0.5$ (see Fig.6) shows that mainly the particles are lost during this phase. The conductivity temperature increases at the same time. The discharge is maintained at a lower energy level. Scrape-off of magnetic islands or large convective cells may be a possible explanation for this anomalous loss. Asymmetric density profiles as mentioned above may be correlated with this

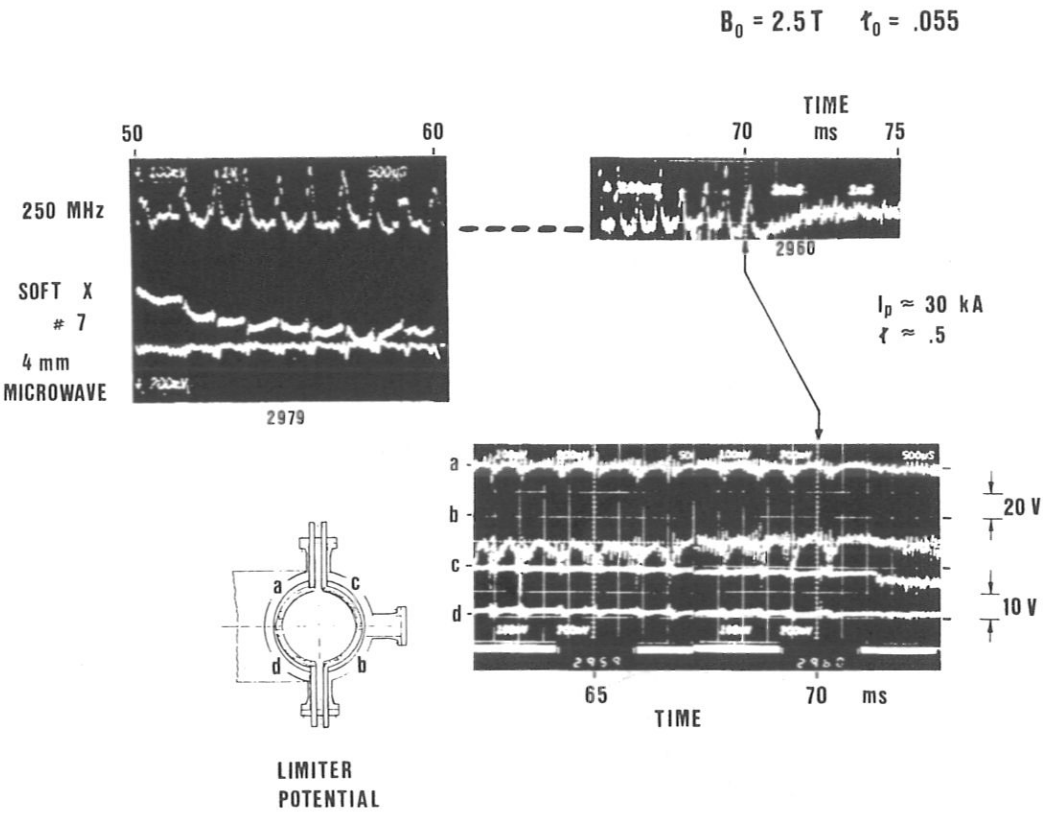

FIG. 7. Sawtooth relaxations and MHD modes at ι_0 = 0.055. Limiter signals are shown in the lower photograph on the right-hand side.

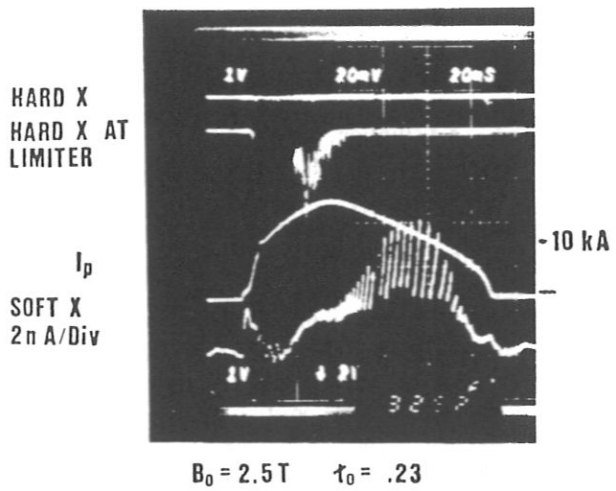

FIG. 8. Sawtooth relaxations at ι_0 = 0.23 and high density shown by the soft X-ray signal (discharge No. 3252).

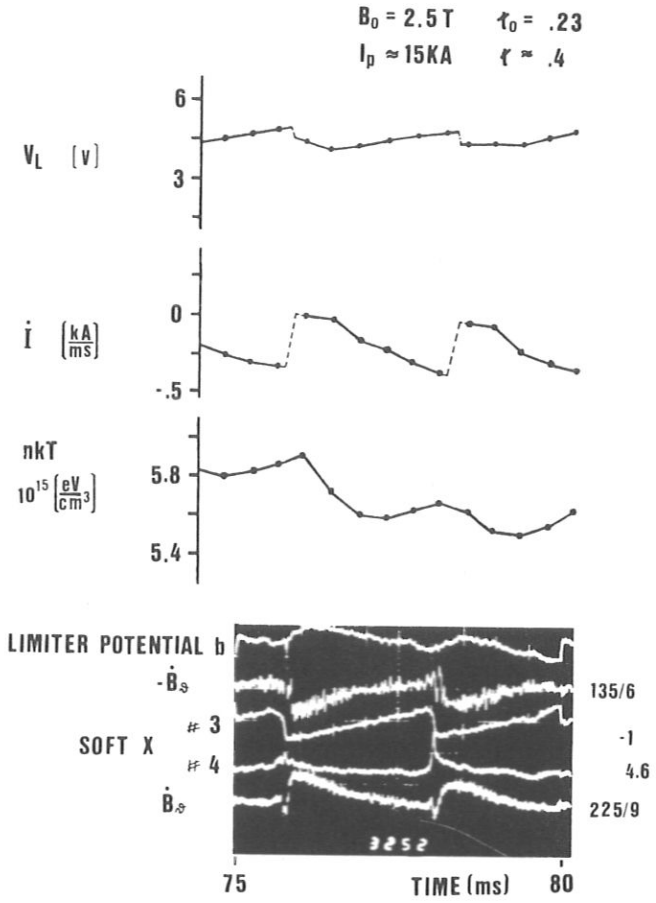

FIG. 9. Sawtooth relaxations and MHD modes of same discharge 3252 for t between 75 and 80 ms, observed by various diagnostics.

effect. Together with this phase of anomalous loss, enhanced radiation of molybdenum, iron and oxygen lines are observed. Bolometric measurements also show an enhanced loss, whereas in the quiescent phase radiation losses do not contribute essentially to the energy balance.

Further investigation of the MHD-modes may clarify these phenomena. Whether the external non-resonant helical field stabilizes the disruption by shaping the plasma profiles or by suppressing the mode coupling mechanism of MHD-modes cannot yet be decided by the present measurements.

c) Sawtooth relaxations

After current build-up sawtooth relaxations and MHD modes are observed at various diagnostics. Under certain conditions, m = 1 and m = 2 modes are identified by means of the Mirnov coils.

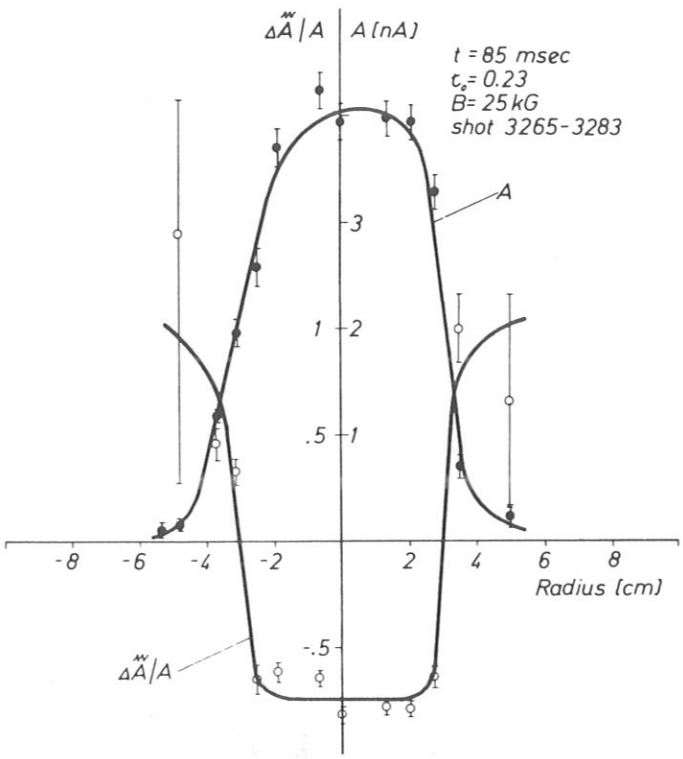

FIG.10. Radial profile of soft X-ray flux A and relative sawtooth amplitude $\Delta\tilde{A}/A$.

For $\epsilon_0 = 0.055$ soft X-ray fluctuations are shown in the upper left part of Fig.7, which are correlated with variations of the 4 mm microwave interferometry signal. Also in coherence with the relaxations, bursts of rf emission are measured with a probe located at the plasma edge. The right half of the figure shows the correlation of the rf bursts with the limiter potentials.

Figure 8 shows the plasma current and soft X-ray waveforms for $\epsilon_0 = 0.23$ at a high electron line density of about 7×10^{18} m^{-2}. Around $t = 80$ msec of the discharge, the large relaxation alone would limit the electron energy confinement time to 7–13 msec. Since τ_E' is around 6 msec for the electrons, the electron energy losses due to the internal relaxations is quite substantial. No hard X-rays are observed at this time.

At high densities, the relaxations are observed in the W VII A-stellarator even at the outside, as shown in Fig.9. The relaxations are observed on the following diagnostic signals: loop voltage, limiter potentials, Rogowski coil, diamagnetic signal ($\Delta nT/nT \approx 3\%$), Mirnov coils and on the soft X-ray fluxes. The light emission in the visible from a limiter segment exhibits a similar feature as the potential signal b over this short time interval.

This simultaneous observation of the internal relaxations indicates that the screening of the internal disruptions by the outer layers of the plasma no longer occurs. In spite of this coherent oscillation over the whole plasma column this does not lead to a termination of the discharge.

For this type of discharge, a radial profile of the soft X-ray flux A is shown in Fig.10 together with the relative sawtooth amplitude $\Delta\tilde{A}/A$. From this follows that the radius, where q is supposed to be unity, is about 3 cm. This is around 30% of the effective plasma radius. Assuming Z_{eff} independent of radius, one obtains from the laser temperature profiles a value of about 5 cm for the q = 1 radius.

SUMMARY AND CONCLUSIONS

The comparison of discharges in "stellarator" operation ($\iota_0 = 0.25, \iota_p \lesssim \iota_0$) and "tokamak" operation ($\iota_0 = 0.055, \iota_p \gg \iota_0$) shows the following results:

At $\iota \leqslant 0.5$ and equal plasma currents the plasma energy increases with increasing external rotational transform. Also the radius of the q = 1 surface grows with ι_0. This leads to a flattening of the density and temperature profiles. Apparently the current density is limited by $q \approx 1$ in the central region.

Gas puffing lead to an increase of the density and the energy confinement time, to heating of the ions and a reduction of Z_{eff} to 1.2.

Close to $\iota = 0.5$ ($\iota_0 = .0.05$) strong MHD-modes [m = 1, m = 0] appear and the energy confinement becomes worse. Disruptive instabilities limit the rotational transform to $\iota \leqslant 0.5$.

In stellarator discharges ($\iota_0 = 0.23$) no disruptions of the current have been observed, even at $\iota = 0.8$ at the edge of the plasma.

At rational values of ι, ($\iota = \frac{1}{3}, \frac{1}{2}, \frac{2}{3}$) strong losses of plasma energy – mainly caused by particle losses – are observed.

Strong internal relaxations are observed in the regime $0.33 \leqslant \iota \leqslant 0.66$, the frequency decreases inversely with density to 200 Hz. The magnetic and electric signals of these oscillations can be seen outside the plasma.

The possibility of changing current distribution, temperature and density profiles by varying the external rotational transform ι_0 and the MHD-behaviour in the stellarator case yields supplementary information about ohmically heated plasmas confined in toroidal devices. Its pronounced effect on the disruptive instability indicates that the helical field is an effective parameter for studying this important problem.

ACKNOWLEDGEMENTS

We should like to thank all engineers, technicians, operators and the whole technical staff of W VII, who have contributed with their work to these first results of W VII. We also thank Mrs. Weikmann for typing the manuscript.

REFERENCES

[1] Proc. 8th SOFT, Noordwijkerhout, EUR 5182 e, 75 (1974).
[2] RAU, F., et al., IPP Report, Garching IPP 2/231 (1976).
[3] HAMADA et al., Report Nagoya University, JPPJ-238 (1975).
[4] HACKER, H., et al., 5th Int. Conf. Plasma Physics and Contr. Fusion, Tokyo (1974) IAEA-CN-33/B1, Vol. II, p.3.
[5] DIKY, A., et al., 5th Int. Conf. Plasma Physics and Contr. Fusion, Tokyo (1974) IAEA-CN-33/B3, Vol. II, p. 45.

DISCUSSION

ON PAPER IAEA-CN-35/D 2

B. COPPI: What makes Z_{eff} so large in the W VII A?

H. WOBIG: We observe $Z_{eff} = 8–9$ in a late phase of the discharge with low density. Before and during the transition phase at rational ι we observe wall contact and an influx of impurities.

B. COPPI: You have a τ_E that tends to increase with T. Is this associated with a decrease in the effects of collisional modes?

H. WOBIG: It might be, but no experimental data are available to support such an assumption.

M.M.K. KEILHACKER: I would like to ask the same question that has been asked with regard to Cleo in stellarator operation. How does the energy confinement time scale with electron density?

H. WOBIG: We observe an increase in confinement time with density ($\tau_E \sim n_e$). However, this dependence has not been checked completely because not all the parameters can be varied independently.

J.L. JOHNSON: Did you observe a higher Z_{eff} for the tokamak mode than for the stellarator mode because the low transform $\iota = 0.055$ could not provide equilibrium control in this mode before the current rises?

H. WOBIG: The experiment has not yet yielded enough data to reveal a difference of Z_{eff} between the stellarator and tokamak modes.

K. MIYAMOTO: I notice that, in the W VII A device too, the radial electron temperature distribution is flatter in stellarator operation than in tokamak operation, despite the fact that the W VII A and Cleo have different pole numbers ($\ell = 2$ and $\ell = 3$, respectively). Have you any explanation for this?

H. WOBIG: No quantitative explanation is available. I believe that anomalous plasma transport within the $q = 1$ surface, which may be correlated with the internal relaxations, leads to the flattening of the profiles.

IAEA-CN-37/H-3

INVESTIGATION OF THE m=2 MODE AT q-VALUES AROUND 2 IN THE W VII-A STELLARATOR

W VII-A TEAM:

B. CANNICI, G. CATTANEI, A. CAVALLO, D. DORST,
A. ELSNER, G. GRIEGER, H. HACKER, J. HOW,
H. JÄCKEL, R. JAENICKE, P. JAVEL, J. JUNKER,
M. KICK, F. LEUTERER, C. MAHN, S. MARLIER,
G. MÜLLER, W. OHLENDORF, F. RAU, H. RENNER,
H. RINGLER, J. SAFFERT, J. SAPPER, P. SMEULDERS,
M. TUTTER, O. VOLLMER, A. WELLER, E. WÜRSCHING,
H. WOBIG, M. ZIPPE
Max-Planck-Institut für Plasmaphysik,
Association Euratom-IPP,
Garching,
Federal Republic of Germany

Abstract

INVESTIGATION OF THE m=2 MODE AT q-VALUES AROUND 2 IN THE W VII-A STELLARATOR.

In the W VII-A stellarator with Ohmic heating, radial profiles of q(r) are similar to those in tokamaks. The m=2, n=1 tearing mode is observed over a wide range of plasma parameters extending to regions where current disruptions usually occur in comparable tokamaks. Typical frequencies are 1–20 kHz; the relative amplitude can reach 2.5% without disruptions. The amplitude of the m=2 mode decreases with increasing helical field or external rotational transform. Simultaneously with the onset of a coupling between the m=1 and m=2 mode, a steep increase of the m=2 amplitude is observed, which is caused either by an increase of the plasma current, by the electron density, or by the content of low-Z impurities. The occurrence of disruptions in tokamaks may be connected with the locking of the m=2 mode at the limiter as observed in W VII-A under these conditions.

INTRODUCTION

The Garching Stellarator WENDELSTEIN VII-A provides an external rotational transform $\iota_o \leq 0.23$ with low shear [1]. For ohmically heated plasmas, radial profiles of j(r) and q(r) derived from measured temperature profiles are similar to those in Tokamaks, but usually the flat internal region within r(q=1) is broader.

Low-frequency fluctuations are observed with mode structures proportional to $\exp i(\omega t - m\theta + n\varphi)$, where θ and φ are the poloidal and toroidal angles, respectively, ω is the angular frequency in the laboratory frame, and m and n are integers.

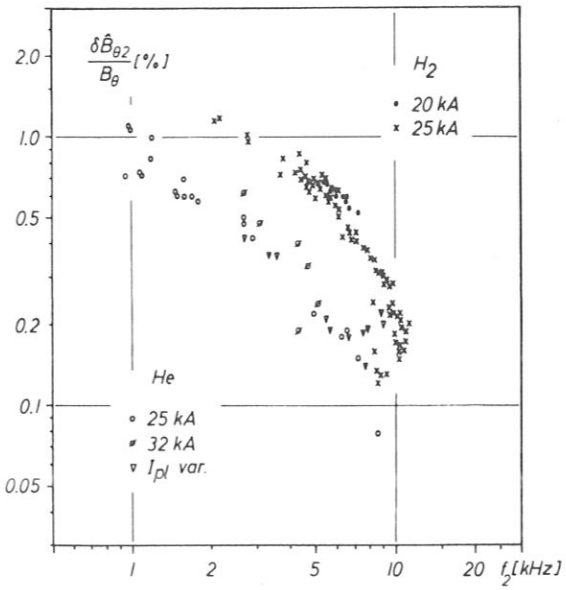

FIG. 1. Relative amplitude as a function of the frequency of the m=2, n=1 mode for H_2 and He and various plasma currents at $B_0 = 3.5$ T and $\iota_0 = 0.11$. I_{pl} var. means that the plasma current has been varied from 8 to 30 kA (cf. Fig. 4).

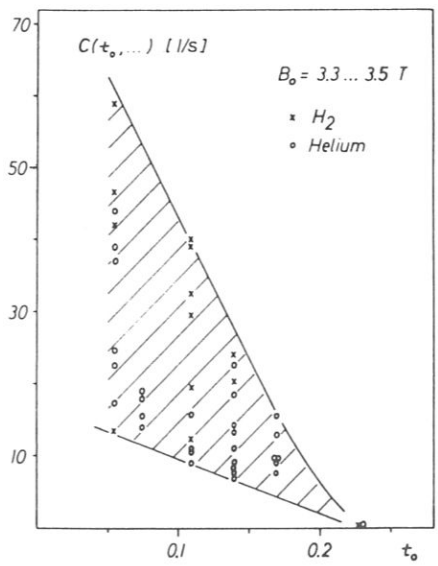

FIG. 2. C versus the external rotational transform ι_0 for discharges in H_2 and He. C describes the dependence of the relative amplitude of the m=2, n=1 mode on ι_0. The spread of the points reflects that C is also dependent on other discharge parameters.

The mode structure is analysed by means of 3x4 poloidal magnetic field probes and 12 soft X-ray diodes. The modes can be attributed to rational magnetic surfaces with a rotational transform $\iota = 1/q = n/m$.

The dependence of the m=2, n=1 mode on various parameters like ι_o, n_e, I_{pl} and its influence on other discharge parameters is discussed in this paper.

DEPENDENCE ON EXTERNAL ROTATIONAL TRANSFORM

At small external rotational transform, $\iota_o \leq 0.11$, the m=2, n=1 mode is the dominant one, similar to the tearing modes in Tokamaks [2,3]. In W VII-A, however, the relative amplitude, $\delta\hat{B}_{\theta 2}/B_\theta$, of the m=2 mode is decreasing with increasing ι_o (B_θ is the poloidal field of the plasma current alone). This indicates that the mode stability is markedly improved by the external helical fields. Figs 1 and 2 will be used to demonstrate this behaviour by separating the dependence of the m=2 amplitude on parameters other than ι_o as far as possible.

In Fig. 1 for a fixed value of $\iota_o = 0.11$ the range of amplitudes and frequencies, f_2, of the m=2 mode is shown for discharges in H_2 and He at various plasma currents, I_{pl}. This figure is obtained by varying the electron density, n_e, and demonstrates that the product

$$\frac{\delta\hat{B}_{\theta 2}}{B_\theta} \cdot f_2 = C$$

is only weakly dependent on f_2, n_e and I_{pl}. Further, it was observed that f_2 is close to the electron diamagnetic drift frequency, $f_{diam.el.}$, which is not explicitly depending on ι_o. Hence, it follows from

$$\frac{\delta\hat{B}_{\theta 2}}{B_\theta} \approx \frac{C}{f_{diam.el.}} = C(\iota_o,\ r(q=2),\ldots?) \cdot B_o \cdot \left.\frac{n_e}{\nabla p_e}\right|_{r(q=2)}$$

that the dependence of the amplitude on ι_o is contained only in the factor C which is shown in Fig. 2. The decrease of the m=2 amplitude with increasing ι_o can clearly be seen, and at $\iota_o = 0.23$ the m=2, n=1 tearing mode has no longer been observed.

DEPENDENCE ON n_e, I_{pl} AND IMPURITIES

Close to Tokamak operation, at $\iota_o = 0.055$, curve a) of Fig. 3 shows the typical behaviour of the m=2 mode amplitude with increasing n_e at constant plasma current. The steep increase of the amplitude in the range between $n_{eo} = 3$ and 4×10^{13} cm^{-3} occurs together with the onset of a coupling between the m=1 and m=2 mode as seen from the soft X-ray signals [2,3,4]. Simultaneously, the sawtooth amplitude decreases [3,4]. Hydrogen and helium discharges show a similar behaviour, but in helium the mode amplitude usually has its increase at somewhat higher densities.

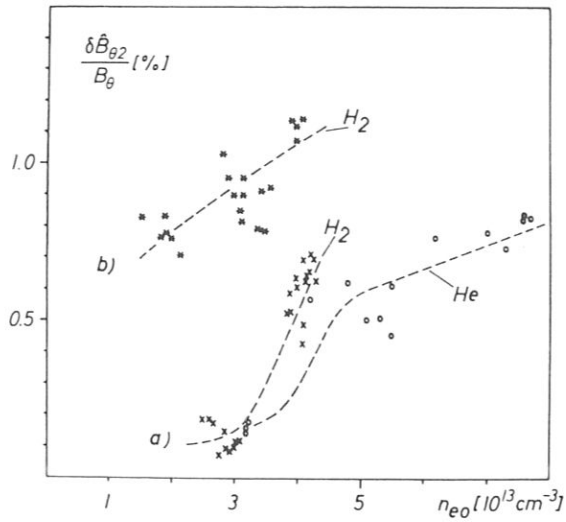

FIG.3. Relative amplitude of the m=2, n=1 mode versus the central electron density n_{e0} for $B_0 = 3.5$ T, $\iota_0 = 0.055$ and for two different plasma currents: (a) $I_{pl} = 25$ kA; $q(a) \approx 3.7$; (b) $I_{pl} = 34$ kA; $q(a) \approx 2.9$. Measurements were taken as a function of microwave line density. For convenience, this was converted into n_{e0} by assuming a parabolic profile.

At higher plasma currents of 34 kA the amplitude of the m=2 mode is considerably larger at low densities (Fig. 3, curve b)). Predisruptions [4] are now seen on the soft X-ray signals close to the q=2 surface which trigger sawteeth at q=1. This may be the cause of the amplitude and frequencies of the m=2 mode being modulated up to $\pm$ 40 % in correlation with the sawteeth. No strong coupling between the m=1 and m=2 mode can be observed in this case. The predisruption phenomenon disappears at higher values of ι_0.

For ι_0 = 0.11 - 0.14 the dependence of the amplitudes and frequencies of different modes on I_{pl} and n_{e0} is shown in Figs 4 and 5. Fig. 4 shows the dependence of the m=2 mode on I_{pl} for nearly constant n_{e0}, and Fig. 5 its dependence on n_{e0} for fixed I_{pl}. In both cases the amplitude of the m=2 mode increases steeply with I_{pl} or with n_e, simultaneously with the onset of a coupling between the m=1 and the m=2 mode.

Progressively with increasing amplitude, the rotation of the m=2 islands is impeded by an interaction with the limiter [3]. The separatrix of the islands seems to be locked to the limiter for an increasingly longer period and therefore the frequency finally goes to zero. For an intermediate situation typical oscilloscope traces are shown in Fig. 6. The phases of the limiter signals shown correspond to the m=2 structure. The distance between the calculated q=2 surface and the effective plasma radius is 1.5 cm. Therefore, if the m=2 islands extend to the plasma edge, their full width would have to be about 3 cm. Similar statements were made by the TFR Group [3].

After having reached a maximum amplitude, either for $q(a) \approx 2.5$ or for $n_{eo} \approx 8 \times 10^{13}$ cm^{-3}, the m=2, n=1 mode is no longer visible. Then a m=3, n=2 mode usually remains, being sometimes coupled with a mode which appears to be m=2, n=2.

Injecting a fixed small quantity of neon into helium discharges of various densities, the maximum of the m=2 amplitude is shifted to lower densities.

Summarizing, to generate the steep increase of the amplitude of the m=2 mode, it is equivalent to increase

(i) the plasma current,
(ii) the electron density, or
(iii) the content of low-Z impurities.

m=2 MODE AND DISRUPTIONS

Fig. 5 shows that for $n_{eo} \approx 7 \times 10^{13}$ cm^{-3} the behaviour of the amplitude and the frequency of the m=2 mode with increasing density is very similar to the time evolution of the m=2 mode in Tokamaks immediately before a disruption [2,3]. In the Stellarator W VII-A these phenomena, which are highly transient in a disrupting Tokamak discharge, can be studied under stationary conditions by varying the density from shot to shot. It is interesting to note that a drastic reduction of the energy confinement time τ_E coincides with the steep increase of the amplitude of the m=2 mode (Fig. 5, upper part)[5]. Since many other plasma parameters like T_e, Z_{eff} or the impurity radiation vary simultaneously, it is difficult to decide whether the m=2 mode is responsible for the decreasing confinement, or whether the change of other parameters diminishes the confinement [6] and causes the m=2 mode to grow at the same time. In a Tokamak the corresponding rapid loss of thermal energy [2] results in an inward shift of the plasma as observed during a disruption, whereas in W VII-A the helical fields provide an equilibrium position for the plasma which helps to avoid disruptions; they are absent if the external rotational transform $\iota_o \gtrsim 0.14$.

Although the circumstances usually leading to disruptions in Tokamaks have been studied in detail in W VII-A, the disruption phenomenon itself has rarely been investigated systematically. The following has been observed: (i) For $\iota_o = 0.055$ and high electron densities it is possible to obtain disruptions with a behaviour of the m=2 mode similar to that in Tokamaks. (ii) At $\iota_o = 0.11$, $q(a) \approx 2$ and high electron densities ($n_{eo} = 1.4 \times 10^{14}$ cm^{-3}), disruptions have also been observed in cases where no m=2 mode was visible, but a small m=3, n=2 mode was dominant. (iii) Under similar conditions, but reducing n_e to 1/10 of the above value, an amplitude of the m=2 mode up to 2.5 % has been measured without occurrence of disruptions.

FURTHER EFFECTS RELATED TO m=2 MODES

Strong m=2 modes modulate the signals also of various other diagnostics in W VII-A, e.g. the total plasma current

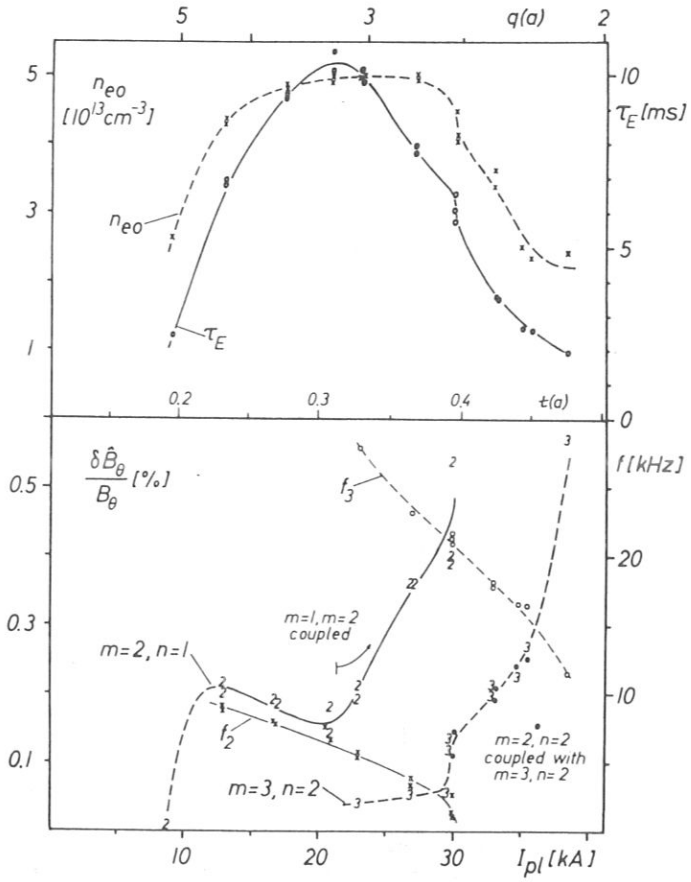

FIG.4. Variation of the relative amplitude and the frequency of the different modes observed with increasing plasma current for helium discharges at $B_0 = 3.5$ T and $\iota_0 = 0.11$. In the upper half the simultaneous variation of the central density n_{e0} and the energy confinement time τ_E derived from the diamagnetic signal is shown. The discharges are performed with identical amounts of He introduced during current build-up.

($\delta I_{pl}/I_{pl} \lesssim 0.1$ %), the microwave density ($\delta n_e/n_e \lesssim 5$ %), the limiter potentials ($\Delta U \lesssim 5$ V), and the H_α or He I emission seen in the limiter plane ($\delta I/I \lesssim 2$ %). Comparing the phases of the m=2 oscillations on the magnetic probes with those of the microwave density and the soft X-ray diodes indicates that the fluctuations of the current density and of the electron temperature are in phase and out of phase to those of the electron density. This seems to be consistent with the model for tearing modes, since for kink modes all three of them should be in phase.

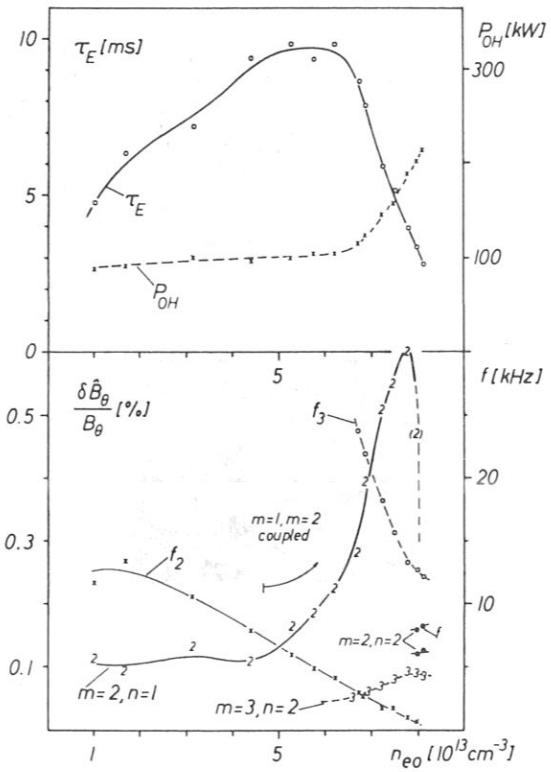

FIG. 5. Variation of the relative amplitude and the frequency of the different modes observed with increasing central density for helium discharges with constant plasma current I_{pl} = 20 kA ($q(a) \approx 2.9$) at B_0 = 3.5 T and ι_0 = 0.14. In the upper half the simultaneous variation of the energy confinement time τ_E and the Ohmic heating power P_{OH} is shown.

m=2 MODE AT q < 2

In correlation with sawteeth, a m=2, n=1 mode can still be observed at q(a) < 2. An example is given in Fig. 7 where the m=2 mode grows already during the risetime of the sawteeth. Usually, only one to two cycles with large amplitude can be seen immediately after the sawtooth disruptions. Presumably, the sawteeth give rise to changes in the profiles, thus creating a m=2 mode for a short time. Since the rational q=2 surface is now beyond the limiter, this could be a m=2, n=1 external kink mode.

SUMMARY

The relative amplitude of the m=2 tearing mode decreases with increasing ι_0, and for ι_0 = 0.23 this mode has no longer been observed.

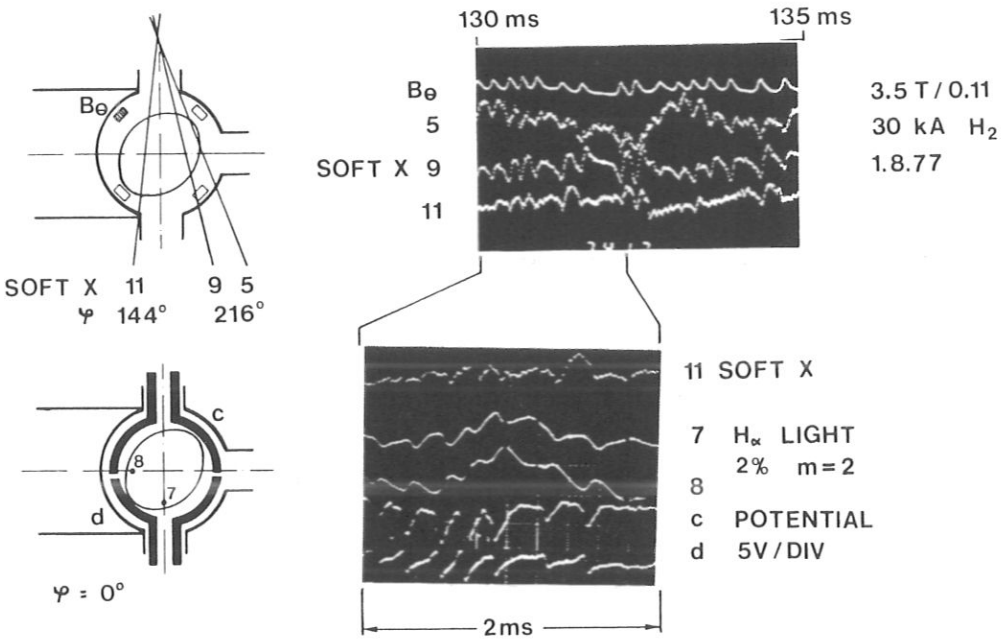

FIG.6. m=2 mode locked to the limiter for irregular intervals. The upper half shows traces of one B_θ coil and of 3 soft X diodes, viewing along different plasma chords (see top insert). In the lower half the corresponding fluctuations of two H_α light signals and two limiter potentials are recorded at an increased sweep. The image points 7 and 8 and the two limiter segments c and d are identified in the lower insert.

A steep increase of the mode amplitude always occurs simultaneously with the onset of a coupling between the m=1 and m=2 modes.

This increase can be generated by increasing I_{pl}, n_e or the content of low-Z impurities.

At large m=2 amplitudes locking of the m=2 islands to the limiter is observed. In comparable Tokamaks this effect usually leads to current disruptions which do not occur in W VII-A if t_o is large enough.

As far as the dependence of the energy confinement on the m=2 amplitude is concerned, no definite answer can be given yet, since several competitive and perhaps even counteracting effects are active at the same time.

ACKNOWLEDGEMENTS

This paper would not have been possible without the continuous endeavours of the technical crew.

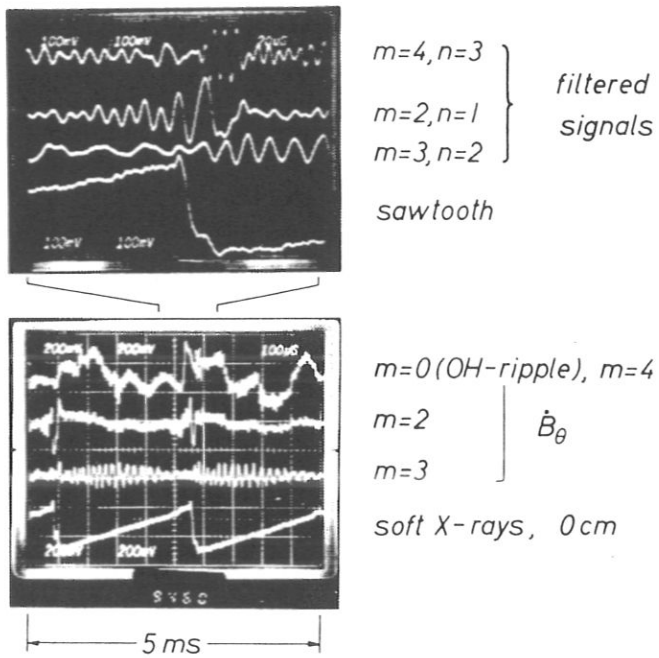

FIG. 7. Time behaviour of different modes and their correlation to sawteeth signals on the central soft X diode for a H_2 discharge at $B_0 = 3$ T, $\iota_0 = 0.23$ and $q(a) \approx 1.65$. By using series connections of B_θ coils, the individual modes have been separated according to their m numbers.

REFERENCES

[1] W VII-A Team, in Plasma Physics and Controlled Nuclear Fusion Research (Proc. 6th Int. Conf. Berchtesgaden, 1976) 2, IAEA, Vienna (1977) 81.

[2] KARGER F., et al., in Plasma Physics and Controlled Nuclear Fusion Research (Proc.6th Int.Conf. Berchtesgaden, 1976) 1, IAEA, Vienna (1977) 267.

[3] EQUIPE TFR, Nucl. Fusion 17 (1977) 1283.

[4] W VII-A Team, in Controlled Fusion and Plasma Physics (Proc. 8th Europ. Conf. Prague 1977) 1 (1977) 127 and 2 (1977) 236;

W VII-A Team, in Controlled Fusion and Plasma Physics (Proc.8th Europ. Conf. Prague 1977) 2 (1977) 73.

[5] Berry, L.A., et al., in Plasma Physics and Controlled Nuclear Fusion Research (Proc.6th Int.Conf. Berchtesgaden, 1976) 1, IAEA, Vienna (1977) 49.

[6] W VII-A Team, paper IAEA-CN-37/H-2, these Proceedings.

DISCUSSION

N. SAUTHOFF: One interpretation of the "locking" of the (2,1) and (1,1) modes and the (3,2) and (2,2) modes is that toroidal – i.e. (1,0) – effects induce mode components of (m ± 1,n). Does this toroidal eigenmode phenomenon correspond to your observations?

R. JAENICKE: There is strong evidence that all the observed modes are different modes, belonging, for example, to different rational surfaces given by $\iota = n/m$.

J.P. FREIDBERG: In a tokamak, increasing the current eventually leads to disruptions. Is there, in a stellarator with fixed Ohmic heating current, any analogous instability anticipated as the amplitude of the stellarator field is increased?

R. JAENICKE: No, but the confinement will eventually be lost, since the current density is limited to $q \geqslant 1$. Therefore, the radius of the $q = 1$ surface approaches the plasma radius, and inside the $q = 1$ surface the transport coefficients can be considered to be infinite.

ENERGY AND PARTICLE CONFINEMENT IN THE OHMICALLY HEATED W VII-A STELLARATOR

W VII-A TEAM:

B. CANNICI, G. CATTANEI, A. CAVALLO, D. DORST, A. ELSNER, G. GRIEGER, H. HACKER, J. HOW, H. JÄCKEL, R. JAENICKE, P. JAVEL, J. JUNKER, M. KICK, F. LEUTERER, C. MAHN, S. MARLIER, G. MÜLLER, W. OHLENDORF, F. RAU, H. RENNER, H. RINGLER, J. SAFFERT, J. SAPPER, P. SMEULDERS, M. TUTTER, O. VOLLMER, A. WELLER, E. WÜRSCHING, H. WOBIG
Max-Planck-Institut für Plasmaphysik,
Association Euratom-IPP,
Garching,
Federal Republic of Germany

Abstract

ENERGY AND PARTICLE CONFINEMENT IN THE OHMICALLY HEATED W VII-A STELLARATOR.

The density regime in the Wendelstein stellerator has been extended to $\bar{n}_e = 10^{20}$ m^{-3} by gas puffing in helium discharges. The density seems to be limited already by small amounts of impurities (i.e. $\leqslant 1\%$ of oxygen). These radiate at the plasma edge, constrict the discharge, and finally terminate it when the losses exceed the available Ohmic heating power. The energy confinement time τ_E increases with electron density but reaches a maximum followed by a rapid decrease connected with strong radiation losses. The particle confinement time shows a similar behaviour. Maximum densities were obtained for stationary helium discharges with $B_0 = 3.5$ T, $I_p = 35$ kA, and the external rotational transform $\iota_0 = 0.14$. For smaller values of the rotational transform the density increase is limited by disruptive instabilities. The ion temperature agrees with neoclassical scaling.

INTRODUCTION

The Wendelstein VII-A stellarator has l=2, m=5 helical windings which, at a main field $B_0 = 3.5$ T, produce an almost shearless external rotational transform $0.055 \leq \iota_0 \leq 0.23$. The major radius is $R_0 = 2.0$ m and the minor radius is defined by the 0.13 m radius of the molybdenum limiter which, because of the elliptical cross-section of the magnetic surfaces, is equivalent to an average plasma radius of ~0.1 m. Results from

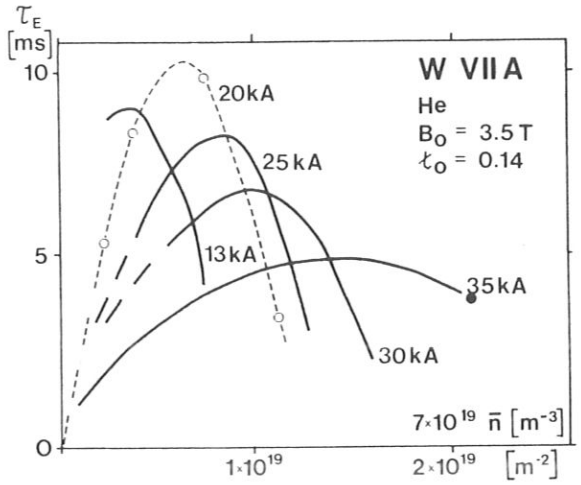

FIG.1. Diamagnetic measurements of the energy confinement time τ_E for helium discharges with various plasma currents I_p. Averaged density $\bar{n} = \int n dA / \int dA$.

ohmically heated plasmas at moderate densities have already been reported at the Berchtesgaden [1] and Prague [2] conferences. Now the investigations have been extended to the high-density regime since high densities are required for sufficient absorption with the nearly perpendicular injection experiment planned for W VII-A. Access to this regime became possible by technical improvements of the OH-circuit, leading to an increase of the control range of the loop voltage from 5 to 10 volts and of the ohmic heating power to 400 kW. Helium was used instead of hydrogen in order to take advantage of the following effects:

For the same temperature the resistivity and thus the available power density rises as Z_{eff} goes from one to two.

Chemical processes leading to a release of oxygen from the wall via the production of water with the impinging atomic hydrogen [3] should disappear in helium discharges. Therefore, the radiation losses should be reduced and the reproducibility improved.

The recycling coefficient ρ is close to one for helium instead of 0.7 for hydrogen [2] so that there is no need for an additional gas feed to maintain stationary conditions.

The main effect found in W VII-A is that even if disruptive instabilities are suppressed, τ_E does not continuously grow with n but goes through a maximum and then steeply decreases. At even higher densities the discharge can no longer be maintained with the available ohmic heating power.

CONFINEMENT AT HIGH DENSITIES

In order to find the optimum confinement conditions for high densities and the physical reason for the density limitation, the external transform, ι_o, and the plasma current, I_p, were varied for B_o = 3.5 T. In Fig. 1 the gross energy confinement time $\tau_E = \frac{W}{P_{OH}}$ is plotted versus n for different currents and ι_o = 0.14, where W is the total plasma energy, and P_{OH} the ohmic input power. All data are taken from quasistationary discharges with pulse lengths >100 ms, where the density was changed by gas puffing during current build-up.

W is calculated from diamagnetic measurements. In hydrogen experiments the values obtained from electron temperature and density profiles measured by Thomson scattering and ion temperatures deduced from charge-exchanged neutrals agreed well with the diamagnetic measurements,but in helium discharges they show a systematic deviation of about -25 %. At lower densities τ_E follows the well-known scaling $\tau_E \sim n$. Also, reduction of τ_E with increasing I_p is observed. Therefore, in this regime τ_E roughly scales with ξ^{-1} where ξ is the drift parameter, $\bar{\xi} \sim \frac{I}{\bar{n}\sqrt{k\bar{T}_e}}$. At higher densities a saturation and a subsequent steep decrease of τ_E is observed. These phenomena are shifted to higher densities if the plasma current is increased. Measurements of the 5015 Å He-I line in three different planes (including that of the limiter) have shown a similar behaviour also for the particle confinement time.

The highest density, $\bar{n} = 10^{20} m^{-3}$ or $\int n dl = 2.2 \times 10^{19} m^{-2}$, was obtained for I_p = 35 kA with $\iota(a) \approx 0.5$ ($q \approx 2$). The input power was 350 kW and $kT_e(o)$ = 200 eV. Fig. 2 gives profiles of n_e and T_e for this discharge. They are flat inside the q=1 surface [1,2], indicating that the transport coefficients are high in this region. The confinement takes place within the rather thin sheath between the q=1 surface and the plasma edge. Rather steep gradients can obviously be balanced there.

Any further increase in n would require an increase of the input power, i.e. of the current density. This could be achieved by lowering the external transform or by increasing B_o. These effects have been observed indeed but, as already stated, a too low external transform ($\iota_o < 0.14$) leads to disruptive instabilities, well known from tokamaks, which prohibit the access to higher densities when approaching q(a) = 2.

In order to illustrate the situation, the ratio of maximum density to maximum current density versus $\iota_p \simeq I_p/B$ is plotted for different values of ι_o in Fig. 3. This procedure is similar to [4] but modified for the inclusion of the stellarator effect. One observes that for larger ι_o, where disruptions are suppressed, the density limit is proportional to the plasma current and to $(1-\iota_o)$. The dependence on B could not be verified since for these experiments B was always between 3 and 3.5 T. Below ι_o = 0.14 the density limit is increasingly determined by disruptions and progressively shifted to lower values. Finally, for

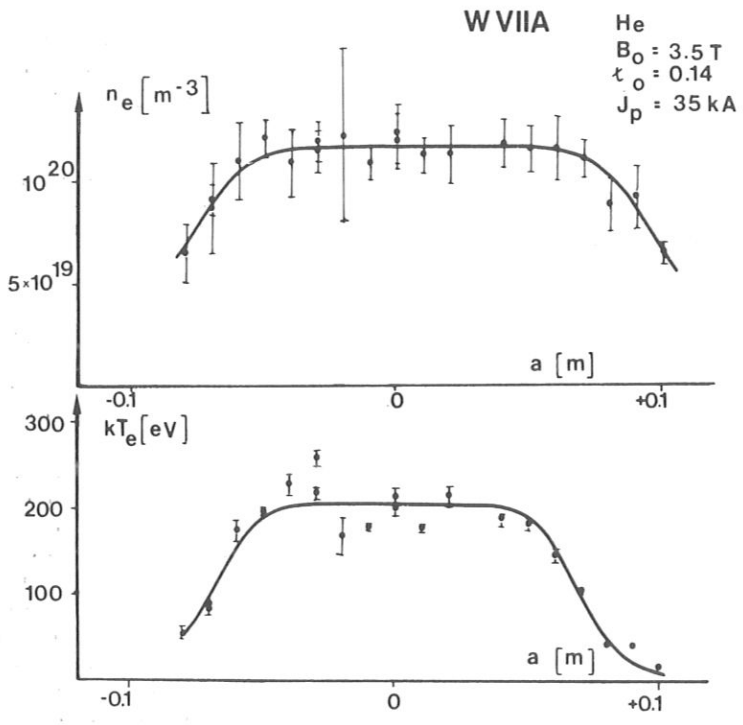

FIG. 2. Measured density and electron temperature profiles at line density 2.2×10^{19} m^{-2} (indicated by ● in Fig. 1).

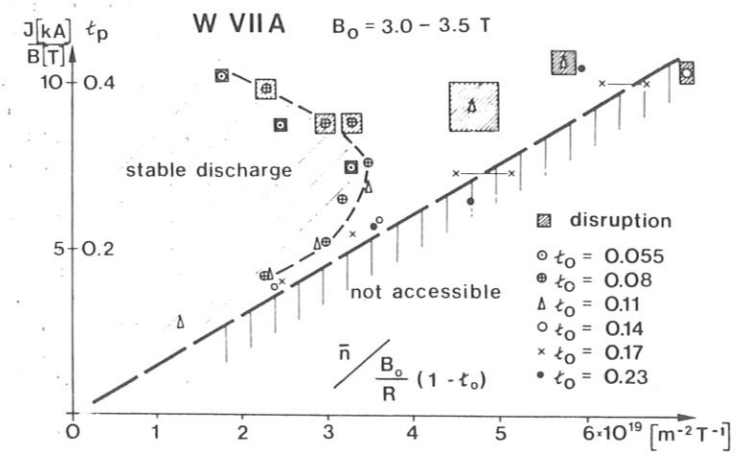

FIG. 3. Density limitations for various I_p and external transforms, ι_0. The average maximum densities divided by the central current densities ($\bar{n}/j(0)$) are plotted versus the internal transform ι_p. The conditions when disruptions determine the discharge are indicated.

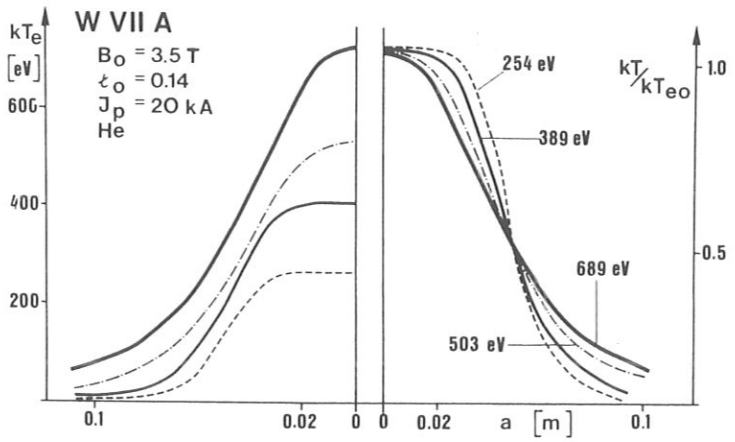

FIG.4. Temperature distributions for the four different discharges marked by ○ in Fig.1. The central temperatures are given for the normalized profiles.

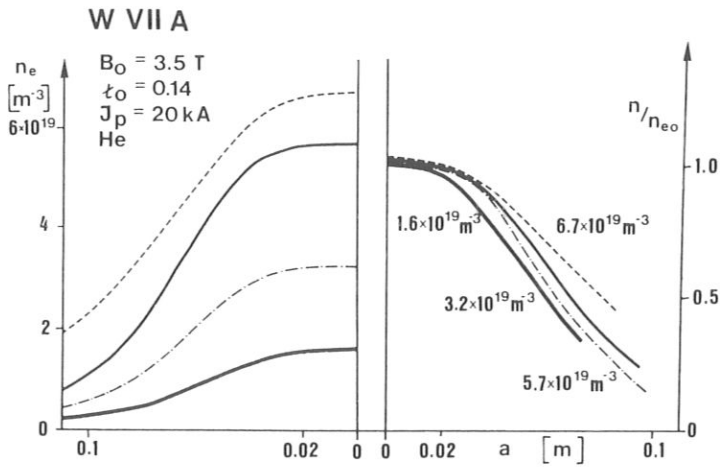

FIG.5. Density profiles corresponding to Fig.4. The central density is given for the normalized profiles.

ι_o = 0.055 the 'disruptive branch' typical for tokamaks is reached. If the density then approaches the critical value for disruptions, a significant change of the MHD modes is observed [5]. At higher external transform, the stronger equilibrium in the helical field may be responsible for maintaining the discharge at higher densities, in spite of the occurrence of phenomena, such as mode coupling and locking to the limiter [5].

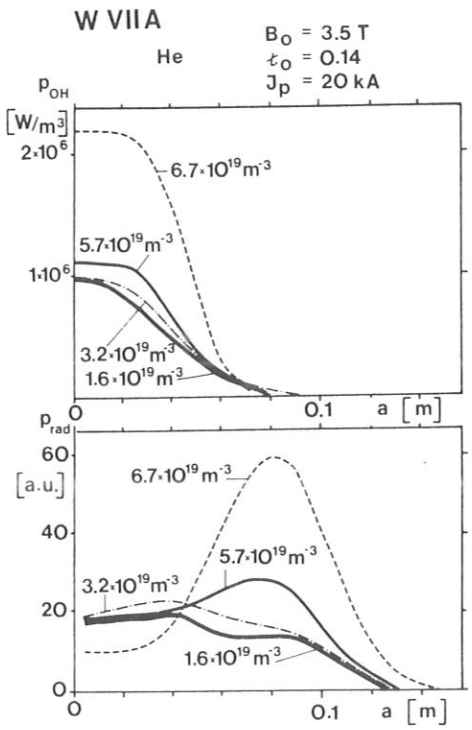

FIG.6. P_{OH}, *heating power density, and relative* P_{rad}, *radiation power density, obtained by Abel inversion from bolometer measurements for the four selected discharges of Figs 4 and 5.* P_{rad} *is given in arbitrary units (a.u.). 100 a.u. are approximately equivalent to* 10^6 $W \cdot m^{-3}$. *The central densities are indicated.*

The dependence of τ_E on n was studied in detail for 20 kA discharges. For a set of density values, Figs 4 and 5 show radial profiles of temperature and density. In addition, the normalized curves were plotted. With increasing n_e the T_e profiles show a strong reduction of T_e in the outer regions as well as a decrease of temperature in the centre. Since the current is kept constant, these effects lead to a concentration of the current towards the centre and, consequently, to an expansion of the q=1 surface since within q=1 the current density is limited to $j \sim \frac{B}{R}(1-\iota_o)$. In this way the region of high transport is expanded and the confinement region reduced by both effects, the expansion of the q=1 surface and the decrease of T_e in the outer regions.

Radially resolved bolometric measurements lead us to believe that the shrinkage of the profiles is caused by radiation cooling of the plasma edge. Fig. 6 shows bolometric measurements for the four discharges of Figs 4 and 5 along with the local ohmic input. At low densities a density increase produces little change in the radial distribution of the radiated power and the ohmic power input as well, indicating that the reduction in

temperature is balanced by a reduction of Z_{eff}. Again one has to keep in mind that I_p is kept constant. The density increase from $3.2 \times 10^{19} m^{-3}$ to $5.7 \times 10^{19} m^{-3}$ and further to $6.7 \times 10^{19} m^{-3}$ does show a definite increase in radiated power at the plasma edge along with an increase of ohmic power in the centre, to account for the additional losses. Since Z_{eff} is around 2 and since the temperature is still more reduced (see Fig. 4), the loop voltage increases to keep up the current.

This radiated power is attributed to impurity radiation. It is responsible for the shrinkage of the T_e profiles and the reduction of the central temperature. It is interesting to note that there is also an indication of radiation from the plasma centre, which seems to decrease for higher densities or decreasing central temperature.

Although the bolometer used has not yet been calibrated with radiation standards, the sensitivity was estimated from its calorimetric properties and the variation of its output signal with the variation of the plasma radiation. This leads to the conclusion that, at least at higher densities, the wall receives about 80 % of the ohmic power input. Another 10 - 20 % of the ohmic power is typically found on the limiter.

RADIATION LOSSES AND IMPURITY CONTENT

In order to look for impurities and their concentration, radial profiles of spectral lines of several species have been taken shot by shot in the UV and VUV region and compared with the bolometer measurements. The spectroscopic measurements give maximum oxygen concentrations of 1 % and Fe concentrations of 0.1 % at $n(o) = 5.7 \times 10^{19} m^{-3}$. These impurities together with the helium radiation may explain the strong radiation losses from the plasma edge (20 - 70 eV) because, as seen from Fig. 5, the electron density at the plasma edge shows a stronger increase than in the centre (for a given temperature, $P_{rad} \sim n_{imp} \times n_e$).

At present there is not a clear picture as far as the comparison with the bolometric measurements is concerned and, in particular, the origin of the radiation from the plasma centre for temperatures above 350 eV is unknown. Photographic recordings, however, with a grazing incidence spectrograph do show many unresolved lines between 60 and 80 Å radiating from the plasma centre. Their identification is not yet clear. If it were Fe, the radiation should extend down to 40 Å and if it were Mo other Mo lines should also occur which were not detected.

To prove that small amounts of impurities radiating from the plasma edge can severely influence the profiles and the confinement, small amounts of Ne were added to the discharges. Neon was selected since, for the conditions of these discharges, it greatly resembles oxygen [6] without showing its intense wall affinity.

Fig. 7 shows τ_E as a function of line density for helium discharges and helium discharges where 10^{17} and 2×10^{17} atoms of

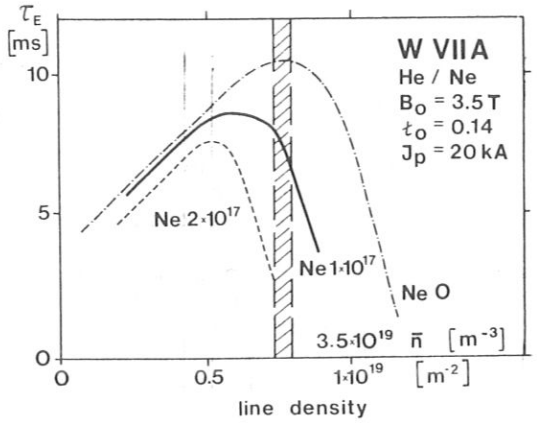

FIG. 7. Energy confinement τ_E versus the density for various neon contents at I_p = 20 kA. At line density 8 × 10^{18} m^{-2} (dashed region), 10^{17} particles correspond to a concentration of 1%.

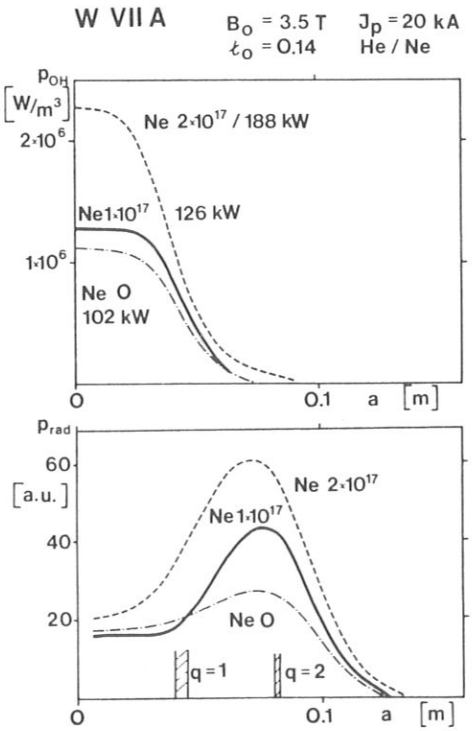

FIG. 8. P_{OH} heating power density and P_{rad} radiation power density for the three cases of Fig. 7 at line density 8 × 10^{18} m^{-2}, central density 5 × 10^{19} m^{-3}.
(P_{rad}: 100 a.u. are approximately equivalent to 10^6 W·m^{-3}.)

Ne had been added. At 8 x 10^{18} m^{-2} line density, this corresponds to 1 % and 2 % impurity content. Again there is little effect at small electron densities, but a drastic change at higher densities. The maximum available density is strongly reduced by this amount of impurity content.

In Fig. 8, radial profiles of radiated power from bolometer measurements along with profiles for the ohmic power input have been plotted. They clearly show the increase of radiated power from the plasma edge. Temperature profiles also shrink for these cases.

So, either by adding small amounts of impurities or by increasing the electron density, one can reach the point where radiative losses influence the temperature profiles and deteriorate the confinement [7] .

Alternatively, the radiation from the plasma centre was increased by adding 3 x 10^{16} atoms of krypton to the discharge. Krypton is expected to radiate from the centre of the discharge, between 200 and 500 eV [6] and the corresponding radiated power was detected by the bolometer. In essence, this leads to a reduction of the effective ohmic heating and thus to a lower central electron temperature. In addition, with increasing helium density the oxygen in the discharge again provides edge cooling and thus a further decrease of the central temperature until the density limit is reached. This confirms the conclusion that edge cooling is responsible for the existence of the density limit rather than radiation losses directly from the plasma centre.

ION HEAT CONDUCTION

An assessment of the contribution of the ion heat conduction to the total energy balance requires the knowledge of the ion temperature and its radial distribution. However, in helium discharges the low charge-exchange rate and the low stripping efficiency do not yield large enough signals to determine the ion temperature by charge-exchange analysis. This problem was circumvented by adding a hydrogen gas puff to the helium discharges and determining the helium ion temperature by measuring the hydrogen ion temperature via charge-exchange analysis. When scanning off the centre, the charge-exchange flux detected by each channel of the energy analyser (0.4 to 2 keV) revealed a strong decrease. In the outer regions, however, the temperature deduced from these signals significantly exceeded the electron temperature. This is not compatible with the electron ion heat-exchange rate, according to which the ion temperature can hardly exceed the electron temperature. For the energy balance it is assumed therefore that the T_e and T_i profiles are proportional to each other.

In Fig. 9 the central values of kT_e and kT_i versus the line density are plotted for the same conditions as in Fig. 7. Theoretical curves for the ion temperature are shown for comparison. They are based on neoclassical ion heat conductivity

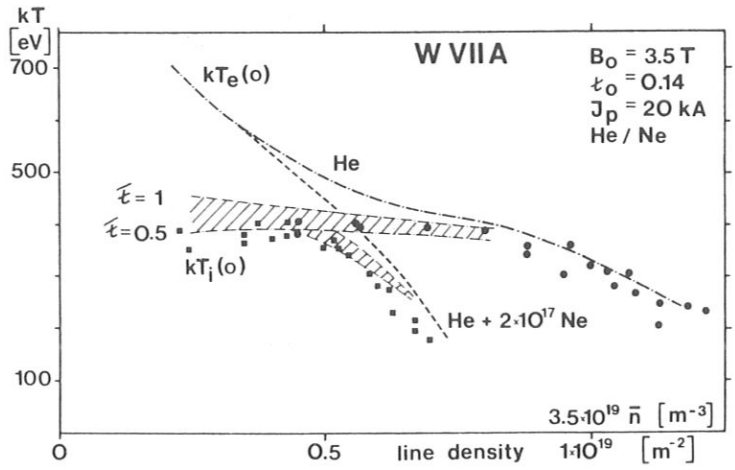

FIG. 9. The variation of the central electron and ion temperatures with density is shown for two different cases; to one of them neon was added. Theoretical curves of the ion temperatures based on the neoclassical heat conductivity for $\bar{\iota}$ = 0.5 and $\bar{\iota}$ = 1.0 are given for comparison (dashed regions).

and on classical heat exchange between electrons and ions. The agreement is quite good. Small deviations between measured and calculated temperatures are probably caused by additional charge exchange losses at low densities and by a transition to the collision-dominated regime at low ion temperatures. In all cases, the power transferred to the ions is only a small fraction of the ohmic power.

SUMMARY

For helium the density range of the Wendelstein VII-A stellarator was extended to $\bar{n}_e = 10^{20}$ m^{-3}.

Low concentrations of impurities, e.g. oxygen less than 1 % at higher densities $\bar{n}_e > 5 \times 10^{19}$ m^{-3}, dominate the confinement by radiation losses at the plasma edge and reduce the temperature. It is interesting to note that this boundary layer may resemble the cold plasma blanket concept. The maximum density is determined by the available ohmic power.

Helium discharges with 1 to 2 % neon added show that the accessible density range is reduced with increasing impurity concentrations since for a given temperature the radiative power increases according to $P_{rad} \sim n_e \times n_{imp}$.

For $\iota_o < 0.14$ the discharge becomes sensitive to disruptive instabilities. The density limit caused by these instabilities coincides with the optimum values obtained in tokamaks related to the restricted current density $j \sim B/R(1-\iota_o)$ within q=1.

Measurements of ion temperature agree with neoclassical expectations. Therefore, the electron - ion heat transfer seems not to be responsible for the reduction of the electron temperature at higher densities.

ACKNOWLEDGEMENTS

This paper would not have been possible without the continuous endeavours of the technical crew.

REFERENCES

[1] W VII-A TEAM, in Plasma Physics and Controlled Nuclear Fusion Research (Proc.6th Int.Conf. Berchtesgaden, 1976) 2, IAEA Vienna (1977) 81.

[2] W VII-A TEAM, in Controlled Fusion and Plasma Physics (Proc.8th Europ.Conf. Prague 1977) 2 (1977) 73.

[3] F. WAELBROECK, H.J. DIETZ, P. WIENHOLD, Rep.Jül.-1448 (1977).

[4] J.W.M. PAUL et al., in Controlled Fusion and Plasma Physics (Proc.8th Europ.Conf. Prague 1977) 2 (1977) 49.

[5] W VII-A TEAM, paper IAEA-CN-37/H-3, these Proceedings

[6] D.E. POST et al., Atomic Data and Nuclear Tables 20 (1977) 397-439.

[7] P.H. REBUT, B.J. GREEN, in Plasma Physics and Controlled Nuclear Fusion Research (Proc. 6th Int.Conf. Berchtesgaden, 1976) 2, IAEA Vienna (1977) 3.

DISCUSSION

R.W. CONN: It has been suggested that τ_e scaling in stellarators is similar to that found in tokamaks and that, given comparable machines, similar confinement is obtained. However, both your paper and the one presented by D.J. Lees (paper H-1) indicate that $\tau_E \propto n$ scaling is not found in stellarators, but that τ_E varies as the drift parameter. What is your opinion on this question at present?

H. RENNER: At low currents the external transform obviously improves the confinement. For high currents (with q = 1 reached in the centre) there is practically no difference between tokamak and stellarator scaling. The increase of external transform changes the profiles and reduces the central temperature. The drift scaling, which includes temperature and density, accordingly fits better over a large parameter range. Introduction of the external transform improves the stability and allows an extension of the parameter range to higher densities, for example where radiation dominates the discharge.

J.D. CALLEN: In tokamaks such as ISX-B the energy confinement time τ_E goes through a maximum as the density is increased. There, the effects of ion heat conduction at the finite plasma current are found to be responsible for the saturation of τ_E with density over the central, confinement region of the plasma. Could such an effect be responsible for the maximum of τ_E with density you have shown?

H. RENNER: No, we exclude the possibility that ion heat losses make any major contribution to the electron energy balance. The W-VII machine would be expected to have a much smaller ion heat conductivity coefficient than ISX owing to the higher toroidal field (3.5 T). Accordingly, in W-VII energy transfer to the ions is reduced, as the difference between ion and electron temperature is smaller at approximately the critical density where τ_E passes through its maximum. It seems that the region with high radiation losses is inaccessible in tokamaks because disruptions restrict the density.

IAEA-CN-37-H-2

Seventh International Conference on Plasma Physics and
Controlled Nuclear Fusion Research

23 - 30 August 1978, Innsbruck, Austria

ENERGY AND PARTICLE CONFINEMENT IN THE OHMICALLY HEATED W VII-A STELLARATOR

W VII-A TEAM

B. CANNICI, G. CATTANEI, A. CAVALLO, D. DORST,
A. ELSNER, G. GRIEGER, H. HACKER, J. HOW,
H. JÄCKEL, R. JAENICKE, P. JAVEL, J. JUNKER,
M. KICK, F. LEUTERER, C. MAHN, St. MARLIER,
G. MÜLLER, W. OHLENDORF, F. RAU, H. RENNER,
H. RINGLER, J. SAFFERT, J. SAPPER, P. SMEULDERS,
M. TUTTER, O. VOLLMER, A. WELLER, E. WÜRSCHING,
H. WOBIG

Max-Planck-Institut für Plasmaphysik
Association EURATOM-IPP
8046 Garching, F.R. Germany

Abstract

The density regime in the Wendelstein stellarator has been extended to $\bar{n}_e = 10^{20}$ m^{-3} by gas puffing in helium discharges. The density seems to be limited already by small amounts of impurities (i.e. $\leq$ 1 % of oxygen). These radiate at the plasma edge, constrict the discharge, and finally terminate it when the losses exceed the available ohmic heating power.

The energy confinement time τ_E increases with electron density but reaches a maximum followed by a rapid decrease connected with strong radiation losses. The particle confinement time shows a similar behaviour.

Maximum densities were obtained for stationary helium discharges with B_o = 3.5 T, I_p = 35 kA, and the external rotational transform ι_o = 0.14. For smaller values of the rotational transform the density increase is limited by disruptive instabilities.

The ion temperature agrees with neoclassical scaling.

INTRODUCTION

The Wendelstein VII-A stellarator has l=2, m=5 helical windings which, at a main field B_o = 3.5 T, produce an almost shearless external rotational transform $0.055 \leq \iota_o \leq 0.23$. The major radius is R_o = 2.0 m and the minor radius is defined by the 0.13 m radius of the molybdenum limiter which, because of the elliptical cross-section of the magnetic surfaces, is equivalent to an average plasma radius of ~0.1 m. Results from ohmically heated plasmas at moderate densities have already been reported at the Berchtesgaden [1] and Prague [2] conferences. Now the investigations have been extended to the high density regime since high densities are required for sufficient absorption with the nearly perpendicular injection experiment planned for W VII-A. Access to this regime became possible by technical improvements of the OH-circuit, leading to an increase of the control range of the loop voltage from 5 to 10 volts and of the ohmic heating power to 400 kW. Helium was used instead of hydrogen in order to take advantage of the following effects:

- For the same temperature the resistivity and thus the available power density rises as Z_{eff} goes from one to two.
- Chemical processes leading to a release of oxygen from the wall via the production of water with the impinging atomic hydrogen [3] should disappear in helium discharges. Therefore, the radiation losses should be reduced and the reproducibility improved.
- The recycling coefficient ρ is close to one for helium instead of 0.7 for hydrogen [2] so that there is no need for an additional gas feed to maintain stationary conditions.

The main effect found in W VII-A is that even if disruptive instabilities are suppressed, τ_E does not continuously grow with n but goes through a maximum and then steeply decreases. At even higher densities the discharge can no longer be maintained with the available ohmic heating power.

CONFINEMENT AT HIGH DENSITIES

In order to find the optimum confinement conditions for high densities and the physical reason for the density limitation, the external transform, ι_o, and the plasma current, I_p, were varied for B_o = 3.5 T. In Fig. 1 the gross energy confinement time $\tau_E = \frac{W}{P_{OH}}$ is plotted versus n for different currents and ι_o = 0.14, where W is the total plasma energy, and P_{OH} the ohmic input power. All data are taken from quasistationary discharges with pulse lengths >100 ms, where the density was changed by gas puffing during current build-up.

W is calculated from diamagnetic measurements. In hydrogen experiments the values obtained from electron temperature and density profiles measured by Thomson scattering and ion temperatures deduced from charge-exchanged neutrals agreed well with the diamagnetic measurements,but in helium discharges they show a systematic deviation of about -25 %. At lower densities τ_E follows the well known scaling $\tau_E \sim n$. Also reduction of τ_E with increasing I_p is observed. Therefore, in this regime τ_E roughly scales with ξ^{-1} where ξ is the drift parameter, $\bar{\xi} \sim \frac{I}{\bar{n}\sqrt{k\bar{T}_e}}$. At higher densities a saturation and a subsequent steep decrease of τ_E is observed. These phenomena are shifted to higher densities if the plasma current is increased. Measurements of the 5015 Å He I line in three different planes (including that of the limiter) have shown a similar behaviour also for the particle confinement time.

The highest density, $\bar{n} = 10^{20} m^{-3}$ or $\int n dl = 2.2 \times 10^{19} m^{-2}$, was obtained for $I_p = 35$ kA with $\iota(a) \approx 0.5$ ($q \approx 2$). The input power was 350 kW and $kT_e(o) = 200$ eV. Fig. 2 gives profiles of n_e and T_e for this discharge. They are flat inside the q=1 surface [1,2] indicating that the transport coefficients are high in this region. The confinement takes place within the rather thin sheath between the q=1 surface and the plasma edge. Rather steep gradients can obviously be balanced there.

Any further increase in n would require an increase of the input power, i.e. of the current density. This could be achieved by lowering the external transform or by increasing B_o. These effects have been observed indeed but, as already stated, a too low external transform ($\iota_o < 0.14$) leads to disruptive instabilities, well known from tokamaks, which prohibit the access to higher densities when approaching q(a) = 2.

In order to illustrate the situation, the ratio of maximum density to maximum current density versus $\iota_p \approx \frac{I_p}{B}$ is plotted for different values of ι_o in Fig. 3. This procedure is similar to [4] but modified for the inclusion of the stellarator effect. One observes that for larger ι_o, where disruptions are suppressed, the density limit is proportional to the plasma current and to $(1-\iota_o)$. The dependence on B could not be verified since for these experiments B was always between 3 and 3.5 T. Below $\iota_o = 0.14$ the density limit is increasingly determined by disruptions and progressively shifted to lower values. Finally for $\iota_o = 0.055$ the "disruptive branch" typical for tokamaks is reached. If the density then approaches the critical value for disruptions, a significant change of the MHD modes is observed [5]. At higher external transform the stronger equilibrium in the helical field may be responsible for maintaining the discharge at higher densities, in spite of the occurrence of phenomena, such as mode coupling and locking to the limiter.[5]

The dependence of τ_E on n was studied in detail for 20 kA discharges. For a set of density values Figs. 4 and 5 show radial profiles of temperature and density. In addition the normalized curves were plotted. With increasing n_e the T_e profiles show a strong reduction of T_e in the outer regions as well as a decrease of temperature in the centre. Since the current is kept constant, these effects lead to a concentration of the current towards the centre and, consequently, to an expansion of the q=1 surface since within q=1 the current density is limited to $j \sim \frac{B}{R}(1-t_o)$. In this way the region of high transport is expanded and the confinement region reduced by both effects, the expansion of the q=1 surface and the decrease of T_e in the outer regions.

Radially resolved bolometric measurements lead us to believe that the shrinkage of the profiles is caused by radiation cooling of the plasma edge. Fig. 6 shows bolometric measurements for the four discharges of Figs. 4 and 5 along with the local ohmic input. At low densities a density increase produces little change in the radial distribution of the radiated power and the ohmic power input as well, indicating that the reduction in temperature is balanced by a reduction of Z_{eff}. Again one has to keep in mind that I_p is kept constant. The density increase from $3.2 \times 10^{19} m^{-3}$ to $5.7 \times 10^{19} m^{-3}$ and further to $6.7 \times 10^{19} m^{-3}$ does show a definite increase in radiated power at the plasma edge along with an increase of ohmic power in the centre, to account for the additional losses. Since Z_{eff} is around 2 and since the temperature is still more reduced (see Fig. 4), the loop voltage increases to keep up the current.

This radiated power is attributed to impurity radiation. It is responsible for the shrinkage of the T_e profiles and the reduction of the central temperature. It is interesting to note that there is also an indication of radiation from the plasma centre, which seems to decrease for higher densities or decreasing central temperature.

Although the bolometer used has not yet been calibrated with radiation standards, the sensitivity was estimated from its calorimetric properties and the variation of its output signal with the variation of the plasma radiation. This leads to the conclusion that at least at higher densities, the wall receives about 80 % of the ohmic power input. Another 10 - 20 % of the ohmic power is typically found on the limiter.

RADIATION LOSSES AND IMPURITY CONTENT

In order to look for impurities and their concentration, radial profiles of spectral lines of several species have been taken shot by shot in the UV and VUV region and compared with the bolometer measurements. The spectroscopic measurements give maximum oxygen concentrations of 1 % and Fe concentrations of 0.1 % at $n(o) = 5.7 \times 10^{19} m^{-3}$. These impurities together with the helium radiation may explain the strong radiation losses

from the plasma edge (20 - 70 eV) because, as seen from Fig. 5, the electron density at the plasma edge shows a stronger increase than in the centre (for a given temperature, $P_{rad} \sim n_{imp} \times n_e$).

At present there is not a clear picture as far as the comparison with the bolometric measurements is concerned and, in particular, the origin of the radiation from the plasma centre for temperatures above 350 eV is unknown. Photographic recordings, however, with a grazing incidence spectrograph do show many unresolved lines between 60 and 80 Å radiating from the plasma centre. Their identification is not yet clear. If it were Fe, the radiation should extend down to 40 Å and if it were Mo other Mo lines should also occur which were not detected.

To prove that small amounts of impurities radiating from the plasma edge can severely influence the profiles and the confinement, small amounts of Ne were added to the discharges. Neon was selected since, for the conditions of these discharges, it greatly resembles oxygen [6] without showing its intense wall affinity.

Fig. 7 shows τ_E as a function of line density for helium discharges and helium discharges where 10^{17} and 2×10^{17} atoms of Ne had been added. At 8×10^{18} m^{-2} line density, this corresponds to 1 % and 2 % impurity content. Again there is little effect at small electron densities, but a drastic change at higher densities. The maximum available density is strongly reduced by this amount of impurity content.

In Fig. 8 radial profiles of radiated power from bolometer measurements along with profiles for the ohmic power input have been plotted. They clearly show the increase of radiated power from the plasma edge. Temperature profiles also shrink for these cases.

So, either by adding small amounts of impurities or by increasing the electron density, one can reach the point where radiative losses influence the temperature profiles and deteriorate the confinement [7] .

Alternatively, the radiation from the plasma centre was increased by adding 3×10^{16} atoms of krypton to the discharge. Krypton is expected to radiate from the centre of the discharge, between 200 and 500 eV [6] and the corresponding radiated power was detected by the bolometer. In essence, this leads to a reduction of the effective ohmic heating and thus to a lower central electron temperature. In addition, with increasing helium density the oxygen in the discharge again provides edge cooling and thus a further decrease of the central temperature until the density limit is reached. This confirms the conclusion that edge cooling is responsible for the existance of the density limit rather than radiation losses directly from the plasma centre.

ION HEAT CONDUCTION

An assessment of the contribution of the ion heat conduction to the total energy balance requires the knowledge of the ion temperature and its radial distribution. However, in helium discharges the low charge exchange rate and the low stripping efficiency do not yield large enough signals to determine the ion temperature by charge exchange analysis. This problem was circumvented by adding a hydrogen gas puff to the helium discharges and determining the helium ion temperature by measuring the hydrogen ion temperature via charge exchange analysis. When scanning off the centre, the charge exchange flux detected by each channel of the energy analyser (0.4 to 2 keV) revealed a strong decrease. In the outer regions, however, the temperature deduced from these signals significantly exceeded the electron temperature. This is not compatible with the electron ion heat exchange rate, according to which the ion temperature can hardly exceed the electron temperature. For the energy balance it is assumed therefore that the T_e and T_i profiles are proportional to each other.

In Fig. 9 the central values of kT_e and kT_i versus the line density are plotted for the same conditions as in Fig. 7. Theoretical curves for the ion temperature are shown for comparison. They are based on neoclassical ion heat conductivity and on classical heat exchange between electrons and ions. The agreement is quite good. Small deviations between measured and calculated temperatures are probably caused by additional charge exchange losses at low densities and by a transition to the collision dominated regime at low ion temperatures. In all cases, the power transferred to the ions is only a small fraction of the ohmic power.

SUMMARY

For helium the density range of the Wendelstein VII-A stellarator was extended to $\bar{n}_e = 10^{20}\ m^{-3}$.

Low concentrations of impurities, e.g. oxygen less than 1 % at higher densities $\bar{n}_e > 5 \times 10^{19}\ m^{-3}$ dominate the confinement by radiation losses at the plasma edge and reduce the temperature. It is interesting to note that this boundary layer may resemble the cold plasma blanket concept. The maximum density is determined by the available ohmic power.

Helium discharges with 1 to 2 % neon added show that the accessible density range is reduced with increasing impurity concentrations since for a given temperature the radiative power increases according to $P_{rad} \sim n_e \times n_{imp}$.

For $\iota_0 < 0.14$ the discharge becomes sensitive to disruptive instabilities. The density limit caused by these instabilities coincides with the optimum values obtained in tokamaks related to the restricted current density $j \sim B/R(1-\iota_0)$ within $q=1$.

Measurements of ion temperature agree with neoclassical expectations. Therefore, the electron - ion heat transfer seems not to be responsible for the reduction of the electron temperature at higher densities.

ACKNOWLEDGEMENTS

This paper would not have been possible without the continuous endeavours of the technical crew.

REFERENCES

[1] W VII-A TEAM, in Plasma Physics and Controlled Nuclear Fusion Research (Proc.6th Int.Conf. Berchtesgaden, 1976) 2, IAEA Vienna (1977) 81

[2] W VII-A TEAM, in Controlled Fusion and Plasma Physics (Proc.8th Europ.Conf. Prague 1977) 2 (1977) 73

[3] F. WAELBROECK, H.J. DIETZ, P. WIENHOLD, Rep.Jül.-1448 (1977)

[4] J.W.M. PAUL et al., in Controlled Fusion and Plasma Physics (Proc.8th Europ.Conf. Prague 1977), 2 (1977) 49

[5] W VII-A TEAM, paper IAEA-CN-37/H-3, these Proceedings

[6] D.E. POST et al., Atomic Data and Nuclear Tables, 20 (1977) 397-439

[7] P.H. REBUT, B.J. GREEN, in Plasma Physics and Controlled Nuclear Fusion Research (Proc. 6th Int.Conf. Berchtesgaden, 1976) 2 IAEA Vienna (1977) 3

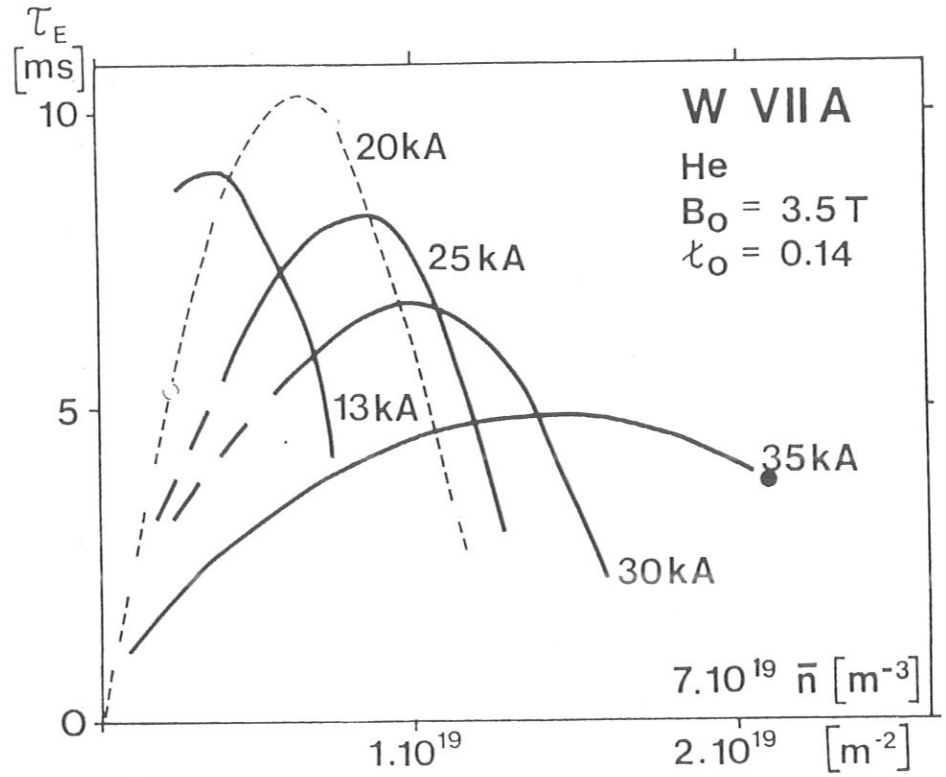

FIG. 1. Diamagnetic measurements of the energy confinement time τ_E for helium discharges with various plasma currents I_p. Averaged density $\bar{n} = \int ndA/\int dA$.

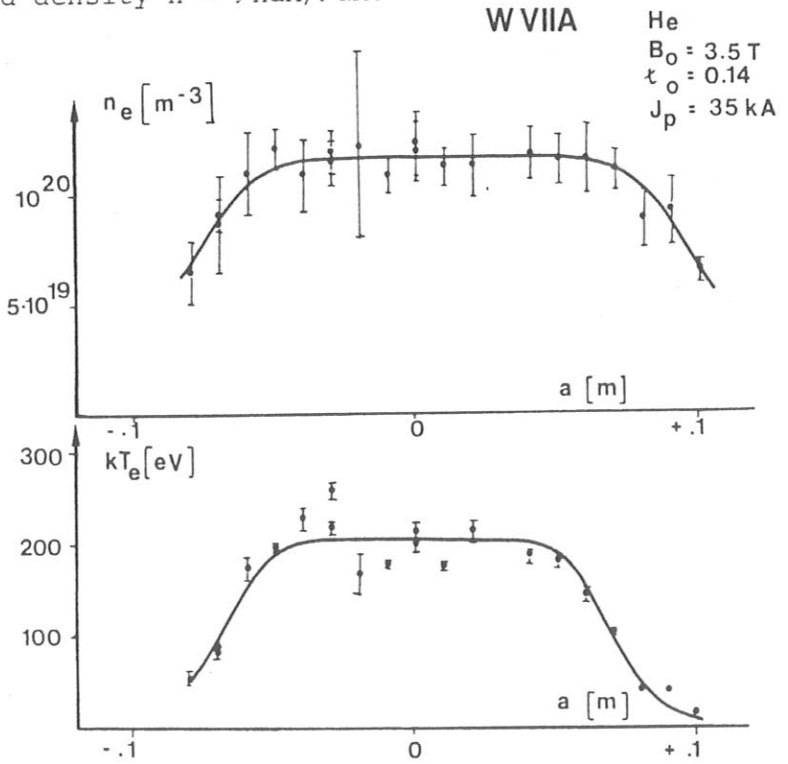

FIG. 2. Measured density and electron temperature profiles at line density 2.2 x 10^{19} m^{-2} (indicated by ● in Fig. 1).

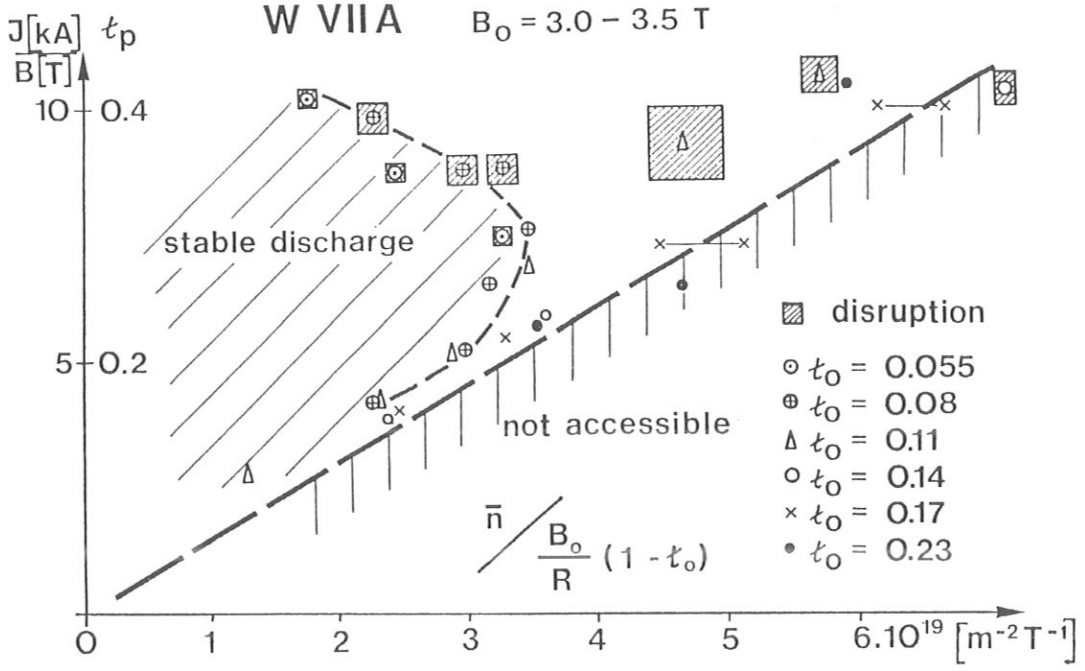

FIG. 3. Density limitations for various I_p and external transforms, t_o. The average maximum densities divided by the central current densities ($\bar{n}$ /j(o) are plotted versus the internal transform t_p. The conditions, when disruptions determine the discharge, are indicated.

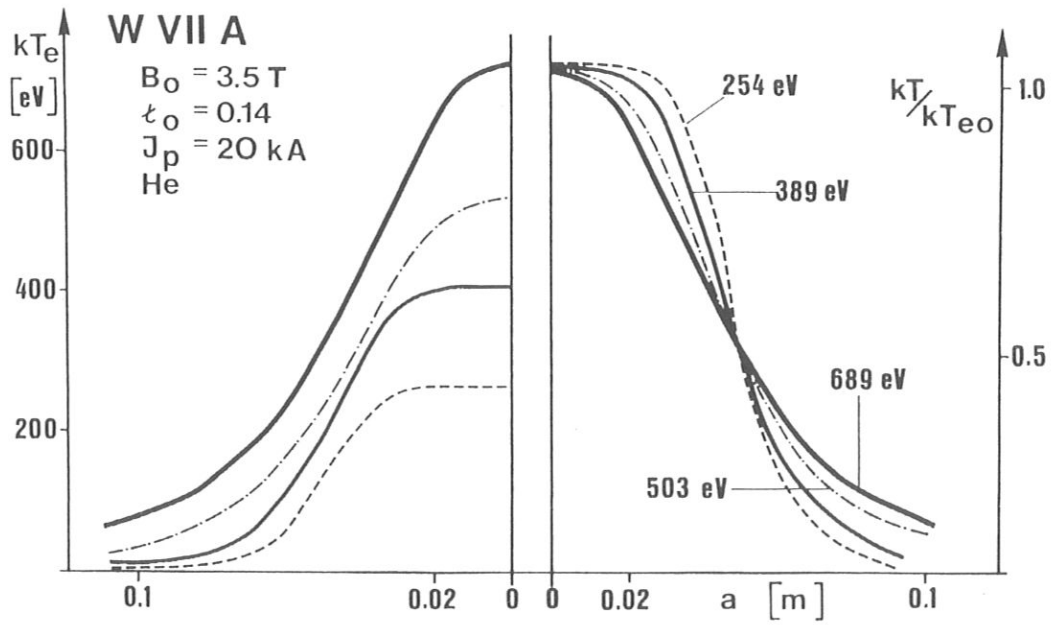

FIG. 4. Temperature distributions for the four different discharges marked by o in Fig. 1. The central temperatures are given for the normalized profiles.

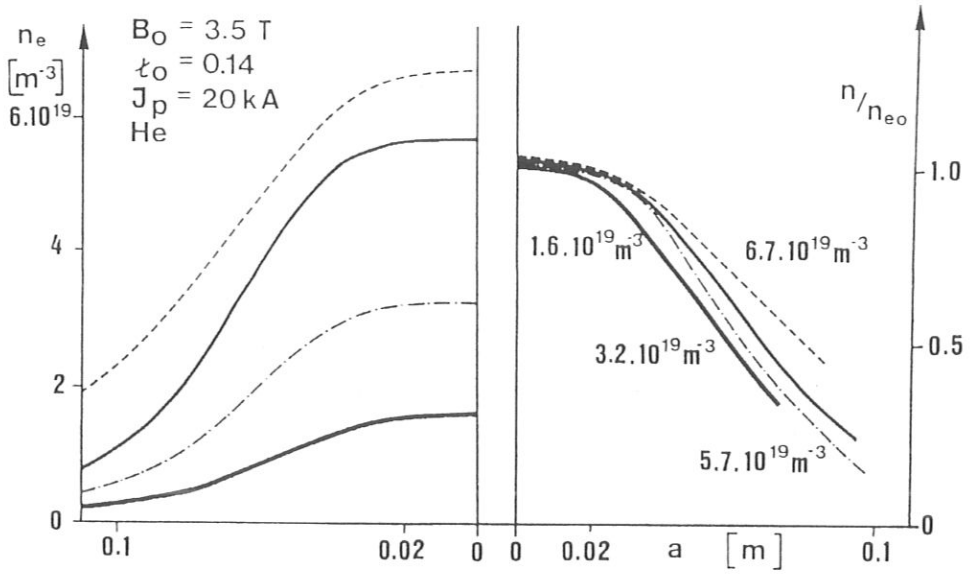

FIG. 5. Corresponding density profiles to Fig. 4. The central density is given for the normalized profiles.

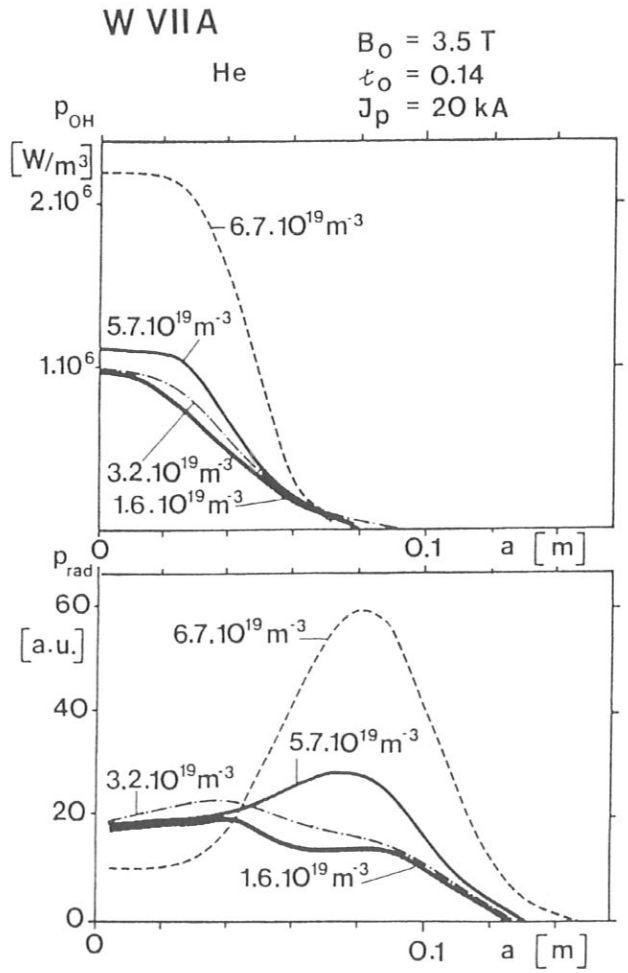

FIG. 6. P_{OH}, heating power density and relative P_{rad}, radiation power density obtained by Abel inversion from bolometer measurements for the four selected discharges of Figs. 4 and 5. (P_{rad} is given in arbitrary units [a.u.]. 100 a.u. are approximately equivalent to 10^6 W/m^3). The central densities are indicated.

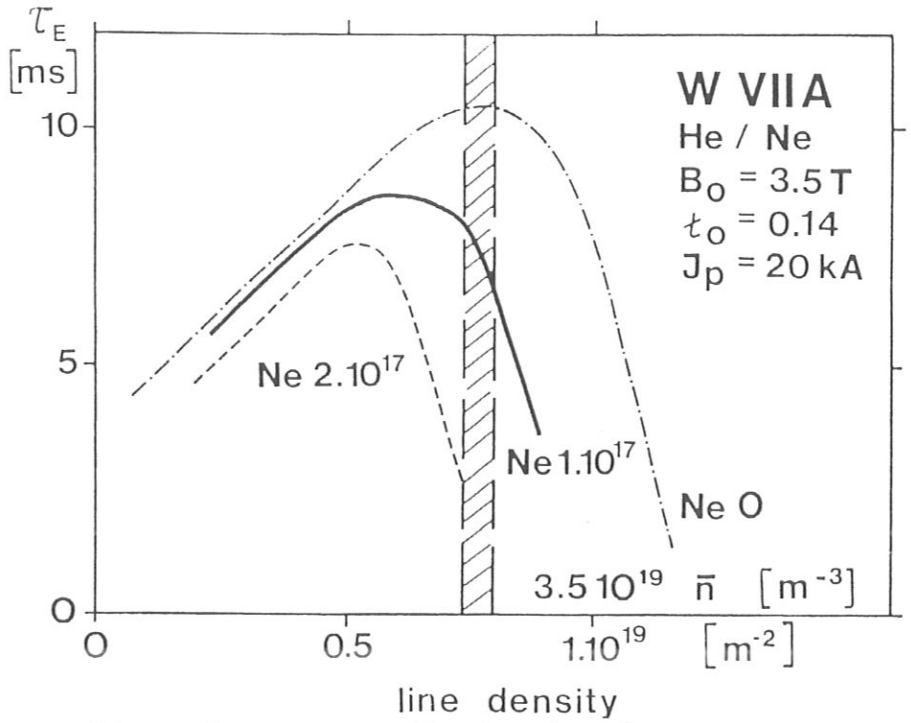

FIG. 7. Energy confinement τ_E versus the density for various neon contents at I_p = 20 kA. At line density 8 x 10^{18} m^{-2} (dashed region), 10^{17} particles correspond to a concentration of 1 %.

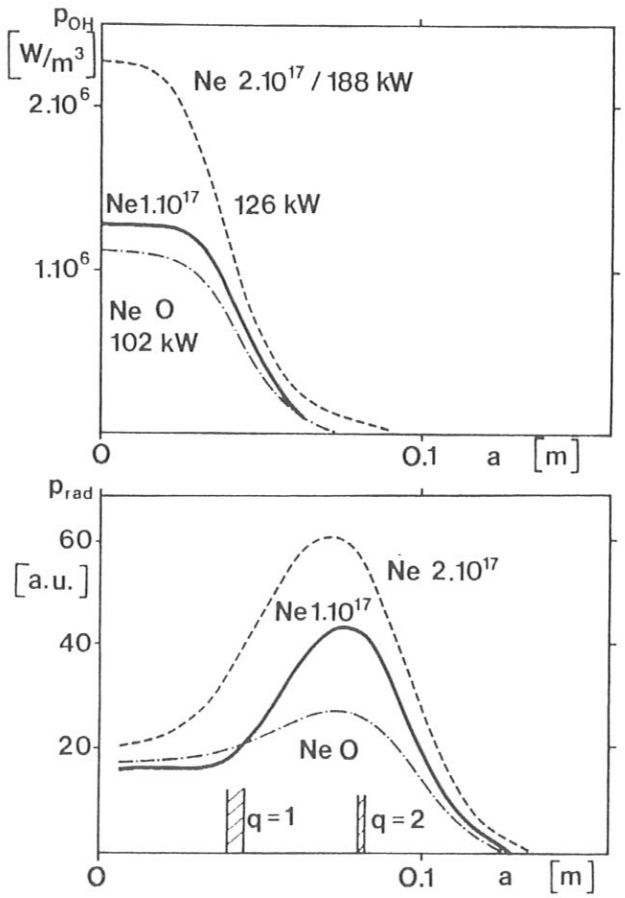

FIG. 8. P_{OH} heating power density and P_{rad} radiation power density for the three cases of Fig. 7 at line density 8 x 10^{18} m^{-2}, central density 5 x 10^{19} m^{-3}.
(P_{rad}: 100 a.u. are approx. equivalent to 10^6 W/m^3).

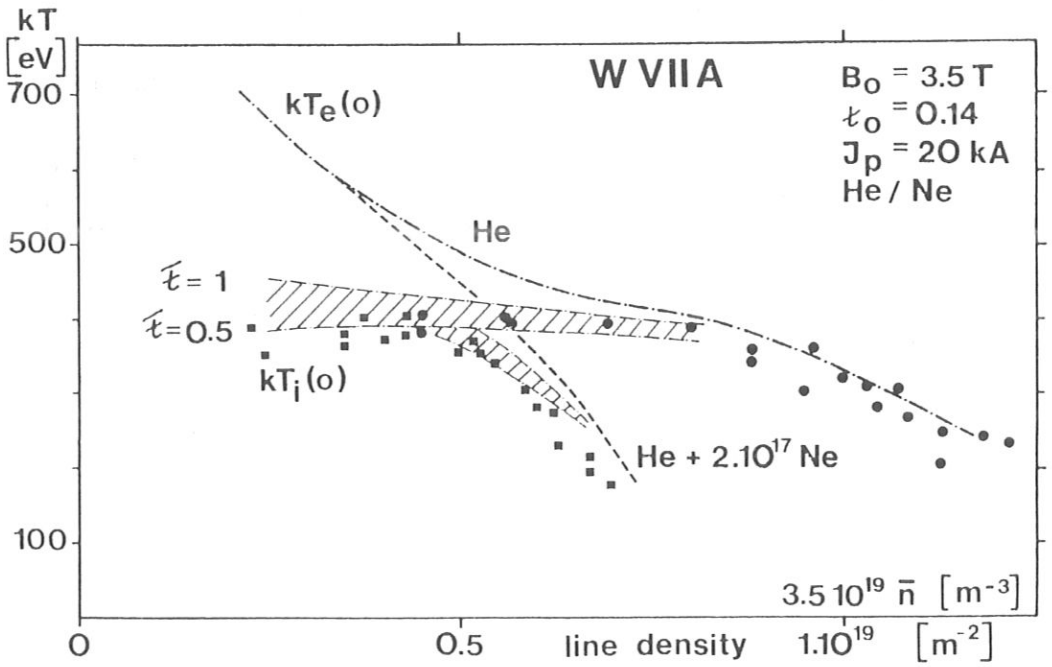

FIG. 9. The variation of the central electron and ion temperatures with density is shown for two different cases, to one of them neon was added. Theoretical curves of the ion temperatures based on the neoclassical heat conductivity for $\bar{\tau}$ = 0.5 and $\bar{\tau}$ = 1.0 are given for comparison (dashed regions).

STABILIZATION OF THE (2,1) TEARING MODE AND OF THE CURRENT DISRUPTION IN THE W VII-A STELLARATOR

W VII-A TEAM*
Max-Planck-Institut für Plasmaphysik,
Association Euratom-IPP,
Garching bei München,
Federal Republic of Germany

ABSTRACT. A numerical code based on a Δ'-analysis is applied to calculate the saturated amplitude of tearing modes dependent on the current density profile. The only stellarator effect included is the additional, shearless external rotational transform ι_0 in the safety factor profile q(r). In this way, the stellarator field shifts the resonant q = 2 surface toward the outside, where the current density gradient is smaller, and stabilizes the (2,1) mode as observed experimentally. Also the measured dependence of the (2,1) mode amplitude on electron density and plasma current can be absolutely predicted by the calculations. – In addition to stabilizing the (2,1) tearing mode, the current disruption is suppressed in Ohmically heated W VII-A discharges for $\iota_0 \gtrsim 0.15$. The experimental findings, together with the calculated island widths, are compared with the predictions of a theoretical model proposed by several authors to explain the current disruption.

1. INTRODUCTION

In many tokamak discharges (see, e.g. Refs [1–3]), a strong correlation between the existence of current-driven tearing modes and the occurrence of the current disruption is observed. In Pulsator, it was found that a small resonant helical field can have a stabilizing effect on the disruptive instability if it is not too large [4]. This could be explained by the flattening of the current density profile close to the q = 2 surface which is due to enhanced electron energy transport.

In the W VII-A stellarator [5] (R_0 = 200 cm, $a \approx 10$ cm, $B_0 \approx 3.5$ T), the external helical field is not in resonance with the pitch of the magnetic field lines in the plasma. It contributes an appreciable part to the total rotational transform $\iota(r) = \iota_p(r) + \iota_0 = 1/q(r)$, where $\iota_p(r)$ is the rotational transform due to the Ohmic heating current. The shear of the external rotational transform $\iota_0 \leqslant 0.23$ produced by the $\ell = 2$ stellarator field is negligible. Therefore, radial profiles of the current density j(r) and the safety factor q(r) are similar to those of tokamaks.

It has been observed on W VII-A that current disruptions do not occur in Ohmically heated discharges if the stellarator field is large enough [6, 7]. Simultaneously, no m = 2, n = 1 or (2,1) tearing mode can be seen under these conditions. The remaining (3,2) mode exhibits only a small amplitude. The threshold for the stabilizing effect of the stellarator field lies in between $\iota_0 = 0.14$ and 0.17.

In the present paper, an attempt is made to explain the behaviour of the (2,1) mode on the basis of the non-linear theory of tearing modes [8, 9], including the effect of the external rotational transform. From the saturated width of the magnetic islands associated with the (2,1) tearing mode, the poloidal magnetic field fluctuations at the Mirnov coils are calculated and compared with the experimental results. Finally, the correlation between the amplitude of the (2,1) tearing mode and the occurrence of current disruptions is investigated.

2. THE MODEL

A pressureless plasma is considered in linear cylindrical geometry. Toroidal curvature and the elliptical plasma cross-section [5] are neglected. The only stellarator effect included is the constant external rotational

* Bartlett, D.V., Cannici, G., Cattanei, G., Dorst, D., Elsner, A., Grieger, G., Hacker, H., How, J., Jäckel, H., Jaenicke, R., Javel, P., Junker, J., Kick, M., Lathe, R., Leuterer, F., Mahn, C., Marlier, S., Müller, G., Ohlendorf, W., Rau, F., Renner, H., Ringler, H., Saffert, J., Sapper, J., Smeulders, P., Tutter, M., Weller, A., Würsching, E., Wobig, H.

transform ι_0 produced by the helical windings. To first order, the total rotational transform $\iota(r)$ is the sum of ι_0 and the rotational transform by the plasma current, $\iota_p(r)$:

$$\iota(r) = \iota_p(r) + \iota_0 = 1/q(r) \tag{1}$$

According to Johnson et al. [10], the free potential energy of tearing modes is given by

$$2\delta W = -8\pi^2 R_0 \int_0^b r dr \left[\left(\frac{d\Psi}{dr}\right)^2 + \frac{A}{r^2}\Psi^2\right] \tag{2}$$

where R_0 is the major radius, $\Psi = ir B_r/m$ is the perturbed helical flux function [11], B_r denotes the radial magnetic field perturbation, and

$$A = m^2 + \frac{mr}{m\iota(r) - n} \frac{\mu R_0}{B_0} \frac{dj}{dr} \tag{3}$$

B_0 is the toroidal magnetic field, $j(r)$ is the unperturbed toroidal current density, and μ is the magnetic permeability. It is assumed that the plasma conductivity is zero outside a radius $r = a$(= effective limiter radius). The wall radius $r = b$ is set to infinity.

The Euler equation of expression (2) is

$$\frac{d}{dr}\left(r\frac{d\Psi}{dr}\right) - \frac{A}{r}\Psi = 0 \tag{4}$$

This equation has been solved by Matsuoka et al. [12] for various current density profiles. They found that the superposition of ι_0 reduces the unstable regions in the $(\iota_0, \iota_p(a))$ parameter space.

In this paper, Eq. (4) is solved for current density profiles observed in the W VII-A experiment. $j(r)$ is assumed to be proportional to $T_e(r)^{3/2}$ with Z_{eff} = const. The electron temperature profile $T_e(r)$ is approximated by a function

$$T_e(r) = T_e(0) \frac{1}{1 + \left(\frac{r}{r_0}\right)^{2\alpha}} \tag{5}$$

The parameter α indicates the steepness of the temperature and, therefore, of the current density profiles; it increases mainly with the electron density n_e. The second parameter, r_0, is the half-width of the temperature profile. It increases mainly with the plasma current. This two-parameter approximation of $T_e(r)$ is sufficient to describe the gross properties of the (2,1) tearing mode in Ohmically heated discharges in W VII-A.

$T_e(0)$, r_0, and α are determined by a least-square fit to the Thomson scattering data, measured along a line through the plasma with 45° inclination to the major axis of the elliptical magnetic surface. This profile is fairly well suited to a cylindrical approximation of the current channel. Nevertheless, to improve this approximation, the half-width r_0 is numerically re-calculated, using the condition $\iota(r = 0) = 1$, since this agrees with the experimental observation that, because of sawtooth oscillations, the total transform $\iota(r)$ is always around one in the plasma centre in W VII-A. The difference between this r_0 and the r_0 from Thomson scattering is less than 10%, and, indeed, with the calculated r_0 the code results agree better with the experimental observations from the Mirnov coils.

From the solution $\Psi(r)$ of Eq. (4), the stability parameter

$$\Delta' = \frac{1}{\Psi(r_s)} [\Psi'(r_s + \epsilon) - \Psi'(r_s - \epsilon)]|_{\epsilon \to 0} \tag{6}$$

is calculated. r_s is the radius of the resonant magnetic surface where $\iota(r_s) = n/m$. Δ' is a function of $\iota_p(a)$, ι_0 and the profile parameter α only. By integrating Eq. (4), it can be shown that Δ' is proportional to $-\delta W$ of Eq. (2). This means that the mode is unstable as long as $\Delta' > 0$ or $\delta W < 0$.

Furthermore, the saturated width w of the magnetic islands can be calculated from

$$\Delta'(w) = \frac{1}{\Psi(r_s)} \left[\Psi'\left(r_s + \frac{w}{2}\right) - \Psi'\left(r_s - \frac{w}{2}\right)\right] \to 0 \tag{7}$$

since Rutherford has shown that the growth rate of the island width is given by $dw/dt \sim \Delta'$ [8]. This method of approximately calculating the saturated island width has been discussed by several authors [13, 14]. A comparison with the results of a resistive non-linear MHD-code showed fairly good agreement.

With $B_r \sim w^2$ [15] the absolute value of the radial magnetic field perturbation can be evaluated from w. Its radial dependence is given by the solution $\Psi(r)$ of Eq. (4). In this way, the relative amplitude $\delta\tilde{B}_\theta/B_\theta$ of the poloidal field fluctuations at the Mirnov coils can be calculated [13] and compared with the experimental results. Here, B_θ is the poloidal field of the plasma current only.

3. RESULTS

To check the applicability of the simplified model described in Section 2, two examples are considered in Sections 3.1 and 3.2, where sufficient information on the current density profiles is available for a detailed comparison between theory and experiment. Only then is the dependence of the (2,1) tearing mode on the stellarator field studied.

3.1. Dependence on density

The electron density n_e of the plasma does not enter the tearing-mode equations directly but a variation of the density changes the current density profile. Figure 1 shows how the plasma becomes colder close to the edge with increasing density, and, consequently the current density decreases at the edge. Owing to the condition $\iota(0) \approx 1$ imposed by the sawtooth oscillations the current density is almost constant at the centre. Therefore, the current channel has to widen close to the centre since the total current is kept constant, and the current density gradient in between has to steepen. This modification of the current density profile can be described by an increase of the profile parameter α from 1.3 to 3.0. Low-Z impurities have a similar effect and also result in an increase of α.

In the lower half of Fig. 2, the measured relative amplitude of the (2,1) mode is shown as a function of the electron density for constant plasma current. From the α-values given in Fig. 1, the α-scale shown in the middle has been deduced, and the mode amplitude $\delta\hat{B}_\theta/B_\theta$ has been calculated as a function of α. This calculation is absolute; no free parameters are adjusted. A comparison between the calculated and the measured curve shows good agreement for large amplitudes. In the upper half of Fig. 2, the calculated island width and Δ' are also presented.

From this agreement we can understand the observed density dependence of the (2,1) mode amplitude. The increase of the amplitude with n_e can be explained by the cooling of the outer plasma region and the resulting steepening of the current density profile inside the q = 2 surface. The radius of the q = 2 surface remains almost constant (see Fig. 1). According to the calculation, the (2,1) tearing mode is stabilized in a quasi-discontinuous manner ($\Delta' \rightarrow < 0$) for $\alpha > 3.1$, since the current gradient immediately inside the q = 2 surface becomes too small. Experimentally even higher densities would have been necessary to check if this stabilization really occurs.

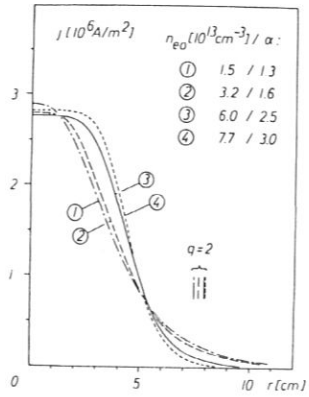

FIG.1. Radial current density profiles calculated from measured electron temperature profiles for helium discharges with constant plasma current, for different electron densities. Discharge parameters: $\hat{B}_0 = 3.5$ T, $\iota_0 = 0.14$, $I_{pl} = 20$ kA, $q(a) = 2.9$. n_{eo} is the central electron density calculated from the microwave line density by assuming a parabolic profile. α is a profile parameter (see Section 2) which has been fitted to the electron temperature profiles, and which increases with n_e.

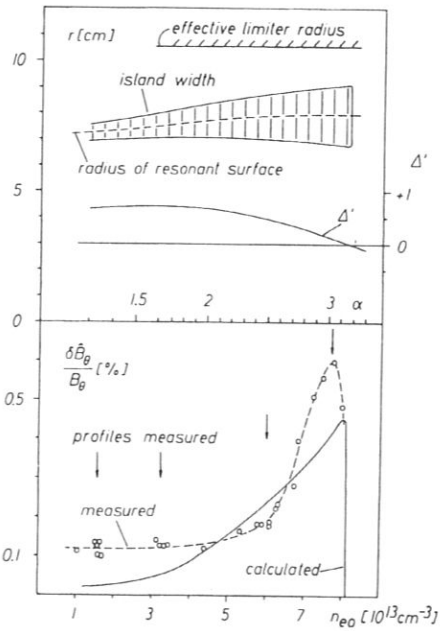

FIG.2. For the discharge parameters given in Fig. 1 the relative amplitude $\delta\hat{B}_\theta/B_\theta$ of the (2,1) mode calculated as a function of α is shown. For comparison also the measured mode amplitude is presented as a function of the density n_{eo}. In the upper half, the corresponding calculated island width and the stability parameter Δ' are given.

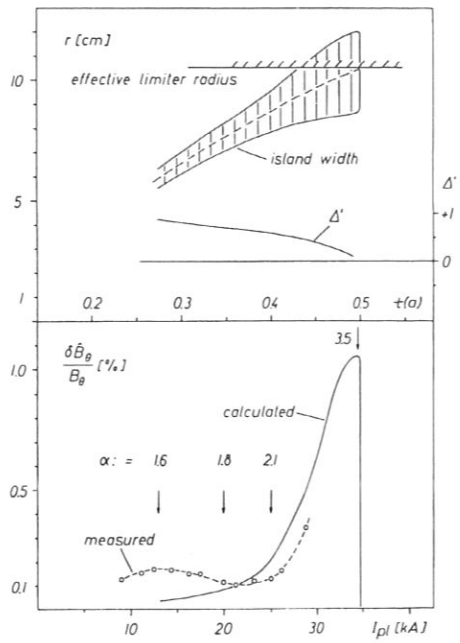

FIG.3. The dependence of the relative amplitude $\delta \hat{B}_\theta / B_\theta$ of the (2,1) mode on the plasma current is studied for helium discharges with $B_0 = 3.5$ T and $\iota_0 = 0.14$. The electron density n_{e0} varies between 2 and 4 X 10^{13}cm^{-3}. The mode amplitude has been calculated as a function of α as in Fig. 2. In the upper half, again the corresponding island width and the stability parameter Δ' are given.

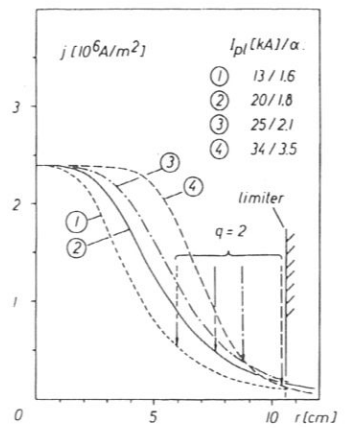

FIG.4. Current density profiles which have been used in the calculation of Fig. 3 to calibrate the α-scale. The α-values given have been derived from measured electron temperature profiles. The central value j(r = 0) has been determined in such a way that ι(0) = 1. The radii of the q = 2 surfaces are indicated by arrows.

3.2. Dependence on plasma current

The dependence of the (2,1) mode amplitude on the plasma current has been discussed in Refs [13, 16] for ORMAK and T-4 discharges. In the W VII-A stellarator, a similar drop of the mode amplitude with q(a) or rise with the plasma current is found for $\iota_0 \lesssim 0.17$ [7].

The procedure described in Sections 2 and 3.1. is applied to calculate the relative amplitude of the (2,1) tearing mode. In Fig. 3, a comparison with experimental data is shown for $\iota_0 = 0.14$. Again the measured and calculated curves agree quite well, but the mode amplitude can no longer be measured above $I_{pl} = 29$ kA. Since the observed frequency of the (2,1) mode goes to zero at this current, probably only the rotation of the islands stops, but the islands do not necessarily vanish. Such a 'locking' [7] or 'stalling' of magnetic islands is also frequently observed in tokamaks [3, 17, 18]. In W VII-A, it was verified for time intervals up to 5 ms (limited by the integration time constant) that the rotation of the islands can be stopped. In the upper half of Fig. 3, it is shown that the calculated island widths extend beyond the limiter for $29 \leqslant I_{pl} \leqslant 35$ kA. The assumption of completely stationary islands is supported by the experimental fact that a clear deterioration of the plasma confinement is observed under these conditions. For $I_{pl} > 35$ kA the resonant q = 2 surface itself is shifted beyond the limiter, and the (2,1) tearing mode can no longer exist. This can be seen from the current density profiles (Fig. 4) used in the calculation.

3.3. Dependence on the stellarator field

In Fig. 5, the calculated relative amplitude of the (2,1) mode is shown as a function of the external rotational transform ι_0 for constant plasma current with α as parameter. In W VII-A, α varies between approximately 1.5 and 4. Therefore, all experimental points should lie within the shaded area, and, in fact, this prediction is upheld quite well for all working gases used.

For $\iota_0 < 0.11$, the mode amplitude grows with α corresponding to increasing electron density and/or low-Z impurity content. If ι_0 is increased to ≈ 0.15, the (2,1) tearing mode is stabilized, or at least its amplitude becomes very small. In the experiment, this stabilization seems to occur at slightly larger values of ι_0 than in the calculation. The transition from instability to stability depends only weakly on the absolute value of the plasma current.

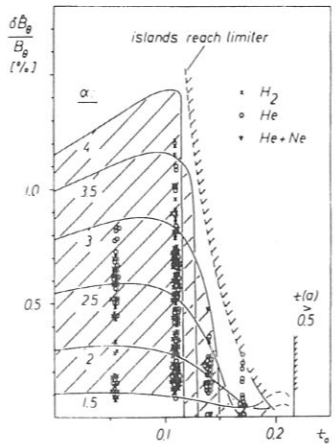

FIG. 5. The solid lines show the calculated relative amplitude $\delta\hat{B}_\theta/B_\theta$ of the (2,1) tearing mode as a function of the external rotational transform ι_0 with α as parameter for $B_0 = 3.5$ T. α, characterizing the current density profile, increases with the electron density. The plasma current is kept constant at 25 kA in the calculation. It varies from 24 to 26 kA for the experimental points shown for different working gases.

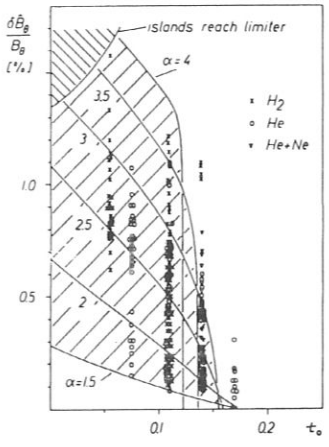

FIG. 7. This figure is similar to Fig. 5, but now the total ι at the limiter is kept constant instead of the plasma current. $\iota(a)$ is 0.35 in the calculation, for the experimental points shown $q(a) = 1/\iota(a)$ varies between 2.8 and 2.9.

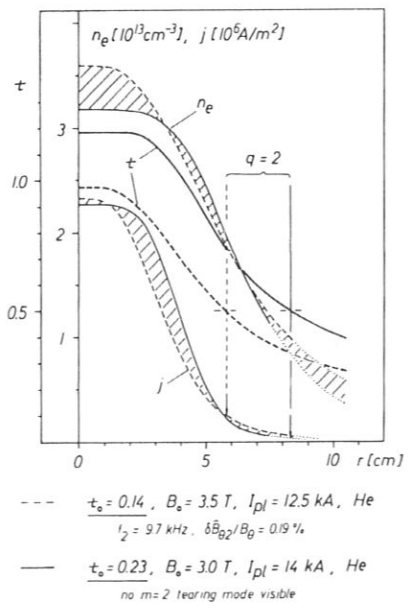

FIG. 6. Two discharges with similar current density profiles $j(r)$ and electron density profiles $n_e(r)$, but different $\iota(r)$ profiles are compared. All profiles are derived from Thomson scattering measurements. The different m = 2 mode behaviour is indicated.

The explanation for the stabilization of the (2,1) mode by the stellarator field can be inferred from Fig. 6. Two discharges with similar current density profiles, but different ι_0 are compared. Owing to the different ι_0 (and toroidal field), the $\iota(r)$ profiles have to be different. The superposition of the stellarator field or, in the case of Fig. 6, the increase of the external rotational transform ι_0 shifts the resonant q = 2 surface toward the plasma boundary. In this region, the gradient of the current density is small, and if the resonant surface is too far away from the steep gradient of j(r) (at $r \lesssim 5$ cm in Fig. 6), the mode becomes stable.

A similar investigation can be made keeping $\iota(a)$ constant instead of the plasma current. The result for $\iota(a) = 0.35$ is presented in Fig. 7. In this case, the $\iota(r)$ profiles depend only slightly on ι_0 since, besides $\iota(a) = \text{const}$, the central value of ι is also constant, because of the $\iota(0) \approx 1$ condition. Consequently, the radius of the q = 2 surface is also practically constant as is demonstrated in Fig. 8. The plasma current has, however, to decrease from 47 to 16 kA for $\iota_0 = 0$ to 0.17, and the current density profile shrinks considerably. This has the same effect on the relative position of the q = 2 surface in the current density profile as in the previous case with constant plasma current. Again the gradient of j(r) around the resonant surface decreases with ι_0. The expected

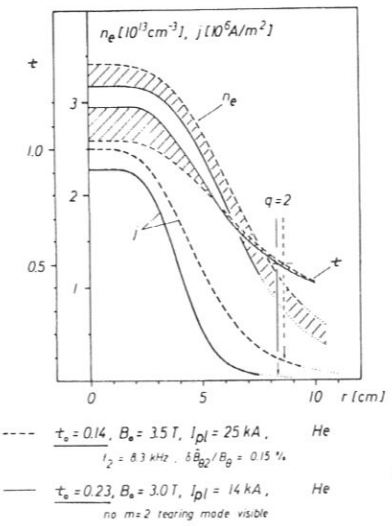

FIG. 8. Comparison of two discharges with similar $\iota(r)$ and $n_e(r)$ profiles, but now the current density profiles $j(r)$ are different. Again the different m = 2 mode behaviour is indicated.

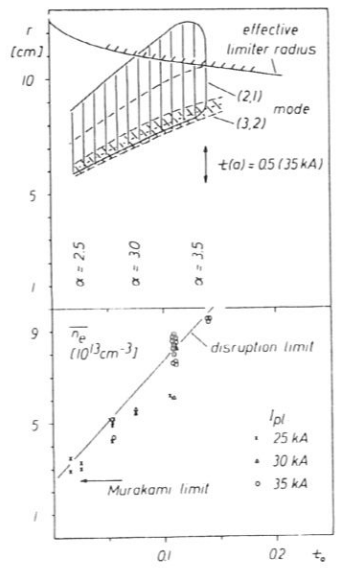

FIG. 9. Disruption limit depending on the line averaged density $\bar{n}_e$ and the plasma current I_{pl} as a function of ι_0 for Ohmically heated discharges in W VII-A with B_0 = 3.5 T. For $\iota_0 > 0.14$ the maximum attainable density decreases again with ι_0, but is limited by the available loop voltage. In the upper half, the island widths for the (2,1) and (3,2) modes, calculated independently of each other, are given for discharge conditions close to the disruption limit. Relevant values of the profile parameter α are indicated.

stabilization of the (2,1) tearing mode can be clearly seen in Fig. 7. Again all the experimental points lie in or slightly outside the shaded area predicted by the numerical calculation.

Under the conditions of Figs 7 and 8 the shear on the resonant surface is almost constant. It varies between 6.5×10^{-2} and 9.5×10^{-2}, and for α = const, it is constant within 10%. Nevertheless, the (2,1) tearing mode can have any amplitude, from very large values to very small. This indicates that there is no straightforward relation between the shear on the resonant surface and the mode amplitude. The more important figure is the gradient of the current density (mainly inside the resonant surface) which enters directly into the right-hand side of Eq. (3).

3.4. Current disruptions in W VII-A

Figure 9 shows that current disruptions have been observed in Ohmically heated discharges on W VII-A for external rotational transforms ι_0 up to 0.14. In the upper half, the island width of the (2,1) tearing mode has been calculated for discharges just stable against current disruptions.

For $\iota_0 \lesssim 0.07$ the islands are inside the plasma, and rotating (2,1) modes are observed experimentally. For $0.07 \lesssim \iota_0 \lesssim 0.14$ the current density profiles are still unstable, but now the islands extend beyond the limiter. No (2,1) mode is observed under these conditions, but the assumption of stationary islands is supported by the calculation (compare with Section 3.2.). For $\iota_0 \gtrsim 0.14$, either the q = 2 surface is beyond the limiter so that the (2,1) tearing mode can no longer exist, or, for smaller plasma currents, the current density profiles are stable for $\alpha \gtrsim 3.5$. Also no current disruptions could be observed for the accessible plasma parameters.

As a result, current disruptions seem to occur as long as the (2,1) tearing mode is unstable, regardless of whether the islands are rotating or stationary. The clear shift of the q = 2 surface with ι_0 toward the limiter seems to have no essential effect on the development of the current disruption.

In the lower half of Fig. 9 it is shown that for $\iota_0 \to 0$ the density limit due to current disruptions corresponds to the well-known Murakami limit [19]. With increasing stellarator field the electron density can be increased by a factor of up to three and the plasma current by a factor of up to 1.4 before reaching the disruption limit [20]. That means that even in the range of ι_0 where the disruptive instability still

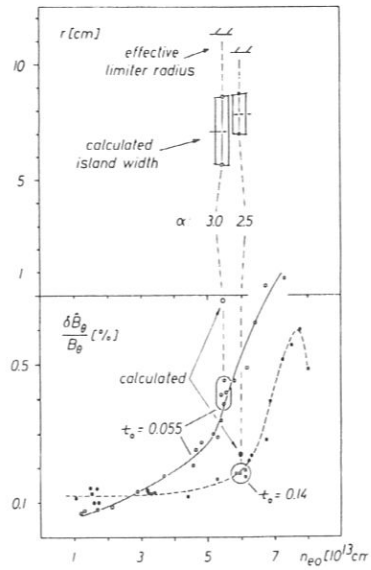

FIG. 10. The measured amplitude $\delta\hat{B}_\theta/B_\theta$ of the (2,1) mode as a function of the density n_{eo} for two helium discharges with different stellarator fields. In both cases, $B_0 = 3.5$ T and $I_{pl} = 20$ kA. At $n_{eo} \approx 5.5 \times 10^{13}$ cm^{-3} electron temperature profiles have been measured so that the island widths could be calculated. A comparison between the measured and calculated $\delta\hat{B}_\theta/B_\theta$ values indicates that the calculated island width for $\epsilon_0 = 0.055$ is somewhat too large.

exists the W VII-A stellarator is considerably more stable against current disruptions than a comparable tokamak (compare also Fig. 3, Ref. [6]).

A possible explanation for this experimental fact is given in Fig. 10. Here, two discharges are compared with all externally controllable parameters equal except the stellarator field. It can be seen that the amplitude of the (2,1) mode is reduced by a factor of roughly two in the range of large amplitudes if ϵ_0 is raised from 0.055 to 0.14. This is also confirmed by calculating the island widths.

Furthermore, we assume in accordance with Fig. 9 that a certain minimum island width is necessary for triggering a current disruption. Consequently, the reduced (2,1) mode amplitude at $\epsilon_0 = 0.14$ has to be increased again to such a threshold value. It follows immediately from Fig. 10 that this can be achieved by increasing the electron density. In Fig. 3 and in Ref. [7], it has been shown that the (2,1) mode amplitude increases with the plasma current for appropriate discharge conditions. Thus the stabilizing effect of the stellarator field on the (2,1) tearing mode can finally be overcome by an increased electron density and/or plasma current. In fact, the (2,1) island widths calculated according to the disruption limit of Fig. 9 depend only slightly on the discharge conditions.

4. CONCLUSIONS

We obtain good agreement between theory and experiment by applying an elementary non-linear code to compute the saturated amplitudes of tearing modes at the Mirnov coils from the condition $\Delta'(w) = 0$. The existence of stationary, i.e. not rotating magnetic islands is concluded from the calculation if the islands are close to or extend even beyond the limiter. This could be verified with the present experimental set-up only for time intervals of approximately 5 ms, which is, however, long compared to the oscillation time of the (2,1) mode under these conditions.

The explanation of the stabilization of the (2,1) mode by the stellarator field turns out to be straightforward. It is due to the fact that the position of the $q = 2$ surface can be moved independently from the other plasma parameters by varying ϵ_0. Thus the $q = 2$ surface can be shifted to regions where the current density profile is sufficiently flat for the (2,1) mode to be stable. Additional stabilizing effects cannot be excluded, but do not seem to be necessary in order to explain the observed dependence on ϵ_0.

It is interesting to compare the experimental findings on the current disruption in W VII-A with the predictions of theoretical models. One proposed mechanism for current disruptions in tokamaks is the non-linear de-stabilization of tearing modes with different helicity, especially the (3,2) mode, by the (2,1) mode [14, 21]. This model is also applicable to the W VII-A stellarator. The onset of the current disruption is expected when the (2,1) and (3,2) islands start to overlap. It can be concluded from Fig. 9 that this condition is fulfilled for the disruptive discharges in W VII-A. According to the simplified calculation used in this paper the (2,1) islands alone extend up to the $q = 1.5$ surface, and the (3,2) mode is unstable. A non-linear, three-dimensional code [14, 21] would probably yield a strong de-stabilization of the (3,2) mode leading to a current disruption.

Another consequence of the model mentioned above is that the key element in avoiding current disruptions should be to control the amplitude of the (2,1) tearing mode. Proposed methods are feedback stabilization and current density profile shaping [21].

A third method is the stabilization of the (2,1) mode by an $\ell = 2$ stellarator field. The results presented in Fig. 9 seem to confirm that this method suppresses current disruptions successfully in stationary discharges.

Another feature of the disruption model could not be verified in the very limited number of disruptions on W VII-A analysed so far. Although the (3,2) mode is frequently observed [22], its explosive growth expected at the beginning of a current disruption could never be clearly seen. This may be due to the very rapid time scale of $\approx 100\ \mu s$, which is of the order of or even faster than the oscillation time. Furthermore, current disruptions are connected with strong m = 0 (profile flattening) and m = 1 (inward shift of the plasma column) perturbations which make simultaneous modulations of the current density due to tearing modes difficult to identify. It should, however, be mentioned that (as for tokamaks [2, 3]) in the case of large (2,1) mode amplitudes, usually a (1,1) mode is observed on soft-X-ray signals [7]. This large (1,1) mode has the same frequency as the (2,1) mode, so there must be some interaction between the two modes. It may play a much more important role than the (3,2) mode in the disruptions observed on W VII-A.

Besides the basic effect of the (2,1) tearing mode on current disruptions, the correlation between the (2,1) mode and the plasma confinement is of great interest [23]. As in ORMAK [13] and T4 [16] such a correlation has been observed in W VII-A [7, 24]. Further results will be reported in a future paper.

ACKNOWLEDGEMENTS

We should like to thank Dr. K. Lackner for preparing and modifying his numerical code and Dr. D. Biskamp for valuable discussions. This work would not have been possible without the continuous endeavours of the W VII technical crew.

REFERENCES

[1] MIRNOV, S.V., SEMENOV, I.B., in Plasma Physics and Controlled Nuclear Fusion Research (Proc. 6th Int. Conf. Berchtesgaden, 1976) Vol. 1, IAEA, Vienna (1977) 291.
[2] KARGER, F., LACKNER, K., FUSSMANN, G., CANNICI, B., ENGELHARDT, W., et al., ibid., 267.
[3] EQUIPE TFR, Nucl. Fusion **17** (1977) 1283.
[4] KARGER, F., WOBIG, H., CORTI, S., GERNHARDT, J., KLÜBER, O., et al., in Plasma Physics and Controlled Nuclear Fusion Research (Proc. 5th Int. Conf. Tokyo, 1974) Vol. 1, IAEA, Vienna (1975) 207.
[5] W VII-A Team, in Plasma Physics and Controlled Nuclear Fusion Research (Proc. 6th Int. Conf. Berchtesgaden, 1976) Vol. 2, IAEA, Vienna (1977) 81.
[6] W VII-A Team, in Plasma Physics and Controlled Nuclear Fusion Research (Proc. 7th Int. Conf. Innsbruck, 1978) Vol. 2, IAEA, Vienna (1979) 265.
[7] W VII-A Team, ibid., 277.
[8] RUTHERFORD, P.H., Phys. Fluids **16** (1973) 1903.
[9] WHITE, R.B., MONTICELLO, D.A., ROSENBLUTH, M.N., WADDELL, B.V., Phys. Fluids **20** (1977) 800.
[10] JOHNSON, J.L., OBERMAN, C.R., KULSRUD, R.M., FRIEMAN, E.A., Phys. Fluids **1** (1958) 281.
[11] GLASSER, A.H., FURTH, H.P., RUTHERFORD, P.H., Phys. Rev. Lett. **38** (1977) 234.
[12] MATSUOKA, K., MIYAMOTO, K., OHASA, K., WAKATANI, M., Nucl. Fusion **17** (1977) 1123.
[13] CARRERAS, B., WADDELL, B.V., HICKS, H.R., Nucl. Fusion **19** (1979) 1423.
[14] BISKAMP, D., Max-Planck-Institut für Plasmaphysik, Garching, private communication (1979).
[15] MATSUDA, S., YOSHIKAWA, M., Jap. J. Appl. Physics **14** (1975) 87.
[16] MIRNOV, S.V., in Plasma Physics and Controlled Nuclear Fusion Research (Proc. 7th Int. Conf. Innsbruck, 1978) Vol. 1, IAEA, Vienna (1979) 433.
[17] NAVARRO, A.P., DUNLAP, J.L., PARE, V.K., BURRIS, R.D., Bull. Am. Phys. Soc. **24** (1979) 936.
[18] GRANETZ, R.S., HUTCHINSON, I.H., OVERSKEI, D.O., ibid., 997.
[19] MURAKAMI, M., CALLEN, J.D., BERRY, L.A., Nucl. Fusion **16** (1976) 347.
[20] W VII-A Team, in Current Disruption in Toroidal Devices (Proc. IAEA Symp. Garching, 1979) Garching (1979) paper D7.
[21] HOLMES, J.A., CARRERAS, B., HICKS, H.R., LYNCH, S.J., WADDELL, B.V., Nucl. Fusion **19** (1979) 1333.
[22] W VII-A Team, in Current Disruption in Toroidal Devices (Proc. IAEA Symp. Garching, 1979) Garching (1979) paper D6.
[23] CALLEN, J.D., WADDELL, B.V., CARRERAS, B., AZUMI, M., CATTO, J.P., et al., in Plasma Physics and Controlled Nuclear Fusion Research (Proc. 7th Int. Conf. Innsbruck, 1978) Vol. 1, IAEA, Vienna (1979) 415.
[24] W VII-A Team, in Controlled Fusion and Plasma Physics (Proc. 9th Europ. Conf. Oxford, 1979) Contributed Papers (1979) 4.

(Manuscript received 9 April 1980
Final manuscript received 8 July 1980)

ELECTRON HEAT TRANSFER AND DENSITY FLUCTUATIONS IN THE WENDELSTEIN VII-A STELLARATOR

W VII-A TEAM:

D.V. BARTLETT, G. CANNICI, G. CATTANEI,
D. DORST, G. GRIEGER, H.H. HACKER,
J. HOW, H. JÄCKEL, R. JAENICKE, P. JAVEL,
J. JUNKER, M. KICK, R. LATHE, J. MEYER,
C. MAHN, S. MARLIER, G. MÜLLER,
W. OHLENDORF, F. RAU, H. RENNER,
H. RINGLER, J. SAPPER, P. SMEULDERS,
M. TUTTER, B. ULRICH, A. WELLER,
E. WÜRSCHING, H. WOBIG, M. ZIPPE

NEUTRAL INJECTION TEAM:

D. COOPER, K. FREUDENBERGER, G. LISTER,
W. OTT, E. SPETH
Max-Planck-Institut für Plasmaphysik,
Association Euratom-IPP,
Garching, Federal Republic of Germany

Abstract

ELECTRON HEAT TRANSFER AND DENSITY FLUCTUATIONS IN THE WENDELSTEIN VII-A STELLARATOR.

The electron energy confinement in the W VII-A stellarator has been studied in Ohmically heated discharges. A low-density regime ($n_e(0) \lesssim 5 \times 10^{13}$ cm^{-3}) has been found, where the coefficient of electron heat conductivity χ_e follows drift parameter scaling closely. This implies a reduction of χ_e with increasing n_e and T_e. An attempt is made to correlate density fluctuations, as measured by microwave scattering, with the observed losses. – With neutral-beam heating, a considerable improvement of confinement has been observed. The confinement time increases with temperature, supporting the results observed in Ohmic heating. – Furthermore, a sharp overall reduction in the density fluctuation level at the beginning of injection is observed and may also contribute to the improved confinement. A brief description of the microwave scattering system is given. – In the high-density regime ($n_e(0) \gtrsim 5 \times 10^{13}$ cm^{-3}), the energy loss is increased by MHD mode activity (the (2,1) mode for $\iota(a) \lesssim 1/2$). Changes in the temperature profile due to magnetic islands have been observed.

W VII-A TEAM and NEUTRAL INJECTION TEAM

Introduction

In this paper we discuss the electron energy confinement in the W VII-A Stellarator for ohmically heated plasmas. First results of experiments with additional neutral beam heating and their effect on density fluctuation level and energy transport are also presented, along with a description of the new microwave scattering diagnostic (appendix). As described in /1/ and /2/, in standard helium discharges (20 kA, 3.5 T, $\iota_0 = 0.14$) there exist two regimes of confinement: the low density regime, where the confinement time is proportional to $\bar{n}_e$, and a high density regime, where the confinement time decreases with density. In the low density regime ($n_e(o) \lesssim 5\times10^{13}\,cm^{-3}$) it is possible to describe the electron heat conductivity $\chi_e(r)$ by a function of the local parameters $n_e(r)$ and $T_e(r)$ with $\chi_e \sim 1/\bar{n}_e \sqrt{\bar{T}_e}$. In the high density regime ($n_e(o) \gtrsim 5\times10^{13}\,cm^{-3}$) more parameters besides n_e and T_e seem to be necessary to describe the local heat conductivity. It is believed that, for $\iota(a) \lesssim 1/2$, growing (2,1) tearing modes /2 & 3/ with islands up to 2.5 cm wide cause the confinement to deteriorate.

Low density regime

The electron heat conductivity is derived from the electron energy balance equation $\chi_e = \dfrac{\int_0^r (P_{OH}(r')-P_{rad}(r')-P_{ei}(r'))r'dr'}{r\, n_e \dfrac{dT_e}{dr}}$.

The temperature profile $T_e(r)$ is described accurately by an analytical expression $T_e(r) = T_e(o)/\left[1+(r/r_0)^{2\alpha}\right]$, where the profile parameters $T_e(o)$, r_0, and α are found by a least squares fit to the measured points obtained by Thomson scattering. The ohmic heating power density $P_{OH}(r)$ is calculated from the temperature profiles assuming $Z_{eff}(r) = \text{const}$. The radiated power density $P_{rad}(r)$ is obtained from bolometric measurements. The electron-ion transfer power density $P_{ei}(r)$ is calculated from the ion temperature profile, where the central temperature has been measured and the profile $T_i(r)$ is assumed to follow the electron density profile. In ohmically heated plasmas, P_{ei} is very much less than P_{OH} and energy losses due to mass flow are negligible.

In contrast to the procedure described in /2/, we have now looked for an analytical approximation for χ_e of the form $\chi_e = A\ n_e^{\nu_n}\ T_e^{\nu_T}$ where

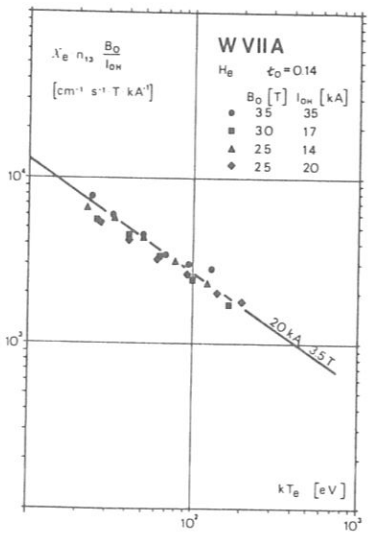

FIG.1. $\chi_e n_{13} B_o/I_{OH}$ *versus temperature.* n_{13} *is the local electron density in units of* 10^{13} cm^{-3}. *The straight line represents results from 20 kA, 3.5 T,* $t_0 = 0.14$ *helium discharges.*

A, ν_n and ν_T are constant factors. We have used values from profiles of different density (which also means different radiation levels /1/) and also different plasma currents, but with I_{OH}/B_o = const (I_{OH} = ohmic heating current and B_o = toroidal magnetic field). Only points outside the q=1 surface have been used. To determine A, ν_n, ν_T, a linear regression method has been applied. The result was $\chi_e = 3\times10^5\ n_e^{-0.97} T_e^{-0.68}\ cm^2 s^{-1}$ (T_e in eV, n_e in $10^{13}\ cm^{-3}$) which is very close to the $\chi_e \sim n_e^{-1} T_e^{-0.66}$ that was obtained by plotting $n_e\chi_e$ vs. temperature. The statistical error in this n-T approximation of χ_e was 12 %. In contrast $\chi_e \sim n_e^{-1}$ alone gives a statistical error of 72 % and is therefore in poor agreement with the measurements.

To study the influence of global parameters on χ_e in the low density regime, the toroidal field B_o and the plasma current I_{OH} have been varied independently. In Fig. 1 we have plotted $n_e\chi_e I_{OH}/B_o$ vs temperature for different combinations of I_{OH} and B_o, thus including a variation of I_{OH}/B_o. The temperature dependence for these cases is clearly the same and it also shows $\chi_e \sim I_{OH}/B_o \times 1/nT^{0.66}$ to be a good approximation to our present results. The external transform t_o was varied between 0.055 and 0.23, but no significant dependence of χ_e on t_o was detected. Also no

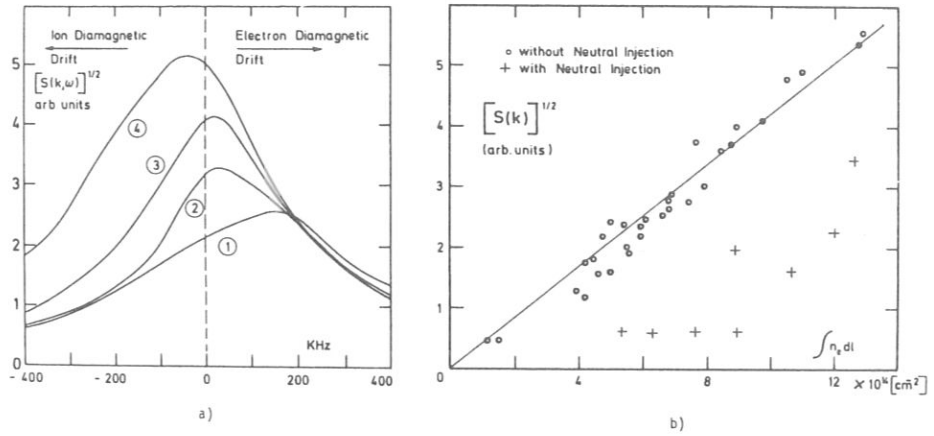

FIG.2. Density fluctuation level $\tilde{n}_e$ as measured by microwave scattering at $k_\perp \approx 11\ cm^{-1} \pm \delta k/2 = 3\ cm^{-1}$.

(a) Scattered amplitude $S(k,\omega)^{1/2}$ (arbitrary units) versus frequency at four different line densities, $\int n_e d\ell \times 10^{14}\ cm^{-1}$ equal to (1) 4.7, (2) 6.0, (3) 8.0, (4) 9.5.

(b) Scattered amplitude $S(k)^{1/2}$ (i.e. density fluctuation level $\tilde{n}_e$ in given $k_\perp$ range) integrated over frequency versus line density with and without neutral injection.

dependence on the local value of $\iota(r)$ (=1/q(r)) could be found. As a result the scaling of χ_e can roughly be described by $\chi_e \sim 1/B_0\bar{\xi}$ where $\bar{\xi} \sim I_{OH}/(\bar{n}_e\sqrt{\bar{T}_e})$ is the average drift parameter ($\bar{n}_e$ = area averaged density, $\bar{T}_e$ = density averaged temperature). These results suggest that a current driven instability might therefore be the cause of the anomalous heat transport in this region. However, results from the microwave scattering diagnostic do not show any clear correlation between the density fluctuation level and the drift parameter.

Fig. 2 shows the fluctuation level $\tilde{n}_e$, integrated over frequency (but not over wavenumber $k_\perp$) vs. line density over a wide range of discharge conditions (helium, deuterium, ι_0 = 0.16-0.23, I_{OH} = 10-20 kA, B_0 = 2.5-3.5 T). It can be seen that the deduced $\tilde{n}_e/n_e$ is constant for all densities, although the confinement time and heat conductivity vary considerably over these conditions. However, the large variation in both frequency and amplitude with line density may obscure a correlation of $\tilde{n}_e/\bar{n}_e$ with χ_e (for example, we expect $\chi_e \sim (\tilde{n}_e/n_e)^2\ \omega$ for flute-like modes, or $\chi_e \sim (\tilde{n}_e/n_e)^2 k_\perp^2$ for the dissipative trapped electron modes /7/, where ω and $k_\perp$ are the wave frequency and perpendicular wave number), so we

cannot yet be conclusive as to the physical processes leading to the drift parameter confinement scaling as described above.

The integrated scattered spectrum shows a weak radial dependence, peaking at r = 8 - 13 cm, and of course this becomes much more peaked towards the outside of the plasma if the amplitude is normalized to the local density. Most of our results are taken with a large scattering volume, with $2 < r < 15$ cm in order to obtain a global average in $\tilde{n}_e$. Almost no dependence on $k_\perp$ is seen over our range of 6 cm^{-1} - 25 cm^{-1}. Preliminary results with CO_2 laser scattering, at $k_\perp \sim 100$ cm^{-1}, confirms the global behaviour observed with microwave scattering with and without neutral injection. However, the fluctuation spectrum is narrower in frequency than that observed with microwave scattering.

Temperature dependence of χ_e

We have carried out some additional experiments to determine whether the favourable T dependence of χ_e is due merely to the fact that we derived it from ohmic heating discharges, where temperature and current are linked together. We have, however, changed the temperature independently of current by adding krypton to the discharge ("negative heating") and keeping all other external parameters constant (I_{OH} = 20 kA, B_o = 35 kG, $\int ndl = 4 \times 10^{14} cm^{-2}$). P_{Rad} in this case peaks at the centre of the discharge resulting in a profile similar to P_{OH} (Fig. 3), thus reducing the central temperature from 500 to 350 eV.

It is found, under these conditions, that the electron thermal conductivity agrees well with the results of Fig. 1, thus confirming the $T_e^{-0.66}$ dependence of χ_e. Neither was a change in the fluctuation level observed, although a narrowing of the spectrum was measured with the reduction of T_e. It should also be noted that in all the profiles mentioned earlier the radiation level and temperature profiles varied substantially with line density /1/.

Supplementary neutral beam heating will also answer the question of electron transport dependence on temperature. These results will be given in the next section.

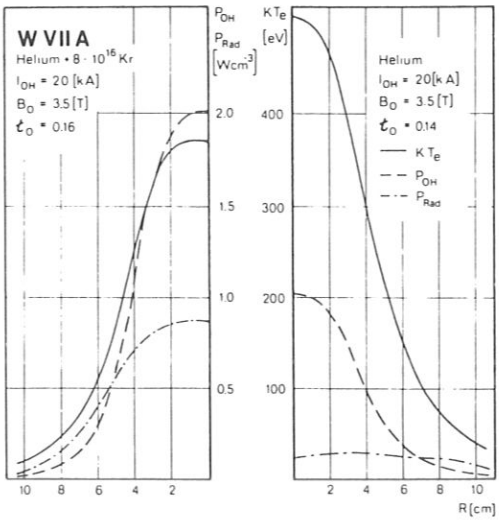

FIG.3. Comparison of a helium and a krypton-doped helium discharge. Both at 20 kA, 3.5 T, $t_0 = 0.14$. Radial distributions for kT_e, P_{OH}, and P_{Rad} are shown.

Neutral beam heating

First results on neutral beam heating experiments /4/ have been analysed. We have used helium and deuterium target plasmas with hydrogen neutral beams. Because of the short interaction length with almost perpendicular injection (84^0 co-injection) the target plasma has to be in the high density regime. Moreover, the density is increased during injection, to improve beam absorption, to a final density above that obtainable without injection. Even then, about 1/3 of the beam power is lost to the opposite wall. Approximately another 1/3 (depending on the external t_0) of the power is calculated to go into loss orbits. The local deposition of the heating power is derived from numerical calculations /4/ on the slowing down of the fast beam particles and the measured ohmic heating power. The power which is lost by transport results from the difference between the input power and the radiated power, the latter being a large fraction of the input power /4/.

In Fig. 4, $\chi_e n_e$ is shown vs. temperature for the time of maximum energy content in a series of discharges with $t_0 = 0.17$ and $I_{OH} = 25$ kA. During injection, the electron heat conductivity is reduced by a factor of 2 to a value below that of the low density curve. Note that the target plasma is in the high density regime, where χ_e normally is anomalously high. Since the density during injection increases even further above the density of the target plasma, a clear improvement of confinement is evident. Moreover,

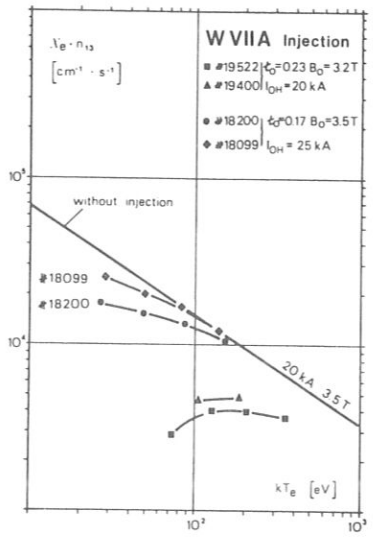

FIG.4. $\chi_e n_{13}$ versus temperature for experiments with additional neutral-beam heating. Straight line refers to Fig.1. The neutral-injection data have been normalized to 20 kA and 3.5 T.

the heat conductivity χ_e for the t_o = 0.23, I_{OH} = 20 kA discharge turns out to be well below the low density values. In this case because of the high rotational transform the Lister Code /4/ predicts 33 % of the power in loss orbits. But even if all this power were deposited in the plasma, it would still only bring χ_e into the low density range.

This leads to two possible conclusions: either the electron heat transport is considerably reduced during neutral injection, particularly at low plasma current and high rotational transform, or more of the injected particles are trapped than theoretically calculated, for example, if the particles on loss orbits experience anomalous improvement in confinement or slowing down.

Although no direct evidence of anomalous slowing down of the beam is available, R.F. probe measurements indicate enhanced ion cyclotron activity which could affect the beam trapping. Microwave scattering measures a broad, low level turbulence in the frequency range 800 - 4000 kHz during injection which could also affect the beam trapping.

An improved confinement during injection may result from the reduced level of density fluctuations observed. A sharp decrease in the fluctuation level occurs above a threshold injection power and within one millisecond of the start of injection. This implies that the change in amplitude is not due to temperature, density or profile changes, since these can only vary on a

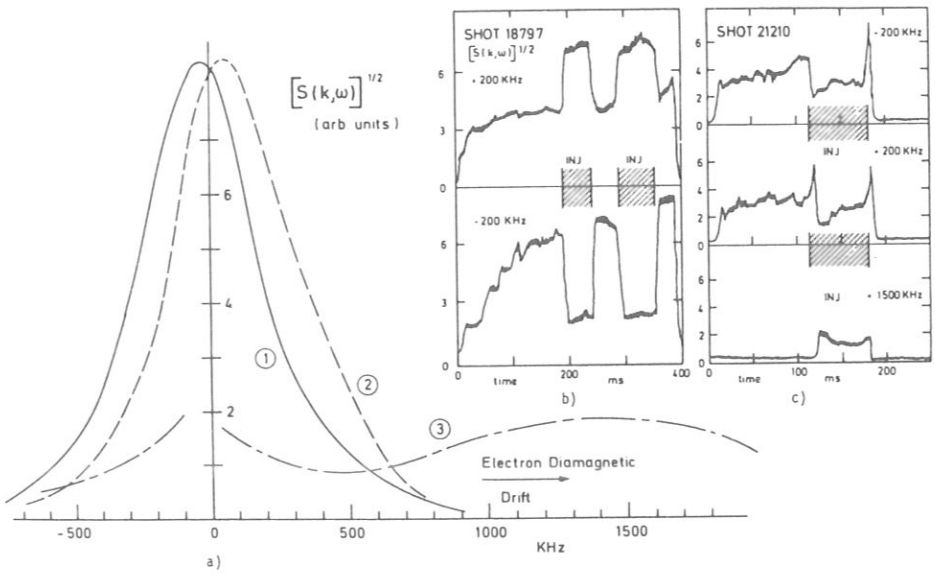

FIG.5. Fluctuation spectra $S(k,\omega)^{1/2}$ (arbitrary units).
(a) Spectra: (1) before injection, (2) with one injector, (3) with two injectors;
(b) Measured scattered amplitude at ± 200 kHz (i.e. electron and ion drift directions) as a function of time, with two consecutive injectors.
(c) Scattered amplitude at ± 200 kHz and + 1500 kHz as a function of time, with three simultaneous injectors.

longer time scale. Fig. 5 shows the scattered spectra before injection, with one injector (below the threshold power) and with two injectors, into a helium plasma. Also shown is the scattered amplitude as a function of time at particular frequencies, showing the time scale of events. It can be seen that injection powers below the threshold value cause a spectrum shift in the electron diamagnetic direction but no amplitude change. This may be associated with a change in poloidal rotation of the plasma. With two or three injectors operating, the low frequency spectrum is reduced, and a broad, low level, high frequency spectrum is seen, extending sometimes as high as 5 MHz. This is possibly associated with the enhanced ion cyclotron activity recorded during injection. Finally, we have plotted the integrated low-frequency (-500 to 500 kHz) spectrum amplitudes on the $\bar{n}_e$ vs. line density scaling graph (Fig. 2). It can be seen that the fluctuation level during neutral injection is much lower than without injection, correlated with the increased confinement.

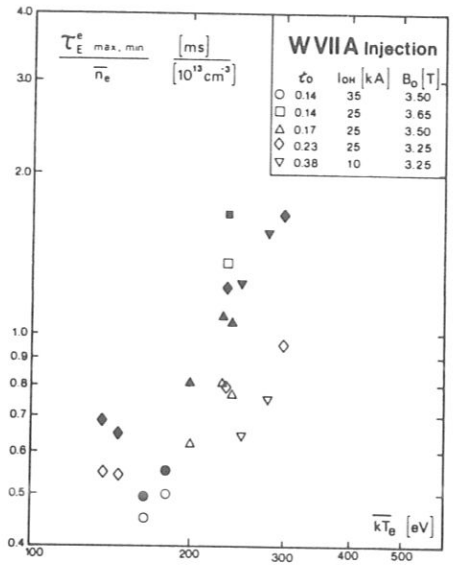

FIG.6. Electron energy replacement time τ^e_E normalized to $\bar{n}_e$, versus average temperature $\bar{T}_e$ (density-averaged). Solid symbols refer to $\tau^e_{E,max} = \int n_e k T_e dV / \int (P_{OH} + P^e_N) dV$, open symbols to $\tau^e_{E,min} = \int n_e k T_e dV / \int (P_{OH} + P^e_N + P^e_{Orbit}) dV$, where P^e_N is the calculated beam power density transferred to electrons and P_{Orbit} the orbit loss power density.

To show whether the electron confinement improves with temperature during injection, we have plotted the energy replacement time τ^e_E normalized by $\bar{n}_e$ vs. the average temperature (density averaged) in Fig. 6.

The normalized confinement time $\tau^e_{E,max}/\bar{n}_e$ (solid symbols) is clearly seen to increase with temperature. $\tau^e_{E,max}$ is calculated from the electron energy content divided by the sum of the ohmic heating power and the calculated /4/ neutral beam power into the electrons. However, even if there were anomalous beam trapping and all the calculated orbit losses were confined in the plasma, the same scaling for τ^e_E is apparent (open symbols $\tau^e_{E,min}$).

High density regime

It has been shown /2,3/ that there exists a very close correlation between the occurence of (2,1) tearing modes, and energy and particle confinement, for densities $n_e(o) \gtrsim 5\times10^{13}$cm^{-3} in standard discharges. Whenever the (2,1) mode activity increases, a deterioration of confinement is observed. This is also true for neutral beam heating experiments /4/.

We have since tried to obtain experimental evidence about the existence of magnetic islands. For this purpose, the triggering of the Pockels-cell

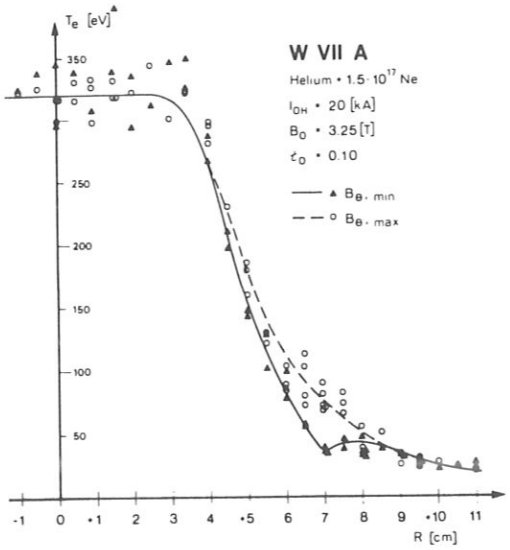

FIG. 7. Temperature profiles measured at the maximum and minimum of the poloidal field fluctuations B_θ. (Typical error 5%.)

for the laser was locked to the Mirnov coil signals. By use of a second laser focussed at the same radial position it was possible to get a measurement of T_e at the minimum and maximum of the poloidal field fluctuations for the same shot. Fig. 7 indicates that there is indeed a difference in the temperature profiles, especially when comparing the two temperature measurements made in the same shot. This difference agrees with the predictions of tearing mode theory /5/, assuming T_e = const on magnetic surfaces. From the perturbed magnetic topology a reduction of the global energy confinement is inferred /6/ but a quantitative calculation at this stage is difficult.

Acknowledgements

The achievement of current free operation would not have been possible without the invaluable support of the W VII-A technical staff. We would also like to thank T.K. Chu (Princeton) for many enthusiastic and fruitful discussions during his visit.

APPENDIX

Microwave Scattering Setup

A microwave scattering diagnostic has been in operation on the W VII-A stellarator for the last eighteen months. It is designed[1] to investigate poloidal-plane electron density fluctuations in the wavelength region from 3 to 10 millimetres, at frequencies from 100 Hz to 1 GHz. The W VII-A diagnostic follows essentially the method used on TFR /7/, with movable emitter and receiver horns. We have, however, incorporated innovations which make this diagnostic more versatile and simpler to use than previous systems.

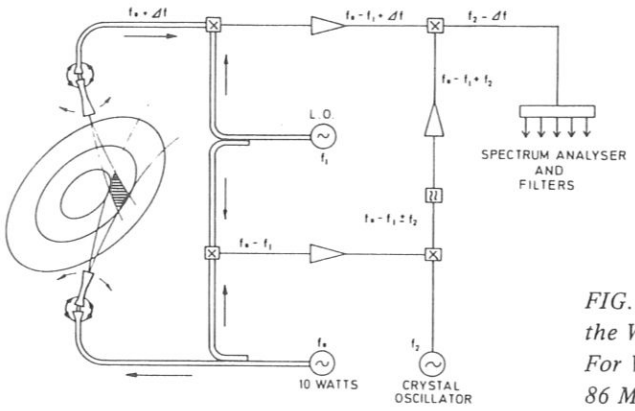

FIG. 8. Microwave scattering system on the W VII-A and CLEO stellarators. For W VII-A, f_0, $f_1 \approx 155$ GHz, f_0-f_1 = 86 MHz, f_2 = 64 MHz.

Fig. 8 shows the experimental arrangement for scattering from the elliptic cross-section of W VII-A. The microwave power is supplied by a Varian Extended Interaction Oscillator (E.I.O.) delivering 10 Watts at 155 GHz. The transmitting and receiving microwave horns (~ 25 dB gain) can be pivoted using a novel flexible waveguide system. Thus most of the cross-section can be viewed, with scattering angles from 0^o to 50^o. This allows a calibration to be carried out at 0^o, and exploration of fluctuations in the wavenumber range 6 cm^{-1} - 25 cm^{-1}. The received signal, consisting of the unscattered "stray" signal and the scattered, doppler shifted spectrum,

[1] The design was carried out in collaboration with Dr. P. Thomas of the CLEO team (Culham), and a similar system has been installed on the CLEO stellarator.

is mixed with a local oscillator to produce an 86 MHz intermediate frequency. The addition of a second mixing stage transfers the scattered spectrum onto a stable crystal oscillator line (64 MHz), removing any frequency drifts and phase noise due to the microwave oscillators (also described in ref. 8). A bank of 16 narrow band filters covering the range $\pm$ 2 MHz around the 64 MHz I.F. is used to give the scattered spectrum as a function of time, and the outputs are low pass filtered and digitally recorded.

References

[1] RENNER, H. and W VII-A TEAM, Proc. 7th Int. Conf. on Plasma Physics and Controlled Nuclear Fusion Research, Innsbruck, II, IAEA Vienna (1979), 265

[2] RINGLER, H. and W VII-A TEAM, Proc. 9th Europ. Conf. on Contr. Fusion and Plasma Physics, Oxford, 1979, A2.4,4

[3] JAENICKE, R. and W VII-A TEAM, Proc. 9th Europ. Conf. on Contr.Fusion and Plasma Physics, Oxford, 1979, BP23,77

[4] W VII-A TEAM and NEUTRAL INJECTION GROUP, paper H-2-2, this conference

[5] HICKS, H.R., et al., ORNL/TM-6096 (Dec. 1977)

[6] CALLEN, J.D., and AZUMI, M., Bull. Am. Phys. Soc. 23 (1978), 885

[7] EQUIPE TFR, Proc. 6th Int. Conf. on Plasma Physics and Controlled Nuclear Fusion Research, Berchtesgaden (1976), IAEA Vienna (1977), Vol. I, 35

[8] DOANE, J.L., Princeton Plasma Physics Laboratory Report PPPL-1595, Nov. 1979

NEUTRAL INJECTION IN THE WENDELSTEIN VII-A STELLARATOR WITH REDUCED OHMIC CURRENT

W VII-A TEAM:

D.V. BARTLETT, G. CANNICI, G. CATTANEI,
D. DORST, G. GRIEGER, H.H. HACKER, J. HOW,
H. JÄCKEL, R. JAENICKE, P. JAVEL, J. JUNKER,
M. KICK, R. LATHE, J. MEYER, C. MAHN,
S. MARLIER, G. MÜLLER, W. OHLENDORF, F. RAU,
H. RENNER, H. RINGLER, J. SAPPER,
P. SMEULDERS, M. TUTTER, B. ULRICH,
A. WELLER, E. WÜRSCHING, H. WOBIG, M. ZIPPE

NEUTRAL INJECTION TEAM:

D. COOPER, K. FREUDENBERGER, G. LISTER,
W. OTT, E. SPETH
Max-Planck-Institut für Plasmaphysik,
Association Euratom-IPP,
Garching, Federal Republic of Germany

Abstract

NEUTRAL INJECTION IN THE WENDELSTEIN VII-A STELLARATOR WITH REDUCED OHMIC CURRENT.

A high-density deuterium plasma with $\beta(0) \leq 0.5\%$; $n_{eo} \geq 10^{20}\,m^{-3}$; T_e, $T_i > 350$ eV can be maintained in the Wendelstein VII-A stellarator with two neutral injectors (27 kV, H_2; $P_N \approx 600$ kW). During the injection phase the plasma current is reduced to zero in 50 ms. The edge value of the rotational transform is kept constant by increasing the current in the helical windings. This procedure prevents MHD instabilities and leads to currentless operation at an external transform of $\iota_0 > 0.5$ without shear. The plasma shows no major instabilities, but the energy balance is dominated by radiation losses. Calculations based on the ODIN code for the conditions of W VII-A with 6° co-injection predict heating efficiencies of $\eta = 17\%$ ($P_{inj} = \eta P_N$; P_N = total neutral power; P_{inj} = net heating power).

1. INTRODUCTION

Studies of plasma behaviour in the Ohmically heated W VII-A stellarator ($R = 2.0$ m, $a = 0.1$ m, $B_0 \leq 3.5$ T; helical windings; $\ell = 2$, $m = 5$, shearless external transform $\iota_0 \leq 0.23$) have demonstrated the deleterious effect of plasma

current on transport and stability [1]. In particular, at high electron density $n_e(0) > 5 \times 10^{19}\,m^{-3}$ the radiation losses from the plasma edge lead to a change of the current profile and a consequent increase in MHD activity [2]. The MHD tearing mode m = 2, n = 1 and the disruptive instability can be stabilized by increasing the external transform ι_0 to values above 0.15, but $\iota(0)$ and the current density $j_{max} \lessapprox (B_0/R)\,(1-\iota_0)$ are limited by sawtooth oscillations in the plasma centre. This limit in the central Ohmic power input determines the maximum achievable temperature and density in Ohmically heated discharges. Whereas the ion heat transport is in agreement with neoclassical predictions, the anomalous electron heat conduction χ_e exceeds the classical value by a factor of 1000. At low density ($n_e(0) < 5 \times 10^{19}\,m^{-3}$) the following scaling law is found: $\chi_e \sim (I_p/B_0)\,n^{-1}\,T_e^{-0.68}$ whereas at higher densities the m = 2 tearing mode and associated islands lead to further increase of the heat losses [3]. Hence, the replacement of Ohmic heating by neutral beam injection promises improvement of plasma confinement and stability. On the other hand, with no plasma current the shear is also zero. This could lead to an increase of shear-suppressed drift instabilities.

2. NEUTRAL INJECTION INTO W VII-A

For heating purposes, four injectors with a total neutral power of more than 1 MW have been installed on the W VII-A stellarator. The specifications of each injector are:

Working gas: hydrogen
Acceleration voltage: 25–30 kV
Beam current: I = 30–35 A
Fraction of neutral power E : E/2 : E/3 = 52:25:23
Injection angle between beam and perpendicular direction to the magnetic field: 6° co-injection (at the port)
Injected neutral power: P_N = 250–350 kW
Pulse duration: $\Delta t \leqslant 200$ ms

Injection heating in W VII-A has to overcome several difficulties:

(a) A large fraction of the beam is not absorbed in the plasma but strikes the opposite wall, which may lead to sputtering and impurity influx.

(b) Near perpendicular injection would be expected to lead to significant orbit losses. These are highly energetic ions, which drift to the wall before being slowed down. The short interaction length of 0.2 m requires a high-density target plasma ($n > 5 \times 10^{19}\,m^{-3}$) to be produced by Ohmic heating for sufficient absorption.

(c) The small aperture of the injection ports ($\emptyset$ = 8.5 cm) requires high beam power densities and careful design of the beam line.

For the experiments reported here two injectors with a total power $P_N = 400–650$ kW have been used. Hydrogen was injected into a helium or deuterium target plasma.

3. MODE OF OPERATION IN W VII-A

With Ohmic heating, a high-density target plasma is only possible after lengthy discharge cleaning at 50 Hz (Ne/He). To reduce the concentration of the main impurity (oxygen) to below 1%, additional titanium gettering is applied before pulse operation.

There are three different types of injection experiments in W VII-A:

(a) Injection at constant plasma current and constant external rotational transform ι_0. Gas puffing is used to increase the density during the injection phase at plasma currents below 35 kA.

(b) Injection with reduction of the plasma current during discharge but with constant external transform.

(c) Reduction of plasma current to zero during the injection phase and a simultaneous increase of the external transform in order to keep $\iota_0 + \iota_p(a) > 0.5$, where $\iota_p(a) =$ transform of plasma current at the boundary.

4. RESULTS

4.1. Constant plasma current, constant external transform

In helium discharges a maximum line density of $\int ndl = 1.5 \times 10^{19}\,m^{-2}$ could be realized only at $I_p = 35$ kA and $\iota_0 = 0.14$. In the first experiments with neutral-beam heating [4] a comparison was made between discharges of different plasma currents ($I_p = 20–35$ kA) but the same density ($\int ndl = 1.5 \times 10^{19}\,m^{-2}$) and the same value of $\iota_0 + \iota_p(a) \approx 0.5$. In these conditions the $m = 2$ tearing mode was suppressed.

Starting with a target plasma at $T_e = 250$ eV, the beam primarily heats the electrons, and the increase of the electron temperature kT_e to 400–500 eV at a central density of $n_{e0} > 10^{20}\,m^{-3}$ reduces the Ohmic power contribution. Neutral injection expands the accessible parameter regime in relation to that of Ohmic heating.

4.2. Reduction of plasma current at constant external transform

The experiments with reduction of plasma current during the discharge were limited by the occurrence of soft disruptions. These disruptions occurred at $\beta_\theta \approx 8$ ($\beta_\theta \sim n(T_e + T_i)/J_p^2$) and were accompanied by strong 3/2 modes

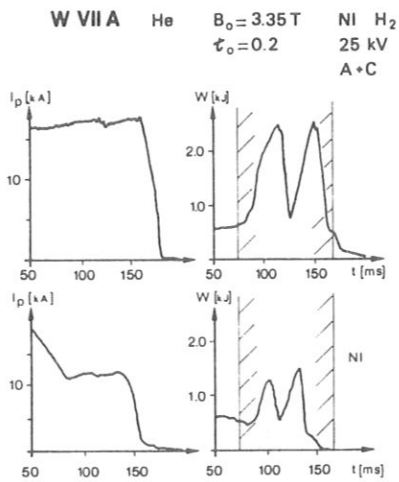

FIG.1. Energy content limits for discharges with NI, different plasma currents and constant rotational transform.

and 2/1 modes. Figure 1 shows two discharges at different plasma currents in relation to the plasma pressure obtained. The very fast rising m = 2 tearing modes (suppressed in OH-discharges at this high external transform of $\iota_0 = 0.23$) have been observed as precursors of the temperature-flattening and the subsequent plasma energy decay. The inward shift of the mode rational surfaces during current reduction, and the change of the current profile due to neutral-beam heating at the edge, destabilized coupled 2/2 and 3/2 modes and consequently the 2/1 tearing modes [5].

To control the position of the q = 2 surface, a feedback system for the current in the helical windings has been developed. During the 50-ms plasma current decay phase, the current in the helical windings is increased so that the total transform $\iota_0 + \iota_p(a)$ is kept above 0.5. This method has successfully prevented soft disruptions, and a phase with a vanishing Ohmic-heating current has been achieved.

4.3. Operation at zero plasma current

Several difficulties are involved in the procedure described above: (a) The reduction of the plasma current to zero has to be made in more than 30 ms in order to prevent strong perturbations of the current distribution. (b) The high external transform leads to a large ellipticity of the magnetic surfaces and a reduction of the effective plasma radius ($\iota_0 = 0.5 \rightarrow a/b = 2$). (c) The target plasma has to start at a plasma current of 16 kA, otherwise a reduction to zero is not possible in the available time. Therefore only a low-density target plasma with $\int ndl = 4.5 \times 10^{18}\,m^{-2}$ is possible, leading to a power absorption of 30% of the neutral beam. (d) The large amount of energy deposited at the wall in the initial phase of injection may release impurities from the wall and enhance the radiation loss. (e) Consequently the density build-up during the injection phase must be carefully adjusted to prevent strong cooling of the electrons.

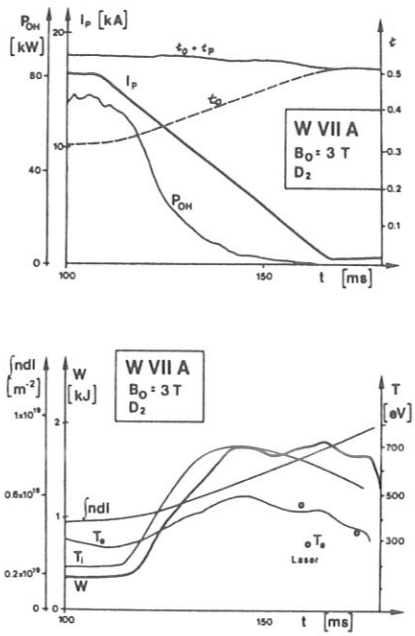

FIG.2. Plasma current reduction during NI. Also shown are Ohmic power P_{OH}, rotational transform $t_0 + t_p$ and t_0. Time variation of line density, electron temperature T_e and ion temperature T_i. (T_e from EC emission with normalization from Thomson scattering; T_i from charge-exchange analysis.) Energy content W by means of diamagnetic loop. Neutral injection during 115–180 ms.

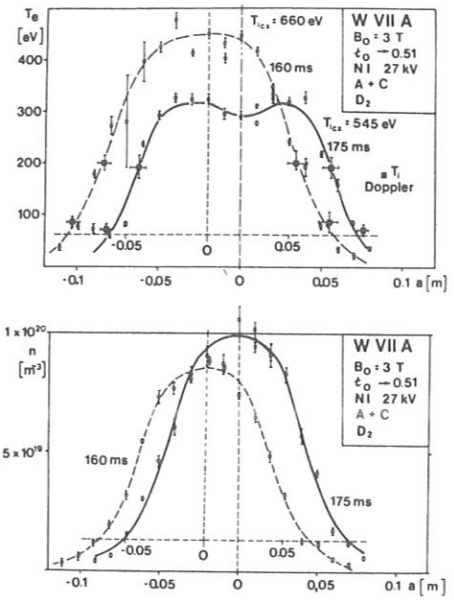

FIG.3. Electron temperature T_e and density n profiles at 160 ms and 175 ms for the discharge parameters of Fig.2. Doppler width and charge-exchange measurements of T_i are indicated.

Deuterium was used as a target plasma since its heating efficiency was calculated to be slightly higher than in a helium plasma.

4.4. Main parameters

The most important parameters of the discharge are given in Fig. 2, which describes the plasma current I_p, the Ohmic power, the line density and the energy content measured by the diamagnetic loop. Figure 3 shows the temperature and density profiles in the currentless phase ($\Delta t = 160$ ms, $\Delta t = 175$ ms).

The ion temperature was measured from the Doppler broadening of the impurity lines in the outer region. The central ion temperature from charge-exchange measurements is, in general, higher than the electron temperature ($T_i = 540$ eV; $T_e = 320$ eV at $\Delta t = 175$ ms). On the other hand, the heating power of plasma ions to electrons as calculated from these data requires a much higher neutral-beam heating of the ions than predicted by classical theory.

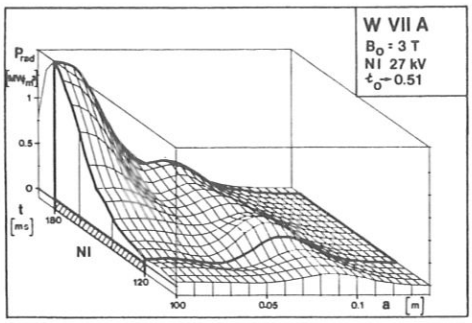

FIG.4. Bolometrically measured radiation power-density profile during NI for the discharge parameters of Fig.2.

4.5. Energy balance and radiation loss

The uncertainties in the ion heating power prevent a detailed analysis of ion heat transport. Some phenomena concerning electron heat conduction have been described in paper IAEA-CN-38/H-2 at this conference [3]. The radiation losses are measured with a bolometer and ultra-soft X-ray diagnostics. The importance of radiation losses on the energy balance is demonstrated in Fig.4. During the neutral injection phase, a significant increase of the central radiation power affects the central electron temperature and may be the reason for the flattening of the temperature profiles. At $\Delta t = 175$ ms the hollow $T_e(r)$-profile indicates that more energy is lost from the central region than the electrons obtain by direct heating. The radiation measurements by ultra-soft diodes (through 1000-Å Al) and the bolometer (without filter) agree in the central region of the plasma. From comparison of intensities through various filters, an average photon energy of around 500 eV is deduced. The spectroscopy documented an increase of emission during the late phase of neutral injection at these photon energies.

The origin of these losses is very likely the impurities O^{6+}, O^{7+}, N^{6+} and C^{5+}. Spectroscopy and soft X-ray diagnostics exclude a significant contribution from iron and molybdenum lines. The strong increase of radiation in the plasma centre cannot be explained by a density and temperature increase only. An increased influx of impurities could not be detected; rather, a reduction of radiation from low ionization states $O^{1+} - O^{5+}$ is observed.

At present, it cannot be decided whether accumulation by diffusion or injection of oxygen by the neutral beam or interaction with the wall is responsible for the strong increase in radiated power. However, it seems unlikely that oxygen in the accelerated beam is responsible alone for the observed impurity effects, since only $\leqslant 3\%$ of oxygen in the beam has been measured in the test stand. Apparently this is not a specific problem of the currentless operation, since all experiments at high plasma currents with injection heating in helium exhibited similar behaviour. Nevertheless, in discharges with Ohmic heating, transport by sawtooth oscillations within the $q = 1$ region may counteract a possible accumulation of impurities in the centre and reduce the increase of radiation.

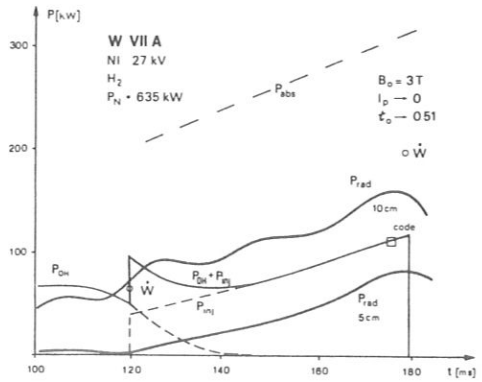

FIG.5. Input power $P_{OH} + P_{inj}$ *versus time: bolometric measurements of radiated power within* $r \leqslant 5$ *cm and* $r \leqslant 10$ *cm.* W *represents the time derivative of the energy content when NI is switched on and off;* P_{abs} *is the calculated absorption power without orbit losses.*

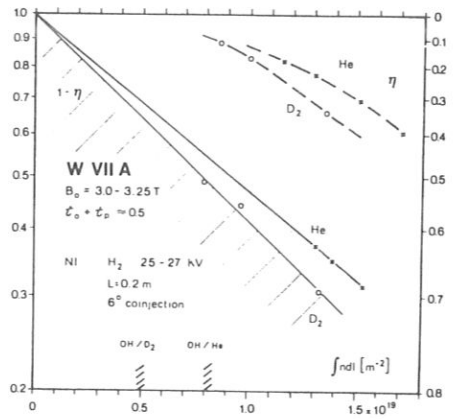

FIG.6. Calculated NI heating efficiency versus line density for He *and* D_2 *targets in W VII-A. The broken and solid curves are with and without the inclusion of orbit losses, respectively.*

Figure 5 gives a picture of the total power balance. The bolometer measurements of radiative losses are compared with the input power $P_{OH} + P_{inj}$. The injection heating power P_{inj} is calculated by Monte-Carlo techniques (ODIN code) with a total neutral power $P_N = 635$ kW. During the stationary phase of the plasma energy, between 140 ms and 180 ms, it can be seen that either the heating power P_{inj} is underestimated or the measured radiation power is too high. Transport to the limiter must also be accounted for in the injection power. The bolometer measurements are reasonably accurate, even after allowance is made for calibration errors, possible toroidal and poloidal asymmetries and interference by particle fluxes. The conclusion is that the calculation of heating efficiency based on classical assumption is too pessimistic. From the energy change W, at the beginning and the end of the injection phase, another estimate for the injection power can be obtained: $t = 120$ ms $\rightarrow P_{inj} = \dot{W} = 70$ kW; $t = 180$ ms $\rightarrow P_{inj} = \dot{W} = 170$ kW. The classical prediction at $t = 175$ ms is 106 kW.

Figure 6 presents the calculations of heating efficiency for discharges in helium and deuterium. These are based on the measured temperature and density profiles at several times during injection. Changing from a helium to a deuterium

TABLE I. PLASMA PARAMETERS ACHIEVED IN W VII-A WITH TWO INJECTORS FOR VARIOUS PLASMA CURRENTS AS SHOWN IN FIG.7

W VII A				NI 25 kV			
		He			D_2		
B_0	[T]	3.5	3.25	3.25	3.25	3.25	3.0
I_p	[kA]	25	20	10	10	10	0
t_0		0.17	0.23	0.38	0.38	0.38	0.51
n_{e0}	[m^{-3}]	1.15	1.2	1.14	1.01	0.89	0.96×10^{20}
$\bar{n}_e$	[m^{-3}]	6.1	5.3	4.8	5.8	3.0	4.3×10^{19}
T_{e0}	[eV]	427	529	403	497	573	316
$\bar{T}_e$	[eV]	229	299	253	250	392	238
T_{i0}	[eV]				495	750	545
W	[J]	2550	2900	1950	2900	2400	1750
$\int ndl$	[m^{-2}]	17.1	15.1	13.0	13.1	8.6	9.6×10^{18}
P_N	[kW]/N	430/2	445/2	600/2	600/2	600/2	635/2
loss: transm.		.31	.32	.38	.31	.49	.45
orbit		.24	.34	.39	.35	.39	.38
heat: ion		.07	.05	.05	.05	.03	.03
electr.		.32	.24	.18	.29	.08	.14
η		.39	.29	.23	.34	.11	.17
$P_{inj.}$	[kW]	168	128	138	204	66	106
P_{OH}	[kW]	108	60	26	16	11	0
$P_{inj.} + P_{OH}$	[kW]	276	188	164	220	77	106
$P_{rad.}$	[kW]	236	190	250	260	170	155
P_{rad} 0.2 μ Be	[kW]			82	50	60	60
$P_{inj.}$ absorbed	[kW]	296	302	372	414	306	349

Note: The last column gives the currentless plasma at 175 ms referred to in Figs 2, 3, 4, 5 and 8.

target gives a slight increase of η. To demonstrate the ineffective absorption of the beam at the beginning of injection, the density accessible by Ohmic heating at $I_p < 20$ kA is indicated. Table I summarizes the most important parameters for different discharges with low and zero plasma current. In all cases the Ohmic power is small compared to the injection power.

An important question is whether the confinement is improved in low-current or currentless operation. In Fig. 7 the energy content of the discharges of Table I are plotted versus input power $P_{OH} + P_{inj}$. The accessible area for Ohmic heating is also indicated for He or D_2. Even if all the orbit losses are neglected and the heating power is assumed to be equal to the total absorbed power $P_{inj} = P_{abs}$, an improvement of the energy replacement time $\tau_E = E/(P_{inj} + P_{OH})$ in low-current discharges during injection can be seen.

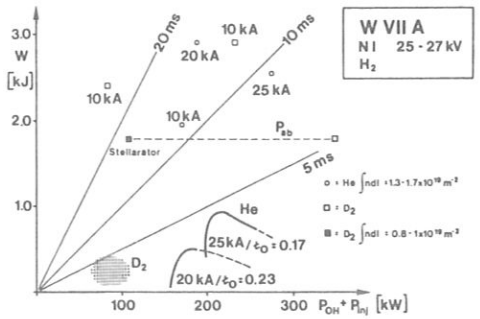

FIG. 7. Energy content versus input power for the discharges listed in Table I. The regions accessible by Ohmic heating alone are marked.

There are some possible explanations of the improved confinement during neutral injection. With the onset of injection, density fluctuations monitored by scattering of CO_2-laser light at $\lambda = 0.5$ mm and microwave scattering at $\lambda = 5$ mm are considerably reduced in the frequency regime $0 < f < 300$ kHz [3]. The fast decrease of the fluctuation level $\delta n/n$ seems to be strongly correlated with the obtainable plasma pressure. Neither the nature of these fluctuations nor the stabilization mechanism by neutral-beam injection is yet understood.

An increase of the neutral-beam heating efficiency above the classical value would require an anomaly in the slowing-down process of the fast ions. HF probes at the plasma edge observe strong ion-cyclotron oscillations of the hydrogen minority after the onset of neutral-beam injection ($\omega = n\omega_{ci}$). These oscillations are apparently excited by the high-energy beam and therefore extract energy from the beam. Since the frequency is the second harmonic of the deuterium ions, the deuterium can be heated by these oscillations. If the mechanism occurs, the measured ion temperature is consistent with such an explanation. The increased power input to the ions compensates the heat transfer to the electrons and the ion heat conduction losses, which according to neo-classical scaling in the plateau regime can exceed the electron heat-conduction losses.

5. NUMERICAL COMPUTATIONS OF HEATING EFFICIENCY IN W VII-A

Earlier numerical computations [6] of the heating efficiency of neutral-beam injection in W VII-A, using a modified version of the FREYA code [7], indicated that a smaller fraction of the energy carried by the 'fast ions' was deposited in the plasma than might be inferred from experimental measurements. To study possible mechanisms for this apparent discrepancy, a considerably faster stellarator Monte-Carlo code, ODIN, has been developed, which incorporates an improved physical model and permits the tracking of more particles, thus reducing the margin for statistical error. In the present computations, the plasma is modelled so that the minor cross-section is elliptic and rotates around the torus with the stellarator

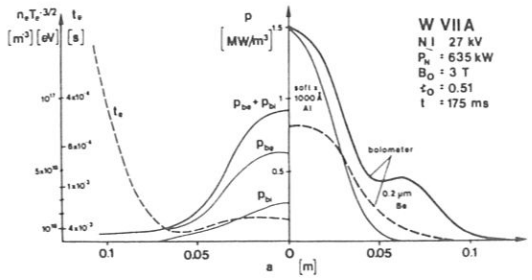

FIG. 8. Calculated deposition profiles for the neutral beam at 175 ms for the discharge of Fig. 2; power to the electrons P_{be}, and to the ions P_{bi}, is given. For comparison, the radiation power density measured by the bolometer with (broken line) and without (solid line) 0.2-μm Be filter is shown together with the soft X-ray profile (1000-Å Al filter). The calculated slowing-down time t_e versus radius is also shown: $t_e \sim T_e^{3/2}/n$.

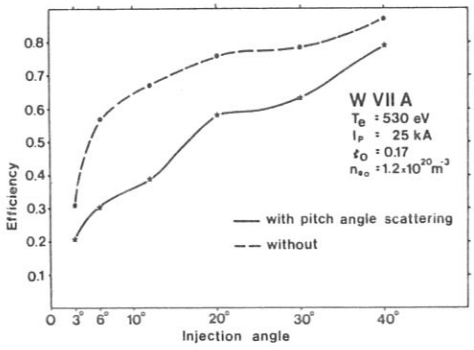

FIG. 9. Efficiency of NI heating as a function of the injection angle. The effect of pitch-angle scattering is demonstrated.

magnetic flux surfaces. Plasma temperature and density profiles are introduced to correspond to the experimental measurements along the line of the Thompson-scattering profile, and values at other points are obtained using a suitable transformation. This model is used in calculating both where the fast ions are generated by the neutral beam and where these ions deposit their energy.

The orbits of the fast ions are followed, assuming the usual ∇B and curvature drifts from magnetic fieldlines, and the $\vec{E} \times \vec{B}$ drift due to possible 'radial' electric fields are also included. The results from the electric field are still under investigation. Coulomb interactions slowing down the fast ions in their path through the plasma are assumed to be classical. Previous calculations assumed that ions whose orbits deviated beyond the limiter radius were lost to the system. The present results allow for the finite width of the limiter and the presence of 'effective limiters' such as the MHD coils and diamagnetic loops.

Differences in heating efficiencies for circular and elliptic plasmas were found to be generally small for the same effective plasma radius, but some changes in the energy deposition profile have been observed. The toroidal current profile has been assumed purely cylindrical throughout, but the effect of 'peaked' and 'flat' current profiles was also found to be small. The inclusion of a purely radial electric field, corresponding to a potential $\phi = 1$ kV across the plasma, has shown some improvement in particle confinement, but results are highly sensitive to the radial dependence of this potential. The inclusion of realistic limiter geometry has resulted, in many cases, in considerable improvement in computed efficiency,

e.g. from 0.2 to 0.3. Considerable improvement in efficiency was also obtained when low-density ($5 \times 10^{17}\,m^{-3}$) and low-temperature (1–5 eV) plasma was allowed to extend beyond the shadow of the limiter. There is some experimental evidence for this. In Fig. 8 we show the power/cm^3 deposited to ions (P_{Be}) and electrons (P_{Bi}) as a function of radius, together with a plot of $n_e/T_e^{3/2}$ (the factor governing slowing-down time due to electrons) for a typical set of parameters in the zero-current stellarator. The effect of slowing down from electrons in the outer region of the plasma is well illustrated.

An important effect in the high fraction of computed orbit losses is that of the pitch-angle scattering, illustrated in Fig.9. Assuming injection of a 'pencil' beam in the mid-plane of the torus, efficiency is plotted as a function of injection angle with and without scattering. For near-perpendicular (3°) injection, confinement is so poor that scattering has little time to have any effect, while for 'tangential' injection (40°) particle orbits are well confined and again the effect of scattering is small. However, for the injection angle (6°) used in W VII-A, the effect of scattering is large, since only a small angle scatter is required to change a confined orbit.

6. SUMMARY AND CONCLUSIONS

Neutral injection into W VII-A can extend the parameter regime beyond that of Ohmically heated plasmas. Operations without Ohmic-heating current could only be obtained by keeping the total rotational transform above 0.5 during the whole discharge in order to suppress the m = 2 tearing mode. Most of the experiments were done with two injectors. The energy content of the plasma in the currentless phase was 1.8 kJ as compared with 0.3 kJ before injection. Preliminary results with three and four injectors (total neutral power 800–1100 kW) indicate that the energy content can be increased to 3.5 kJ. Despite the uncertainties in actual heating power from the neutral beam, the energy confinement is improved in relation to Ohmically heated discharges. However, even if the anomalous electron thermal conductivity were reduced in currentless operation a considerable improvement of the total energy confinement cannot be expected since the electron energy loss is dominated by radiation,and ion heat conductivity becomes the dominant transport loss. The ions are in the plateau regime where the theoretical conductivity χ_i scales with $T_i^{3/2}$. The increase of radiation during injection seems to be correlated with the direct energy deposition by the beam on the wall. Adjustment of the beam power and the density increase may reduce these problems. The increase of high-energy radiation from the plasma centre in the last phase of injection can only be understood by an increase of the density of highly ionized impurity ions, especially oxygen.

The energy balance of the plasma requires a stronger ion heating than predicted by classical calculations. If the slowing-down mechanism of injected ions can be enhanced by the observed ion-cyclotron waves, this would lead to a reduction of the orbit losses and higher heating efficiencies. In stellarator operation ($I_p \rightarrow 0$, shear $\rightarrow 0$) a plasma beta $\beta(0) \approx 0.5\%$ was obtained. So far no MHD activity has been observed although, according to theoretical computations, β approaches the critical regime of localized MHD modes [8].

Another remarkable effect is the strong reduction of the fluctuation level at the onset of injection as observed with the CO_2 laser and μ-wave scattering diagnostics. Since changes of the plasma profiles occur on a time scale of tens of ms, this must be the direct effect of the neutral beam and of the presence of fast hydrogen ions in the plasma. There are some indications of a correlation in the level and frequency of fluctuations with plasma confinement but this has to be investigated further.

In summary, neutral-beam injection has been shown to be a powerful method for producing and maintaining a high-density plasma in a stellarator field.

ACKNOWLEDGEMENTS

The achievement of current-free operation would not have been possible without the invaluable support of the W VII-A technical staff. We should also like to thank T.K. Chu (Princeton) for many enthusiastic and fruitful discussions during his visit.

REFERENCES

[1] W VII-A TEAM, in Plasma Physics and Controlled Nuclear Fusion Research 1978 (Proc. 7th Int. Conf. Innsbruck, 1978) Vol.2, IAEA, Vienna (1979) 265.
[2] W VII-A TEAM, in Proc. 9th Europ. Conf. Controlled Fusion and Plasma Physics, Oxford, 1979, Papers BP23 and BP24.
[3] W VII-A TEAM, Paper IAEA-CN-38/H-2-1, these Proceedings.
[4] W VII-A TEAM AND NEUTRAL INJECTION GROUP, in Proc. 9th Europ. Conf. Controlled Fusion and Plasma Physics, Oxford, 1979, Papers BP24 and BP74.
[5] W VII-A TEAM, Inst. Plasma-Physik, Garching, Rep. IPP 2/250 (1980).
[6] FAULKNER, J.E., et al., in Proc. 9th Europ. Conf. Controlled Fusion and Plasma Physics, Oxford, 1979, Paper BP27.
[7] LISTER G.G., et al., in Proc. 3rd Symp. Plasma Heating in Toroidal Devices, Varenna, 1976 (SINDONI, E., Ed.), Editrice Compositori, Bologna (1976) 303.
[8] LORTZ, D., NÜHRENBERG, J., Nucl. Fusion **17** (1977) 125.

DISCUSSION

ON PAPERS H-2-1 AND H-2-2

J.C. WESLEY: It appears that the increase in central radiation that you observe is very similar to what is seen in Doublet III in a type 'O' discharge, i.e. one without central MHD activity. Do your discharges in fact show a similar absence of central MHD?

H. RENNER: In the currentless phase no MHD perturbations were observed. A high current ($q = 1$ at the centre) with sawtooth activity seems to prevent a strong increase in central radiation.

J.G. CORDEY: Have you considered whether charge-exchange recombination of the impurities by the neutral beam may be responsible for the large increase in radiation seen on injection? This process produces a sharp rise in radiation coincident with the beam switch-on. Do the O^{6+} lines, for example, show a sharp increase?

H. RENNER: We have considered this mechanism but do not believe it has a significant effect. In particular, the time behaviour of the central radiation is not consistent with the process you suggested. The intensity rises during the injection phase but no sudden increase is observed at beam switch-on.

D. PALUMBO: In the expression you give, I presume χ_e decreases with T. Is that right?

H. RENNER: Yes.

D. PALUMBO: And what was the current?

H. RENNER: The plasma current in our experiments varied between 14 and 35 kA and the main field from 2.5 to 3.5 T.

G.H. WOLF: In discussing the power balance, you explained that even if you made the unrealistic assumption that all your neutral-beam power of 365 kW was absorbed by the plasma and if you subtracted the measured radiated power of about 155 kW, you arrived at an absolute minimum possible plasma-transport-dominated confinement time of $\tau_E \approx 10$ ms. Can you give a plausible estimate on the basis of your diagnostic information of that component of the energy confinement time which is due to plasma transport only?

H. RENNER: We can use the time behaviour of the plasma energy on beam switching to estimate the heating power: $\dot{W} \sim P_{inj} \sim 180$ kW. If this value is correct, then by subtracting just the central radiation losses within 5 cm ($P_{rad} \sim 80$ kW) we get an energy exchange time of about 18 ms.

H. FURTH: A critical question appears to be whether the bulk plasma ions are heated by the beam ions in the classical manner or by some anomalously fast process. You have suggested that there may be an anomalous energy transfer through the coincidence of cyclotron harmonics of the beam and plasma ions. In that case, the heating should be diminished in ^{3}He plasmas.

H. RENNER: That is an interesting suggestion.

DISCUSSION

S.M. HAMBERGER: Have you considered the effects of a radial electric field on the trapping of the hot ions? This field might be indicated by the plasma rotation detected by the microwave scattering.

H. RENNER: The code calculations show that the electric fields have a small effect on the heating efficiency but this depends very much on the radial field distribution. Analyses of the scattered microwave and CO_2-laser spectra give contradictory results. For further explanation we have to wait for the spectroscopic measurements.

NEUTRAL-INJECTION HEATING IN THE WENDELSTEIN VII-A STELLARATOR

W VII-A TEAM
G. CATTANEI, D. DORST, A. ELSNER, G. GRIEGER,
H. HACKER, J. HARTFUSS, H. JÄCKEL, R. JAENICKE,
J. JUNKER, M. KICK, H. KROISS, C. MAHN, S. MARLIER,
G. MÜLLER, W. OHLENDORF, F. RAU, H. RENNER,
H. RINGLER, F. SARDEI, M. TUTTER, A. WELLER,
H. WOBIG, E. WÜRSCHING, M. ZIPPE

NI GROUP
K. FREUDENBERGER, G.G. LISTER, W. OTT,
F.-P. PENNINGSFELD, E. SPETH

Max-Planck-Institut für Plasmaphysik,
Euratom-Association, Garching,
Federal Republic of Germany

Abstract

NEUTRAL-INJECTION HEATING IN THE WENDELSTEIN VII-A STELLARATOR.

A high-density deuterium plasma with $\beta(0) \leqslant 1\%$ at $B_0 = 3.2$ T, $n_{e0} \geqslant 10^{14}$ cm^{-3}, $T_i = 1$ keV, $T_e = 0.6$ keV, is maintained in the Wendelstein VII-A Stellarator by neutral injection (27 kV, H_2, $P_N \approx 1$ MW). This was achieved by increasing the density of the target plasma by the ablation of an injected D_2 pellet. Oxygen is the dominant impurity. Contamination of the plasma has been reduced by various means, lowering the radiation losses, so that the "currentless" phase could be extended from 10 ms to 150 ms. The plasma in the currentless phase shows no instabilities. Analysis of the energy balance describes the ion heat loss in agreement with the neoclassical prediction. The electron conduction loss seems to follow the empirical scaling $\chi_e \sim 1/nT^{2/3}$. The beam-heating efficiency as predicted by the ODIN code, especially for the ions, is smaller than its observed value.

1. INTRODUCTION

"Currentless" operation of the Wendelstein VII-A Stellarator by neutral-injection (NI) heating was achieved in 1980 [1]. The plasma exhibits very favourable properties:

(a) No MHD instabilities, which would cause deterioration in the confinement at residual plasma current I_p, are observed.
(b) The level of density fluctuations is significantly reduced.

(c) The improved confinement allows a plasma to be maintained at remarkably high pressure.

However, radiative losses increasing strongly with time restrict the duration of the currentless phase. A detailed analysis of the power balance was uncertain owing to the dominant radiative power losses. In the meantime, significant progress has been made in diminishing the plasma contamination and consequently in extending the duration of the currentless phase [2]. The full NI power $P_N \approx 1$ MW was applied to heat the plasma.

2. MODE OF OPERATION

Four neutral injectors, using H_2, are available with 200–350 kW power each at an accelerating voltage of 27 kV. The W VII-A Stellarator (main radius R = 2 m; plasma radius a = 0.1 m; main field $B_0 \leqslant 3.5$ T; helical windings $\ell = 2$, m = 5; shearless external transform $\iota_0 \leqslant 0.6$) with medium-sized geometry, allows only almost perpendicular injection, 84°, to the direction of the magnetic field. Consequently, large losses (orbit losses and shine-through even at high target densities $\int ndl > 1 \times 10^{15}$ cm^{-2}, $n_{e0} > 10^{14}$ cm^{-3}) must be taken into account.

The deuterium target plasma is produced by Ohmic heating at a maximum line density $\int ndl \approx 0.5 \times 10^{15}$ cm^{-2} with 20 kA plasma current, which is programmed down at the start of NI. To avoid catastrophic energy losses due to growing tearing modes, especially (2,1) and (3,2) modes during this transition, the location of the resonance surfaces within the plasma must be controlled. This is mainly done by feedback control of the current in the helical windings with the condition $\iota_0 + \iota_p \approx 0.5$ for the total rotational transform at the plasma boundary.

By proper adjustment of the NI power, and of the cold gas flux by programmable gas valves, a fast current reduction (20 ms) a sufficient suppression of the (2,1) tearing mode even at $\iota_0 + \iota_p = 0.45 < 0.5$ is possible. The current reduction is the most critical part during the transition to the currentless discharge with a shearless profile of the transform t.

A residual current of 0.5–3 kA is observed in the parameter range of the W VII-A plasma with resistive voltage kept near zero. This current is higher by an order of magnitude than predicted for bootstrap or Ohkawa current. There may be a number of reasons for this residual current:

(a) The plasma pressure.

(b) Non-stationarity of the plasma parameters may introduce dynamic voltages by positional shift of the plasma column.

(c) Unfortunately there is a large voltage ripple in the primary OH system at zero loop voltage, and the current may therefore result from rectified eddy currents at the plasma boundary.

Apparently the residual current modifies the magnetic configuration and consequently influences the confinement. Further investigations at stationary conditions are necessary to clarify this observation.

(d) Since the particle transport in W VII-A is faster than neoclassical transport, the diffusion-driven currents must also be expected to deviate from neoclassical predictions. An increased particle loss could result in an increased bootstrap current.

3. RESULTS

3.1. Parameter range

The refinement of the scenario for the transition to currentless plasma finally leads to improved plasma parameters. Two examples will be described in detail. Figure 1 presents the main parameters of a "clean" standard discharge "A". Starting with the target plasma, the plasma current I_p, the external transform t_0, and the edge value $t_0 + t_p$ are plotted. Three injectors are used. By the use of Ti-gettered ion sources, the amount of light impurities in the beam has been significantly reduced [3]. A steady cold gas flux maintains broad density profiles, as seen in Fig. 2. The corresponding electron temperature stays at $T_e \approx 400$ eV. Figure 1 shows the energy content W, electron temperature T_e determined by soft-X-ray measurements, ion temperature T_i measured by charge-exchange analyser as well as that derived from neutron flux from D-D reactions. An ion temperature profile at t = 180 ms obtained by active charge-exchange analysis using a diagnostic beam is included in Fig. 2. At the boundary region, values for T_i derived from Doppler width measurements from C V lines are added. Figure 3 shows the time behaviour of the total radiation within the indicated radii measured by bolometer. The distribution of the local radiative power density is plotted for this discharge in Fig. 4. When it is taken into account that the line density is growing steadily, the slight increase of central radiation indicates an effective reduction of the impurity flow compared to previous discharges.

The operation with refined beams and the subsequent reduction of impurity inflow allows the full use of four injectors. In a second example (Fig. 5) a discharge "B" with $P_N \approx 1$ MW is described. During this discharge at t = 124 ms, a D_2 pellet (0.6 mm diameter, 500 $m \cdot s^{-1}$ velocity) has been ablated. Practically all particles remain in the plasma, which results in density increase by a factor of 2. From

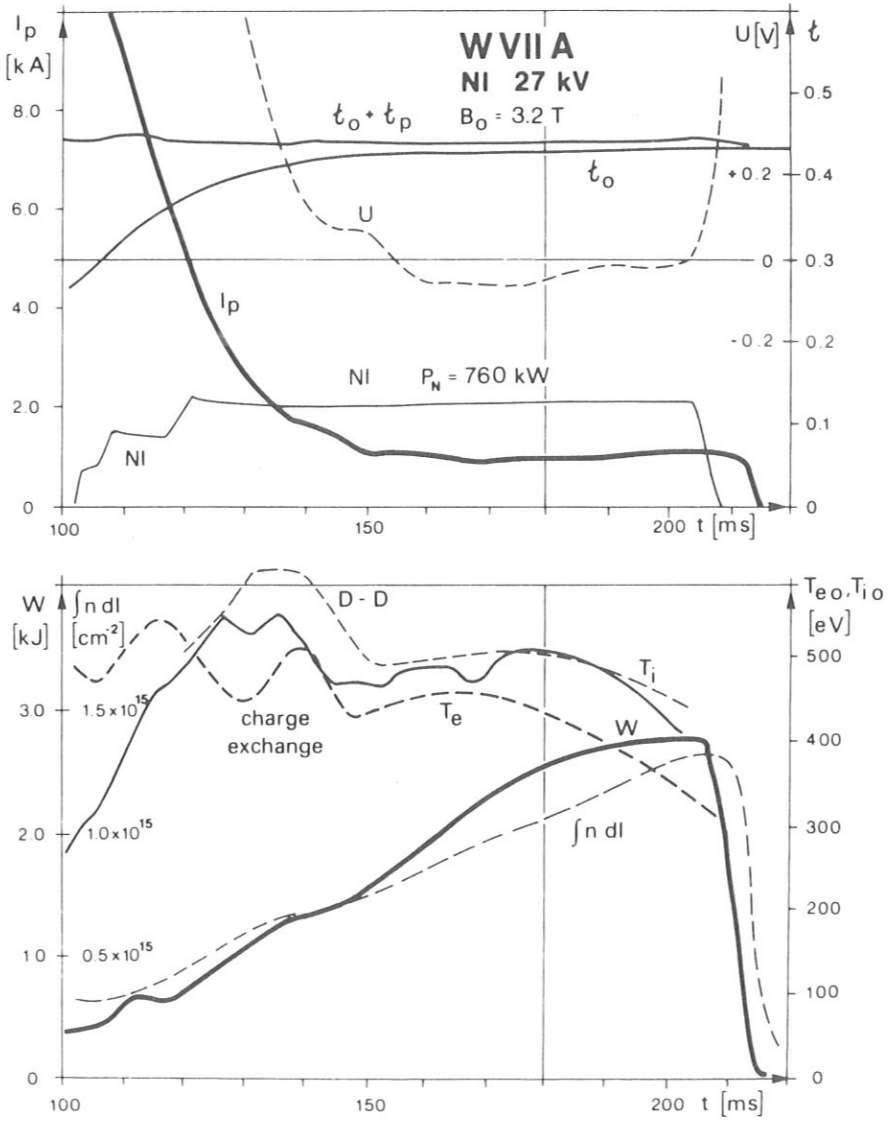

FIG.1. Discharge "A": plasma current reduction I_p, "currentless" phase with resistive voltage U during NI, P_N = 760 kW (Ti gettering). Main parameters: t_0, $t_0 + t_p$–rotational transform; $\int ndl$–line density; W–energy content; T_{e0}–electron temperature (soft X-ray); T_{i0}–ion temperature (charge-exchange, D-D neutrons).

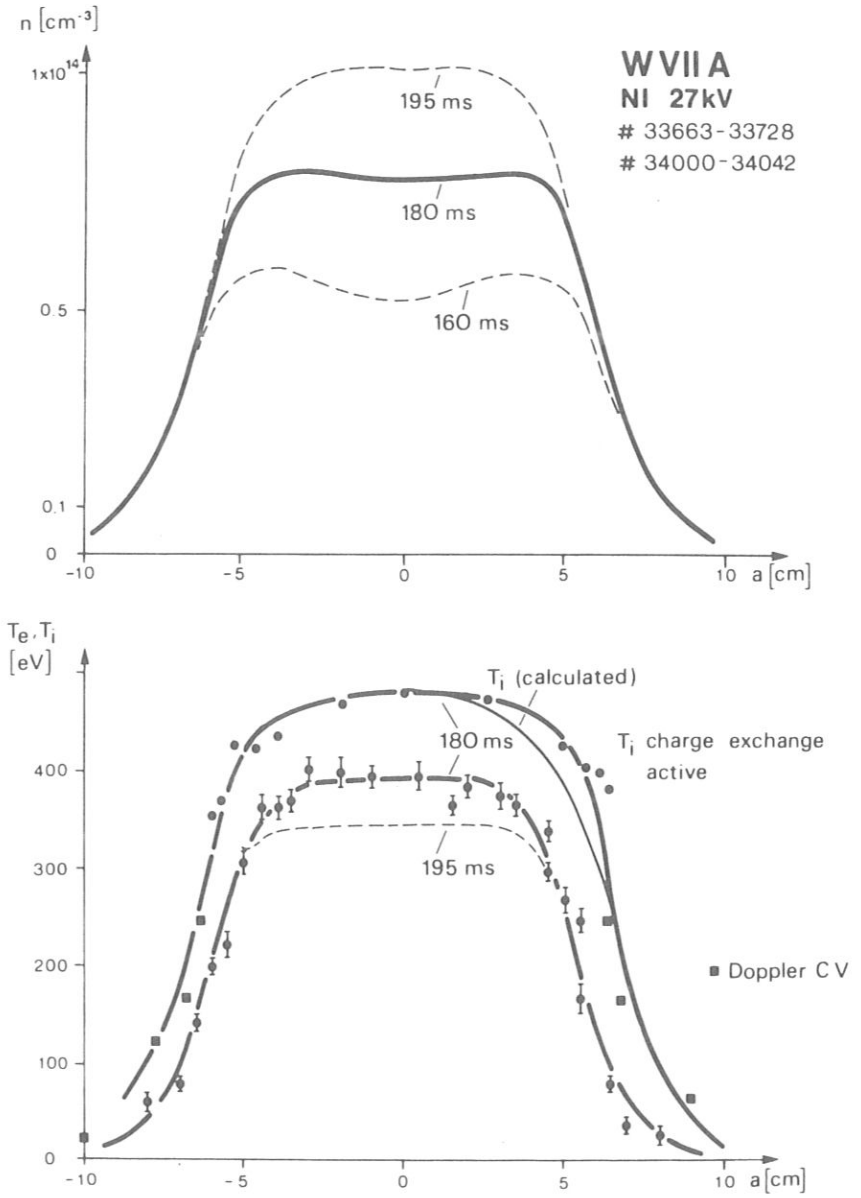

FIG.2. Temperature and density profiles for discharge "A". The approximate T_i profile (transport analysis) is indicated at $\Delta t = 180$ ms.

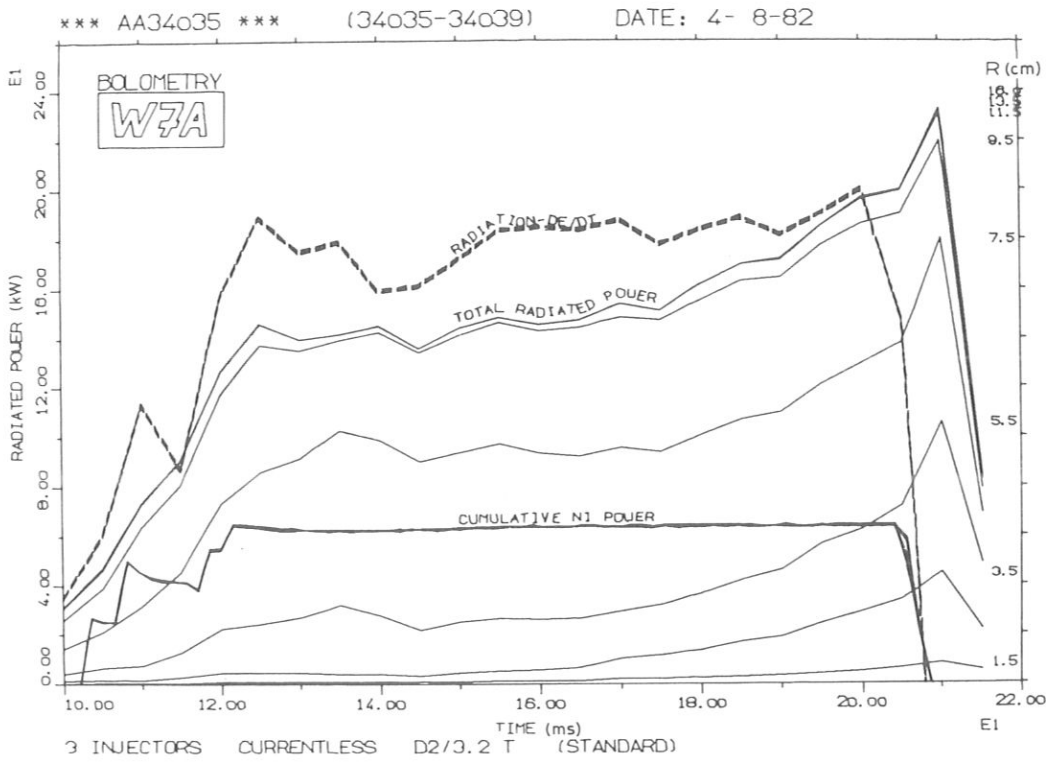

FIG.3. Total radiative loss P_{rad} obtained by bolometer ("A"). Integrated values for different radii. P_{rad} – W is included.

this density increase in the early phase of the currentless discharge, the higher heating efficiency leads to a higher energy content. Addition of the fourth injector drives the ion temperature up to $T_i \approx 1$ keV. Figure 6 illustrates the temperature and density profiles for this well documented discharge. From the central plasma parameters $n_{e0} = 1.1 \times 10^{14}$ cm^{-3}, $T_e = 0.6$ keV, $T_i = 1$ keV for $B_0 = 3.2$ T, a central $\beta(0) = 0.8\%$ is calculated. For singular shots, values exceeding $\beta(0) \approx 1\%$ have been reached.

3.2. Energy balance

Rough estimates of the energy balance in W VII-A have already been carried out, but the non-stationarity of the parameters, the dominant radiative losses and the uncertainties of the beam power deposition have impeded this analysis. Improvement of the discharge and the diagnostics has now provided a more secure basis.

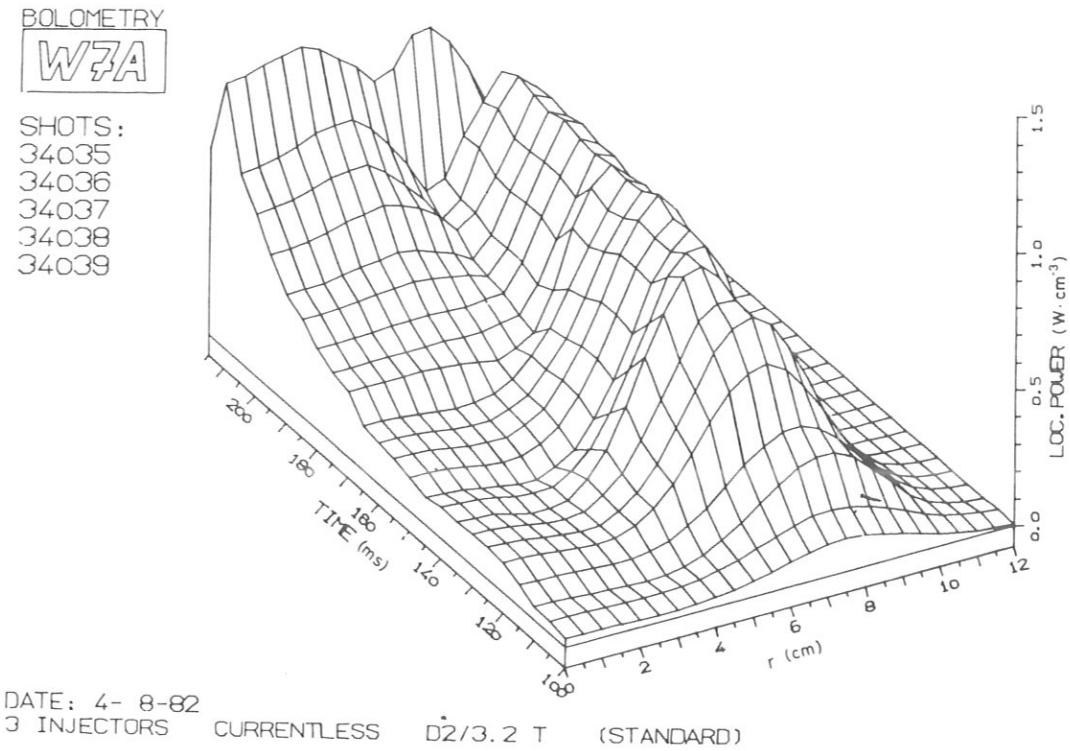

FIG.4. Radiative power density profiles for discharge "A".

3.2.1. Global energy balance

A numerical code, ODIN [4], modified for application to W VII-A, has been used to calculate the heating efficiencies with measured density and temperature profiles of the plasma. The NI power P_N can be taken from the response of the internal calorimeters in W VII-A. There is no doubt about the shine-through losses, which are measured and found to be in agreement with the calculation. The orbit losses, however, appear to have been overestimated. The build-up of radial electric fields can lead to better confinement of the hot injected ions. The resulting poloidal rotation has been confirmed by spectroscopic measurements. Doppler-shift measurements of impurity lines during NI are consistent with poloidal velocities $v \approx 10\ km \cdot s^{-1}$, corresponding to several hundred volts per cm radial field strength. Experimentally, the heating efficiencies can be derived by analysis of the transient behaviour of the plasma during stepwise changes of the injection power. Some results are presented in Fig. 7. For several discharges, including the standard case "A", one additional injector has been used for 10–20 ms. For

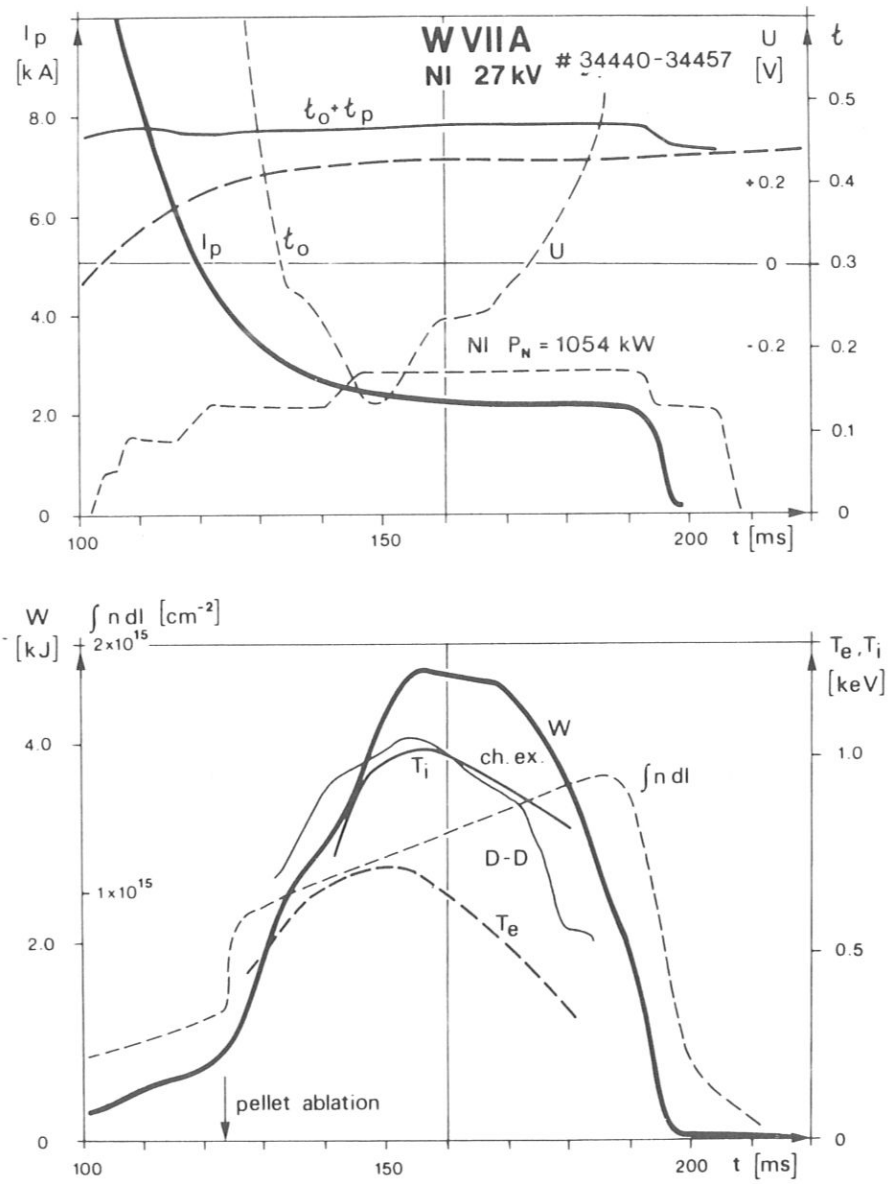

FIG.5. Discharge "B": neutral injection $P_N = 1056$ kW. Main parameters as in Fig.1. Pellet injection at $\Delta t = 124$ ms (D_2 ⌀ 0.6 mm, 500 $m \cdot s^{-1}$).

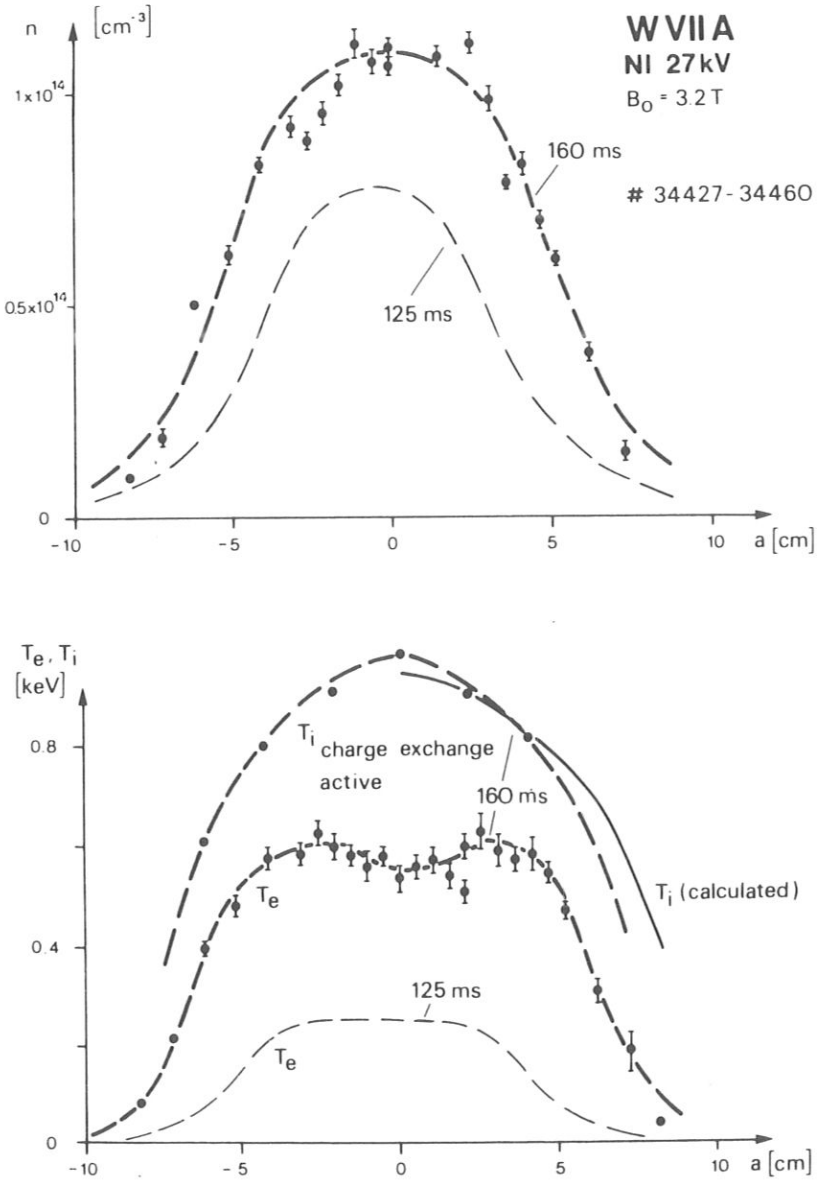

FIG.6. Temperature and density profile for discharge "B" at 125 ms and 160 ms after pellet injection. The approximated T_i profile (transport analysis) is included.

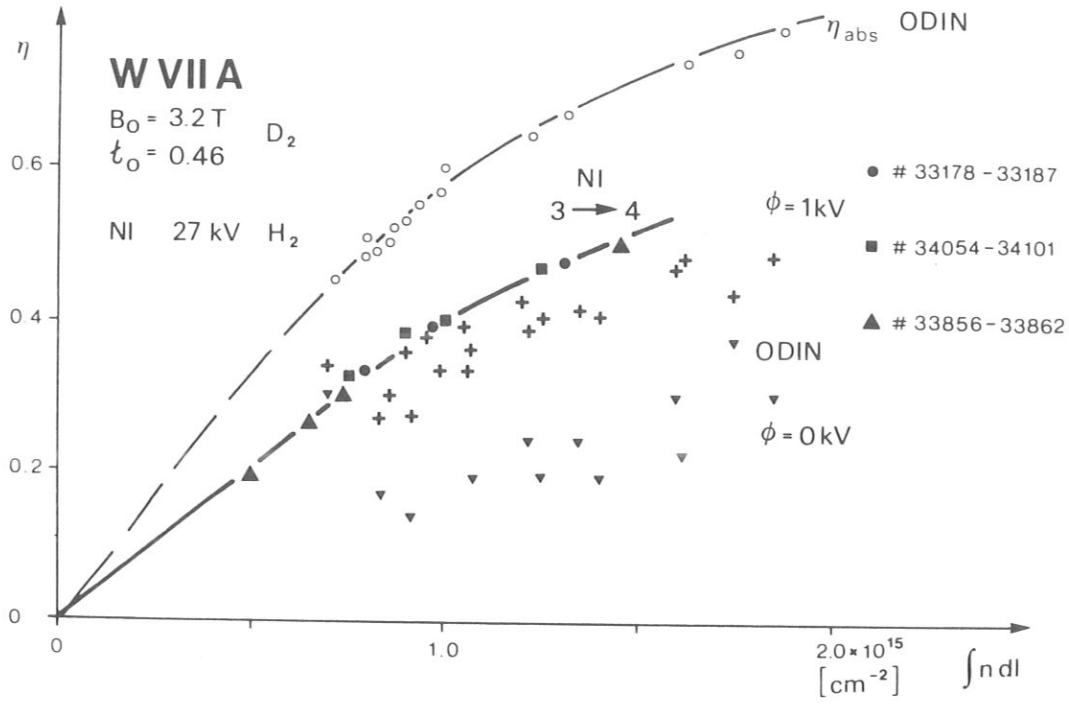

FIG. 7. Total heating efficiency η for NI versus line density ∫ndl for various discharges as calculated by the ODIN code: η_{abs} is trapping efficiency; η corrected for the orbit losses at radial potential difference. For comparison, experimental values for η are plotted. +: φ = 0 kV. ▼: φ = 1 kV.

comparison, the heating efficiency from the ODIN calculations, assuming a radial potential difference $\phi = 0$ or $\phi = 1$ kV, are also given in Fig. 7. The calculation for $\phi = 1$ kV agrees with those values for the heating efficiency obtained in the experiment, although for a detailed analysis the different density and temperature profiles have to be taken into account.

For the two selected discharges, the energy replacement time τ_E can be calculated at the time of the profile measurements. The time variation of the internal parameters is relatively small: $\tau_E = W/(P_{IN}-W)$, where W is the internal energy and P_{IN} the effective heating power (see Table I).

The radiative losses P_{rad}, especially in the internal region $P_{rad}/5.5$ cm within a = 5.5 cm, reduce the available heating power signficantly. P_{th} is calculated from the transport analysis discussed in the next section.

3.2.2. Energy transport analysis

The transport calculations are based on the neoclassical heat conduction $\kappa_{i,plateau} = n\chi_i \approx n_i T_i^{3/2}$ and the empirical electron heat conduction $\kappa_e = n\chi_e \approx 1/T^{2/3}$

TABLE I. DISCHARGE PARAMETERS

Discharge	W (kJ)	W (kW)	P_N (kW)	$\int ndl$ (cm^{-2})	η_{exp}
A	2.6	30	760	1×10^{15}	0.4
B	4.7	−10	1054	1.2×10^{15}	0.45

Discharge	P_{rad} (kW)	P_{rad}/5.5 cm	P_{th} (kW)	P_{IN} (kW)	τ_E (ms)
A	180	40	260	304	9.0
B	200	100	370	474	10.0

κ_e was verified for Ohmic discharges not affected by MHD perturbations [5]. With measured profiles for density, temperature and radiative losses, the unknown quantities in the energy balance are reduced to the beam deposition profiles for ions p_{bi} and electrons p_{be}, which can be compared with ODIN code predictions. By trial and error, p_{bi} is varied until the measured T_i profiles are approximated. The electron heat conduction equation is solved for p_{be}, taking into account the measured $T_e(r)$ and radiation profile. For the classical energy transfer P_{ie}, the composition of the ion component H^+, D^+ and oxygen is included. Heating of electrons by impurity ions and charge-exchange losses are neglected. In Figs 2 and 6 the approximated ion temperature profiles T_i are indicated for comparison.

The global energy balances for discharges "A" and "B" are presented in Fig.8. The following results are obtained:

(a) The necessary ion heating $p_{bi} \lesssim 2.5 - 9\ W \cdot cm^{-3}$ is concentrated within $r \leqslant a/2$ and exceeds the ODIN calculations even for a radial potential difference of 1 kV.

(b) The necessary electron heating $p_{be} < 1 - 1.5\ W \cdot cm^{-3}$ peaks at $r \approx 1/2 - 2/3$ a.

(c) The main part of the power is deposited in the centre and transferred to the ions, contrary to the predictions of the ODIN code. The necessary total heating power p_{th}, however, is fairly consistent with the P_{IN} predictions.

(d) In discharges with low central radiative losses, ion heat conduction is the essential loss for the central region, whereas electron heat conduction becomes dominant at the plasma edge.

Within these assumptions, the ions need almost all the heating power available by neutral injection. The electrons are heated by the ions and almost no direct

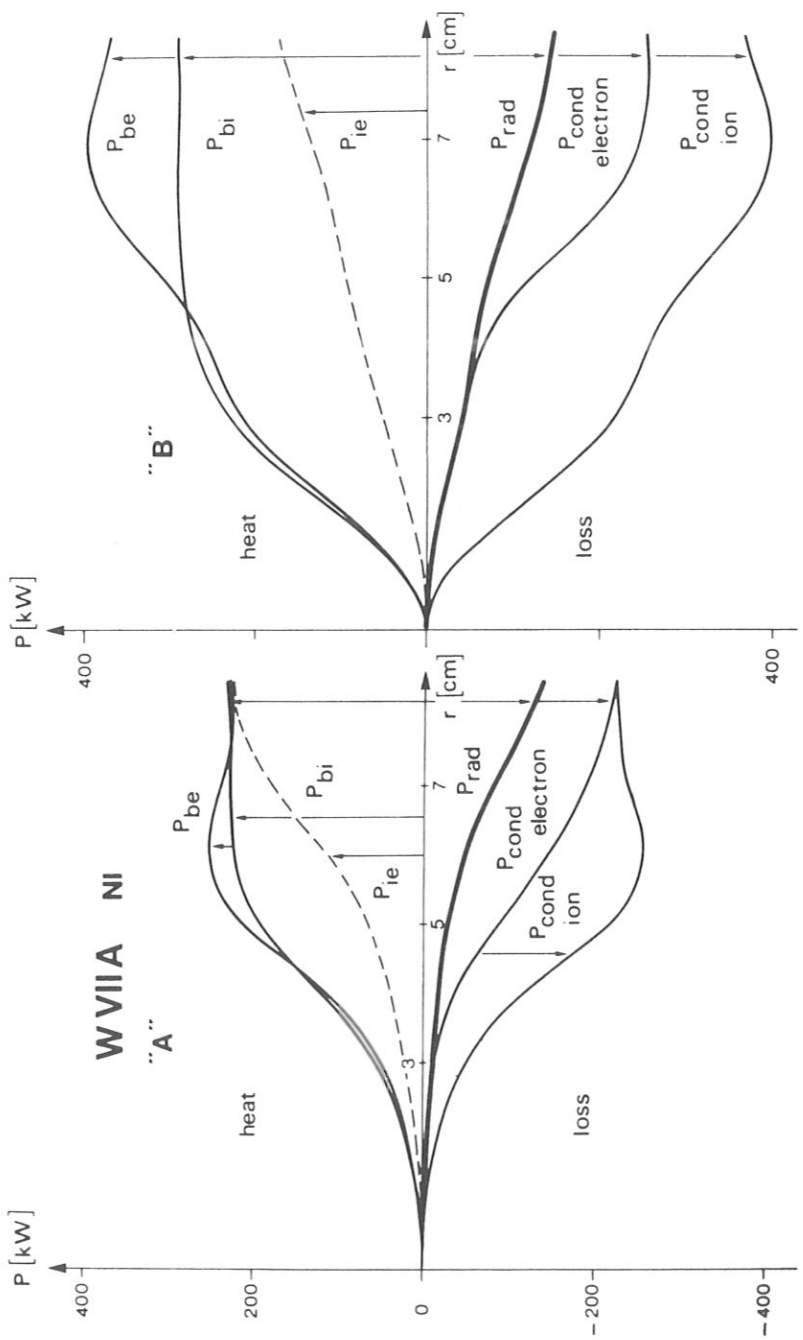

FIG. 8. Global energy balance for discharge "A" at 180 ms and "B" at 160 ms. Measured radiation loss P_{rad}, calculated conduction loss P_{cond}, NI heating to electron P_{be} and to ions P_{bi} versus radius.

electron heating is necessary. This picture is consistent with the hollow electron temperature profiles of discharge "B" (Fig. 6).

3.3. Radiation losses

Towards the end of the "currentless" phase of neutral-beam-heated discharges, a strong increase of the central impurity radiation is usually observed. Local radiation of up to 3 $W \cdot cm^{-3}$ could be deduced from a turnable 10-channel bolometer system. Nearly the same values are obtained from ultrasoft-X-ray measurements with an array consisting of 30 Si diodes which are sensitive to radiation with energy $\geqslant 350$ eV. Radiation levels of this order finally exceed the power deposited by NI, and lead to temperature decay and termination of the discharge.

The increase of impurity radiation in time may have several causes:
(a) improved confinement for all particle species during the "currentless" phase;
(b) contamination of the neutral beam with oxygen and a very effective trapping of beam impurities by the plasma; (c) additional influx of impurities during current decay, as indicated by an increase of the radiation from low ionization stages; the impurities remain trapped during the "currentless" phase.

3.3.1. Density increase and particle confinement

There is strong experimental evidence for substantial increase in particle confinement during the currentless plasma phase. From H_α/D_α signals at various ports round the machine, beam fuelling is found to be the main source of particle production.

If all beam particles that are trapped, including the fraction of particles introduced into lost orbits and an oxygen impurity content of 5% (see below), are taken as the main particle source, we estimate particle confinement times of the order of 100 ms (assuming 0.7 for the recycling coefficient as found in Ohmically heated discharges), which is less than the neoclassical confinement time by a factor of 5 to 10.

3.3.2. Impurities

The central radiation consists mainly of O VIII and O VII line radiation with wavelengths of 19 Å and 22 Å respectively. This is deduced from the observations of the line radiation in the range 14 – 19.5 Å by crystal spectrometer. The importance of the 22-Å radiation can be roughly estimated from the O VII line at 18.6 Å. Moreover, pulse-height spectra taken with a windowless Si(Li) soft-X-ray detector ($\Delta E \approx 200$ eV) during different time intervals show a peak in the distribution at about 650 eV ($\cong 19$ Å). To investigate the sources of impurities and the main impurity species in the plasma centre, the following experiments have been made:

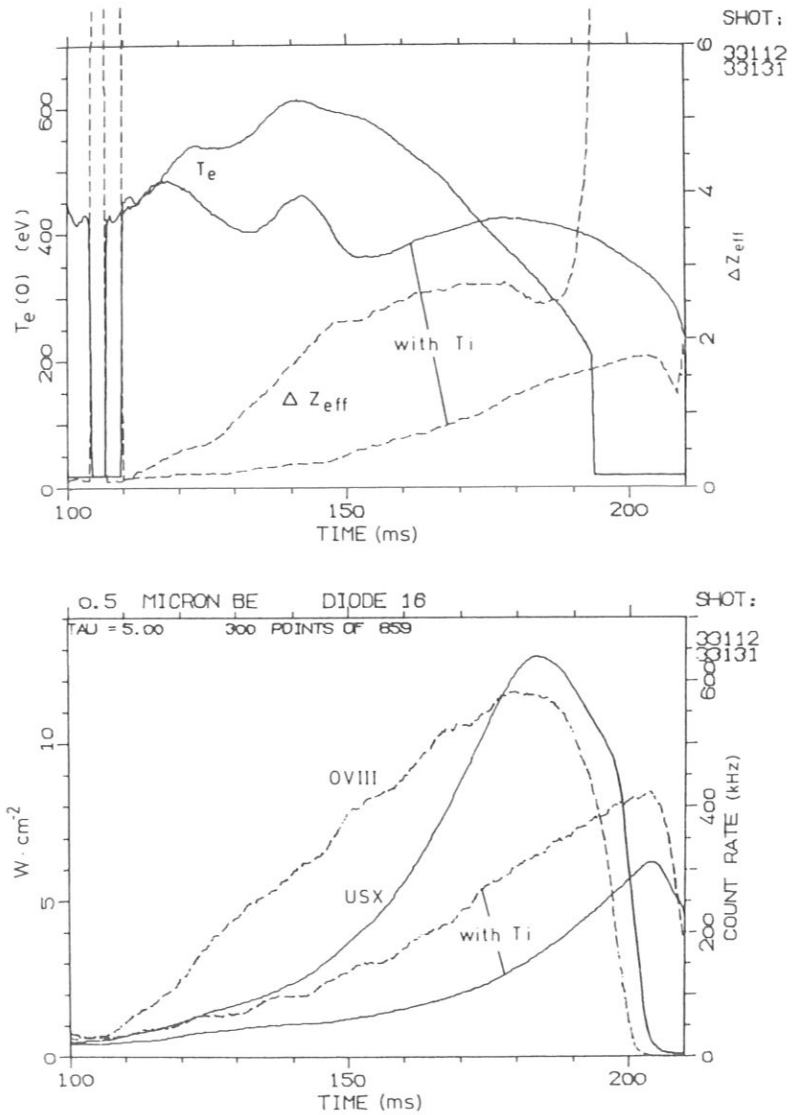

FIG. 9. Reduction of Z_{eff} and electron temperature decay rate in the plasma centre (extracted from X-continuum radiation) for "clean" discharge (upper diagram). The lower diagram shows the corresponding effect on the central soft X radiation (>500 eV) and O VIII line radiation.

(a) Unlike hydrogen, beam-injected oxygen is expected to be absorbed almost completely by the plasma, even at moderate densities. This is confirmed by measurements of sputtered molybdenum in front of the beam dump by laser fluorescence [6]. Because of the high sputtering yield of oxygen, the contribution of the oxygen impurities in the hydrogen beam dominates the Mo sputtering. With plasma, the Mo sputtering is reduced by a factor of 10, whereas for H sputtering a reduction by only a factor of 2 would be expected because about 50% of the

beam power is still transmitted through the plasma. Therefore, oxygen must have been primarily absorbed in the plasma.

(b) In addition, computations with a modified version of the ODIN neutral beam deposition code have shown [7] that a considerable fraction of injected oxygen is thermalized in a high ionization state near the plasma centre (up to 80% within a 5-cm radius). Central deposition is even increased if radial electric fields, which have been shown to exist, are included.

(c) Titanium gettering of the ion sources has led to a considerable reduction of the light-impurity content contamination of the extracted fast ion beam as detected by the mass spectrometric measurements [3].

Figure 9 demonstrates the reduction of the central radiation losses if "cleaned" neutral beams are used and the heating rate of the NI is carefully adjusted to avoid additional impurity influx from the wall via m = 2 islands which may evolve during the current decay. The relative change of both the central USX signal and the O VIII radiation at 19 Å also indicates the important role of the oxygen line radiation.

These optimized discharges also do not show the strong decrease of electron temperature during NI, therefore allowing for a further extension of the duration of the discharge. Moreover, the central Z_{eff} value obtained from the central flux of the continuum radiation above about 3 keV is drastically reduced.

(d) A direct method of studying the effect of beam-injected oxygen was applied by using an additional 20-ms injection pulse from a fourth injector with no titanium gettering. Figure 10 shows the effect of additionally running the fourth injector (144 – 164 ms) on the evolution of the central temperature (measured by the X-ray filter method) and Z_{eff} (from X-ray continuum radiation). After an initial rise of the electron temperature (150 – 160 ms), a faster decrease due to enhanced line radiation is observed. Z_{eff} has increased by 0.5 after the end of the 20-ms injection pulse. Assuming that the oxygen injected with the neutral beam is completely deposited inside a radius of 5 cm, a 2.5% oxygen contamination of the ungettered injector can be evaluated. During a 60-ms operation period, with three gettered injectors only, the increase in Z_{eff} is about 1, corresponding to 0.6% oxygen content of each beam, well consistent with direct measurements of the beam impurity concentration.

(e) Controlled impurity contamination of the plasma with neon has shown that fast neon neutrals (via injection) are effectively deposited in the plasma centre during the "currentless" phase. Cold neon only penetrates if the gas puff coincides with the plasma current decay [8].

(f) Since iron is also present in the plasma centre, as detected by resonance lines of Fe XVII (15 Å and 17 Å) and Fe XVIII (14.2 Å), the relative contribution

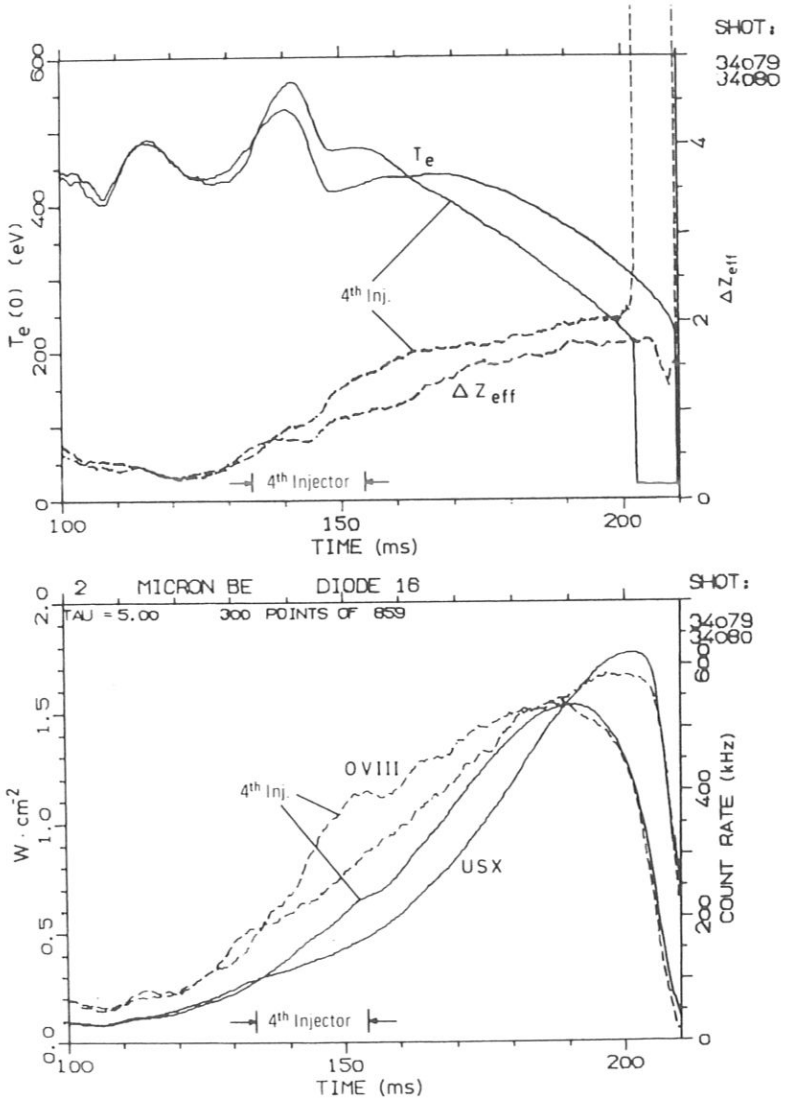

FIG.10. Enhancement of Z_{eff}, O VIII line radiation (19 Å), USX radiation (>500 eV) and the decay rate of the central electron temperature by use of an additional 20 ms injection pulse.

of Fe line radiation to the whole central radiation (above about 350 eV, USX diodes) was determined by Fe-laser blow-off at different times during the discharge. A strong increase of the Fe XVII radiation was observed just after the Fe ablation, whereas the relative increase of the USX radiation was much smaller (Fig. 11). A contribution of 10–20% of the Fe line radiation to the total central radiation losses can be estimated.

(g) The time behaviour of the central radiation can be well explained by a mixture of O VIII and O VII line radiation, with a shift towards O VII in the case

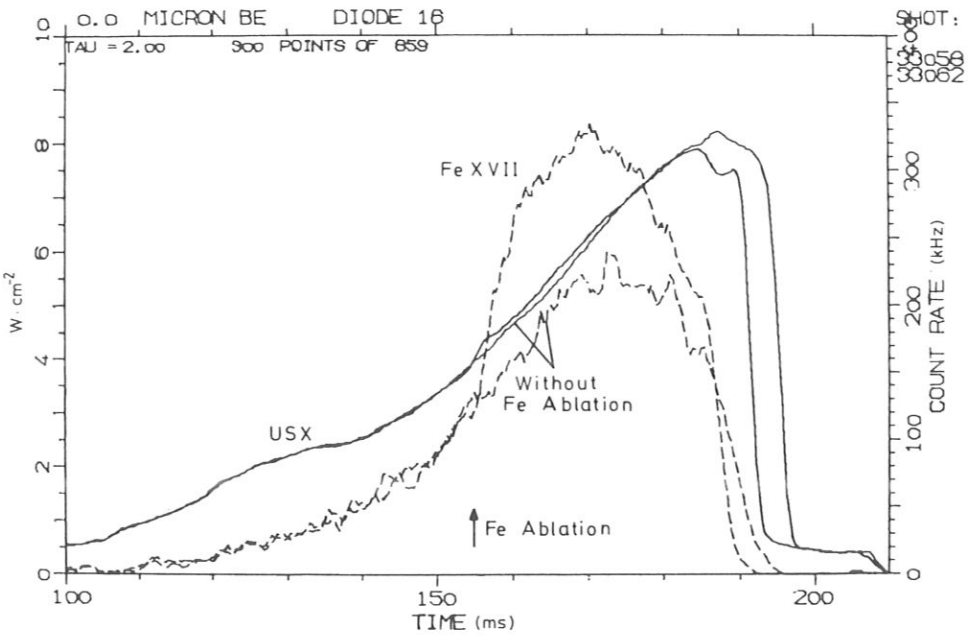

FIG.11. Effect of Fe ablation by laser blow-off at 154 ms on the Fe XVII line radiation (15 Å) and the central USX radiation (>350 eV).

of electron temperature decay below about 400 eV by progressive radiation cooling. About 50 ms after the start of injection, strongly increasing iron radiation is observed which adds to the final radiation level by about 20%. Although radiation from iron is lower than oxygen, the steep increase of Fe XVIII in the centre, even with decreasing temperature, and the simultaneous reduction of the radiation from lower Fe charge states, may be an indication of an inward flow of impurities.

3.3.3. Confinement of injected impurities

The laser ablation technique has been used to obtain some information on the confinement of impurities. Si and Fe have been ablated at various times during the discharge. 3×10^{16} particles are estimated to reach the plasma, as compared to the total number of particles ($\approx 2 \times 10^{19}$) present in the plasma.

During the Ohmic-heating phase, $t < 100$ ms, the intensity of Si XII (499.43 Å) normalized to the line-integrated electron density decays with a time constant of 16 ms (Fig. 4). From radial profile measurements we conclude that Si XII is representative of the central part of the plasma. The same time constant is deduced from the decay of the Fe XVII (15 Å) line radiation for iron ablation.

With NI in the currentless phase, an increase of the time constant by a factor of 2 to 3 is observed. As an example, Si XII/$\int$ndl versus time is shown during this phase. The electron temperature has been kept constant except for the first 5 ms;

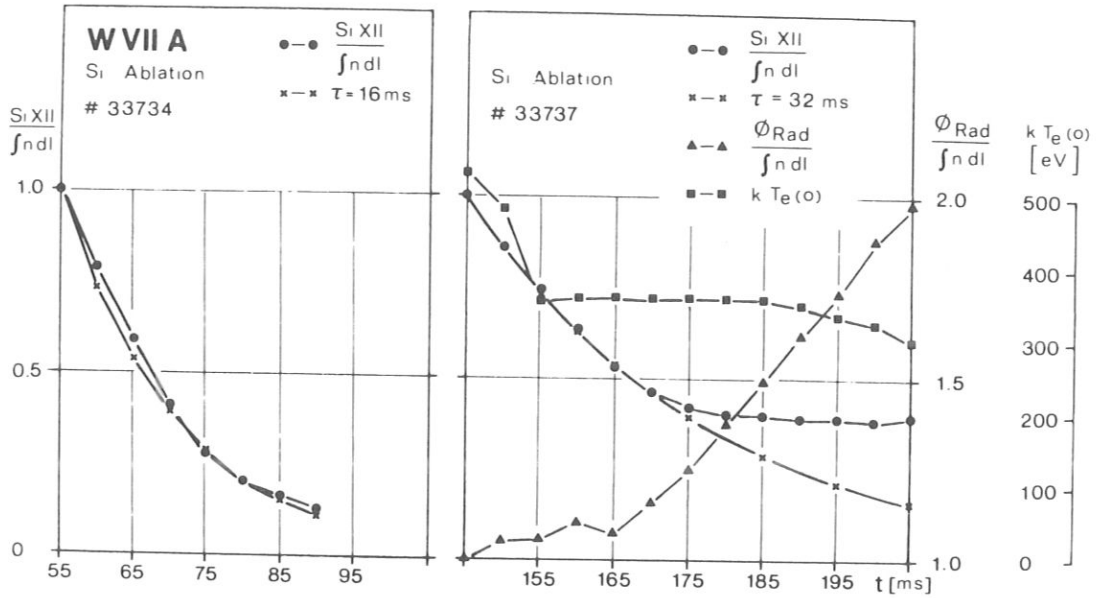

FIG.12. Decay of Si XII/∫ndl signals after ablation (time of ablation 50 ms and 140 ms). Exponential decay curves are given for comparison. Central radiation $\phi_{rad}/\int ndl$ from USX diodes and $kT_e(0)$ are shown as a function of time.

the time of ablation was 140 ms. In this case, an exponential decay with a 32 ms time constant fits the experimental decay only within the first 25 ms of the decay. Later in time, the decay of the Si XII signal is much longer. This time behaviour is also confirmed by measurements of the continuum radiation as seen by X-ray diodes. From this result, one is led to the conclusion that either the confinement has further improved or a change in the density and temperature profiles during the final stage of the current decay around 145 ms causes a change in the transport of the impurities, resulting in an inward transport. Temperature profiles have been found to change from triangular shape to flat profiles.

Although this inward transport cannot be excluded, there is evidence of improved confinement if a further reduction of density fluctuations, as measured by microwave scattering around 160 ms, is related to the confinement of particles. The central radiation from USX diodes, again normalized to ∫ndl, is plotted in Fig. 12 and can be taken as a measure of the impurity content. It is interesting that the observed linear increase starts at about the same time that the exponential decay of the line radiation is considerably reduced. This behaviour is also seen from the line radiation of intrinsic impurities in the plasma.

4. SUMMARY AND CONCLUSIONS

In spite of the geometry of the device ($a \leqslant 0.1$ m) and the small effective heating power ($P_{IN} < 500$ kW), remarkable plasma parameters have been achieved

in W VII-A with NI. So far no saturation due to β-limiting effects has been observed. Certainly the effect of the residual current in the "currentless" phase on the configuration must be carefully investigated. Long pulse operation (a pulse duration $\Delta t > 150$ ms has already been established) may favour these investigations in excluding dynamic effects resulting from the current decay. Experiments are under way to substitute plasma build-up and heating by RF application for Ohmic heating. This may finally prevent the difficulties, especially during the transition phase to currentless plasma.

The inclusion of radial electric fields seems to explain the reduction of the orbit losses and thus the increased heating efficiency observed. The mechanism for preferential coupling of the beam power to the ions still needs to be investigated. Ion-cyclotron waves, which have been observed in correlation with NI, may turn out to be responsible for this increased ion heating.

The improvement of energy confinement seems to be supported by the disappearance of sawtooth instabilities and tearing modes with vanishing plasma current. It may be concluded from the transport analysis that the electron conduction, even in the currentless case, can be described by the empirical scaling $\chi_e \approx 1/(nT_e^{2/3})$, which has been derived from Ohmic discharges. In the case of Ohmic heating, this favourable scaling at high temperatures is not applicable in the whole plasma region as a result of those instabilities. Ion heat conduction seems to be in agreement with neoclassical predictions and becomes dominant for high ion temperatures ($\chi_i \approx T_i^{3/2}$). As a consequence of the weak coupling of the beam to the electrons, the ions must also transfer a large fraction of the power to the electrons operating at high densities. The electron temperature profile is very sensitive to the impurity content and to the coupling to the ions. This coupling mechanism has been investigated at densities low enough for the temperature difference between electrons and ions to be accurately enough documented. Experiments with additional electron heating by a small plasma current are consistent with that picture.

The oxygen contamination of the plasma has been significantly reduced by various means. There is an unavoidable influx of impurities by the beam and from the wall, and in the case of continuous density increase, still observed for the long pulse discharges, this leads to radiative losses exceeding the power input from NI. An accumulation by an increased inward flow of impurities can at present be neither affirmed nor excluded.

ACKNOWLEDGEMENTS

The progress of the W VII-A Stellarator experiments would have been impossible without the efforts of the technical staff. Dr. Büchl and Mr. Schiedeck were responsible for pellet injection. Dr. Scherzer contributed by analysing

exposed carbon probes. The support of the Jülich group, especially Dr. Bogen and Dr. Schweer for laser fluorescence measurements, and Dr. Schlüter for preparation of the crystal spectrometer, is gratefully acknowledged.

REFERENCES

[1] W VII-A TEAM, NI GROUP, in Plasma Physics and Controlled Nuclear Fusion Research 1980 (Proc. 8th Int. Conf. Brussels, 1980) Vol. 1, IAEA, Vienna (1981) 185.
[2] W VII-A TEAM, NI GROUP, in Proc. 3rd Joint Varenna-Grenoble Int. Symp. Heating in Toroidal Plasma, Grenoble, 1982, Vol.2 (1982) 813.
[3] OTT, W., et al., ibid., Vol. 1, p. 123.
[4] W VII-A TEAM, NI GROUP, Proc. 2nd Joint Varenna-Grenoble Int. Symp. Heating in Toroidal Plasma, Como, 1980, Vol. 2 (1980) 789.
[5] W VII-A TEAM, Bull. Am. Phys. Soc. **26** (1982) 891, 2U 11.
[6] BOGEN, P., et al., in Proc. 5th Int. Conf. Plasma Surface Interaction in Controlled Fusion Devices, Gatlinburg, 1982.
[7] LISTER, G.G., et al., in Proc. 3rd Joint Varenna-Grenoble Int. Symp. Heating in Toroidal Plasma, Grenoble, 1982, Vol. 1 (1982) 103.
[8] W VII-A TEAM, Bull. Am. Phys. Soc. **26** (1982) 891, 2U 10.

DISCUSSION

R. GOLDSTON: It seems to me that you could learn a great deal about beam ion thermalization in W VII-A by measuring the charge-exchange energy spectra of the fast ions at a number of angles and poloidal and toroidal locations. Have you done anything along these lines?

H. RENNER: We have analysed slowing-down spectra: the flat energy distribution obtained may indicate increased thermalization. Corresponding predictions of the Monte-Carlo calculations, including radial electric fields or higher collision frequencies, confirm these observations. Unfortunately, the energy resolution of our analyser is rather poor, and access to the plasma is limited.

M. NAGAMI: In tokamak experiments with neutral-beam injection, the electron energy confinement time is proportional to the plasma current, indicating that the intensity of the poloidal field is essential in electron energy transport. Your electron heat conductivity expression for W VII-A shows no B_p dependence. Have you checked this against experiments?

H. RENNER: In the experiments with Ohmic heating in W VII-A no explicit dependence on the poloidal field has been found for variation of $1 > t > 0.2$ at B_0 from 2 T to 3.5 T. The currentless operation with a restricted accessible parameter range (3.2 T, $t_0 \approx 0.5$) allows no significant proof.

T.K. CHU: The W VII-A has been used for currentless experiments in which energetic neutral beams were injected with a rotational transform from about 0.25 to greater than 0.5. Are there any experimental results indicating that a high rotational transform is desirable?

H. RENNER: A lower transform allows operation at a higher field value and leads to more circular cross-sections of the plasma column. Hence operation at $t_0 < 0.5$ is preferred, as long as the dangerous (2, 1) mode can be suppressed during the current reduction.

T.K. CHU: Does improved particle confinement time, and therefore impurity accumulation and radiation loss, appear as a real limitation on steady-state operation of a stellarator?

H. RENNER: Certainly restrictions may occur if no measures are taken against the accumulation. I am hopeful that efficient control of the impurity flow, which may critically depend on the density and temperature profiles, will be possible. Possible measures include gas flow, magnetic perturbations by formation of islands, etc.

IAEA-CN-41/Q-5

CONCEPT OF AN ADVANCED STELLARATOR

U. BROSSMANN, W. DOMMASCHK,
F. HERRNEGGER, G. GRIEGER,
J. KISSLINGER, W. LOTZ, J. NÜHRENBERG,
F. RAU, H. RENNER, H. RINGLER, J. SAPPER,
A. SCHLÜTER, H. WOBIG
Max-Planck-Institut für Plasmaphysik,
Euratom-Association, Garching,
Federal Republic of Germany

Abstract

CONCEPT OF AN ADVANCED STELLARATOR.

In classical stellarators, the Shafranov shift of magnetic surfaces determines the limit of the equilibrium β-value: $\beta_{eq} \approx \iota^2/A$; ι = twist number, A = aspect ratio. In an Advanced Stellarator (AS), the β-limit is higher than this value; the increase in the β-limit is obtained by reducing the Pfirsch-Schlüter currents $j_\parallel$ relative to $j_\perp = |\nabla p|/B$. As an example of an Advanced Stellarator, the W VII-AS configuration – a modification of the W VII-A stellarator – is described. Pfirsch-Schlüter currents and neoclassical transport losses in W VII-AS are by a factor of two smaller than those in an equivalent $\ell = 2$ stellarator. – A modular coil set of 45 coils generates the vacuum field with the parameters: B = 3.0 T, ι = 0.39, 5 field periods. The magnetic-field configuration, its properties and the modular coils are described in the paper.

1. INTRODUCTION

The justification of fusion research in the stellarator line is based mainly on two facts: the reactor potential of the stellarator and the encouraging results of stellarator experiments in recent years. Also theoretical studies on equilibrium, MHD-stability, and neoclassical diffusion have lead to new ideas and better understanding of threedimensional plasma equilibria [1]. Conventional stellarators are characterized by one dominating helical field component of the $\ell = 2$ or $\ell = 3$-type. With increasing pressure the plasma equilibrium is subject to the Shafranov shift, which then sets an upper limit on the achievable β-value given by $\beta_e \lesssim \iota^2/A$ (ι = twist number or angle of rotational transform/2π, A = aspect ratio). Therefore a large value of β_e requires either a large twist of the field and/or a small aspect ratio. A strong poloidal field requires large currents in their helical windings with all their technical difficulties and a small aspect ratio limits access to the plasma. From the reactor point of view a stellarator with large aspect ratio ($A \geq 10$) is to be preferred.

In an Advanced Stellarator the Shafranov shift is reduced by proper shaping of the vacuum magnetic field. While the plasma pressure determines the diamagnetic current $j_\perp$, the detailed choice of the vacuum field determines the Pfirsch-Schlüter currents $j_\parallel$ arising from finite pressure. The vertical field of these currents is causing the Shafranov shift. Plasma equilibria with zero Pfirsch-Schlüter currents ($j_\parallel = 0$) have already been investigated by D. Palumbo [2], who has shown that in this special case the drift surfaces of all particles including trapped particles and magnetic surfaces coincide. Coulomb collisions can only cause classical diffusion in this type of configuration. The equilibria discussed in [2], however, were MHD-unstable.

The present paper describes a practical scheme how to find a vacuum magnetic field which allows a plasma equilibrium with reduced Pfirsch-Schlüter currents and a magnetic well to ensure at least low-β MHD-stability.

Particle orbits and transport in these optimized configurations are studied by use of a Monte-Carlo code [3]. As expected the transport losses of an Advanced Stellarator in the Pfirsch-Schlüter regime and plateau regime are smaller compared with those of a conventional $\ell = 2$ or $\ell = 3$ stellarator.

Another important component of the Advanced Stellarator is the modular coil set which replaces the helix-TF-coil system of a conventional stellarator or torsatron (TF = toroidal field). Rather than calculating the magnetic field of given coils the problem here is to find the coils for a given vacuum field of the Advanced Stellarator. The "natural" solution of this problem leads to a set of poloidally closed and twisted coils.

If desired the magnetic field can also be generated by helical windings; it would require a superposition of $\ell = 0,1,2,3$ - windings and a toroidal field. However, in order to avoid the technical difficulties of complex helical windings a method has been worked out how to construct a coil system consisting of poloidally closed modular coils for any vacuum magnetic field. These modular coils are a generalization of the concept of twisted coils proposed by S. Rehker and H. Wobig [4].

Studies of Advanced Stellarators have been extended to a large variety of configurations. The example described in this paper is W VII-AS, an upgrade version of the W VII-A stellarator in Garching. The optimized field configuration W VII-AS was selected under several constraints coming from the W VII device.

These constraints did not allow to incorporate a large $\ell = 1$ field component which according to theory leads to a strong re-

duction of the Pfirsch-Schlüter currents [1]. In W VII-AS the Pfirsch-Schlüter currents are reduced by a factor of two compared to those of an equivalent $\ell = 2$ stellarator, a factor large enough for experimental investigation.

The aims of the W VII-AS experiment are

- to investigate plasma behaviour in an optimized magnetic field configuration
- to investigate a plasma without ohmic heating currents
- to make use of the modular set of poloidally closed coils instead of the conventional helix/TF coil system

Improved access for various heating methods and increase of plasma radius to twice the radius of W VII-A are further aims of this experiment. The paper describes the physics aspects of the W VII-AS concept and some technical properties of the modular coil system.

2. THE PRINCIPLES OF OPTIMIZATION

One principle for optimizing a stellarator is the choice of the vacuum field as to minimize $j_{\parallel}/j_{\perp}$ on all magnetic surfaces. For low β-values and small twist number per period this ratio $j_{\parallel}/j_{\perp}$ is governed by the variation of $Q = \int d\ell/B$ on magnetic surfaces where the integration is performed along a vacuum field line over one field period. Reducing the variation of Q on each magnetic surface therefore is the guide line for the choice of a vacuum field. For this purpose the vacuum field is composed from Dommaschk-potentials [5] and the coefficients are calculated by minimizing the variation of Q. Several constraints on the admissible shape of the plasma column are imposed on the minimization procedure. For stability at $\beta \to 0$ the existence of an averaged magnetic well is required, while for particle confinement an approximation to an absolute MIN-B-configuration is desired.

These latter conditions narrow the parameter space of optimized configuration appreciably, since otherwise plasma equilibria without Shafranov shift can be found easily. A significant reduction of $j_{\parallel}/j_{\perp}$ over all the plasma cross-section can only be achieved if the effect of toroidal curvature is overcome with the help of $\ell = 1$ field components which increase the local curvature and, unavoidably, also the population of localized particles. Therefore the danger exists that in configurations with reduced $j_{\parallel}/j_{\perp}$ and optimized drift orbits of

passing particles enhanced trapped particle losses occur in the low collisionality regime. These localized particles can, however, be chosen to be situated in the region of small curvature of the field line, so that their drift velocity is small. In the resulting configuration, which could also be described as toroidally linked mirrors, trapped particle losses are not essentially larger than in a classical stellarator.

3. THE COIL SYSTEM

The procedure of constructing the coil system starts with the optimized field given in Dommaschk potentials. In any torus surrounding the magnetic surfaces a sheath current is uniquely determined which produces the given field inside the torus. The discretization of such a sheath current yields the coil system. In order to avoid distortion of the magnetic surfaces by the gaps between the coils, a minimum number of 8 - 10 coils per field period appears necessary. Although the torus carrying the sheath current can be chosen arbitrarily its proper choice is very important for technical reasons. Adjustment of the torus to the shape of the magnetic surfaces is the ideal choice with respect to the geometry of the coils and the electromagnetic forces. In practical cases, however, the coil system has to be positioned outside the separatrix of the magnetic surfaces.

In case of W VII-AS the choice of the coil system has been made under the condition of maximum magnetic field strength and maximum distance between plasma boundary and vacuum tube. The details of the procedure are described elsewhere [6]. Starting point was a configuration ASC 742 with 5 field periods, the coil system reproducing this configuration was modified in two directions. The first modification reduces the variation of the magnetic field on the magnetic axis the second modification introduces 5 special large coils in order to provide access for tangential neutral beam injection. Due to these changes the resulting magnetic field slightly deviates from the optimized configuration ASC 742, but the increase in $j_{\parallel}/j_{\perp}$ and the change of drift orbits of passing particles are small.

This modified coil system consists of 45 modular coils, it is designed to produce B = 3 T on the magnetic axis and a constant twist $\iota = 0.39$.

Plane TF-coils are superimposed in order to vary the rotational transform within the limits $0.24 \leq \iota \leq 0.6$. The maximum additional toroidal field is 0.5 T. A view on the coil set is shown in Fig. 1.

Parameters of W VII-AS:

Major radius	$R = 2.0$ m
Averaged plasma radius	$a = 0.2$ m
Aspect ratio	$A = 10$
Magnetic field	$B_o = 3.0$ T
Rotational transform	$\iota = 0.39$
Shear	$\Delta\iota/\iota < 10^{-2}$
Number of field periods	$m = 5$
Number of coils	45
Magnetic well	$\Delta V'/V'(o) = -2$ %
Variation of $\|B\|$ on magnetic axis	$\delta B/B = 3.3$ %
Variation of $\|B\|$ on last magnetic surfaces	$\delta B/B = 28$ %

A vertical field system and an ohmic heating transformer of the W VII-A experiment is available. The large injection coils will be energized separately thus allowing a change of the field ripple introduced by these coils. The standard magnetic field of W VII-AS is generated by one coil set. The additional coils allow to vary the field parameters in a wide range.

4. MAGNETIC FIELD CONFIGURATION

The magnetic field of this coil set can be considered as a superposition of $\ell = 0,1,2,3$ components. The cross section of the magnetic surfaces as calculated from this coil set changes at different azimuts from an elliptical to a triangular shape (Fig. 2) the average aspect ratio is about 10. Increase of ι by superimposing the additional toroidal field yields smaller magnetic surfaces, at $\iota \simeq 0.6$ the aspect ratio is about 20. A reduction of ι below the standard value $\iota = 0.39$ leads to larger magnetic surfaces. The shear of the W VII-AS magnetic field is negligibly small, therefore the MHD-stability at $\beta \to 0$ relies on the existence of a magnetic well. This magnetic well can be changed by superimposing a vertical field of $\pm$ 0.06 T. An inward shift of the magnetic surfaces by the vertical field yields a further reduction of the Pfirsch-Schlüter currents, the magnetic well, however, vanishes. Extensive studies of the fine structure of the magnetic surfaces show islands around $\iota = 5/N$, $N = 9, 10, 11 \ldots$. These "natural" islands strongly grow, if resonant error fields are superimposed. Because of the very small shear of the W VII-AS configuration these dangerous regions of ι always can be avoided

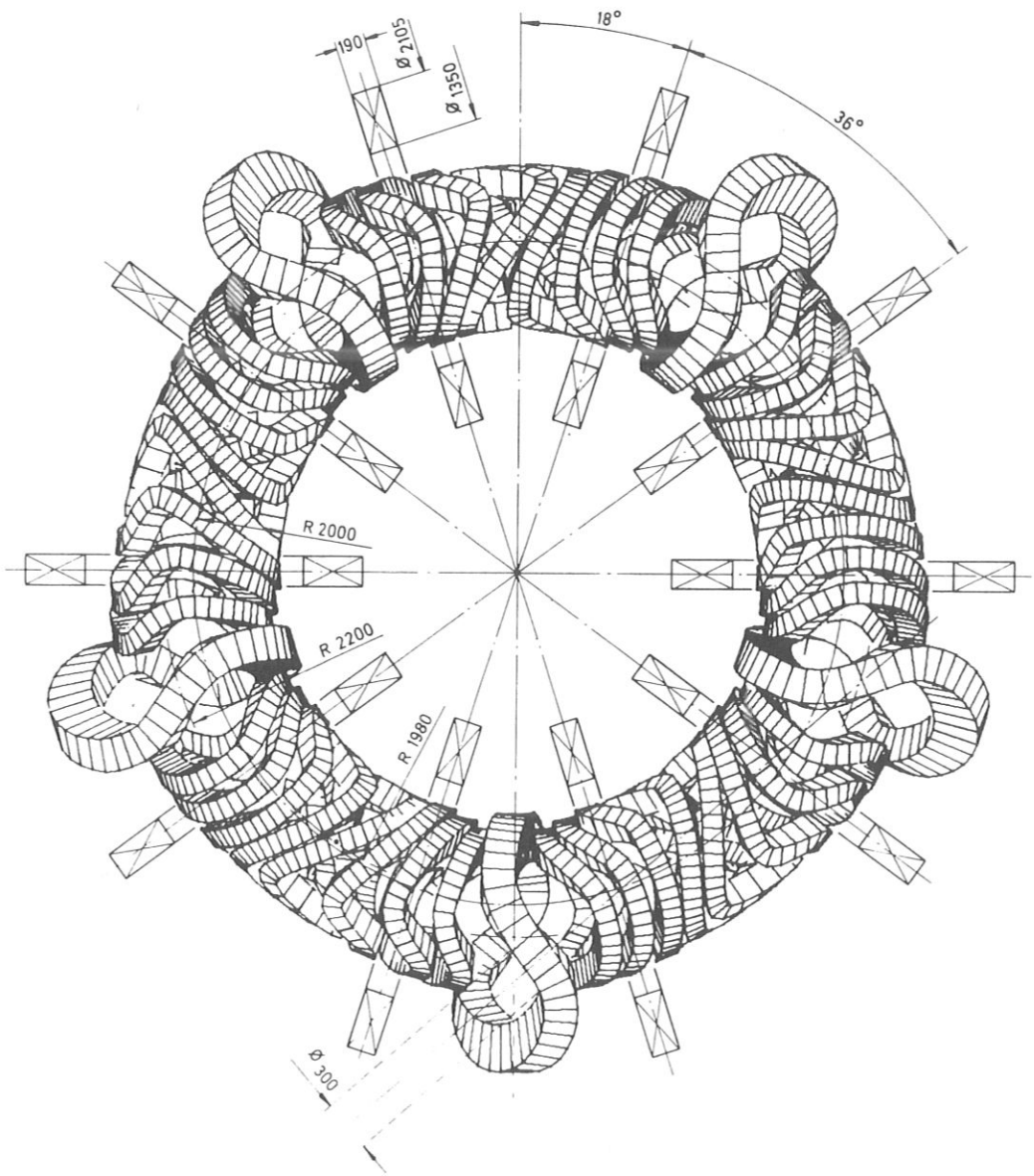

FIG. 1. Top view on the coil set of W VII-AS. Average diameter of one modular coil d = 1 m.

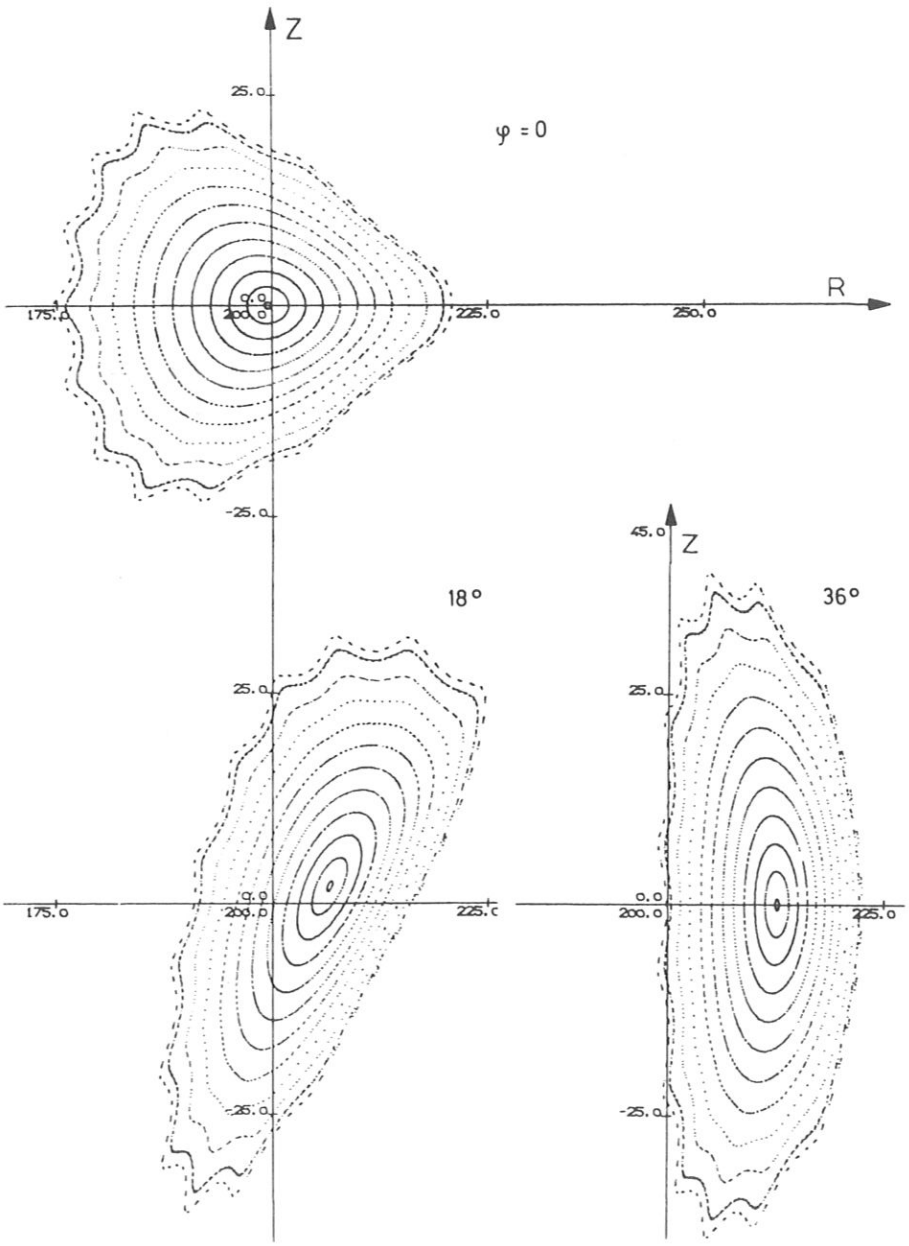

FIG. 2. Magnetic surfaces of the W VII-AS coil set. Cross-section in three different poloidal planes with azimuthal angles $\varphi = 0^\circ, 18^\circ, 36^\circ$.

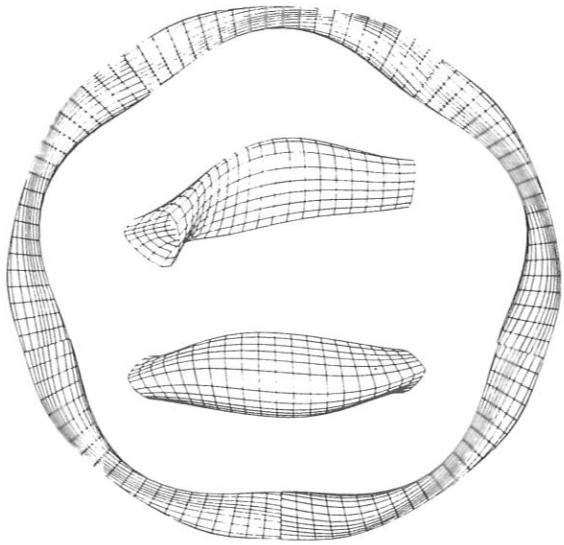

FIG.3. Shape of magnetic surface of JOK 744 configuration. This field is an analytic approximation to the W VII-AS field.

by the proper choice of the superimposed toroidal field. The standard case of W VII-AS without an extra toroidal field has a rotational transform between 10/25 and 5/13. In regions outside the "forbidden" values of ι error fields of the order of 0.2 % of the main toroidal field can be tolerated without destroying the magnetic surfaces.

5. PFIRSCH-SCHLÜTER CURRENTS, PLASMA EQUILIBRIUM AND STABILITY

In order to study plasma equilibrium, diffusion and particle orbits an analytic approximation of the actual W VII-AS magnetic field in terms of Dommaschk potentials has been constructed. A top view of one magnetic surface of this approximation (JOK 744) is exhibited in Fig. 3. The reduction of the Pfirsch-Schlüter currents is mainly caused by the M + S-effect which can be seen in Fig. 3. The ratio $j_{\parallel}/j_{\perp}$ is proportional to $(Q - \overline{Q})/\overline{Q}$ ($\overline{Q}$ = poloidal average of Q). This ratio depends on toroidal and poloidal angle but only weakly on the radial coordinate. The maximum value of $j_{\parallel}/j_{\perp}$ in 4 different poloidal planes is shown in Fig. 4. The comparison with an $\ell = 2$ stellarator at the same rotational transform clearly shows a factor of 2 reduction of $j_{\parallel}/j_{\perp}$ for all values of ι. The analytical approximation JOK 744 has a slightly larger reduction factor than W VII-AS, this difference is caused by the special injection coils. In order to

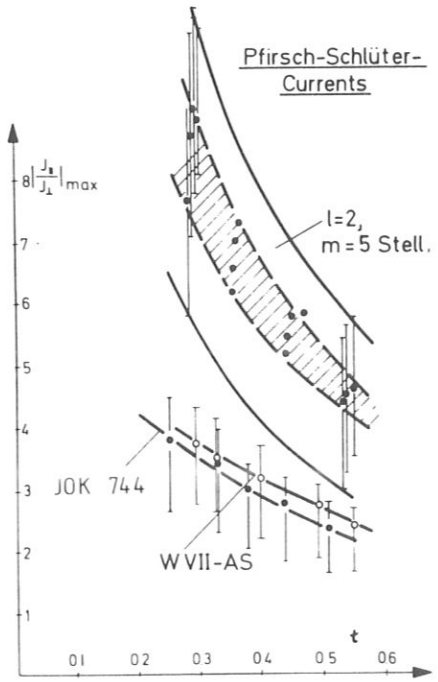

FIG. 4. Maximum ratio $|j_{\parallel}/j_{\perp}|_{max}$ versus rotational transform. Vertical bars correspond to variation of $|j_{\parallel}/j_{\perp}|_{max}$ within one field period. Dots ($\ell = 2$ stellarator) indicate $|j_{\parallel}/j_{\perp}|_{max}$ for different magnetic surfaces.

study the effect of reducing $j_{\parallel}/j_{\perp}$ the plasma equilibrium in W VII-AS was investigated with the NYU-code BETA [7] and the Garching CS-code [8]. The standard version with its actual field structure (including the effect of the injection gap) was used in the CS-code; the code BETA started from JOK 744.

In the code BETA, the actual shape of the outermost vacuum flux surface has been approximated and a sequence of equilibria with increasing β-values were computed. The maximum value of β considered was $\beta_{max} = 4.5$ % (corresponding to $\langle\beta\rangle = 1.5$ %) (Fig. 5). In a similar field configuration (ASC 742) with a larger rotational transform $\iota = 0.54$ but also larger aspect ratio $A \sim 14$, the corresponding β-values was $\beta_{max} = 7.5$ % ($\langle\beta\rangle = 2.5$ %). The Shafranov shift (location of the magnetic axis as function of β) is plotted in Fig. 6. For $\beta_{max} = 2.0$ % the toroidally averaged shift (displacement of the axis compared to its position at $\beta = 0$) is approximately 2.0 cm. In the equivalent $\ell = 2$-stellarator about twice this amount has to be expected. Calculations with the CS-code starting from the given vacuum magnetic field of W VII-AS confirmed the reduction of the Shafranov shift.

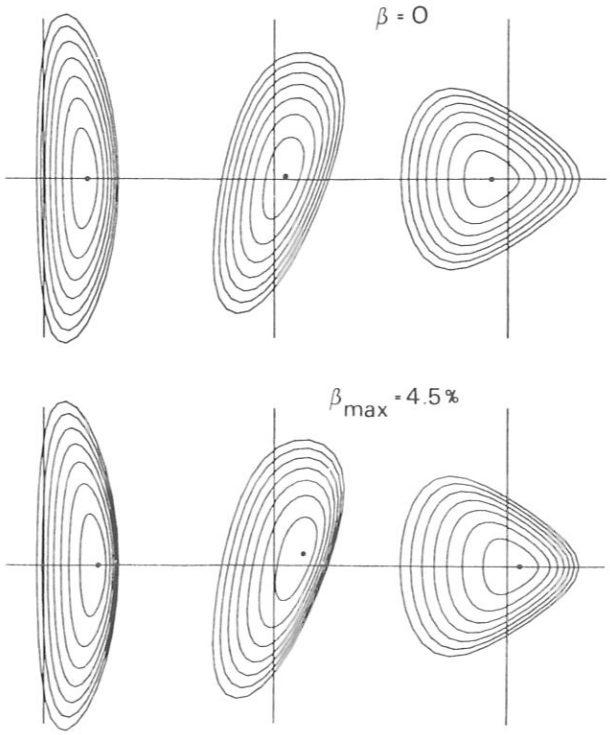

FIG.5. Flux surfaces of equilibria corresponding to vacuum field configuration of W VII-AS. Result of the BETA code at different azimuths ($\varphi = 0°, 18°, 36°$).

With respect to MHD-stability, no definite conclusion can as yet be drawn. However, the following remarks can be made.

The standard W VII-AS case has a modest magnetic well securing MHD stability at very low β. The residual shift at finite β deepens this well (beyond the trivial diamagnetic deepening of the well). Although this might not be sufficient for the stability of internal modes, it should at least remove the grossly unstable behaviour of the straight $\ell = 2$-stellarator. Results obtained with the expansion around the magnetic axis [1] indicate that the stability β limit of the type of configuration represented by W VII-AS is comparable to that of the standard toroidal $\ell = 2$ stellarator, i.e. $\langle\beta\rangle_s \sim 0.5\,\%$. β_s is the limit according to a necessary stability criterion.

The stability of gross internal MHD modes in W VII-AS will be studied with the new version of code BETA [9] in cooperation with NYU. A preliminary result [10] indicates that the reference design value $\iota = 0.39$ should safely avoid the possible instability of the 2,1 and 3,1 modes resonating with $\iota = 1/2$ and $\iota = 1/3$ respectively. Experimentally, W VII-AS will have the flexibility to

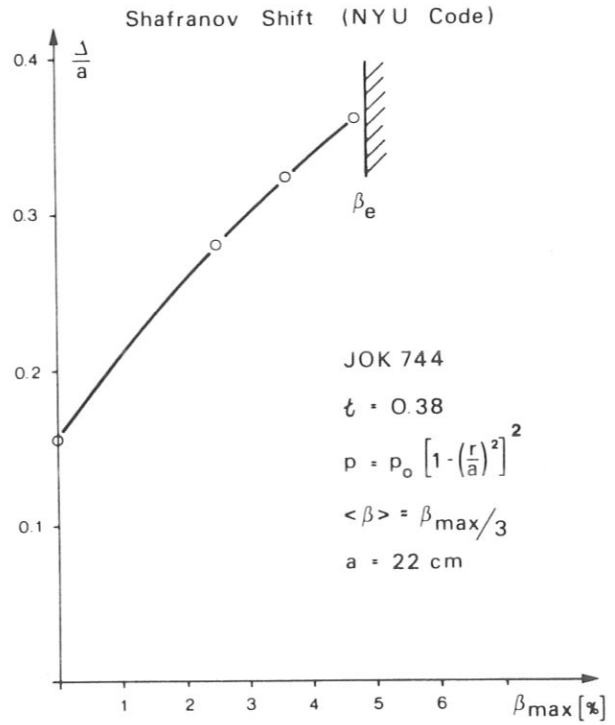

FIG.6. Toroidal shift Δ of magnetic axis normalized with average plasma radius a as a function of β_{max} for W VII-AS. Result of BETA code.

contribute by i) operating under magnetic well and magnetic hill conditions, ii) varying the resonance condition for gross modes by variation of ι, iii) achieving the estimated β-limits $\langle\beta\rangle_s \sim 0.5$ %.

6. PARTICLE ORBITS AND DIFFUSION LOSSES

Extensive studies of particles orbits have been made showing the expected large deviation from those of a classical stellarator. The drift surfaces of passing particles stay closer to the magnetic surfaces than in the $\ell = 2$ stellarator. Similar to the reduction of $j_{\parallel}/j_{\perp}$ the factor is about 2. Trapped particle behaviour is rather complicated, besides localized particles, which remain trapped in a local mirror, a certain class of particles exists, which make rapid transition between the trapped state and the passing state. Due to the quasi-straight section of the magnetic axis (see Fig. 3) particles localized to this region ($\varphi = 0$) only experience a small vertical drift depending on the pitch angle. Two other local mirrors exist - one caused by the neutral beam

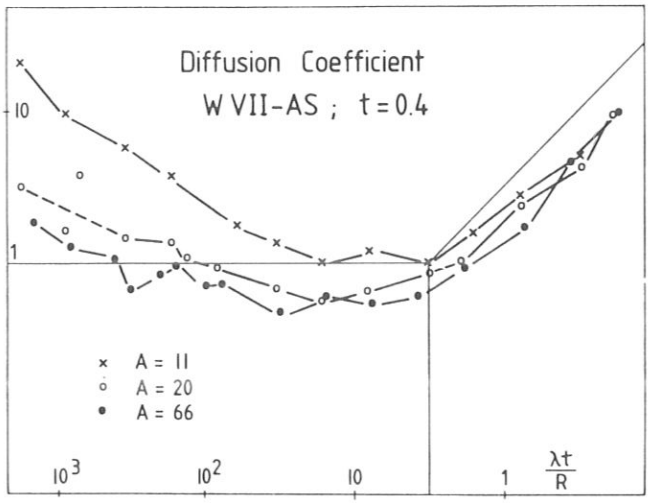

FIG. 7. Diffusion coefficient of monoenergetic ions versus collisionality $(\lambda t/R)^{-1}$. *Diffusion coefficient is normalized to plateau value. Three curves correspond to surfaces of different aspect ratios. Result of the Garching Monte-Carlo code taking into account actual W VII-AS field.*

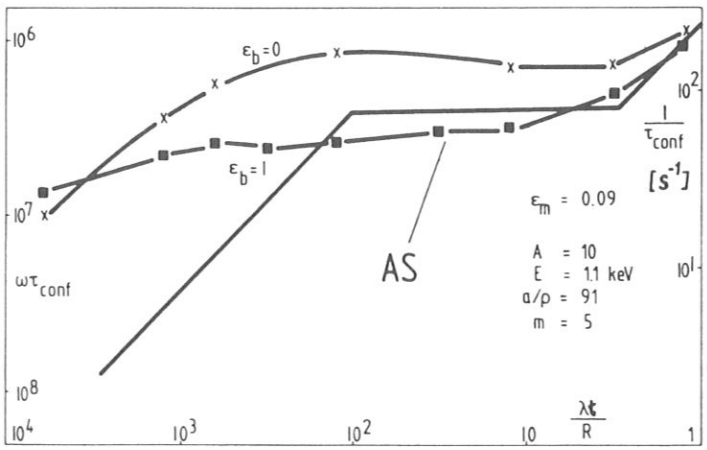

FIG. 8. Loss rate of monoenergetic ions in model field of advanced stellarator $(B=B_0 \times (1-\epsilon_a \cdot r/R \cos\theta)(1-\epsilon_b \cos m\varphi) + \epsilon_m \cos m\varphi, \epsilon_a, \epsilon_b, \epsilon_m = \text{const})$. *Rotational transform* $\iota = 1/3$. *Parameter* ϵ_b *controls drift of localized particles. Result of modified Boozer-Kuo-Petravic code.*

injection coil - where the vertical drift of localized particles follows the standard drift $v_D = (\rho/R) \cdot v_{th}$, ρ = gyroradius. The $\delta B/B$ of these mirrors is comparable with the helical ripple of the $\ell = 2$ stellarator.

Diffusion losses relying on guiding center drifts in actual fields have been calculated using a Monte-Carlo code [3] and a modified version of the Boozer - Kuo-Petravic code [11]. The diffusion coefficient for monoenergetic ions is shown in Fig. 7. The magnetic field used in this case is calculated from the coils including the injection coils; in the modified Boozer - Kuo-Petravic code, however, a model field is used. In the Pfirsch-Schlüter regime and the plateau regime the diffusion coefficient is smaller by a factor of 2 compared with the $\ell = 2$ stellarator, in the long mean free path regime the diffusion coefficient is about equal. These results are obtained for a large value of a/ρ_i ($a/\rho_i > 10^3$; a = plasma radius) in the W VII-AS experiment, however, $a/\rho_i \simeq 10^2$ has to be expected. Under these conditions also velocity space diffusion into the loss cones becomes important. The modified Boozer-Kuo-Petravic code and a model field was used to calculate the loss rate under stationary conditions rather than the diffusion coefficient. These calculations show that for realistic plasma parameters ($a/\rho_i \simeq 10^2$) the $1/\nu$-scaling of the diffusion losses does not occur. From this result the conclusion is drawn that in W VII-AS the collisional ion losses, even in the low collisionality regime are not larger than the losses in the plateau regime (Fig. 8).

7. HEATING METHODS AND EXPECTED PLASMA PARAMETERS

Various heating methods are foreseen in the W VII-AS device. The coil system allows radial access, both for ion cyclotron heating and electron cylotron heating. These methods in combination with neutral beam injection will be used for the build up of a net current free plasma. The power envisaged for these three methods is: ECRH (600 kW) ICRH (3MW), neutral beam injection (1.2 MW). Special attention is given to neutral beam injection: tangential injection and the large penetration length of 2 m will allow to use or moderate density plasma ($\bar{n} \gtrsim 2 \cdot 10^{19} m^{-3}$) as a target plasma.

The injected particles (E = 40 keV) are born as passing ions, their slowing down is faster than scattering into the trapped particle region. According to numerical calculation about 600 kW power should be available as net heating power into the ions. Under the assumption of neoclassical ion heat conduction this power should be sufficient to heat the ions to temperatures between 1.5 keV and 2.0 keV. The expected β-values are $\beta_{max} = 1\text{-}2\ \%$.

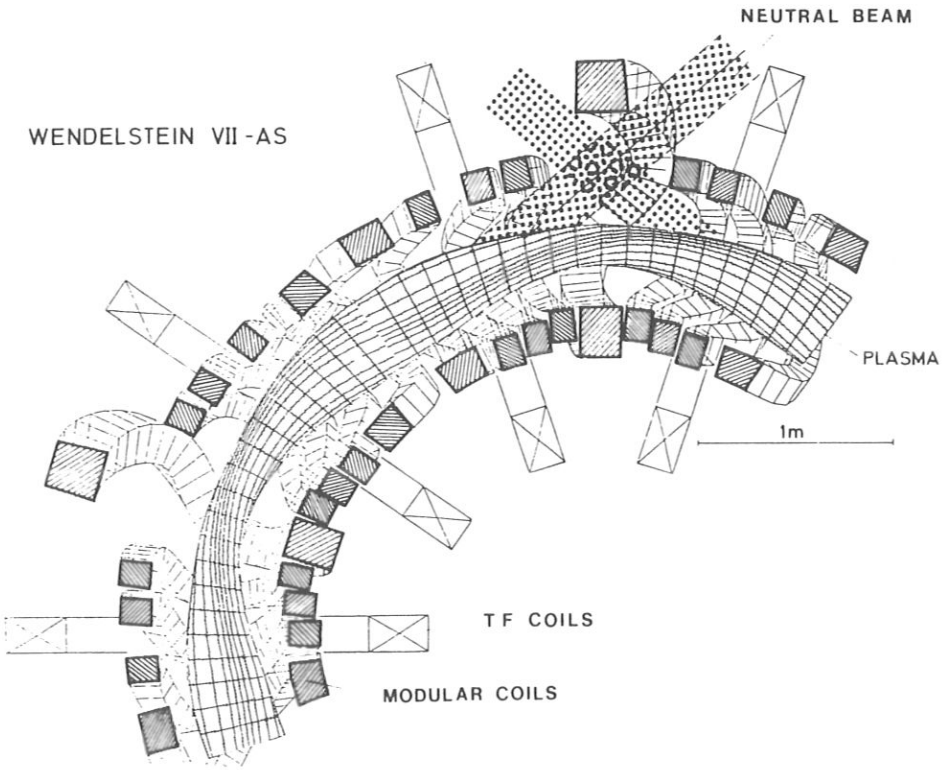

FIG. 9. Cut through horizontal plane. Schematic view indicating geometry of injection beam.

This value does not reach the equilibrium limit (4.5 %), but it is sufficient to investigate the reduction of Shafranov shift and instabilities.

The neoclassical particle confinement time which is determined by the electrons is in the order 0.5 - 1 s. For this reason a pulse length of τ_p > 1s is planned for the heating methods.

8. TECHNICAL PROBLEMS

As already demonstrated the concept of an Advanced Stellarator requires a coil system with a complex geometry. In addition the vacuum tube is adjusted to the shape of the magnetic surfaces and deviates strongly from the axisymmetric vacuum tubes used in most fusion experiments. In contrast to previous stellarators there are no electromagnetic forces acting upon the vacuum tube, which alleviates its construction despite its geometrical complexity. These new properties involve new technical problems and require new solutions. In addition to the radial forces

toroidal and poloidal forces occur in every coil. The integral toroidal and radial forces are of comparable size but far below the design values of the W VII-A TF-coil system. The poloidal and toroidal forces are compensated within one field period. This suggests to build the coil set of one field period as one module, the integral radial forces on each module are oriented in the direction of the major radius like in a standard TF-coil system. The stresses in the coils are not larger than 120 MPa tension and 25 MPa shear. Studies done by an industrial firm have shown that the manufacturing of the twisted coils does not require new development of special material.

The complex shape of the coils requires a new winding technique in order to avoid the spring back effect, solutions to this problem have been found. Effects of coil errors and mounting errors on the magnetic field have been studied in order to determine tolerances for manufacturing and mounting the coils [6]. Perturbations which preserve the 5-fold symmetry of the system have little effect on the magnetic surfaces. This concerns a motion of the coil system due to electromagnetic forces or thermal expansion. Perturbations which break the 5-fold symmetry, especially an m = 1 perturbation, are more dangerous. The result of the numerical studies shows

- at ι = 1/3 and 1/2 small field errors of the order of $\delta B/B = 10^{-4}$ generate large islands. These values of ι have to be avoided;
- in the gaps between the ι-values ι = 5/N, N = 9,10,... field errors up to $2 \cdot 10^{-3}$ can be tolerated. Even a horizontal field of $5 \cdot 10^{-3}$ B_o does not destroy the standard configuration W VII-AS. These field errors are within the tolerances of manufacturing and assembling the coil set.

The position of the large injection coils will be adjustable in certain limits. Thus it will be possible to correct field errors if necessary.

Further technical details of the W VII-AS will be published in [12].

REFERENCES

[1] Chodura, R., Dommaschk, W., Herrnegger, F., Lotz, W., Nührenberg, J., Schlüter, A., IEEE Transactions of Plasma Science, December 1981, Vol. PS-9, No 4

[2] Palumbo, D., Il Nuovo Cimento, 53B (1968) 507

[3] Lotz, W., Nührenberg, J., Proc. of the Annual Meeting on Theoretical Aspects of Contr. Thermonucl. Res., Austin 1981, paper 3/641, and Chodura, R., Dommaschk, W., Herrnegger, F., Lotz, W., Nührenberg, J., Schlüter, A., US-JAPAN Workshop on 3-D Studies for Toroidal Devices, Oct. 19-21, 1981, Oak Ridge Tennessee

[4] Rehker, S., Wobig, H., Proc. of the Symp. on Fusion Technology, Grenoble 1972, p354, Max-Planck-Institut for Plasmaphysics, Report IPP 2/215 (1973)

[5] Dommaschk, W., Z. f. Naturforschung, 36a, (1981) 251

[6] Kisslinger, J., Rau, F., Wobig, H., Proc. of the 12th Symp. on Fusion Technology (SOFT) Jülich 1982 and IPP-Report 2/259 (1981)

[7] Bauer, F., Betancourt, O., Garabedian, P., A Computational Method in Plasma Physics, New York, Springer Verlag (1978)

[8] Chodura, R., Schlüter, A., Comput. Phys. 41 (1981), 68

[9] Bauer, F., Betancourt, O., Garabedian, P., Phys. Fluids 24 (1981), 48

[10] Betancourt, O., Herrnegger, F., Merkel, P., Nührenberg, J., private communication

[11] Boozer, A. H., Kuo-Petravic, G., Phys. Fluids 24 (1981), 851

[12] Brossmann, U., Mukherjee, S., Sapper, J., Proc. of the 12th Symp. on Fusion Technology, Jülich 1982

DISCUSSION

T.K. CHU: Dr. Lyon (paper CN-41/Q-3) contended that rotational transform per field should be kept low, whereas according to Dr. Yoshikawa (paper CN-41/Q-4) it should be high. What do your studies indicate is the effect of changing the rotational transform per field period?

H. WOBIG: If the rotational transform in W VII-AS is changed the Pfirsch-Schlüter currents increase with decreasing ι and decrease with increasing ι. For the purpose of achieving a high equilibrium limit, a large ι is better; from a technical point of view a small rotational transform is preferred.

R. GOLDSTON: You presented results indicating enhanced transport losses for collisionless particles. It almost seems inappropriate to ask this in the light of the anomalously good W VII-A results, but how do you intend to put together ICRF heating – with its concomitant high-energy perpendicular tail – and non-axisymmetric geometry? In addition to simple orbit losses, impurity generation and confinement in such an arrangement seem less favourable than with co-tangential injection.

H. WOBIG: The losses of highly energetic particles with $v_\perp \gg v_\parallel$ must be considered together with a radial electric field which might lead to improved confinement of these localized particles.

PLASMA CONFINEMENT AND THE EFFECT OF ROTATIONAL TRANSFORM IN THE WENDELSTEIN VII-A STELLARATOR

ABSTRACT

The confinement of NI-heated (B = 3 T) and ECR-heated (B = 1 T) currentless plasmas in W VII-A is strongly influenced by the particular values of the rotational transform. Compared to irrational values of iota, island formation and convective losses may deteriorate the confinement for rational values of the transform at the plasma edge: $\iota(a) = m/n$; e.g. 1/2, 1/3, 2/3.... Consequently, a plasma current $I_p < 2$ kA originating from the plasma pressure, $\beta(o) \lesssim 1$ %, or produced by the heating mechanism as well as the external transform have to be controlled for stationary operation in the shearless ($\Delta \iota_o/\iota_o < 1$ %) magnetic configuration of W VII-A to maintain optimum confinement.

Neutral injection heating in W VII-A leads to build up of radial electric fields. These radial electric fields increase the heating efficiency η by the reduction of orbit losses and even influence the ion heat transport. Collisional slowing-down is found by neutron measurements for D^o injection into D^+ plasmas as well as by cx-measurements.

1. INTRODUCTION

By application of neutral injection (NI) heating favourable transport and stability properties with $\beta(o) \simeq 1$ % at $B_o = 3$ T have been achieved for "currentless" operation of the W VII-A Stellarator at particular values of the rotational transform $\iota(a) = 0.52$ and $\iota(a) = 0.45$ /1,2,3/. Recent investigations using a 28 GHz VARIAN gyrotron at 1 T succeeded to substitute ohmic heating for preionization, plasma build up and heating /4/. In future a combination of electron cyclotron resonance heating (ECRH) and NI will be possible at main fields $B_o = 2.5$ T by means of the 70 GHz VARIAN gyrotron which has already been delivered to IPP Garching.

A combination of different non-ohmic heating methods: ECRH, NI, and ion cyclotron resonance heating (ICRH) seems mandatory to explore in a wide parameter range stability and transport properties of the plasma as a function of the particular magnetic field configuration. For the optimization of the different Stellarator configurations various detailed properties of the particular heating mechanism (mass flow, power deposition profile, current drive) have to be taken into account.

2. PLASMA BEHAVIOUR IN W VII-A

2.1 Parameter range
ß-limits

In contrast to the HELIOTRON E /5/ magnetic configuration, possessing high transform and high shear, the helical winding system (l = 2, m = 5) of W VII-A produces a rotational transform of $\iota_o \leq 0.6$ with low shear ($\Delta\iota_o/\iota_o < 1$ %) for $B_o \leq 3.5$ T.

"Currentless" plasmas with neutral injection heating (4 injectors, 27 kV, typically $H^o \rightarrow D^+$ with $P_N \simeq 1$ MW) have been studied at B_o = 2.5 - 3.5 T. In spite of the moderate size of W VII-A (R = 2 m main radius, a = 0.1 m plasma radius) high ß-values have been obtained at densities $n_e \approx 10^{14}$ cm^{-3} and temperatures $T_e < T_i \simeq 1$ keV. For various discharges fig. 1 shows the central ß as a function of heating power. The highest values correspond already to about half the equilibrium limit of W VII-A.

For ECRH at 1 T (28 GHz, 200 kW, heating efficiency $\eta \simeq 0.5$) plasmas could be maintained with $n_{eo} \lesssim n_{cutoff} \approx 10^{13}$ cm^{-3} and $T_i < T_e \lesssim 1.5$ keV. In fig. 2 theoretical predictions /6,7/ for both stability and equilibrium betas are compared with experimental data. Only a significant increase of the heating power would allow to approach critical ß values, because of the dependence of the transport on B and ι. So far, no MHD instabilities have been observed within the accessible ß range.

The energy replacement time $\tau_E = W/P_{IN}$ varies from τ_E = 10-20 ms for NI at 3 T to τ_E = 1-2 ms for ECRH at 1 T for "currentless" discharges at optimum confinement.

2.2 NI Heating

For NI heated discharges in W VII-A a local energy transport analysis has always been difficult. The power deposition profiles as well as the local transport properties are strongly affected by the radial electric fields that are built up by the almost perpendicular NI. Both high heating efficiencies and preferential ion heating have been postulated /1,2,3,8/ to explain the experimental results.

2.2.1 Heating efficiency

Measurements of power input agree with code predictions if electric fields deduced from poloidal plasma rotation measurements are included /2,8/. For the almost perpendicular injection, radial electric fields have strong influence on particle trajectories and thus on lost orbits, which in turn determine the electric field to achieve ambipolarity. By measuring sputtered Fe-atom densities ($n_{Fe} \simeq 1.5 \times 10^8$ cm^{-3}) via laser induced fluorescence, the existence of orbit losses has been shown in positions of the vacuum vessel, where the calculations predict the orbits to intersect the stainless steel wall.

In addition, experiments have been done with all currents and magnetic fields reversed which leaves the magnetic configuration unchanged. In this case, both ∇B drift and ExB poloidal rotation have to change sign, whereas the radial electric field remains unchanged. The orbit losses are now expected to be deposited on the opposite side of the vacuum vessel. Both effects have been verified experimentally. Reversing currents and fields also corresponds to a change from co- to counter-injection, for which direction the heating efficiency is expected to be smaller /8/. From the experiment no difference in heating efficiency was found. The higher poloidal velocity, $\simeq$ 30 km s^{-1} as compared to 20 km s^{-1} for co-injection, is in agreement with this observation.

2.2.2 Preferential ion heating

The simultaneous existence of central ion and electron temperatures of 1 keV and 0.6 keV respectively and of neoclassical ion heat conduction could only be explained if in the central plasma region ($r \lesssim a/2$) all the beam power were primarily transferred to the ions /2/.

Ion cyclotron emission has been measured: therefore neutral beam (NB) driven ion modes have been considered as possible candidates for preferential ion heating. Theoretically, the transient slowing down distribution function has been found unstable to low harmonic ion cyclotron modes after switching on the NB /9/. In the case of stationary slowing down, however, the distribution function based on Coulomb scattering was found to be stable, except for a very small regime around the injection energies, resulting in strong instability at the plasma resonance with frequencies above the lower hybrid frequency. These instabilities, however, would smooth the distribution function only in the vicinity of the injection energies. Therefore, only a small energy transfer from the beam to the waves would be expected. Thus, for stationary conditions, the slowing down of the beam particles should mainly be determined by Coulomb scattering.

2.2.3 Slowing down

Any mechanism leading to preferential ion heating would necessarily be connected with a faster slowing down of the injected fast ions. Therefore, considerable effort has been put into measuring both the stationary ion distribution function and ion slowing down times by switching off one or more of the injectors /10/. To clarify the energy transfer mechanism, further experiments have been carried out based on the idea that beam plasma interaction may be localized at the injection port. Therefore, one injector , operated with deuterium (D) was pulsed for 20 ms into a standard currentless deuterium discharge (B_o = 3.2 T, $\epsilon < 0.5$) maintained by 3 H^o- beams. The neutron flux from the reaction $D + D \rightarrow n + He^3$ was measured at various positions around the machine by a He^3 proportional counter . Except for some enhancement at the injection port, a symmetric